Proceedings of the Ninth Lomonosov Conference on Elementary Particle Physics

PARTICLE PHYSICS *at the start of the* NEW MILLENNIUM

Editor

Alexander I Studenikin

PARTICLE PHYSICS

at the start of the

NEW MILLENNIUM

This page is intentionally left blank

INTERREGIONAL CENTRE
FOR ADVANCED STUDIES

Proceedings of the Ninth Lomonosov
Conference on Elementary Particle Physics

PARTICLE PHYSICS
at the start of the
NEW MILLENNIUM

20–26 September 1999, Moscow

Editor
Alexander I Studenikin
Department of Theoretical Physics
Moscow State University, Russia

World Scientific
Singapore • New Jersey • London • Hong Kong

Published by

World Scientific Publishing Co. Pte. Ltd.

P O Box 128, Farrer Road, Singapore 912805

USA office: Suite 1B, 1060 Main Street, River Edge, NJ 07661

UK office: 57 Shelton Street, Covent Garden, London WC2H 9HE

British Library Cataloguing-in-Publication Data
A catalogue record for this book is available from the British Library.

PARTICLE PHYSICS AT THE START OF THE NEW MILLENNIUM

Copyright © 2001 by World Scientific Publishing Co. Pte. Ltd.

All rights reserved. This book, or parts thereof, may not be reproduced in any form or by any means, electronic or mechanical, including photocopying, recording or any information storage and retrieval system now known or to be invented, without written permission from the Publisher.

For photocopying of material in this volume, please pay a copying fee through the Copyright Clearance Center, Inc., 222 Rosewood Drive, Danvers, MA 01923, USA. In this case permission to photocopy is not required from the publisher.

ISBN 981-02-4644-7

Printed in Singapore by World Scientific Printers

NINTH LOMONOSOV CONFERENCE ON ELEMENTARY PARTICLE PHYSICS

Mikhail Lomonosov
1711-1765

Sponsors

Russian Foundation for Basic Research

Interregional Centre for Advanced Studies

Ministry of Science and Technology of Russia

Supporting Institutions

Faculty of Physics and Institute of Theoretical Microphysics of Moscow State University

Joint Institute for Nuclear Research (Dubna)

Instituto Superior Tecnico - CENTRA (Lisbon)

Institute of Theoretical and Experimental Physics (Moscow)

Institute for Nuclear Research (Moscow)

Institute for High Energy Physics (Protvino)

Programme Committee

V.Bagrov (Tomsk State Univ.), V.Belokurov (MSU), V.Braginsky (MSU),
G.Diambrini-Palazzi (Univ. of Rome),
J.Dias de Deus (IST/CENTRA, Lisbon),
D.Ebert (Humboldt Univ., Berlin), R.Faustov (NSK, RAN & ICAS, Moscow),
D.Galtsov (MSU), V.Kadyshevsky (JINR, Dubna),
A.Logunov (IHEP, Protvino), V.Matveev (INR, Moscow),
V.Melnikov (Russian Grav. Soc., Moscow),
V.Mostepanenko (PTI, St.-Petersburg),
A.Mourao (IST/CENTRA, Lisbon),
A.Nikishov (Lebedev Physical Inst., Moscow),
L.Okun (ITEP, Moscow), V.Ritus (Lebedev Physical Inst., Moscow),
V.Rubakov (INR, Moscow), V.Savrin (MSU), F.Selleri (Univ. of Bari),
D.Shirkov (JINR, Dubna), Yu.Simonov (ITEP, Moscow),
A.Slavnov (MSU & Steklov Math. Inst., Moscow),
A.Smirnov (INR, Moscow & ICTP, Trieste),
P.Spillantini (INFN, Florence), A.Studenikin (MSU & ICAS, Moscow),
V.Trukhin (MSU), V.Zhukovsky (MSU)

Organizing Committee

G.Diambrini-Palazzi (Univ. of Rome),
J.Dias de Deus (IST/CENTRA, Lisbon),
A.Egorov (MSU & ICAS, Moscow) - Secretary,
R.Faustov (Russian Academy of Sciences & ICAS, Moscow),
V.Galkin (Russian Academy of Science & CAS, Moscow),
A.Kataev (INR, Moscow), O.Khrustalev (MSU), P.Kashkarov (MSU),
V.Melnikov (Russian Grav. Soc., Moscow), V.Mikhailin (MSU),
A.Mourao (IST/CENTRA, Lisbon), N.Nikitina (MSU),
P.Nowosad (Univ. of Sao Paulo), Yu.Popov (MSU),
V.Rubakov (INR, Moscow), P.Silaev (ITM, Moscow State University)
A.Sisakian (JINR, Dubna),
A.Slavnov (MSU & Steklov Math. Inst., Moscow),
A.Studenikin (MSU & ICAS, Moscow) - Chairman,
V.Trukhin (MSU), Yu.Vladimirov (MSU)

FOREWORD

The 9th Lomonosov Conference on Elementary Particle Physics was held at the Moscow State University (Moscow, Russia) on September 20-26, 1999.

The conference was organized by the Faculty of Physics of the Moscow State University and the Interregional Centre for Advanced Studies in co-operation with the Institute of Theoretical Microphysics of the Moscow State University and supported by the Joint Institute for Nuclear Research (Dubna), the Instituto Superior Tecnico-CENTRA (Lisbon), the Institute of Theoretical and Experimental Physics (Moscow), the Institute for High Energy Physics (Protvino) and the Institute for Nuclear Research (Moscow). The Ministry of Science and Technology of Russia and the Russian Foundation for Basic Research also sponsored the conference.

It was eighteen years ago when the first of the series of conferences (from 1993 called the "Lomonosov Conferences"), was held at the Department of Theoretical Physics of the Moscow State University (June 1983, Moscow). The second conference was held in Kishinev, Republic of Moldavia, USSR (May 1985).

After the four years break this series was resumed on a new conceptual basis for the conference programme focus. During the preparation of the third conference (that was held in Maykop, Russia, 1989) a desire to broaden the programme to include more general issues in particle physics became apparent. At subsequent meetings of this series (Minsk, Republic of Byelorussia, USSR, 1990; Yaroslavl, Russia, 1992) a wide variety of interesting things both in theory and experiment of particle physics, field theory, gravitation and astrophysics were included into the programmes. During the conference of 1992 in Yaroslavl it was proposed by myself and approved by numerous participants that these irregularly held meetings should be transformed into regular events under the title "Lomonosov Conferences on Elementary Particle Physics". It was also decided to enlarge the number of institutions that would take part in preparation of future conferences.

Mikhail Lomonosov (1711-1765), a brilliant Russian encyclopaedias of the era of the Russian Empress Catherine the 2nd, was world renowned for his distinguished contributions in the fields of science and art. He also helped establish the high school educational system in Russia. The Moscow State University was founded in 1755 based on his plan and initiative, and the University now bears the name of Lomonosov.

The 6th Lomonosov Conference on Elementary Particle Physics "Cosmomicrophysics and Gauge Fields" was held at the Moscow State University (1993). The publication of the volume containing articles written on the basis of presentations at the 5th and 6th Lomonosov Conferences was supported by the Accademia Nazionale dei Lincei (Italy).

The 7th and 8th Lomonosov Conference (1995 and 1997) were also held in Moscow and the proceedings of these meetings entitled "Problems of Fundamental Physics" and "Elementary Particle Physics" were published by the Interregional Centre for Advanced Studies.

The physics programme of the 9th Lomonosov Conference included 27 review talks and 45 session reports on various topics in particle physics, as fundamental symmetries, electroweak theory, tests of standard model and beyond, heavy quark physics, non-perturbative QCD, neutrino physics, astroparticle physics, quantum gravity effects.

On behalf of the Organizing Committee I should like to warmly thank the session chairpersons, the speakers and all of the participants of the 9th Lomonosov Conference.

We are grateful to the Dean of the Faculty of Physics of the Moscow State University, Vladimir Trukhin, the Directors of the Joint Institute for Nuclear Research, Vladimir Kadyshevsky, the Director of the Institute of Theoretical and Experimental Physics, Mikhail Danilov, and the Dean of the Faculty of Physics of the Instituto Superior Tecnico-CENTRA, Jorge Dias de Deus, for the support in organizing the conference.

I should like to thank Lev Okun and Andrey Kataev for their help in planning of the scientific programme of the meeting. Special thanks are due to Ana Mourao, Andrei Kounine and Boleslaw Pietrzyk for their valuable help in inviting speakers for the topical sessions of the conference.

Furthermore, I am very pleased to mention Andrey Egorov, the Scientific Secretary of the conference, and Alexey Illarionov for their very efficient work in preparing and running the meeting.

These Proceedings were prepared for publication and sponsored by the Interregional Centre for Advanced Studies with support by the Ministry of Science and Technology of Russia and the Russian Foundation for Basic Research.

Alexander Studenikin

CONTENTS

Sponsors and Committees v

Foreword vii

On the Fundamental Symmetries in Particle Physics 1
E. Shabalin

Chiral Symmetry in Lattice QCD 13
A. Slavnov

NA48 Rare Decay Results 21
B. Vallage

Two Photon Physics at LEP 33
G. Passaleva

Adler Function from $R^{e+e-}(s)$ Measurements: Experiments vs QCD Theory 43
A. Kataev

Perturbation Theory with Convergent Series for Large Values of Coupling Constant: A Calculation of β-Function in φ^4 Model 53
V. Belokurov, E. Shavgulidze, Yu. Solov'yov and I. Yudin

Two-Dimensional QCD and Instanton Contribution 58
A. Bassetto, F. Vian and L. Griguolo

Color Reconnection and Bose–Einstein Correlations at LEP2 65
Th. Ziegler

Analytic Approach to QCD and the Interquark Potential 72
A. Nesterenko

A NLO QCD Analysis of the Spin Structure Function g_1 and Higher Twist Corrections 78
E. Leader, A. Sidorov and D. Stamenov

Leptonic Decays of Ds 85
J. Putz

Heavy Quark Asymmetries 89
A. Tricomi

Experimental Signature of a Fermiophobic Higgs Boson 96
L. Brüecher and R. Santos

S-Channel Higgs Physics beyond the Standard Model 106
G. Boyarkina

Quantum Field of Nonstationary Polaron 112
O. Khrustalev, M. Tchitchikina and E. Spirina

Dirac's Equation, SU(2) Model and Octanions 119
S. Kopylov

Irreducible Darboux Transformations 123
V. Bagrov and B. Samsonov

The AMS Experiment: First Results and Physics Prospects 128
J. P. Vialle

Possible Observational Evidences of Non-Compact
(Non-Baryonic) Microlenses ("Neutralino Stars") 141
A. Zakharov

Neutrino Conversions in Active Galactic Nuclei 147
A. Husain

Lepton Production by Neutrinos in an External Electromagnetic Field 153
A. Borisov and N. Zamorin

Propagation of Axions in a Strongly Magnetized Medium 159
A. Borisov and P. Sizin

Mixing and CP Violation with Quasidegenerate Majorana Neutrinos 165
G. Branko, M. Rebelo and J. Silva-Marcos

Solar Neutrino Oscillations in Extensions of the Standard Model 172
O. Boyarkin
Covariant Treatment of Neutrino Spin (Flavour) Conversion in Matter under the Influence of Electromagnetic Fields 178
M. Dvornikov, A. Egorov, A. Lobanov and A. Studenikin

Pulsar Velocity Puzzle and Nonstandard Neutrino Oscillations 182
R. Horvat

Kinematic Projecting of Pulsar Profiles 187
V. Bordovitsyn, V. Epp and V. Bulenok

Neutral Particle Radiation in Electromagnetic Field 193
A. Lobanov and O. Pavlova

Radiation of Relativistic Particles in a Quasi-Homogeneous Magnetic Field 198
V. Epp and T. Mitrofanova

Spin-Orbital Motion and Thomas Precession in the Classical and Quantum Theories 203
V. Bordovitsyn and A. Myagkii

Late Gravitational Collapse, Quantum Miniholes and the Birth of a New Universe 209
M. Fil'chenkov

On Adelic Strings 214
B. Dragovich

Collider Searches for TeV Scale Quantum Gravity with Compact Extra Dimensions 219
P. Azzurri

Dynamics of Event Horizon Creation 232
A. Shatsky

Conference Programme 235

On the Fundamental Symmetries in Particle Physics

E.Shabalin
ITEP, Moscow, Russia

Abstract. At present, the limit on possible CPT-odd contribution into CP violating part of the decay amplitude of the neutral Kaons does not look as the restrictive one: $A(CP-odd, CPT-odd)/A(CP-odd, CPT-even) \sim 0.3$ and the further more accurate measurements are highly desirable. As for CP violation itself, a picture of the possible effects originated by various sources of CP breakdown is presented both for the flavour-changing and flavour-conserving processes.

1 What is known on CPT invariance

The standard field theory of the microscopic processes is invariant under the product of charge conjugation (C), space reflection (P) and time reversal (T) [1], [2]. Consequently, a test of CPT invariance is really a test of correctness of the modern particle theory. Is it possible to imagine something that could break CPT or imitate such a breaking? The answer is YES. It could take place in the theories without locality, or Lorentz-invariance [3], or in the open quantum-mechanics [4], or in a theory incorporating new force acting differently between the matter and antimatter.

One of the consequences of CPT invariance is the equality of masses and lifetimes of a particle and its antiparticle [2] and this prediction is the object of a study in many experiments. The most decisive results collected by PDG-94 [5] are the following:

$$(m_{e^+} - m_{e^-})/m_e < 4 \cdot 10^{-8} \ , \tag{1}$$

$$\tau_{\mu^+}/\tau_{\mu^-} = 1.00002 \pm 0.00008 \ , \tag{2}$$

$$(m_P - m_{\bar{P}})/m_P = (2 \pm 4)10^{-8} \ , \tag{3}$$

$$\mid m_{K^0} - m_{K^0} \mid /m_{K^0} < 9 \cdot 10^{-19} \tag{4}$$

The last result is announced in ref. [5] as "the best test of CPT invariance". But it is not obtained by the direct measurement of $m_{K^0} - m_{\bar{K}^0}$. This result follows from some theoretical ideas on description of the weak decays of $\{K^0, \bar{K}^0\}$ system by neglecting, moreover, a possible direct CPT violation in the decay amplitudes. More accurate estimate of $m_{K^0} - m_{\bar{K}^0}$ is one order less restrictive and it corresponds to conclusion that CPT invariance is tested in $\{K^0, \bar{K}^0\}$ system with the accuracy 0.08%!

To clarify the situation let's consider the case when CP violating interaction incorporates the part conserving T invariance. Then, the wave functions of $K_{S,L}$ acquire the form [6], [7], [8]

$$K_S = [K_1 + (\varepsilon + \Delta)K_2]/\sqrt{1 + \mid \varepsilon + \Delta \mid^2} \ ,$$
$$K_L = [K_2 + (\varepsilon - \Delta)K_1]/\sqrt{1 + \mid \varepsilon - \Delta \mid^2} \ , \tag{5}$$

where

$$K_1 = (K^0 + \bar{K}^0)/\sqrt{2} \ , \ \ K_2 = (K^0 - \bar{K}^0)/\sqrt{2}$$

are the CP eigenstates, with opposite CP properties and the parameters ε and Δ describe CPT conserving and CPT violating parts of the $K_{S,L}$ wave functions.

Besides, if CP and CPT is violated in the direct transitions $K^0, \bar{K}^0$ into final states, the additional parameters appear:

$$a = A(K_2^0 \to 2\pi;\ I=0)/A(K_1^0 \to 2\pi;\ I=0)\ ,\ \ CPT=-1 \tag{6}$$

$$\frac{1-y_l}{1+y_l} = \frac{A(K^0 \to l^+\nu\pi^-)}{A^*(\bar{K}^0 \to l^-\tilde{\nu}\pi^+)}\ ,y_l \neq 0 \text{ corresponds to } CPT=-1\ , \tag{7}$$

$$\varepsilon' = \frac{1}{\sqrt{2}}A(K_2^0 \to 2\pi\ ;\ \ I=2)/A(K_1^0 \to 2\pi\ ;\ \ I=0)\ ,\ \ CPT=1 \tag{8}$$

As a result, the known CP-odd effects in the decay of $\{K^0\ ,\ \bar{K}^0\}$ system are described by the following formulae:

$$\eta_{+-} \equiv \frac{A(K_L \to \pi^+\pi^-)}{A(K_S \to \pi^+\pi^-)} \cong \varepsilon - \Delta + \varepsilon' + a\ ; \tag{9}$$

$$\eta_{00} \equiv \frac{A(K_L \to \pi^0\pi^0)}{A(K_S \to \pi^0\pi^0)} \cong \varepsilon - \Delta - 2\varepsilon' + a\ ; \tag{10}$$

$$\delta_L = \frac{\Gamma(K_L \to l^+\nu\pi) - \Gamma(K_L \to l^-\nu\pi)}{\Gamma(K_L \to l^+\nu\pi) + \Gamma(K_L \to l^-\nu\pi)} \cong 2Re(\varepsilon-\Delta) - 2Rey_l - Re(x_l - \bar{x}_l)\ . \tag{11}$$

In the last formula, the parameters x_l and $\bar{x}_l$ correspond to possible violation of the $\Delta Q = \Delta S$ rule and in the world without CPT invariance x_l and $\bar{x}_l$ could be different in general. With the known quark content of the theory this rule is violated in the second order in G_F, so that $x_l(\bar{x}_l)$ is of order $G_F m_K^2 \leq 2\cdot 10^{-6}$.

It is clear from eqs.(9)-(11), that the data on the decays of K_L mesons do not allow to conclude whether the CP violation entails CPT violation or not. One needs the data on K_S decays too, because the last ones are expressed in terms of the $(\varepsilon+\Delta)$ contribution. In particular,

$$\delta_S = \frac{\Gamma(K_S \to l^+\nu\pi) - \Gamma(K_S \to l^-\nu\pi)}{\Gamma(K_S \to l^+\nu\pi) + \Gamma(K_S \to l^-\nu\pi)} \cong 2Re(\varepsilon+\Delta) - 2Rey_l + Re(x_l - \bar{x}_l)\ . \tag{12}$$

From (11) and(12), one obtains

$$Re\Delta \cong \frac{1}{4}(\delta_S - \delta_L) \tag{13}$$

The first estimate of $Re\Delta$ and $Im\Delta$ was obtained in [9] from the reanalysis of the old data on K_{e3}^0 and $\bar{K}_{e3}^0$ decays with the result

$$Re\Delta = 0.018 \pm 0.020; \quad Im\Delta = 0.021 \pm 0.037 \tag{14}$$

The recent more accurate measurement of the same rates by CPLEAR Collaboration [10] gave

$$Re\Delta = (2.4 \pm 2.8)\cdot 10^{-4}; \quad Im\Delta = (-1.5 \pm 2.3)\cdot 10^{-2} \tag{15}$$

A limit on $Re\Delta$ was lowered by two orders , but a precision in measurement of $Im\Delta$ remained practically the same as in [9]. The limit on $Im\Delta$ can be considerably lowered using the Bell-Steinberger unitarity relation [11] with the result

$$Im\Delta = (2.4 \pm 5.0)\cdot 10^{-5}\ . \tag{16}$$

For other CPT violating parameters CPLEAR Collaboration has found

$$Rey_l = (0.3 \pm 3.1) \cdot 10^{-3}; Imx_l = (-2.0 \pm 2.7) \cdot 10^{-3}; Re\bar{x}_l = (-0.5 \pm 3.0) \cdot 10^{-3}. \quad (17)$$

Let's dwell on the determination of $m_{K^0} - m_{\bar{K}^0}$. The general expression for this mass difference is [7], [8]

$$m_{K^0} - m_{\bar{K}^0} = 2(m_L - m_S)(Re\Delta - Im\Delta \cdot tan^{-1}\Phi_{SW}) \quad (18)$$

Consequently, using the results (15) and (16) one concludes:

$$\mid m_{K^0} - m_{\bar{K}^0} \mid / m_{K^0} \leq 1.2 \cdot 10^{-17}. \quad (19)$$

This result is by one order less restrictive than given by PDG-94 (see eq. (4)). But the latter was obtained by neglecting the last two terms in the curved brackets of the theoretical formula

$$(m_{K^0} - m_{\bar{K}^0})/m_{K^0} = \frac{2(m_L - m_S)}{m_{K^0}}\{\mid \eta \mid (\frac{2}{3}\Phi_{+-} + \frac{1}{3}\Phi_{00} - \Phi_{SW}) \times$$
$$\times \sin^{-1}\Phi_{SW} + a + Im(\frac{1}{\Gamma_S}\sum_f \alpha_f)\cot\Phi_{SW}\} \quad (20)$$

and by using the data on η_{+-} and η_{00} which yield

$$\mid \eta \mid (\frac{2}{3}\Phi_{+-} + \frac{1}{3}\Phi_{00} - \Phi_{SW})\sin^{-1}\Phi_{SW} \cong (-0.19 \pm 1.6) \cdot 10^{-5}. \quad (21)$$

But the experimental upper limit on the last term in eq. (19) is

$$Im(\frac{1}{\Gamma_S}\sum_f \alpha_f) \leq 1.4 \cdot 10^{-4} \quad (22)$$

and the only estimate of a previously available from the literature was [8]

$$a = (-0.75 \pm 6) \cdot 10^{-3} \quad (23)$$

It is obvious that, in such a situation, the use of only the first term in the curved brackets of eq.(20) for determination of $m_{K^0} - m_{K^0}$ is not justified.

But from comparison of the eqs. (17) and (19) one can obtain a new estimate of the parameter a, considerably better than the estimate (23). Namely,

$$\mid a \mid \leq 8 \cdot 10^{-4} \quad (24)$$

From eqs.(15) and (22) one can conclude that the upper bound on strength of CPT violation is only by 3 times lower than the known strength of CP violation in the Kaon decays characterized by the parameter $\mid \eta \mid \cong 2.3 \cdot 10^{-3}$.

The further investigation of the possible CPT violation in the decays of neutral and charged kaons [12] is extremely desirable.

Besides, as very promising look the experiments with antihydrogen where a measurement of the frequency $(1s - 2s) - \gamma$ transitions can give an information on $[m(H) - m(\bar{H})]/m(H)$ at the level $10^{-15} - 10^{-18}$ [J.Eades].

If there is the interaction with $\Delta B = 2$, one more precise test of CPT would be possible. If $m_n \neq m_{\bar{n}}$, but $\Delta m_{n\bar{n}} \leq 1/t$ where t is the free-flight time of the neutron beam, then the observation of $n \to \bar{n}$ transition would give an upper limit $\Delta m_{n\bar{n}} \leq 10^{-22} - 10^{-23}$ [13].

2 What about CP violation itself?

2.1 The Standard Model prediction for $\{K^0,\ \bar{K}^0\}$ system.

The main efforts were dedicated to clarification of the mechanism of CP breakdown, in particular, to check-up whether the Kobayashi-Maskawa (K-M) mechanism is the only source of CP violation. This mechanism is a natural ingredient of the Standard Model (SM) where the coupling constants of $W^{\pm}$ bosons to the changing-flavour currents can be the complex numbers. Such a source can violate CP directly in the decay amplitude in G_F^1 order and indirectly - in G_F^2 order in the transitions changing a flavour by two units, such as $K^0 \to \bar{K}^0$, $B^0 \to \bar{B}^0$ and so on. The last ones cause a transition between CP-odd and CP-even combinations of K^0 and $\bar{K}^0$ or B^0 and $\bar{B}^0$.

Beyond the SM such a transitions could take place due to the so-called superweak interaction [14] of the type

$$L_{SW} = ig_{SW}^{(K)} K^2 + ig_{SW}^{(B)} B^2 + ... + H.c. \tag{25}$$

In the last case, the parameter ε' in the expressions (9) and (10) would have a zero value. The recent experimental data of KTeV [15] and NA48 [16] Collaborations show that $\varepsilon' \neq 0$:

$$(\varepsilon'/\varepsilon)_{KTeV} = (2.80 \pm 0.41) \cdot 10^{-3}; \quad (\varepsilon'/\varepsilon)_{NA48} = (1.85 \pm 0.75) \cdot 10^{-3}, \tag{26}$$

confirming the old non-zero result of NA31 Collaboration [17]: $(2.30 \pm 0.65) \cdot 10^{-3}$ for the above mentioned ratio.

Therefore, the superweak interaction is excluded as the only source of CP violation. But together with other sources of CP breakdown generating ε' it remains as a candidate contributing into ε.

An existance of other than CKM complex constants sources of CP violation can resolve the problem of inconsistency the above experimental results on ε'/ε with the theoretical ones expected in the framework of SM [18–21]:

$$(\varepsilon'/\varepsilon)_{SM} = 10^{-4} \cdot \left\{ \begin{array}{r} (6.7 \pm 0.7) \\ (3.1 \pm 2.5) \\ (4 \pm 5) \\ (17 + 14(-10)) \end{array} \right. .$$

The slight theoretical magnitudes for the direct CP violation in $K \to 2\pi$ decays are partially a consequence of the considerable cancellation between contributions of the so-called gluonic and electroweak penguin diagrams. It diminishes ε' by one order.Such a cancellation takes no place for the decay $K^{\pm} \to \pi^{\pm}\pi^{\pm}\pi^{\mp}$ and it would be interesting to search for CP effects in this decay. The observable effects are

$$\Delta\Gamma = \frac{\Gamma(K^+ \to \pi^+\pi^+\pi^-) - \Gamma(K^- \to \pi^-\pi^-\pi^+)}{\Gamma(K^+ \to \pi^+\pi^+\pi^-) + \Gamma(K^- \to \pi^-\pi^-\pi^+)} \tag{27}$$

and

$$\Delta g = \frac{g^{(+)} - g^{(-)}}{g^{(+)} + g^{(-)}} \tag{28}$$

where $g^{(\pm)}$ are determined by the relation

$$| K^{\pm}(k) \to \pi^{\pm}(p_1)\pi^{\pm}(p_2)\pi^{\mp}(p_3) |^2 \sim 1 + g^{\pm}(s_3 - s_0)/m_\pi^2 + ... \tag{29}$$

and $s_0 = m_K^2/3 + m_\pi^2$, $s_3 = (k - p_3)^2$. The expected magnitudes of $\Delta\Gamma$ and Δg calculated in the framework of SM with respect to next-to-leading order corrections in momentum expansion of the amplitudes are [22, 23]

$$| \Delta\Gamma | = 2 \cdot 10^{-6} \mid sin\delta \mid; \tag{30}$$

$$| \Delta g | = (2.3 \pm 0.9) \cdot 10^{-5} \mid sin\delta \mid . \tag{31}$$

2.2 The SM predictions for $\{B^0, \bar{B}^0\}$ system.

A smallness of CP violation in $\{K^0, \bar{K}^0\}$ system has an accidental character.

It is connected with a smallness of the parameters $s_i = \sin\theta_i$ in KM matrix, with the dependence

$$| \varepsilon_K | \sim | s_2 s_3 \sin\delta | \simeq 10^{-3}$$

and with the circumstance that the direct CP violation does not play a considerable role in $K_L \to 2\pi$ transitions.

For $\{B^0, \bar{B}^0\}$ system ε_B^{Phys} also is small, of order $10^{-4} - 10^{-3}$. But CP-odd parts of the subprocesses

$$b \to c\bar{c}s \tag{32}$$

$$b \to u\bar{u}d \tag{33}$$

are large and they are governed by the "tree" diagrams. For this reason CP violation can cause the time-dependent asymmetries in some processes at the level $few \cdot 10\%$. In particular, in the processes

$$B^0, \bar{B}^0 \to J/\Psi K_S \tag{34}$$

$$B^0, \bar{B}^0 \to \pi^+\pi^- \tag{35}$$

the CP-violating asymmetry

$$A_B = \frac{\Gamma(B^0 \to f) - \Gamma(\bar{B}^0 \to f)}{\Gamma(B^0 \to f) + \Gamma(\bar{B}^0 \to f)} \tag{36}$$

is expected to be (see [24] and refs. therein).

$$A_B(J/\Psi K_S) \sim \sin 2\beta = \frac{2\eta[\eta^2 + \rho(\rho - 1)]}{[\eta^2 + (1-\rho)^2](\eta^2 + \rho^2)} \tag{37}$$

$$A_B(\pi^+\pi^-) \sim \sin 2\alpha = \frac{2\eta(1-\rho)}{\eta^2 + (1-\rho)^2} \tag{38}$$

where η and ρ are the parameters of the quark mixing matrix taken in the form [25] ($\lambda = \sin\theta_C$)

$$V = \begin{pmatrix} 1 - \frac{\lambda^2}{2} & \lambda & A\lambda^3(\rho - i\eta) \\ -\lambda[1 + A^2\lambda^4(\rho + i\eta)] & 1 - \frac{\lambda^2}{2} & A\lambda^2 \\ A\lambda^3[1 - (1 - \frac{\lambda^2}{2})(\rho + i\eta)] & -A\lambda^2[1 + \lambda^2(\rho + i\eta)] & 1 \end{pmatrix} . \tag{39}$$

The mean value of $\sin 2\beta$ is estimated to be ~ 0.7. Then, the integrated asymmetry [26]

$$A_B(J/\Psi K_S) \cong -0.47 \sin 2\beta \sim 30\% \tag{40}$$

The recent measurement of this asymmetry [27] gave

$$sin2\beta = 0.79 \pm 0.43 \tag{41}$$

Though the mean value of $sin2\beta$ very close to the expected one from the experimental constraints on CKM matrix elements, the error bars in (42) are too large for the confident conclusion. Let me remind that the previous measurements had given the non-physical mean values $sin2\beta > 1$.

The asymmetry in decay of B_S^0, $\bar{B}_S$ mesons is expected at the following level [28]

$$A_{B_s}(\psi\Phi,\ D_s\bar{D}_s) \sim 0(\text{few}\%) \tag{42}$$

For the charged B mesons, the asymmetries are estimated to be $\sim$ few% or smaller [29].

The asymmetry in the semileptonic decays are estimated to be [30]

$$A_{B_d}(l^{\pm}\nu X) \leq (1-3)10^{-3},\ \ A_{B_s}(l^{\pm}\nu X) \leq 0(10^{-4}) \tag{43}$$

2.3 CP violation in Hyperon decays.

The corresponding CP-odd asymmetries can be studied at the proton-antiproton machines:

$$p\bar{p} \to \bar{\Lambda}\Lambda,\ \ \bar{\Sigma}\Sigma,\ \ \bar{\Xi}\Xi,\ \ ... \tag{44}$$

with the further search for decay

$$Y \to B + \pi \tag{45}$$

The amplitude

$$A(Y \to B\pi) = S + P\vec{\sigma}\vec{q} \tag{46}$$

where $\vec{q} \equiv \vec{q}_\pi$ in the rest frame of Y.

$$S = \sum_i S_i e^{i(\Phi_i^S + \delta_i^S)}\ , P = \sum_i P_i e^{i(\Phi_i^P + \delta_i^P)} \tag{47}$$

where δ_i are the strong scattering phases (the same for Y and $\bar{Y}$) and Φ_i are the weak CP violating phases ($\Phi_i(Y) = -\bar{\Phi}_i(\bar{Y})$). In the rest frame of Y, one of the possible CP-odd asymmetry is

$$A = \frac{\alpha + \bar{\alpha}}{\alpha - \bar{\alpha}} \tag{48}$$

where $\bar{\alpha}$ - the corresponding quantity for $\bar{Y}$ and

$$\alpha = 2Re(S^* P)/(\mid S \mid^2 + \mid P \mid^2).$$

The expected values are [31]

$$\begin{array}{ccccc} & \text{SM} & & \text{Weinberg} - \text{Higgs} & & \text{Superweak} & \\ A_\Lambda = & -(0.5-1.5)10^{-5} & ; & -2.5 \cdot 10^{-5} & ; & 0 & ; \end{array} \tag{49}$$

At present, an accuracy in measurement of A_Λ is 0.02 [32].

2.4 CP violation in the flavour-conserving processes.

SM with $\Theta = 0$.

If the K-M phase is the only source of CP violation, the CP-odd effects in the flavour-conserving processes have to be very tiny. They occure in the second order of weak interaction and in addition depend on dynamics of strong interaction. As a result, SM without Θ-term in QCD lagrangian gives Electric Dipole Moment of the neutron $d_n \sim 10^{-32}$ e cm [33–35]

$$Br(\eta \to 2\pi) \leq 2 \cdot 10^{-27}; \;\; Br(\eta' \to 2\pi) \leq 4 \cdot 10^{-29}$$

These results are discouraging for those who believe that KM phase is the only source of CP breakdown and would like to search for these effects experimentally. But for those who look for the other sources of CP violation these results are encouraging because they open a golden possibility to search for d_n and $\eta \to 2\pi$ decay in very broad region of the magnitudes smaller than existing experimental bounds.

SM with $\Theta \neq 0$.

In particular, if the QCD lagrangian contains the so-called Θ-term [36]

$$L^{\Theta}_{QCD} = -\Theta \frac{g^2}{32\pi^2} G^a_{\mu\nu} \tilde{G}^a_{\mu\nu} \;, \;\; CP = -1 \tag{50}$$

which appears because of the complicated topological structure of the QCD vacuum, d_n and $Br(\eta \to 2\pi)$ are expected at the levels (see [37] and refs. therein and also [38,39])

$$d_n^{th} \sim (2-3) \cdot 10^{-16} \Theta \text{ ecm} \tag{51}$$

$$Br(\eta \to 2\pi)^{th} \simeq 350 \cdot \Theta^2 \tag{52}$$

Comparing the prediction (53) with the experimental limit on $d_n^{exp} \leq 1.2 \cdot 10^{-25}$ e cm one obtains

$$\Theta \leq 5 \cdot 10^{-10} \tag{53}$$

Then

$$Br(\eta \to 2\pi) \leq 10^{-16} \tag{54}$$

2.5 CP violation in a theory with both explicit and spontaneous CP breakdown.

The SM with an extended sector of Higgs bosons containing no less than three Higgs doublets has one more source of CP-violation – spontaneous and explicit CP breakdown allowing a mixing between various charged and neutral Higgs fields [40], [41]. The diagrams in fig.1 show the contributions of this new mechanism of CP violation to the parameters ε and ε'. The magnitudes of these contributions depend on the quantity

$$ImA = Im \frac{< 0 \mid \Phi_1^+ \Phi_2^{+*} \mid 0 >}{\lambda_1^* \lambda_2} \tag{55}$$

where $\lambda_1 =< 0 \mid \Phi_1^0 \mid 0 >$, $\lambda_2 =< 0 \mid \Phi_2^0 \mid 0 >$. Being extracted from comparison of calculated ε^{th} with ε^{exper} and inserted into the formula for ε'^{th}, this ImA gives too large value of $\mid \varepsilon'/\varepsilon \mid^{th}$ compared with $\mid \varepsilon'/\varepsilon \mid^{exp}$ [42], [43], [44]. In addidion,it was shown that ImA extracted from ε leads to the value of d_n by

one order larger than d_n^{exp} [45]. Therefore, the Weinberg mechanism of spontaneous breakdown of CP invariance as the only source of CP violation is excluded. It can not give the main contribution into parameter ε, but it can make a considerable contribution to ε'. [46].

The constraints on ImA can be extracted - somewhat surprisingly - from CP conserving decay $b \to s\gamma$ [47].The problem was studied in ref. [48], but neglecting the contribution of intermediate t quark. Taking into account this contribution, the upper limit on allowed magnitude of ε'/ε turns out to be

$$\varepsilon'/\varepsilon \leq 10^{-3} \cdot \begin{cases} 2.18 \cdot [1-2.5], & m_H = 100GeV \\ 1.30 \cdot [1-3.5], & m_H = 175GeV \\ 0.905 \cdot [1-4.7], & m_H = 300GeV \end{cases}$$

m_t is taken 175 GeV. The uncertainties in the above relation are connected with the uncertainty in value of the CKM parameter $s_2 = sin\theta_2$. Therefore,it is not excluded that the value of ε'/ε observed in the last experiments is originated by CP violation in Higgs-quarks interaction. Then the predictions for d_n and $Br(\eta \to 2\pi)$ become

$$\begin{aligned} d_n &\leq 0.1 d_n^{exp} \\ Br(\eta \to 2\pi) &\leq 2 \cdot 10^{-15} \end{aligned} \tag{56}$$

Let's note that the uppper limit on $Br(\eta \to 2\pi)$ is 20 times as great as the upper limit on this quantity due to the Θ-term of QCD.

The above predictions are related to CP violation in charged Higgs interactions and to the case when the flavour-changing neutral currents are absent. If the flavour-changing $\bar{q}qH_i^0$ interactions are allowed, CP violation can take place in a theory with two Higgs doublets [49] due to transition between scalar and pseudoscalar components of $H_{1,2}^0$. This mechanism could generate d_n and d_e with the magnitudes close to existing experimental limits for these quantities [50], [51], [52].

CP violation in $\bar{q}qH^{\pm}$ interaction can considerably change the prediction of SM for magnitude of CP-odd effects in $K^{\pm} \to \pi^{\pm}\pi^{\pm}\pi^{\mp}$ decays.The existing constraints do not exclude at least a doubling of the corresponding CP violating effects [53].

2.6 Effect of Supersymmetry particles and their interactions on CP violation.

In SUSY generalization of SM, a necessity for many new particles opens the doors for the emergence of new CP violating parameters. In particular, the gaugino Majorana masses, squark masses and scalar trilinear interaction coupling can be complex. These sources alter the predictions of SM because of two various effects.

First - through new diagrams involving in the intermediate state superpartners of the usual particles. CP violation will be proportional to δ_{KM}, but a strength will be different from SM prediction.

Second - due to new phases independent of δ_{KM}.

As an illustration of the situation, I'll show the results of alteration of the parameters ε_K, d_n, ε'_K in SO(10) minimal supersymmetric model obtained in ref. [54]. The gluino-mediated box diagram gives for $\Delta S = 2$ transition

$$| \varepsilon_K |^{\tilde{g}} \simeq 2 \cdot 10^{-2} \sin(\phi_d - \phi_s)(\frac{300\text{GeV}}{M_3})^2 \mid \frac{V_{ts}V_{td}}{4 \cdot 10^{-4}} \mid^2 \cdot \mid \frac{180\text{MeV}}{m_s + m_u} \mid^2 \tag{57}$$

where M_3 is a mass of the bottom squark and ϕ_d, ϕ_s are the new phases appearing in SO(10) model.

$$d_n \cong 4 \cdot 10^{-26}_{ecm} \times \frac{m_b(M_3)}{2.7\text{GeV}} \mid \frac{V_{td}}{0.01} \mid^2 \cdot (\frac{300\text{GeV}}{M_3})^2 \frac{A_b + \mu \tan\beta}{M_3} \cdot \cdot \sin(\phi_d - 2\beta) \tag{58}$$

where A_b and μ are the parameters of trilinear scalar interaction and β is a function of δ_{KM}.

$$\mid \frac{\varepsilon'_K}{\varepsilon_K} \mid^{\tilde{g}}_{SO(10)} = 3 \cdot 10^{-4} (\frac{300\text{GeV}}{M_3})^2 \frac{A_b + \mu \tan\beta}{M_3} \cdot \cdot \frac{\sin(\phi_d - \beta) + \sin(\phi_s - \beta)}{2} \tag{59}$$

In general, the common conclusion is that the SUSY contribution to $\varepsilon'_K/\varepsilon_K$ is rather small. But in some special case this ratio could be of order $3 \cdot 10^{-3}$ [55].

The parameters ε_B, ε'_B also are altered by New Physics and their values can be different from the expected in SM. In particular, the asymmetry in B^0_s, $\bar{B}^0_s$ decays can reach a magnitude [56]

$$A(B_s \to \psi\Phi) \sim \sin 2\zeta_{NewPhys} \tag{60}$$

with $2\zeta \sim 1$. An observation of such high asymmetry would be the evidence for New Physics, because the SM predicts

$$A(B_s \to \psi\Phi)_{SM} \sim 0 \ \ (\text{few}\%) \tag{61}$$

The electric dipole moments of the neutron and electron in SUSY could be close to their experimental limits [57], [58], [59], [60].

3 Conclusions and outlook

CPT: is tested in the decays of $\{K^0, \bar{K}^0\}$ system with accuracy of order 0.1%. The further investigations in this field are highly desirable.

CP: The situation with a search for the origin of CP violation is complicated. The possible sources are

1. Superweak CP violation in the transitions changing a flavour by two units: $\Delta S = 2$, $\Delta B = 2$, ...
2. The $K - M$ phase in SM.
3. θ-term in QCD lagrangian.
4. Spontaneous and explicite CP breakdown in extended Higgs sector.
5. New complex parameters appearing in SUSY.
6. New complex coupling constants in the theories with flavour-changing neutral currents or in the theories with broken left-right symmetry and so on.

Every single source can be identified because of rather definite predictions for a set of processes including flavour changing and flavour-conserving transitions.

But if a few sources act simultaneously, the situation can occur very uncertain and may require the huge efforts to clarify the origin of CP violation.

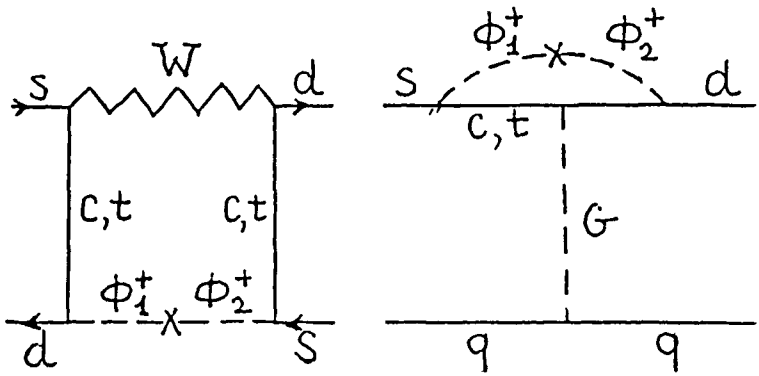

Fig.1

References

[1] Schwinger J., Phys.Rev. 1951, v.**82**, p. 914;
Luders G., Dansk.Mat.Fys.Medd. 1954, v.**28**, p.17.

[2] Grawert G.,Luders G.,Rollnik G.,Fortsch.Phys.,1959,v.**7**,p.291.

[3] Bais F.A. and Frere J.M., Phys.Lett. 1981, v.**98B**, p. 431.

[4] Ellis J., Mavromatos N.E. and Nanopoulos D.V., Preprint CERN-TH.6896/93; CERN-TH.6897/93.

[5] Particle Data Group, Phys.Rev. 1994, v.**D50**, p. 1173.

[6] Shubert K.R. et al., Phys.Lett. 1970, v.**31B**, p. 662.
Cronin J.W., Rev.Mod.Phys. 1981, v.**53**, p. 373.

[7] Barmin V.V. et al., Nucl.Phys. 1984, v.**B247**, p. 293.

[8] Tanner N.W. and Dalitz R.H., Ann.Phys. 1986, v.**171**, p.463.

[9] Demidov V.,Gusev K. and Shabalin E., Phys.Atomic Nucl. 1995, v.**58**, p.968.

[10] Angelopoulos A. et al.(CPLEAR Collaboration), Preprint CERN-EP/98-154, 1998.

[11] Bell J.S. and Steinberger J., Proc.Oxford Int.Conf. on Elementary Particles, 1965, p. 195.
[12] Demidov V.S. and Shabalin E.P., The DAPhNE Physics Handbook, Ed. by L.Maiani,J.Pancheri and N.Paver, LNF-INFN,1992, p.45.
[13] Abov Yu.G.,Djeparov F.S. and Okun L.B., Pisma ZhETF, 1984, v.**39**, p.493.
[14] Wolfenstein L., Phys.Rev.Lett. 1964, v.**13**, p. 569.
[15] Alavi-Harati A.et al.(KTeV Collaboration), Phys.Rev.Lett.,1999, v.**83**, p.22.
[16] Fanti V. et al. (NA48 Coll.), Preprint CERN-EP/99-114, 1999.
[17] Barr C.D. et al., Phys.Lett. 1993, v.**B317**,233.
[18] Buras A., Jamin M., Lautenbacher M., Nucl.Phys. 1993, **B408**, 209.
[19] Ciuchini M., Franko E., Martinelli G. and Reina L., in The Second DAΦNE Physics Handbook, ed. by L.Maiani, G.Pancheri and N.Paver. INFN-LNF, 1995, p. 27.
[20] Bertolini S. and Eeg J.O., Preprint SISSA 103/95/EP, 1995.
[21] Bertolini S. et al., Nucl.Phys.,1998 v.**B514**, 93.
[22] Shabalin E.P., Phys.Atomic Nucl. 1998, v.**61**, p.1372.
[23] Shabalin E., Nucl.Phys. 1993, v.**B409**, p.87.
[24] Nir. Y., in Proc.of XX SLAC Summer Institute on Particle Physics, 1992, SLAC-Report-412, p.81.
[25] Wolfenstein L., Phys.Rev.Lett., 1983, v.**51**, p.1945.
[26] Nelson H.M., in Proc. of XX SLAC Summer Institute on Particle Physics, 1992;SLAC-Report-412, p.47.
[27] Damet J., Report at XV Particles and Nuclei Interaction Conf. June 10-16, 1999, Uppsala, Sweden.
[28] Bigi I.I. and Sanda A.I., Nucl.Phys., 1981, v.**B193**, p. 85.
[29] Simma H.,Eilam G.,Wyler D.,Nucl.Phys.1991,v.**B352**,p.367.
[30] Bigi I.I. et al., CP-violation, Ed. C.Jarlskog (World Scientific, Singapore 1988)
[31] Donoghue J.F.,et al., Phys.Rev. 1986, v.**D34**, p. 833.
[32] Barnes P.D. et al., Nucl.Phys., 1991, v.**A526**, p. 575; see also E.Gonzalez, J.Illana, preprint CERN-PPE/94-33, 1994.
[33] Shabalin E.P., Usp.Fiz.Nauk. 1983, v.**139**, p. 561. [Sov.Phys.Usp. 1983, v.**26(4)**. p. 297.
[34] Khriplovich I., Phys.Lett. 1986, v.**B173**, p. 193.
[35] Jarlskog C. and Shabalin E., Phys.Rev., 1995, v.**D52**, p. 248.
[36] t'Hooft G., Phys.Rev.Lett. 1976, v.**37**, p. 8.
[37] Shabalin E., Yad.Fiz. 1994, v.**57**, p.1854 [Physics of Atomic Nuclei, 1994, v.**57**].
[38] Crewther R.J. et al., Phys.Lett. 1979, v.**88B**, p. 123.
[39] Shifman M.A., Vainshteion A.I. and Zakharov V.I., Nucl.Phys. 1980, v.**B166**, p. 494.
[40] Weinberg S., Phys.Rev.Lett., 1976, v.**37**, p. 657.
[41] Deshpande N.G. and Ma E., Phys.Rev. 1977, v.**16**,p.1538.
[42] Deshpande N.G., Phys.Rev. 1981, v.**D23**, p. 654.
[43] Sanda A.I., Phys.Rev. 1981, v.**D23**, p. 2647.
[44] Jarlskog C. and Shabalin E., Phys.Rev.1995, v.**D52**, 6327.
[45] Khriplovich I.,Zhitnitskii A.,Sov.J.Nucl.Phys.1981,v.**34**,p.95.

[46] Shabalin E.,Proc. of "Workshop on K Physics", Orsay, France, May 30-June 4 ,1996, p.71.
[47] Grossman Y. and Nir Y., Phys.Lett. 1993, v.**B313**, p.126.
[48] Shabalin E., Phys.Reports 1999, v.**320**, p.355.
[49] Lee T.,Phys.Rev.1973,v.**D8**,p.1226;Phys.Rep.1974,v.**9C**,145.
[50] Barr S. and Zee A., Phys.Rev.Lett. 1990, v.**65**, p.21 and (E)-ibid.1990, v.**65**, 2920.
[51] Das A. and Kao C., Phys. Lett. 1996, v.**B372**, p.106.
[52] Bramon A. and Shabalin E.,Phys.Lett. 1997, v.**B404**, p.115.
[53] Shabalin E.P.,Phys.Atomic Nucl., 1999, v.**62**, p.1552.
[54] Barbieri R., Hall L. and Strumia A., Preprint LBL-36907, 1995.
[55] Masiero A.,Murayama H.,Phys.Rev.Lett.1999,v.**83**,p.907
[56] Bigi I.I., in Proc. of Les Recontres de Physique de La Vallee d'Aoste, La Thuile, March 6-11, 1994, p. 137.
[57] Ellis J., Ferrara S. and Nanopoulos D.V., Phys.Lett. 1982, v.**B114**, p.231.
[58] Polchinski J. and M.B.Wise,Phys.Lett. 1983, v.**125B**, p. 393.
[59] del Aguila F.et al., Phys.Lett. 1983, v.**126B**, p. 71.
[60] Dugan M..Grinstein B.,Hall L.Nucl.Phys.1985,v.**B255**,p.413.

Chiral symmetry in lattice QCD

A.A.Slavnov
Steklov Mathematical Institute,
Gubkina st. 8, GSP-1, 117966 Moscow, Russia, and
Moscow State University

Abstract. The problem of chiral symmetry preservaton in lattice QCD is discussed. A new multifield lattice QCD model is discussed in details. The model is free of spectrum doubling and preserves all nonanomalous chiral symmetries up to exponentially small corrections.

1 Introduction

Chiral symmetry is the old problem for lattice gauge theories. A naive discretization of the Dirac gauge invariant action in Euclidean formulation may be written as follows

$$I = \sum_{x,\mu} -\frac{1}{2ia}[\bar{\psi}(x)\gamma_\mu U_\mu(x)\psi(x+a_\mu) - \bar{\psi}(x+a_\mu)U_\mu^+(x)\gamma_\mu\psi(x)] \tag{1}$$

Here the fermion fields are defined in the sites of a rectangular lattice with the spacing a, and the gauge fields $U_\mu(x)$ on the links connecting the sites x and $x+a$ in the direction μ. The gauge field U_μ belongs to the gauge group $\Omega(x)$ and under the gauge transformations changes as follows

$$U_\mu(x) \to \Omega(x)U_\mu(x)\Omega^{-1}(x+a_\mu) \tag{2}$$

It may be presented in the exponential parametrization as $U_\mu = \exp\{-aA_\mu(x)\}$ where A_μ belongs to the Lie algebra of the gauge group.

If the field ψ transforms under the gauge transformations as

$$\psi(x) \to \Omega(x)\psi(x) \tag{3}$$

the action (1) is obviously gauge invariant. This is valid for any gauge group. Moreover, if the action (1) is also invariant under the global chiral transformations

$$\bar{\psi}(x) \to \bar{\psi}(x)\exp\{i\gamma_5\alpha\}, \quad \psi(x) \to \exp\{i\gamma_5\alpha\}\psi(x) \tag{4}$$

leading to the conservation of a corresponding current.

Assuming that in the continuum limit $a \to 0$ eq. (1) gives the action of some physical model, one would get in this way a manifestly chiral invariant regularization of arbitrary gauge theory. This certainly cannot be true as some chiral symmetries are affected by quantum anomalies. The resolution of the paradox is obtained if one notices that the naive disretization (1) does not provide a correct spectrum.

The quadratic form generated by the action (1) in momentum representation looks as follows

$$I_0 = \int_{-a^{-1}\pi}^{a^{-1}\pi} d^4p\bar{\psi}(p)\sum_\mu[a^{-1}\gamma_\mu\sin(p_\mu a)]\psi(p) \tag{5}$$

The corresponding dispersion relation after transition to Minkovsky space acquires the form

$$\sinh^2(Ea) = \sum_{i=1}^{3} \sin^2(p_i a) \tag{6}$$

One sees that the states with a given energy are degenerate. For example $E = 0$ corresponds not only to $p_i = (0,0,0)$, but also to the states of the form $p = (\pi a^{-1}, 0, 0)$, $p = (\pi a^{-1}, \pi a^{-1}, 0)$, e.t.c. Altogether in the $4d$ space one has 16 degenerate mass states, all of them surviving in the continuum limit. Moreover, if one starts with the continuum Lagrangian describing the fermions of definite chirality, then the lattice action (1) describes 8 massless exitations of positive chirality and 8 exitations of negative chirality. So the model is actually not chiral but vectorlike.

Of course the naive discretization (1) is not the only possibility, and one may try some other discretizations to get rid off unwanted spectrum degeneracy and to describe a chiral theory. However there is no simple way to do that. H.Nielsen and R.Ninomiya 1 proved the "no-go" theorem which states that any chiral invariant lattice action satisfying some natural physical requirements like locality, hermiticity e.t.c. leads to a degenerate fermion spectrum. To kill the doubler states one has to sacrifice either chiral symmetry or some other physical requirement. Of course a real physics is described by the continuum model and breaking chiral symmetry on the lattice is not a disaster, if it is restored in the continuum limit. However this restoration is not automatic - to get a chiral invariant target theory one has to introduce noninvariant counterterms like nonzero bare fermion mass. From the point of view of nonperturbative calculations that means fine tuning of several parameters which complicates considerably computer simulations and leads to some other problems. Moreover, numerical computations are done for a nonzero lattice spacing. That leads to additional noninvariant order a corrections. In practical simulations the lattice spacing a is not too small and these corrections are not negligible. Therefore it is very important to have a formulation which preserves chiral symmetry on the lattice or at least provides vanishing of chirality breaking effects in the continuum limit and their minimization for a finite lattice spacing.

A possible way to bypass the "no-go" theorem is to consider the actions which include infinite series of fields. In our paper 2 it was shown that continuum anomaly free models like the Standard model do allow a manifestly chiral invariant regularization if one introduces a regularized action containing infinite number of fermion fields. Application of this idea to lattice theories lead to the models which have no spectrum doubling and posess exact chiral invariance in the continuum limit 3, 4. The method was also checked by nonperturbative simulations of some $2d$ models 5. R.Narayanan and H.Neuberger showed 6 that this approach is closely related to the five dimensional domain wall model proposed by D.Kaplan 7. Introduction of an infinite series of fermion fields may be considered as a discretization of the fifth dimension.

Although originally it might seem that considering an infinite series of fermions is too high price, by now it is widely accepted that it is the only way to preserve the exact chiral symmetry without tuning additional parameters. Many present approaches like overlapp formalism 8 or different versions of domain wall fermions 9, 10 use this idea.

The main question is whether these approaches allow efficient nonperturbative calculations. Considering realistic chiral gauge models on the lattice seems at present

to be too hard for computer simulations. On the top of the usual problem of simulating fermion determinants there is an additional difficulty, as a chiral determinant being complex does not allow straightforward Monte-Carlo simulations. So it seems reasonable to start with the study of vectorial models like QCD and to try to deal with the breaking of the global chiral symmetry.

The multifermion models like truncated overlapp 11 or domain wall fermions 10 have been applied to the study of QCD and first numerical simulations 12, 13 gave promising results. The chirality breaking effects, in particular fermion mass renormalization, were also discussed 14, 15.

In the present paper I propose a new multifield formulation of lattice fermion models. This formulation was used successfully for the analysis of $SU(2)$ global anomaly with the help of lattice regularization 16. Being applied to the lattice QCD this formalism provides a model which has no species doubling, does not require any fine tuning to calculate arbitrary gauge invariant amplitudes and does not contain any dimensional parameter except for a lattice spacing. For a finite lattice spacing all chirality breaking effects are suppressed exponentially. Although the model includes an infinite number of fermion species, the convergence of the corresponding series is very fast, and one can hope that it may be truncated by a small finite number of terms.

2 The effective action for the QCD quark determinant

Our goal is to construct an effective action for lattice QCD which reproduces in the continuum limit the chiral invariant QCD determinant without tuning any chiral noninvariant counterterms. For a finite lattice spacing the chirality breaking effects are suppressed exponentially.

A possible way to remove the degeneracy of the fermion spectrum was proposed by K.Wilson 17, who noticed that instead of the "naive" action (1) one can use the following action

$$I = \sum_{x,\mu} -\frac{1}{2}[\bar{\psi}(x)\gamma_\mu(D_\mu + D_\mu^* - \kappa a D_\mu^* D_\mu)\psi(x)] \tag{7}$$

$$D_\mu = \frac{1}{a}[U_\mu(x)\psi(x+a_\mu) - \psi(x)] \tag{8}$$

Here the first term represents the chiral invariant part of the action and the second term is so called Wilson term, breaking chiral invariance. In this equation κ is a dimensionless parameter, which we choose in the interval $0 < \kappa < 1$. In a formal limit $a \to 0$ the Wilson term vanishes and therefore this action is also a possible candidate for a lattice regularization of QCD. However the fermion propagator generated by the quadratic part of the action (7) describes the spectrum, different from the eq.(1):

$$S(p) = [\sum_\mu a^{-1}\gamma^\mu \sin(p_\mu a) + \kappa a^{-1}\sum_\mu (1 - \cos(p_\mu a))]^{-1} \tag{9}$$

This propagator has the pole only when all the components of p are equal to zero. When one of the components is close to the end of the Brillouin zone $p = \pi a^{-1}$ the

Wilson term is proportional to a^{-1}. Therefore all doubler states acquire the masses of the order of the lattice cut-off and decouple in the continuum limit.

The modified action (7) solves the problem of the fermion spectrum degeneracy, but breaks explicitely the chiral symmetry for a finite lattice spacing. This breaking is rather strong. It requires chiral noninvariant fermion mass renormalization and also leads to order a chirality breaking corrections. Much softer symmetry breaking may be achieved by using the multifield effective action of the following form

$$I = \sum_{x,\mu} \sum_{n=-\infty, n\neq 0}^{\infty} -\frac{1}{2}\bar{\psi}_n(x)[\gamma_\mu(D_\mu + D^*_\mu) - \\ -n\kappa D^*_\mu D_\mu)]\psi_n(x), \tag{10}$$

The first term in the eq.(10) represents the chiral invariant part of the action and the second term is the Wilson term multiplied by n. The dimensionless parameter κ is chosen in the interval $0 < \kappa < 1$.

Let us consider some fermion loop diagram with L vertices, which may be presented by the following integral:

$$\Pi_L = \int_{-\pi a^{-1}}^{\pi a^{-1}} d^4p \sum_{n=-\infty, n\neq 0}^{\infty} (-1)^n \\ \mathrm{Tr}\,[\,G(p)\Gamma_i(p, q_1)G(p+q_1)\ldots] \tag{11}$$

Here G are the Green function of the fields ψ_n, Γ_i are the interaction vertices and q_l is a total momentum entering the corresponding vertex. Taking the trace we can present Π_L as the following sum:

$$\Pi_L = \int_{-\pi a^{-1}}^{\pi a^{-1}} d^4p \sum_{n=-\infty, n\neq 0}^{\infty} \\ (-1)^n \frac{F_0(p,q) + n^2 F_1(p,q) + \ldots}{(s^2 + m^2 n^2)(s_1^2 + m_1^2 n^2)\ldots} \tag{12}$$

where

$$s^l_\mu = a^{-1}\sin[(p + q_1 + \ldots + q_l)_\mu a] \tag{13}$$

$$m_l = \kappa a^{-1} \sum_\mu (1 - \cos(p + q_1 + \ldots + q_l)_\mu). \tag{14}$$

Let us consider this equation for the case when all the momenta q_l are external. In this case we can assume that

$$|q_l| < \epsilon a^{-1}, \quad L\epsilon < 1. \tag{15}$$

The integration domain in the eq.(12) may be separated into two parts:

$$V_1 : |p| < \epsilon a^{-1}; \\ V_2 : |p| > \epsilon a^{-1}. \tag{16}$$

In the domain V_2 the integrand may be expanded in terms of $q_l a$. Therefore integration over this domain produces only local counterterms. To calculate the integral over V_1 we replace the sum in the eq.(12) by the following integral in the complex plane

$$\int_C \pi \frac{(F_0 + z^2 F_1 + \ldots) F(p,q)}{\sin(z\pi)(s_0^2 + m_0^2 z^2)\ldots} dz \tag{17}$$

Here the contour C encloses the real axis except for a vicinity of the point $z = 0$. By Cauchi theorem this integral is equal to the integral over the large circle plus the sum of the residues at the poles situated on the imaginary axis at the points

$$z = 0, \quad z^2 = -\frac{s_l^2}{m^2}. \tag{18}$$

The residue at $z = 0$ gives

$$\frac{F_0 F(p,q)}{s_0^2 \ldots s_{L-1}^2} \tag{19}$$

which is the manifestly chiral invariant expression for the integrand of a massless fermion diagram. The integral over large circle vanishes and the residues at the remaining poles are proportional to

$$[\sinh(\frac{s_l}{m_l})]^{-1} \sim \exp\{-[(p + q_1 + \ldots + q_l)a\kappa]^{-1}\}. \tag{20}$$

One sees that for external momenta much smaller than the cut-off these terms are exponentially suppressed.

So we proved that any one loop quark diagram is equal to a manifestly chiral invariant expression which coincides with the corresponding diagram in massless QCD with "naive' fermion action and cutted Brillouin zone $|q_l a| < \epsilon$ plus local counterterms. As our procedure is obviously gauge invariant, the amplitude obtained in this way is also gauge invariant.

Global chiral invariance of multiloop diagrams requires a special study. Individual fields ψ_n generate chiral noninvariant terms like fermion mass counterterm. However it was shown in our paper 19 that after summation over all these fields the noninvariant counterterms cancel. The idea of the proof may be illustrated by the two loop diagram. One can show that individual noninvariant counterterms have the following structure:

$$n f(n^2) \bar{\psi}_n K \psi_n \tag{21}$$

Here K is some local operator, which may depend on the gauge fields, but has no dependence on n. The function $f(z)$ is analytic in the complex z plane cutted along the imaginary axis from $\frac{2i}{\kappa\epsilon}$ to $-\frac{2i}{\kappa\epsilon}$. The integrand of the diagram with the counterterm insertion may be presented in the form similar to eq.(17):

$$\int_C \frac{(\tilde{F}_0 + z^2 \tilde{F}_1 + \ldots)}{(s_0^2 + m_0^2 z^2)\ldots(s_{L-1}^2 + m_{L-1}^2 z^2)} \times \frac{\pi z^2 f(z^2) K F(p,q)}{\sin(z\pi)} dz$$

The integration contour again encloses the real axis except for a vicinity of zero. Transforming the integration contour as before we shall have again exponentially small contribution from the poles at the imaginary axis and also the contribution

from thr intrgral enclosing the cut from $\frac{2i}{\kappa\epsilon}$ to $\frac{2i}{\kappa\epsilon}$. However due to the symmetry properties of the integrand this integral is equal to zero, and we arrive to the same conclusion as in the one loop case. Two loop diagrams posess global chiral invariance up to exponentially small corrections. This proof is easily generalized to diagrams with arbitrary number of loops.

Now we prove that the currents assosiated with nonanomalous global chiral symmetries are conserved up to exponentially small terms.

Let us consider the action (10) with the source term for a chiral current:

$$I_V = I + \sum_{x,\mu} V^b_\mu(x) J^b_\mu(x) \tag{22}$$

Here J_μ is the axial current which in the continuum case is equal to

$$J^b_\mu(x) = \sum_{n=-\infty, n\neq 0}^{\infty} \bar{\psi}_n(x)\gamma_5\gamma_\mu T^b \psi_n(x) \tag{23}$$

T^b being the generators of the chiral symmetry group. V_μ is the source term. In the continuum chiral invariant theory this current is covariantly conserved

$$\partial_\mu J^b_\mu + g t^{bcd} J^c_\mu V^d_\mu = 0 \tag{24}$$

For the lattice action (22) including the Wilson term the corresponding equation is modified. Firstly, the Neuther current has a contribution from the Wilson term, and secondly, as the Wilson term breaks the chiral symmetry, the r.h.s. is nonzero. The analogue of the eq.(24) for the action (22) may be written as follows

$$\partial_\mu J^b_\mu + g t^{bcd} J^c_\mu V^d_\mu = \sum_{n=-\infty,\ n\neq 0}^{\infty} n \sum_x \bar{\psi}_n(x) W(x) \psi_n(x) \tag{25}$$

where ∂ is a lattice derivative. The r.h.s. of eq.(25) is due to the Wilson term and in the quantum theory is responsible for the chiral anomaly. A particular form of W is not essential for our discussion. It is important that the r.h.s. of eq.(25) is bilinear in ψ and proportional to n.

Being integrated with the exponent of the action (22) the eq.(25) leads to the chiral Ward identity broken by the Wilson term

$$a^{-1}\sin(k_\mu a)\Gamma^{bc_1\ldots c_n}_{\mu\nu_1\ldots\nu_n}(k, q_1\ldots q_n) + \tag{26}$$

$$+ g t^{bcd} \int d^4p \Gamma^{cc_1\ldots c_n}_{\mu\nu_1\ldots\nu_n}(k-p, q_1\ldots q_n) V^d_\mu(p) = \sum_{n=-\infty,\ n\neq 0}^{\infty} n W_n$$

Here W_n stands for the sum of diagrams generated by the r.h.s. of the eq.(25).

We shall use the differential form of this identity, obtained by differentiating it over k_μ and putting $k = 0$:

$$\Gamma^{bc_1\ldots c_n}_{\mu\nu_1\ldots\nu_n}(0, q_1\ldots q_n) + \tag{27}$$

$$+gt^{bcd}\int d^4p\partial_\mu\Gamma^{cc_1\ldots c_n}_{\mu\nu_1\ldots\nu_n}(-p,q_1\ldots q_n)V^d_\mu(p)=\sum_{n=-\infty,\quad n\neq 0}^{\infty} n\frac{\partial W_n}{\partial k_\mu}|_{k=0}$$

Here is the important difference between anomalous and nonanomalous theories. Passing from the eq.(26) to the differential identity (27) we assumed that $\frac{\partial\Gamma}{\partial k_\mu}$ is not singular at $k=0$. It is not true for anomalous models: the anomalous triangle diagram is singular at $k=0$. Therefore the eq.(27) is equivalent to the identity (26) only if anomaly is absent.

Now we shall show that the r.h.s. of the eq.(27) is exponentially small. To prove the absence of anomaly it is sufficient to consider one loop diagrams. The diagrams representing the r.h.s. of eq.(27) are obtained from the QCD amplitudes which we considered in the previous section by insertions of the additional vertices $n\frac{\partial W}{\partial k_\mu}|_{k=0}=n\mu$, corresponding to zero external momentum. In other words they may be considered as momentum dependent counterterms which shift the Wilson term $nm\to n(m+\mu)$. The sum over n gives for such diagrams the result analogous to the eq.(??)

$$\Pi^L=\int_{-\epsilon a^{-1}}^{\epsilon a^{-1}} d^4p[\frac{A_l(p,q)}{s_l^2}- \tag{28}$$

$$-\sum_{l=0}^{L-1}\frac{\pi A_l(p,q)}{(m_l+\mu)\sqrt{s_l^2}\sinh(\pi\sqrt{s_l^2}(m_l+\mu)^{-1})}]+c.t.$$

where $c.t.$ stands for local counterterms. As was explained above the sum of the first terms and local counterterms is equal to the gauge invariant QCD amplitudes without insertions of μ and the remaining terms are proportional to $exp\{-\frac{\pi s_l}{\mu+m_l}\}$. The diagrams with k insertions of μ are given by the k-th term of the formal Taylor expansion of this exponent in terms of μ near the point $\mu=0$. All these terms are exponentially small. So we proved that to any nonanomalous global chiral symmetry corresponds a current which is covariantly conserved up to exponentially small corrections. At the same time the global $U(1)$ anomaly is present as it was explained before the differential Ward identity (27) does not hold in this case.

3 Discussion

It was shown in the previous section that the path integral of the exponent of the effective action (10) in the continuum limit reproduces exactly the quark determinant of massless QCD without any chiral noninvariant counterterms. For a finite lattice spacing chirality breaking corrections are exponentially small

$$\sim O(\exp\{-(\kappa\epsilon)^{-1}\}),\quad \epsilon\sim|q|a$$

Finite quark masses may be easily incorporated into our scheme. One should simply add to the effective action (10) a common mass term. It will lead to the following modification of the sum in the eq.(12):

$$\sum_{n=-\infty,n\neq 0}^{\infty}\frac{(-1)^n}{\Pi_l(s_l^2+(m_l n+m_0)^2} \tag{29}$$

This sum may be transformed as before to the integral in the complex plane using Watson-Zommerfeld transformation. The residue at $z = 0$ gives the amplitude for the quark of mass m_0:

$$\sim \Pi_l (s_l^2 + m_0^2)^{-1} \tag{30}$$

and the remaining terms produce exponentially small corrections. Of course in this case the chiral invariance is explicitely broken by the bare quark mass.

For practical simulations one has to truncate the sum over n by some finite number N. Such a truncation obviously introduces additional corrections. To compute the contribution of individual ψ_n field one has to deal with the usual Wilson QCD action and the well known tecnique may be used. However to get an exponentially small corrections one has to apply this technique N times. Obviously this procedure makes sence for practical simulations only if N is not too big. So the main question is the estimation of the rate of convergence of the series over n. This problem is at present under investigation.

Acknowledgements

This work is supported in part by Russian Basic Research Foundation under grant 99-01-000190 and INTAS-96-370.

References

[1] H.B.Nielsen, M.Ninomiya, Nucl.Phys. B105 (1981) 219.
[2] S.A.Frolov, A.A.Slavnov, Phys.Lett. B309 (1993) 344.
[3] S.A.Frolov, A.A.Slavnov, Nucl.Phys. B411 (1994) 647
[4] A.A.Slavnov, Phys.Lett. B348 (1993) 344.
[5] A.A.Slavnov, N.V.Zverev, Phys.Lett. B420 (1998) 323.
[6] R.Narayanan, H.Neuberger, Phys.Lett. B302 (1993) 62.
[7] D.B.Kaplan, Phys.Lett. B288 (1992) 342.
[8] R.Narayanan, H.Neuberger, Nucl.Phys. B412 (1994) 574.
[9] Y.Shamir, Nucl.Phys. B406 (1993) 90.
[10] V.Furman, Y.Shamir, Nucl.Phys. B439 (1995) 54.
[11] H.Neuberger, Phys.Rev. D57 (1998) 5417.
[12] T.Blum, A.Sony,Phys.Rev.Lett. 79 (1997).
[13] T.Blum, Talk delivered at LATTICE'98.
[14] S.Aoki, Y.Taniguchi, hep-lat/9711004.
[15] Y.Kikukawa, H.Neuberger, A.Yamada, hep-lat/9712022.
[16] A.A.Slavnov, Phys.Lett. B388 (1996) 147; Proceedings of the 6th International Conference on Path Integrals, p.80.World Sci. Singapour, 1999.
[17] K.G.Wilson, Phys.Rev.D10 (1974) 2445; New Phenomena in Subnuclear Physics (A.Zichichi ed.), Plenum Press, New York, 1977.
[18] A.A.Slavnov, Theor.Math.Phys. 57 (1983) 4.
[19] A.A.Slavnov, Nucl.Phys. B544 (1999) 759.

NA48 RARE DECAY RESULTS

Bertrand VALLAGE [a], on behalf of the *NA48* Collaboration
DAPNIA/SPP, CE de Saclay, 91191 Gif sur Yvette CEDEX, FRANCE

Abstract. New results from the *NA48* Collaboration at *CERN* on rare K_L Dalitz and double Dalitz decays : $K_L \to \gamma^{(*)}\gamma^{(*)}$ are presented. The status of the $\mathcal{CP}$-violating $K_L \to \pi^+\pi^-e^+e^-$ is also discussed. Preliminary results on the $\Xi^0 \to \Lambda\gamma$ and $\Xi^0 \to \Sigma^0\gamma$ branching ratios and the precise determination of the Ξ^0-mass are also sketched. All results are compared with corresponding values from the dedicated rare decay experiment *E799-II*.

1 Introduction

The primary goal of the *NA48* experiment at *CERN* is the precise determination of the *direct* $\mathcal{CP}$-violation parameter $Re(\varepsilon'/\varepsilon)$ in the kaon system, from the study of the $K_{L,S} \to \pi^+\pi^-, \pi^0\pi^0$ decay rates [1]. The high beam intensities give the experiment a good sensitivity to '*medium rare*' K_L decays, as well as to hyperon decays from the K_S target. This talk will focus on the $K_L \to \gamma^{(*)}\gamma^{(*)}$ data recorded in 1997 and where one or two γ are virtual and convert to an l^+l^- pair, and on $K_L \to \pi^+\pi^-e^+e^-$ data recorded in 1998.

2 *NA48* as a rare decay experiment

The proton beam intensity of 1.5×10^{12} on the K_L target every 14.4 seconds is optimized for the ε' running of the experiment, and is also suitable for rare decays studies, although the experiment is not dedicated to this physics goal as its competitor, the *E799-II* part of the *KTeV* experiment at *Fermilab*. The *NA48* detector, described in detail elsewhere [2], offers very good features for rare decay measurements :

- high resolution detectors are used, and achieve a good particle identification and background rejection. Charged particles are detected with a magnetic spectrometer consisting of 4 very "*transparent*" drift chambers, giving a low probability for γ conversion and electron bremsstrahlung. Neutral particles are measured with a high granularity electromagnetic calorimeter offering good space and time resolution, as well as an excellent knowledge of the energy scale ($< 0.1\%$).
- all subdetectors have a time resolution below $1ns$, which is a powerfull tool in removing backgrounds due to accidental coincidences in the detector
- the versatility of the programmable charged and neutral triggers, as well as the high data taking capability in excess of $100Mbytes/s$, allow the experiment to record the rare decay dataset concurrently to the ε' data. However, triggers based on the clusters counting in the calorimeter are limited to a decay range of the order of 3 τ_{K_S}, resulting in a limited integrated K_L flux or 3×10^9 in 1997, relatively modest compared to the 2.7×10^{11} collected by *E799-II* in the same period.

[a] e-mail: Vallage@hep.saclay.cea.fr

Most of the results presented here are based on 1997 data, corresponding to $\simeq 10\%$ of the final dataset.

3 K_L Dalitz and double Dalitz decays

In this family, one finds : $K_L \to e^+e^-\gamma$, $K_L \to \mu^+\mu^-\gamma$, $K_L \to e^+e^-e^+e^-$, $K_L \to e^+e^-\mu^+\mu^-, \ldots$. These decays allow the study of the long distance contributions to the amplitudes, since they probe the structure of the $K_L \to \gamma\gamma^*$ and $K_L \to \gamma^*\gamma^*$ vertex. This is of particular importance for modelling the long range dispersive component to the decay $K_L \to \mu^+\mu^-$. For the $K_L \to l^+l^-\gamma$ case, *Bergström, Massó and Singer* (*BMS*) [3] parametrize the form factor of the long distance contribution by α_{K^*}, a free parameter which weights the relative strenght of *the pseudoscalar pseudoscalar* (*P-P*: π^0, η, η') and *vector vector* (*V-V*: ρ, ω, ϕ) transitions :

$$F[K_L \to \gamma\gamma^*] = \frac{F[K_L \to \gamma\gamma]_{exp}}{1 - m_{ll}^2/m_\rho^2} + \alpha_{K^*} \times \frac{N_A A_{K^*}(m_{ll})}{1 - m_{ll}^2/m_{K^*}^2}$$

Shifman, Vahnstain and *Zakharov* explained the enhancement of the *P-P* transitions by the gluonic penguin diagrams, contributing only to the first term of the *RHS* of the equation above. The probabilities for internal conversion have been estimated in this '*BMS*' model, and assuming the $\Delta I = 1/2$ rule, a value $|\alpha_{K^*}| = 0.2 - 0.3$ is predicted, which means a small but non-zero contribution from the *V-V* part.

3.1 $K_L \to e^+e^-\gamma$

The $e^+e^-\gamma$ final state has been recently studied by *NA48* [4]. The total number of events selected is 6864, with very small background, mainly due to $K_S \to \pi^0\pi^0_D$ (7.2 ± 1.2 events) and $K_L \to \pi e\nu$ with an additional "accidental" photon (2.9 ± 0.6 events). The correlation plot between the squared and scaled e^+e^- invariant mass and the $e^+e^-\gamma$ mass is shown in *Figure* 1.

The branching ratio is determined to be:

$$B(K_L \to e^+e^-\gamma) = [1.06 \pm 0.02_{stat} \pm 0.02_{sys} \pm 0.04_{br}] \times 10^{-5},$$

using as normalization a set of 4060 $K_L \to \pi^0\pi^0_D$ decays. The value is in good agreement with the *BMS*-based theoretical prediction of 9.9×10^{-6}, and with previous experimental results : $(9.1 \pm 0.5) \times 10^{-6}$. The $KTeV$ $e^+e^-\gamma$ signal accounts to $\simeq$ 16K events, but no branching ratio as been released yet.

The parameter α_{K^*} which appears in the form factor, can be extracted from the shape of the $x = (m_{ee}/m_K)^2$ distribution. Data are compared in *Figure* 2 with the prediction of the *BMS* model for $\alpha_{K^*} = -0.36$, as well as with a pure QED model with trivial form factor. A formfactor is clearly needed to describe the distribution at intermediate and large $m(e^+e^-)$, which - according to the *BMS* model - is achieved by the *vector vector* contribution given by α_{K^*}. Ten sets of Monte Carlo samples have been produced including radiative corrections [5] for different values of α_{K^*}. The χ^2 between data and Monte Carlo is minimized as shown in *Figure* 3 for the value :

$$\alpha_{K^*} = -0.36 \pm 0.06_{stat} \pm 0.02_{sys},$$

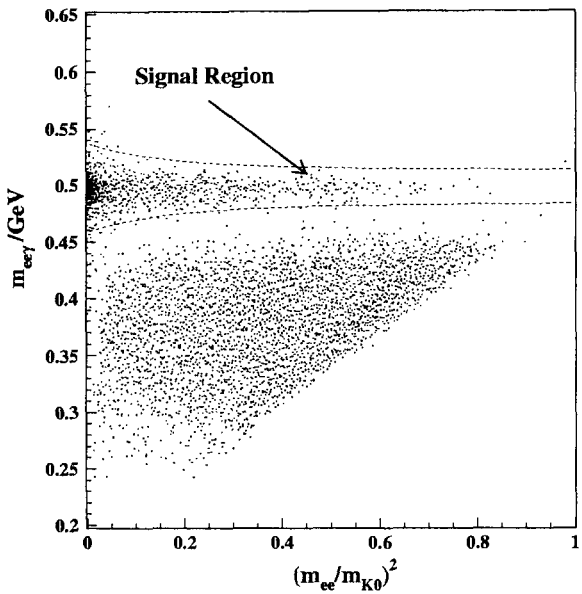

Figure 1: Scatter plot of the $e^+e^-\gamma$ mass versus m_{ee}^2/m_K^2.

where the statistical error corresponds to a χ^2 increase of one. This result is consistent with the *BMS* model, and compares well with earlier measurements in this channel : $\alpha_{K^*} = -0.28 \pm 0.08$ (*NA31, E845*). It should be stressed that without radiative corrections, the value of α_{K^*} above would be -0.15 ± 0.05; the difference arises because at high m_{ee} the probability of emission of internal bremsstrahlung increases, and the resulting $ee\gamma\gamma$ events are lost from our sample.

3.2 $K_L \to \mu^+\mu^-\gamma$

Up to now, published results on the $\mu^+\mu^-\gamma$ channel suffer poor statistics : 207 events from *KTeV* and 45 events from *NA48*. Unlike the $e^+e^-\gamma$ channel which allow the determination of α_{K^*} from the shape of the m_{ee}^2/m_K^2 distribution, lepton mass effects make the $m_{\mu\mu}^2/m_K^2$ distribution rather normalisation sensitive to α_{K^*}. Current published data favor a small value, *e.g* $\alpha_{K^*} = -0.04 \pm 0.22$ [6], one sigma away from that determined using the $e^+e^-\gamma$ channel.

Both experiment will soon update their earlier results, with 6700 events from *KTeV*, and 2061 candidates from the 1998 dataset of *NA48*. The reconstructed invariant mass distribution of this last sample is shown in *Figure* 4, together with the background estimate coming from $K_L \to \pi^+\pi^-\pi^0$ with lost γ and $K\mu3$ accompanied with accidental γ and subsequent in flight pion decay.

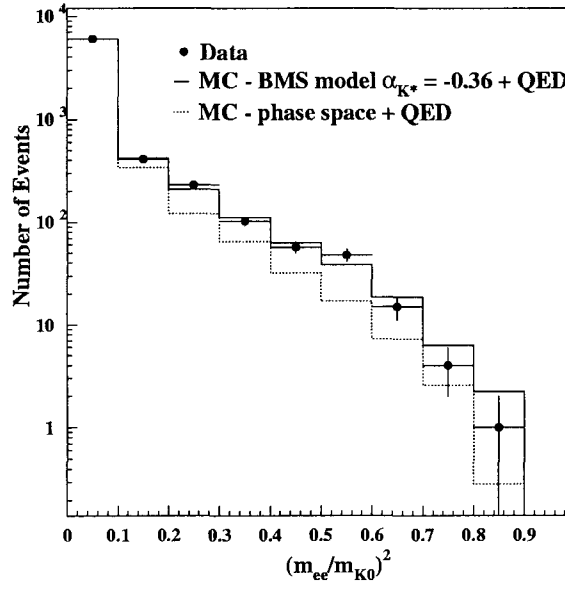

Figure 2: Comparison of m_{ee}^2/m_K^2 distribution in data (points with error bars) and Monte Carlo sample generated using $\alpha_{K^*} = -0.36$ (solid line) and form factor f(x)=1 (dotted line).

3.3 $K_L \to e^+e^-\gamma\gamma$

For the understanding of kaon decays with photons and leptons in the final state, the precise knowledge of radiative corrections is important. The decay $K_L \to e^+e^-\gamma\gamma$ in itself is of considerable interest, as it constitutes the major background to the very rare decay $K_L \to \pi^0 e^+e^-$, which is expected to be dominated by direct $\mathcal{CP}$-violation [5].

Figure 5 shows the $K_L \to e^+e^-\gamma\gamma$ mass plot of the data taken in 1997 and 1998. In the signal region between 482-514 MeV, 503 events are found, (7.3 ± 2.7) of which are estimated to be due to $K_L \to \pi^0\pi^0_D$ and (14.2 ± 1.2) events are due to $e^+e^-\gamma$ *plus* a photon from external electron bremsstrahlung in the detector material. The **preliminary** branching ratio for a minimum photon energy of 5 MeV in the K_L center-of-mass system is calculated to be:

$$B(K_L \to e^+e^-\gamma\gamma) = [5.82 \pm 0.27_{stat} \pm 0.45_{sys} \pm 0.16_{norm}] \times 10^{-7},$$

using $K_L \to e^+e^-\gamma$ events for normalization. The result is in good agreement with earlier measurements, and with the recent result from $KTeV: 6.31 \pm 0.45 \times 10^{-7}$ based on 1988 events with an estimated background of 76.6 ± 3.3 events. The branching ratio is $\simeq 5$ order of magnitude above the standard model expectation of the $K_L \to \pi^0 e^+e^-$, for which the best limit is $\leq 5.64 \times 10^{-10}$ (90% CL) [7].

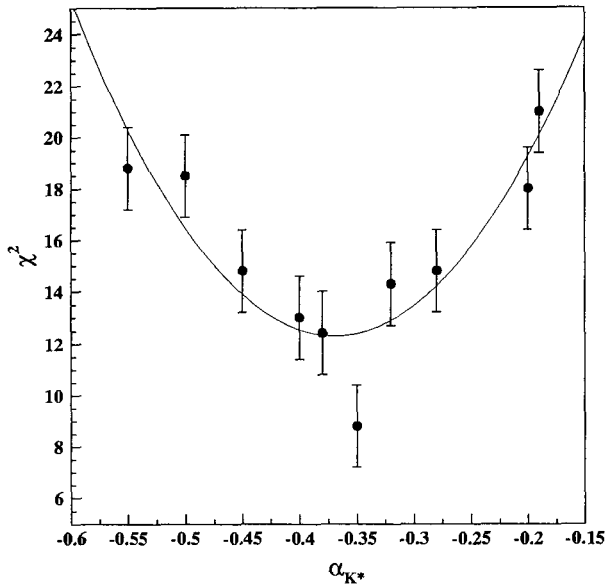

Figure 3: χ^2 distribution for data vs Monte Carlo comparison, as a function of the parameter α_{K^*}.

3.4 $K_L \to e^+e^-e^+e^-$

This decay is due to double *internal* photon conversion of $K_L \to \gamma^*\gamma^*$ in e^+e^- final states. It suffers from substantial background from $K_L \to \gamma\gamma$ and $K_L \to e^+e^-\gamma$ decays with subsequent *external* conversion in the material of the detector. To reject these events, a minimal track distance of 2 cm at the spectrometer drift chambers before the magnet is required, corresponding to a cut on the minimal virtuality of the intermediate γ^*. Requiring a small transverse momentum w.r.t. to the beam direction of $p_T^2 < 0.0005\mathrm{GeV}^2/\mathrm{c}^2$, 84 $K_L \to e^+e^-e^+e^-$ candidate events are selected with negligible background. The $KTeV$ experiment signal accounts to 430 events, also with negligible background, but none of the collaborations released the branching ratio whose theoretical expectation is $\simeq 3.5 \times 10^{-8}$.

In analogy to the classic determination of the π^0-parity, the angle between the two e^+e^--planes contains information about the $\mathcal{CP}$-parity of the initial state. For the $\mathcal{CP}$-eigenstates belonging to the eigenvalues $\pm$ 1, the distribution is given by $dN/d\phi \propto 1 + \alpha \cos 2\phi$, with α depending on the kinematics of the event. A $\mathcal{CP}$-odd (*resp.* even) state would result in α = -0.19 (*resp.* +0.19). The fit to the angular distribution give $\alpha = -0.32 \pm 0.15$ (see *Figure* 6), corresponding to a 60% probability for $\mathcal{CP}(K_L)$=−1 and a 1.5% probability for $\mathcal{CP}(K_L)$=+1.

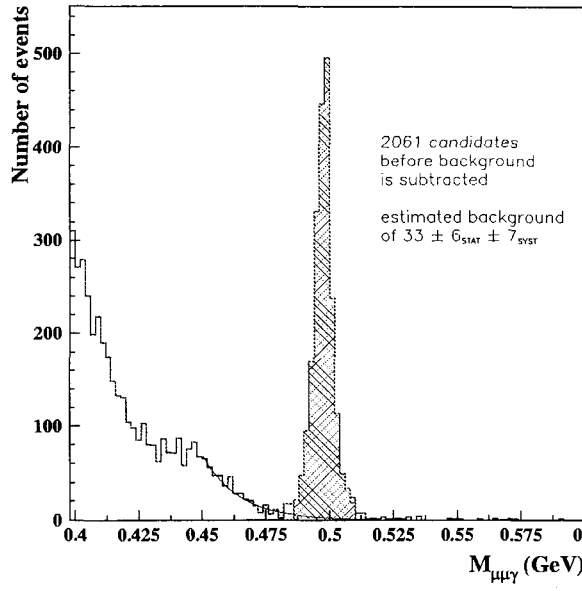

Figure 4: Reconstructed $\mu^+\mu^-\gamma$ mass compared to the background estimate.

4 Status of $K_L \to \pi^+\pi^-e^+e^-$

The decay $K_L \to \pi^+\pi^-e^+e^-$ is expected to proceed mainly through a $\pi^+\pi^-\gamma^*$ state. Two dominant components contribute to the amplitude : an indirect $\mathcal{CP}$-violating $K_L \to \pi^+\pi^-$ with inner bremsstrahlung, and a $\mathcal{CP}$-conserving photon M1 direct emission followed by internal conversion. The interference of these two amplitudes results in a $\mathcal{CP}$-violating circular polarization of the γ^*, which can be probed by studying the correlation of the e^+e^- plane relative to the $\pi^+\pi^-$ plane : the ϕ angle between these planes is a T odd variable. In the model of *Sehgal and Wanniger* [8], the angular distribution in ϕ is :

$$\frac{d\Gamma}{d\phi} = \Gamma_1 cos^2\phi + \Gamma_2 sin^2\phi + \Gamma_3 cos\phi sin\phi$$

Effects are particularly visible in the $\mathcal{CP}$-violating asymmetry defined as :

$$Asymmetry = \frac{N_{\cos\phi\sin\phi>0} - N_{\cos\phi\sin\phi<0}}{N_{\cos\phi\sin\phi>0} + N_{\cos\phi\sin\phi<0}}$$

for which the prediction of [8] is 14.4%.

A dedicated 4-tracks trigger was implemented for the 1998 *NA48* data taking which corresponds to an integrated K_L flux of $\simeq 5 \times 10^{10}$. A total of 458 signal events was

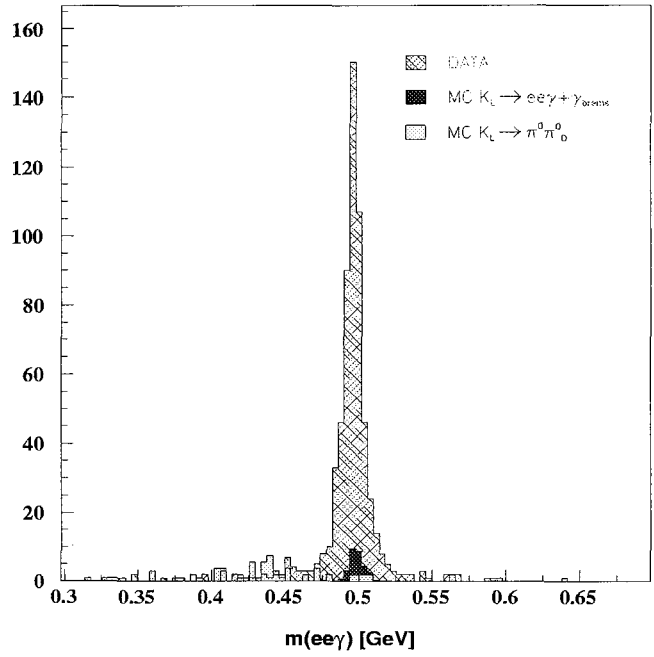

Figure 5: Invariant mass of $e^+e^-\gamma\gamma$ system.

selected, with 12.4 background events coming mainly from $K_L \to \pi^+\pi^-\gamma$ with conversion $\gamma \to e^+e^-$, overlayed $K_L \to \pi^-e^+\nu_e$ and $K_L \to \pi^+e^-\bar{\nu}_e$, and $K_L \to \pi^+\pi^-\pi^0_D$ with $\pi^0_D \to e^+e^-\gamma$. Figure 7 shows the $\pi^+\pi^-e^+e^-$ invariant mass distribution. The branching ratio is found to be :

$$BR(K_L \to \pi^+\pi^-e^+e^-) = (2.90 \pm 0.15(stat)) \times 10^{-7} \ \textbf{(Preliminary)}$$

using a normalization of $1M$ $K_L \to \pi^+\pi^-\pi^0_D$ decays, which is in good agreement with the theoretical prediction of $\sim 3 \times 10^{-7}$ (*Sehgal and Wanniger*).

The $\mathcal{CP}$-violating asymmetry is maximal where the interference of the M1 direct emission and the inner bremsstrahlung is the biggest. The experimentaly observed asymmetry is the convolution of this interference with the detector acceptance, which enhance the observed effect. As a result, full simulation of the detector shows that in the absence of interference the observed asymmetry is zero, whereas a generated asymmetry of 14% gives rise to a 22% reconstructed asymmetry. Figure 8 shows the observed asymmetry of $(20 \pm 5)\%$ together with a Monte Carlo simulation of the angular distribution. The unfolding of the effect is in progress, and should be released soon. The $KTeV$ experiment recently reported [9] a branching ratio of $BR = (3.63 \pm 0.11(stat) \pm 0.14(syst)) \times 10^{-7}$ based on a total kaon flux of 2.4×10^{11}), and an observed asymmetry of $23.3 \pm 2.3\%$ based on 1811 events, yielding an acceptance corrected asymmetry of $13.6 \pm 2.5(stat) \pm 1.2(syst)\%$ in good agreement with the prediction of [8].

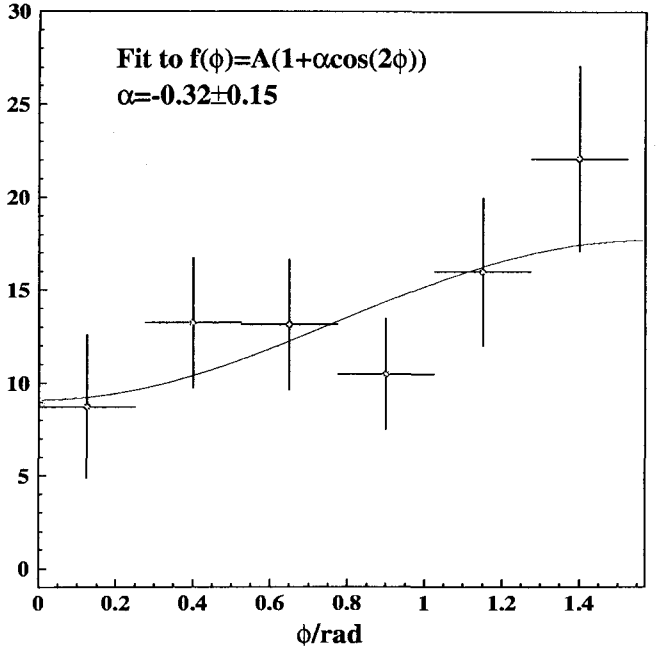

Figure 6: Distribution of the ϕ angle between the e^+e^- planes, together with the fit for the parameter α.

5 Hyperon studies

Radiative Ξ^0-decays are difficult to calculate due to their non-leptonic weak interaction nature, and theoretical predictions show a wide variation.

The *NA48* double beams setup includes a "*close*" target used to produce the necessary K_S component for the ε'/ε determination. This target is also a source of neutral short-lived particles like Λ^0 and Ξ^0. The proton beam intensity of 3×10^7 on this target is optimized for the ε' and could be highly increased for specific K_S or hyperon decays studies. Radiative Ξ^0 decays are selected requiring a reconstructed $\Lambda \to p\pi^-$ in the spectrometer and at least one γ in the calorimeter.

NA48 has analysed a sample of 31 $\Xi^0 \to \Lambda\gamma$ decays, with an acceptance of 6.7% and almost free of background, yielding a **preliminary** value for the branching ratio of :

$$B(\Xi^0 \to \Lambda\gamma) = [1.90 \pm 0.34_{stat} \pm 0.19_{sys}] \times 10^{-3}.$$

Twenty candidates for the $\Xi^0 \to \Sigma^0\gamma \to \Lambda\gamma\gamma$ decay have also been observed, with an acceptance of 3.1% and 15% background mainly coming from $\Xi^0 \to \Lambda\pi^0$ decays. A **preliminary** value for the branching ratio of :

$$B(\Xi^0 \to \Sigma^0\gamma) = [3.14 \pm 0.76_{stat} \pm 0.32_{sys}] \times 10^{-3}$$

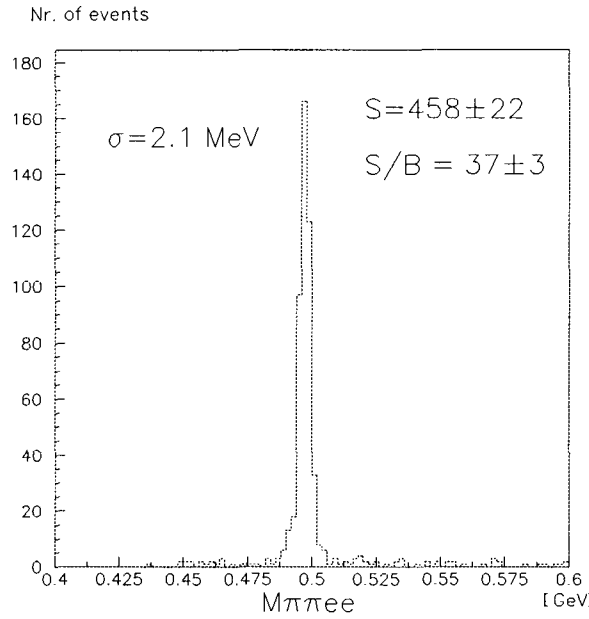

Figure 7: $\pi^+\pi^-e^+e^-$ invariant mass distribution.

has been determined. In both cases a sample of 6669 $\Xi^0 \to \Lambda\pi^0$ decays was used for normalization, with an acceptance of 2.8%.

While these branching ratios are statistically less precise than earlier determinations, the Ξ^0-mass measurement is systematically limited and can be drastically improved given the precise tracking and small uncertainty of the momentum scale in the *NA48* detector. Using $\Xi^0 \to \Lambda\pi^0$ decays, the vertex is calculated from the π^0-mass constraint; the nominal π^0 and Λ masses are used as additional constraints. The resulting Ξ^0-mass resolution is about 1 MeV, as can be seen in *Figure* 9. The limiting systematic error comes from the knowledge of the vertex position, which has been conservatively estimated to be ± 50 cm. The **preliminary** Ξ^0 mass value of :

$$m(\Xi^0) = 1314.83 \pm 0.06_{stat} \pm 0.20_{sys}\text{MeV}$$

constitutes a factor 4 improvement *w.r.t.* previous measurements.

6 Summary and future

A new analysis on $K_L \to e^+e^-\gamma$ has been presented. Preliminary results on $K_L \to e^+e^-\gamma\gamma$, $K_L \to e^+e^-e^+e^-$ and $K_L \to \pi^+\pi^-e^+e^-$ have been shown, as well as progress on $K_L \to \mu^+\mu^-\gamma$. Preliminary results on radiative Ξ^0-decays and a precise determination of the cascade mass were discussed.

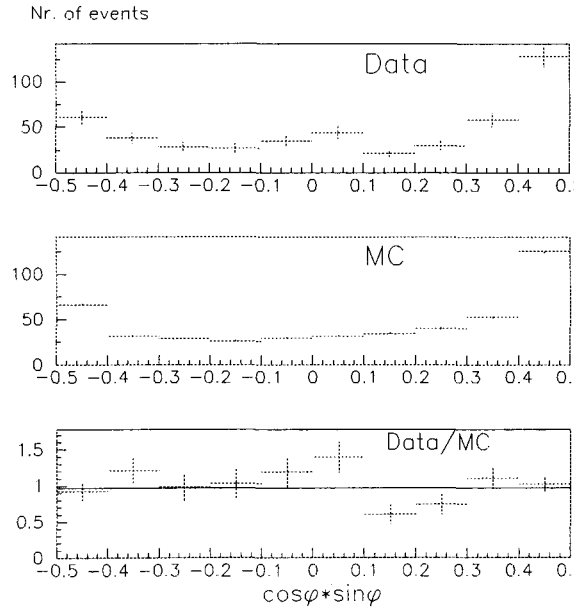

Figure 8: $\cos\phi \sin\phi$ distributions. *Top* : observed in the data, *Center* : MC simulation, *Bottom* : ratio data/MC.

In a close future, results based on 1998-1999 data will be finalized, corresponding to $\sim 3 \times 10^{10}$ decays for Dalitz decay studies, and $\sim 1.3 \times 10^{11}$ decays for the $K_L \to \pi^+\pi^-e^+e^-$ channel, yielding an accuracy $< 3\%$ on the $\mathcal{CP}$-violating asymmetry.

The future *NA48* program is still uncertain, since the destruction of the drift chambers on November 11th. Nevertheless, proposals have been written for dedicated K_S rare decay studies [10], as well as direct $\mathcal{CP}$-violation searches using charged kaons beams in a modified *NA48* setup [11].

Acknowledgments

I would like to thank in particular *Julien Cogan, Lutz Köpke, Matthew Needham*, and *Slawek Wronka* for providing *NA48* results and plots, and helping me to prepare the talk. I also greatly acknowlegde the help of *Taku Yamanaka* in providing numbers and plots from the *KTeV E799-II* competitor experiment.

References

[1] "A new measurement of direst $\mathcal{CP}$-Violation in two pion decays of the neutral kaon", NA48 Collaboration, V. Fanti et al., Phys. Lett. B 465 (1999) 335-348.

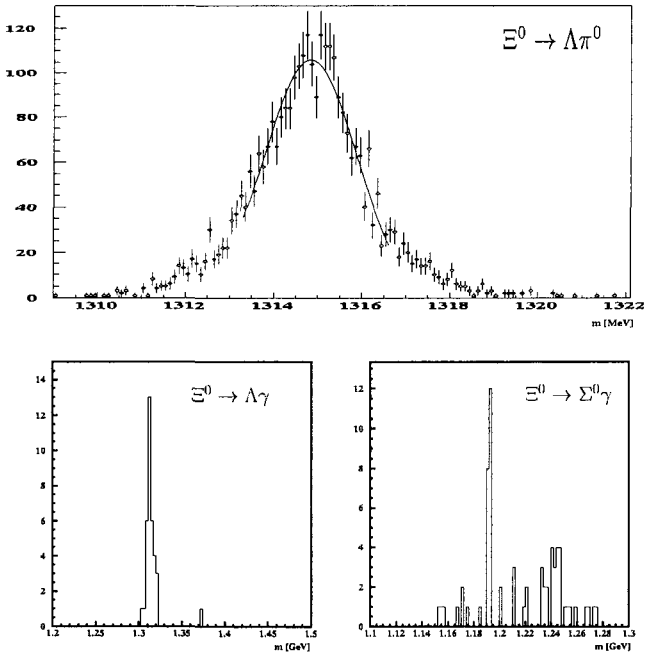

Figure 9: $\Lambda\pi^0$ mass distribution (top). Radiative hyperon decays. Evidence for $\Xi^0 \to \Lambda\gamma$ (bottom left) and $\Xi^0 \to \Sigma^0\gamma \to \Lambda\gamma\gamma$ (bottom right). In both cases the $\Lambda\gamma$ invariant mass distribution is shown.

[2] "The Beam and Detector for the Precision $\mathcal{CP}$-Violation Experiment NA48", to be submitted to Nucl. Inst. Meth.

[3] "Testing the origin of the $\Delta I = 1/2$ rule through K_L Dalitz decays", L. Bergström, E. Massó and P. Singer, Phys. Lett B131 (1983) 229-233.

[4] "Measurement of the Decay Rate and Form Factor Parameter α_{K^*} in the Decay $K_L \to e^+e^-\gamma$", NA48 Collaboration, V. Fanti et al., Phys. Lett. B 458 (1999) 503.

[5] "Background to $K_L \to \pi^0 e^+e^-$ from $K_L \to e^+e^-\gamma\gamma$", H.B. Greenlee, Phys. Rev. D42 (1990) 3724-3731.

[6] "Measurement of the Decay Rate and the Parameter α_{K^*} in the Decay $K_L \to \mu^+\mu^-\gamma$", NA48 Collaboration, V. Fanti et al., Z. Phys. C 76 (1997) 653-657.

[7] "KTeV rare decay results", Taku Yamanaka, Moriond Electroweak Conf. (1999).

[8] "$\mathcal{CP}$ violation in the decay $K_L \to \pi^+\pi^-e^+e^-$", L. M. Sehgal and M. Wanniger, Phys. Rev. D46 (1992) 1035-1041.

[9] "Observation of $\mathcal{CP}$ violation in $K_L \to \pi^+\pi^-e^+e^-$ decays" KTeV Collaboration, A. Alavi et al, hep-ex/9908020, 5 Aug 1999. Sub. to Phys. Rev. Lett.

[10] "A high sensitivity investigation of K_S and neutral hyperon decays using a modified K_S beam", NA48 Collaboration, R. Batley et al., CERN/SPSC 2000-002, SPSC/P253 ADD.2, 12 Dec 1999.

[11] "Addendum for a precision measurement of charged kaon decay parameters with an extended NA48 setup", NA48 Collaboration, R. Batley et al., CERN/SPSC 2000-003, SPSC/P253 ADD.3, 14 Dec 1999.

TWO PHOTON PHYSICS AT LEP

G. PASSALEVA [a]

INFN Florence, Largo E. Fermi 2, I-50121 Florence, Italy

*Abstract.*LEP offers an excellent opportunity to measure two photon processes over a large kinematical range and thus study the complex nature of the photon. This article reviews the experimental status of "Two Photon Physics" at LEP. The recent results on multi-hadron production and photon structure functions are discussed.

1 Introduction

Over the past decade two photon physics has proven to be a very productive source of information about QED, QCD and hadron spectroscopy. The Feynman diagram responsible for a two photon collision process at LEP is shown in Figure 1, where the high energy incident electrons and positrons split off virtual photons and the scattered electrons take most of the beam energy.

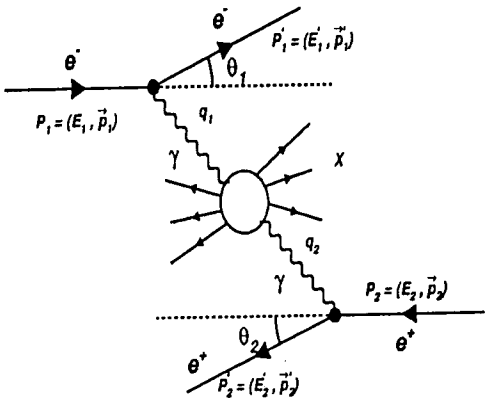

Figure 1: $\gamma\gamma$ *collision in* e^+e^- *scattering*

These two photons then can interact to form a state X with mass $W_{\gamma\gamma}$. The four-momentum transfer q_i to the photons depends on the angle and energy of the scattered electrons[b]. When neither of the scattered electrons is detected (untagged events), the virtual photons are referred to as nearly real i.e. $q_1^2 \approx q_2^2 \approx 0$. This class of events allows several tests of QCD by studying hadronic resonances, the inclusive hadron cross section and jet production rates. If there is detection of one of the scattered electrons $Q^2 = -q_1^2$ (single tagged events), it is possible to probe the other photon $q_2^2 \approx 0$ regarded as a "target" and study its structure. Finally, if both the scattered electrons are detected $Q_i^2 = -q_i^2, (i = 1, 2)$ (double tagged events), the structure of

[a] e-mail: giovanni.passaleva@cern.ch

[b] Electron stands for electron and positron throughout this article

the reaction of highly virtual photons is probed. In the following sections, a review is given of the $\gamma\gamma$ results obtained at LEP, with special attention to recent results.

2 The Two Photon Total Cross-section

At LEP II energies, the two photon process $e^+e^- \to e^+e^-\gamma^*\gamma^* \to e^+e^-hadrons$ is a copious source of hadron production. In this reaction the photons either interact as a point-like particle or undergo quantum fluctuation (resolved photon) into a resonant(VMD) or non-resonant virtual states opening up all the possibilities of hadronic interactions as shown in Figure 2. These interactions can be described in terms of Regge poles [1,2], (Pomeron or Reggeon exchange).

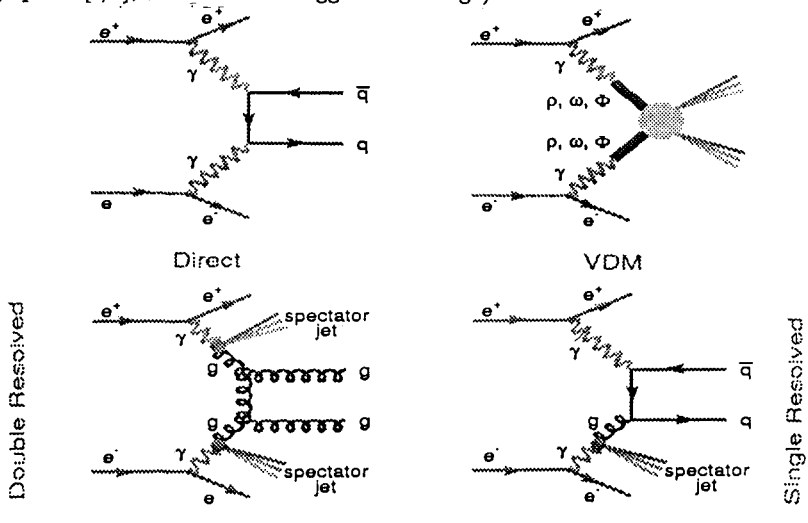

Figure 2: *Some diagram contributing to hadron production in $\gamma\gamma$ collisions at LEP.*

A measurement of the total hadronic cross section as a function of $\sqrt{s}$, improves our understanding of the hadronic nature of the photon. At LEP, using the high energy runs above the Z peak, L3 and OPAL have measured the cross section [3,4] $\sigma(\gamma\gamma \to hadrons)$ in the range $5 \leq W_{\gamma\gamma} \leq 145$ GeV as shown in the Figure 3.
The cross-section measurement of the two experiments show a clear rise at high energies, described by a "Soft Pomeron" and the data of the L3 experiment show a fast decrease at low energies due to "Reggeon exchange". The rise of $\sigma_{\gamma\gamma}$ is faster than the one observed in hadron-hadron or γp collisions; a simple factorization ansatz [5] $\sigma_{\gamma\gamma} = \sigma^2_{\gamma p}/\sigma_{pp}$ is excluded as can be seen in Figure 3 from the predictions of Schuler and Sjostrand [6]. The data are rather well described by the dual parton model of Engel and Ranft [7] or by analytical calculations which take into account the importance of QCD effects at high transverse momentum. In Figure 3, the mini-jet model of Godbole and Pancheri [8] is also represented. One has to notice that all models has some dependence which can change the cross section predictions by 10-30%. The Monte Carlo models PYTHIA and PHOJET which are used to correct the data, differ

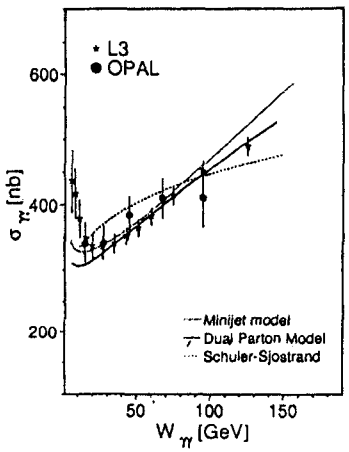

Figure 3: *The measured cross-section $\sigma(\gamma\gamma \to hadrons)$ as a function of $W_{\gamma\gamma}$.*

by ≈20% in the absolute normalization. In future, improvements in the theoretical predictions especially the description of diffractive processes are desirable.

3 Single Particle and Jet Production

Inclusive production of charged hadrons, K_s^0 mesons and jets has been studied at LEP by the OPAL experiment. Figure 4(a) shows a measurement of the differential cross-section for charged hadrons produced in collision of the two quasi-real photons in the range 10 GeV< $W_{\gamma\gamma}$ <125 GeV as a function of transverse momentum [9] p_T . The results are reasonable agreement to NLO perturbative QCD calculations [10]. These data demonstrate the dominance of the direct component at large p_T.
Also shown in figure 4(b) is the comparison of the $\gamma\gamma$ data to p_T measured in γp and (π,K)p interactions normalised at the same value at low p_T. It can be seen that there is a significant increase of rates in the $\gamma\gamma$ process above a p_T of 2 GeV. The clear deviation from the hadronic interactions shows the effect of the direct component in the $\gamma\gamma$ interactions. Similar studies of p_T distributions of the K_s^0 mesons are in reasonable agreement with NLO calculations [9].

The OPAL experiment has performed a very nice measurement of dijet production in two-photon collisions at $\sqrt{s} = 161$ and 172 GeV. Their results [12] demonstrate that it is possible to distinguish between direct and resolved processes in the dijet events with the help of the variable x_γ, which is the estimator of the fraction of the target photon's momentum carried by the parton which produces jets. Figure 5 shows the measured distribution of the parton scattering angle θ^* for direct and double-resolved processes, compared to the relevant QCD matrix element calculations [13]. One observes a clear distinction between the direct process $\gamma\gamma \to q\bar{q}$ ($x_\gamma > 0.8$), where a quark is exchanged in the t channel and the doubly resolved one ($x_\gamma < 0.8$),

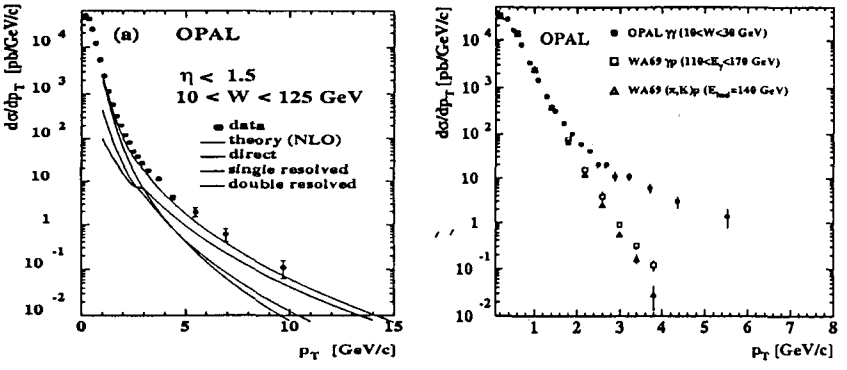

Figure 4: *a) Differential inclusive charged hadron cross-section and b) the* p_T *distribution measured in* $\gamma\gamma$ *interactions compared to the* γp *and* $(\pi,K)p$ *interactions.*

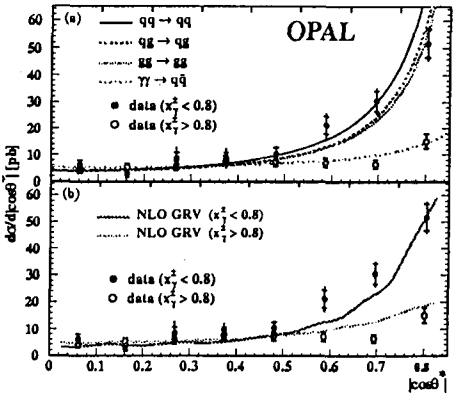

Figure 5: *The angular distribution in the dijet center-of-mass system for "Direct" and "Resolved" events*

dominated by the gluon exchange. The strong rise in $\cos\theta^*$ distribution near $\cos\theta^*=1$ is due to a large double-resolved contribution, as expected from QCD.

4 Heavy Quark Production

The study of heavy quark (c,b) production in two photon collisions at LEP provides not only an excellent test of perturbative QCD but also gives an estimate of the gluon density in the photon. At LEP energies, the direct and resolved photon processes are predicted to give comparable contributions to the charm and beauty quark production cross-sections [14]. The resolved process is dominantly quark-gluon fusion: $\gamma g \to q\bar{q}$ so that these measurements provide information about the gluon content of the photon. The cross-section of the processes $e^+e^- \to e^+e^- c\bar{c}, b\bar{b}$ X has been measured by the L3 [15] and OPAL [16] experiments. At L3, the charm and beauty quark are identified by tagging leptons (e, μ) from semileptonic charm and beauty decays. Charm quark were also identified by the reconstruction of $D^{\pm *}$ meson decays, where $D^* \to D^0\pi^\pm$, and OPAL tags charm quark with $D^* \to D^0\pi^\pm$ and $D^0 \to K^-\pi^+, K^-\pi^+\pi^0, K^-\pi^+\pi^-$.

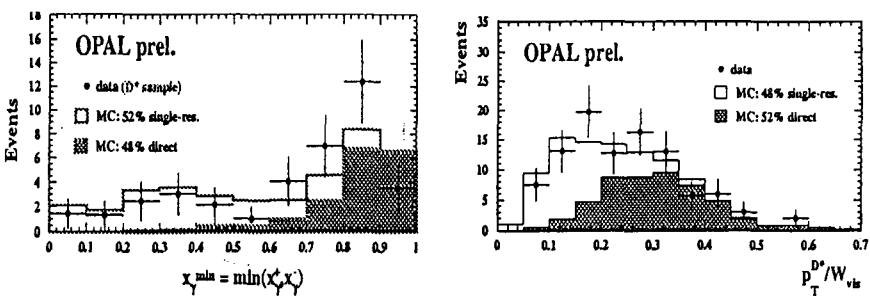

Figure 6: *The x_γ distribution of dijet events containing a D^* and the p_T distribution of the D^* normalised to the visible mass of the event.*

A good separation of direct and resolved processes is obtained by associating the D^* to a dijet analysis or by inspection of the p_T distribution of the D^* (See figure 6). As predicted the direct and resolved processes contribute roughly equally to the observed distribution. The differential D^* cross section agrees well with the NLO predictions and is independent of the Monte Carlo models used to correct the data over the range of detector acceptance. The total inclusive cross-sections are plotted in Figure 7 together with previous measurements. The data are compared to NLO QCD calculations [14]. The direct process $\gamma\gamma \to c\bar{c}, b\bar{b}$, shown with dotted line, is insufficient to describe the data, even if real and virtual gluon corrections are included. The cross sections requires contributions from the resolved processes which are dominantly $\gamma g \to c\bar{c}, b\bar{b}$. The data therefore requires a significant gluon content in the photon.

The $b\bar{b}$ cross section is measured for the first time in two photon collisions by the L3 experiment. The preliminary value of b cross section lies somewhat above QCD predictions.

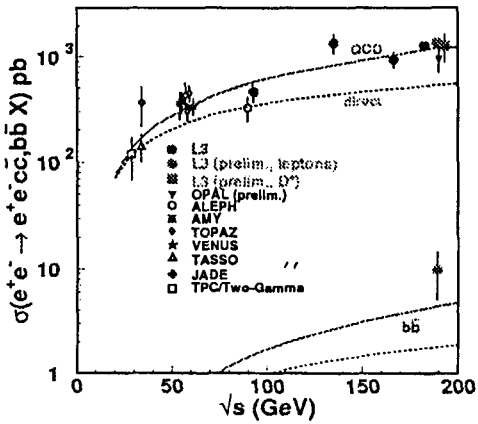

Figure 7: *The cross-section for heavy quarks production as measured at LEP and at previous* e^+e^- *colliders*

5 Hadronic structure function $F_2^{\gamma,QCD}$

The measurement of the hadronic structure function, $F_2^{\gamma,QCD}$ has been performed at LEP in the range $0.0025 < x < 1$ and $1.2\ \mathrm{GeV}^2 < Q^2 < 279\ \mathrm{GeV}^2$ [20, 21, 22, 23]. The physical interest in the analysis of the hadronic photon structure function is twofold. Firstly, to measure the shape of F_2^γ, especially at small values of x, at fixed Q^2, where HERA experiments observe a strong rise of the proton structure function. Secondly the Q^2 evolution of F_2^γ is investigated. The F_2^γ measurements from L3 and OPAL are shown in Figure 8 (a) in the Q^2 interval from 1.2 to 9.0 GeV^2. The x range is $0.002 < x < 0.1$ at $\langle Q^2 \rangle = 1.9\ \mathrm{GeV}^2$ and $0.005 < x < 0.2$ at $\langle Q^2 \rangle = 5.0\ \mathrm{GeV}^2$. For the low values of x, the data agree better with the parton density prediction of GRV [17], whereas SaS-1d [19] prediction is lower.

A compilation of the results for different experiments on the Q^2 evolution of F_2^γ in various ranges of x are shown in Figure 8 (b). The measured values of F_2^γ show clearly the linear growth with $\ln Q^2$ expected by QCD. The predictions of the GRV-LO [17] and SaS-1d [19] models are also shown. With all the statistics available at the end of LEP data taking, one hopes to extract the effective scale parameter Λ_{QCD} at large x.

6 $\gamma^*\gamma^*$ Collisions

The cross-section of $\gamma^*\gamma^*$ collisions has been measured at LEP with L3 [24] and OPAL [25] experiments in the range of $3\ \mathrm{GeV}^2 < Q_{1,2}^2 < 37\ \mathrm{GeV}^2$. Since the two photons are highly virtual and - unlike the proton - they do not contain constituent quarks with an unknown density distribution, one may hope to have a complete perturbative QCD calculation under particular kinematical conditions. An alternative

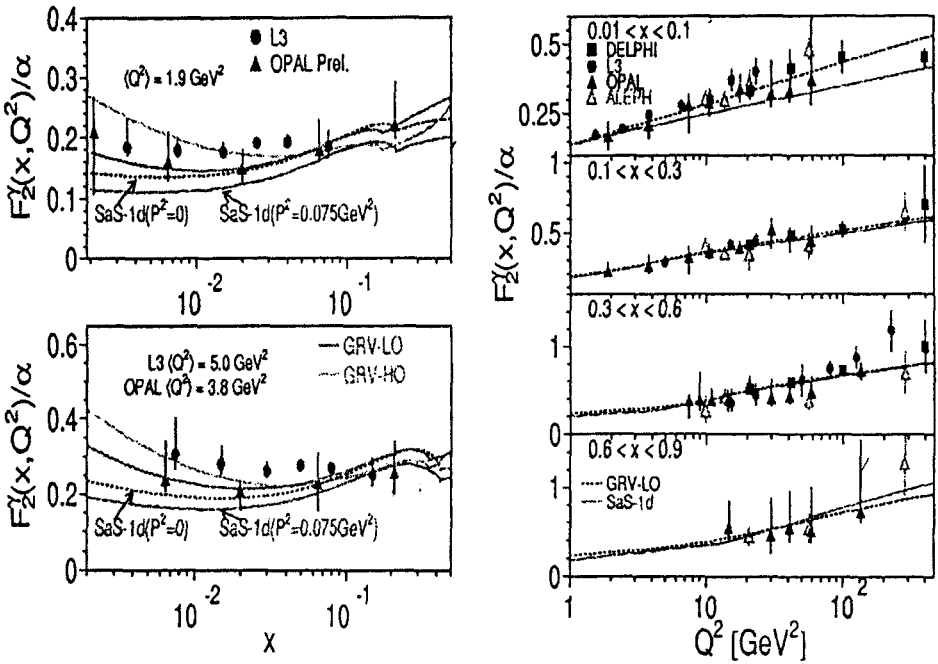

(a) (b)

Figure 8: *(a) The measured F_2^γ at $\langle Q^2 \rangle = 1.9\ GeV^2$ and $5.0\ GeV^2$ and (b) evolution of F_2^γ as a function of Q^2 for different range of x values.*

QCD approach is based on the BFKL equation [26]. Here the highly virtual two-photon process, with $Q_1^2 \simeq Q_2^2$, is considered as the "golden" process where the calculation can be verified without phenomenological inputs [27,28]. The $\gamma^*\gamma^*$ interaction can be seen as the interaction of two $q\bar{q}$ pairs scattering off each other via multiple gluon exchange. In this scheme the cross-section for the collision of two virtual photons [27,28] depends upon the "hard Pomeron" intercept $\alpha_P - 1 = 0.53$ [27,28] in the LO, whereas in the next-to-leading order the BFKL contribution is calculated to be smaller, $\alpha_P - 1 \simeq 0.17$ [29]. The results from L3 and OPAL (figure 9(a)) show that the events are well described by the PHOJET Monte Carlo model which uses the GRV-LO parton density in the photon and leading order perturbative QCD. The LO BFKL calculations shown in the figure 9(b), with dotted line are too high. By leaving α_P as a free parameter in the LO calculations, a combined fit to the L3

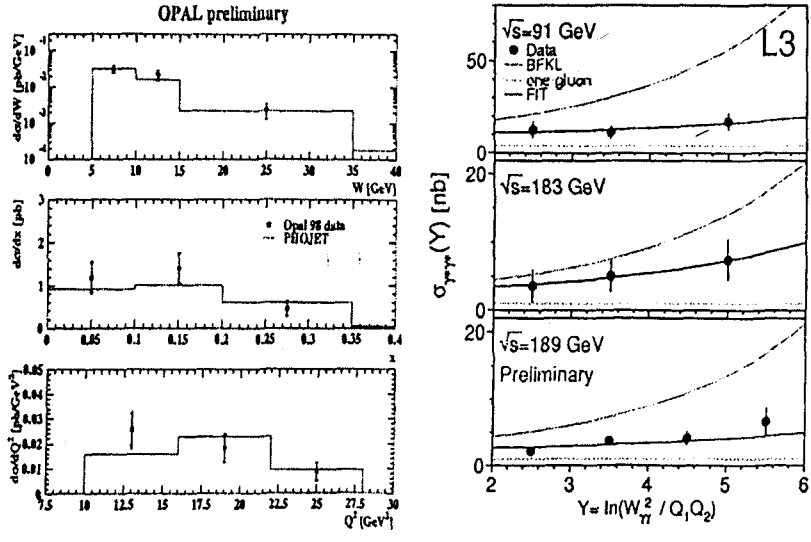

(a) (b)

Figure 9: *(a) The differential cross-section of double tag events compared to PHOJET Monte Carlo predictions and (b) the two photon cross-sections at LEP1 and LEP2 compared to LO-BFKL calculations after subtraction of the direct contribution*

data obtained at $\sqrt{s} \approx 91$, 183 and 189 GeV gives a value of $\alpha_P - 1 = 0.29 \pm 0.025$ with χ^2/d.o.f =7/9.

7 Outlook

Progress in the field of the two photon physics at LEP is significant, most notable are multi-hadron production and photon structure functions. With the statistics of 500 pb^{-1} luminosity available at the end of LEP II data taking the experimental

measurements will reach a high level of precision such that an improvement from the theoretical point of view will be desirable in order to have reliable interpretations of the experimental results.

Acknowledgements

I would like to thank all the colleagues from LEP experiments for their kind collaboration in the preparation of this paper. Many thanks also to the organizers of the conference and in particular to Prof. A. Studenikin and Dr. A. Egorov. They provided a very warm and fruitful atmosphere and gave us the opportunity to have a feeling of the new as well as the ancient Russia.

References

[1] P. D. B. Collins, Introduction to Regge theory (Cambridge U.P., Cambridge, 1977)
[2] Review of Particle Physics, *Phys. Rev.* D **54**, 191 (1996)
[3] L3 Coll., M. Acciarri et al., *Phys. Lett.* B **408**, 450 (1997);
L3 Coll., M. Acciarri et al., Submitted to EPS, Tampere, 1999
[4] OPAL Coll., G. Abbiendi et al., CERN-EP/99-076.
[5] V. N. Gribov and L. Ya. Pomeranchuk, *Phys. Lett.* B **8**, 343 (1962).
[6] G. A. Schuler and T. Sjöstrand, *Nucl. Phys.* B **407**, 539 (1993);
G. A. Schuler and T. Sjöstrand, *Z. Phys.* C **73**, 677 (1997)
[7] R. Engel, *Z. Phys.* C **66**, 203 (1995);
R. Engel and J. Ranft, *Phys. Rev.* D **54**, 4246 (1996)
[8] R.M.Godbole and G.Pancheri, hep-ph/9903331 (1999)
[9] OPAL Coll., K. Ackerstaff et al., *Eur. Phys. J* **C6**, 253 (1999)
[10] J. Binnewies, B. A. Kniehl and G. Kramer, *Phys. Rev.* D **53**, 6110 (1996)
[11] OMEGA Coll., R. J. Apsimon et al., *Z. Phys.* C **43**, 63 (1989)
[12] OPAL Coll., K. Ackerstaff et al. , *Z. Phys.* C **73**, 433 (1997);
OPAL Coll., G. Abbiendi et al. , *Eur. Phys. J* **C 6**, 253 (1999)
[13] H. Kolanoski, Two-Photon Physics at e^+e^- Storage Rings, Springer-Verlag(1984);
B. L. Combridge et al., *Phys. Lett.* B **70**, 234 (1977);
D. W. Duke and J. F. Owens, *Phys. Rev.* D **26**, 1600 (1982)
[14] M. Drees et al., *Phys. Lett.* B **306**, 371 (1993)
[15] L3 Coll., M. Acciarri et al., Submitted to EPS, Tampere, 1999
[16] OPAL Coll., G. Abbiendi et al. , Submitted to EPS, Tampere, 1999
[17] M. Glück, E. Reya and A. Vogt,*Phys. Rev.* D **45**, 3986 (1992);
M. Glück, E. Reya and A. Vogt,*Phys. Rev.* D **46**, 1973 (1992)
[18] H. Abramowicz, K. Charchula and A. Levy, *Phys. Lett.* B **269**, 458 (1991)
[19] G. A. Schuler and T. Sjöstrand, *Z. Phys.* C **68**, 607 (1995);
G. A. Schuler and T. Sjöstrand, *Phys. Lett.* B **376**, 193 (1996)
[20] ALEPH Coll., R.Barate et al., *Phys. Lett.* B **458**, 152 (1999)
[21] DELPHI Coll., Igor Tyapkin in " Workshop on Photon Interactions and the Photon structure", LUND 1998

[22] L3 Coll., M. Acciarri et al., *Phys. Lett.* B **436**, 403 (1998);
L3 Coll., M. Acciarri et al., *Phys. Lett.* B **447**, 147 (1999)
[23] OPAL Coll., K. Ackerstaff et al., *Z. Phys.* C **74**, 33 (1997);
OPAL Coll., K. Ackerstaff et al., *Phys. Lett.* B **411**, 387 (1997);
OPAL Coll., K. Ackerstaff et al., *Phys. Lett.* B **412**, 225 (1997). OPAL Coll., G. Abbiendi et al., Submitted to EPS, Tampere, 1999
[24] L3 Coll., M. Acciarri et al., *Phys. Lett.* B **453**, 333 (1999);
L3 Coll., M. Acciarri et al., Submitted to EPS, Tampere, 1999
[25] OPAL Coll., G. Abbiendi et al. , Submitted to EPS, Tampere, 1999
[26] E.A. Kuraev, L.N. Lipatov and V.S. Fadin, Sov. Phys. JETP **45** (1977) 199;
Ya.Ya. Balitski and L.N. Lipatov, Sov. J. Nucl. Phys. **28** (1978)822
[27] S.J. Brodsky, F. Hautmann and D.E. Soper, *Phys. Rev.* D **56**, 6957 (1997)
[28] J. Bartels, A. De Roeck and H. Lotter, *Phys. Lett.* B **389**, 742 (1996);
J. Bartels, A. De Roeck, C. Ewerz and H. Lotter, hep-ph/9710500
[29] S.J. Brodsky, V.S. Fadin, V.T. Kim, L.N. Lipatov and G.B. Pivovarov, hep-ph/99101229

Adler function from $R^{e^+e^-}(s)$ measurements: experiments vs QCD theory

A.L. Kataev
Institute for Nuclear Research of the Academy of Sciences of Russia, 117312 Moscow, Russia

Supported in part by the Russian Foundation of Basic Research, Grant N 99-01-00091

*Abstract.*An experimental QCD analysis of the behaviour of the Adler D-function in the Eucledian region is described. It is stressed that by taking into account of b-quark mass-dependent α_s^2-effects one obtains better agreement between theoretical predictions and experimentally motivated behaviour of the D-function at large Euclidian momentum transfer. A more detailed analysis of QCD predictions, including information on quark and gluon condensates, requires more precise data on $e^+e^- \to hadrons$, particularly in the energy regions $E < M_{J/\Psi}$ and $M_{J/\Psi} < E < 3.6\ GeV$. Use of experimenental determination of the D-function to test the generalized Crewther relation is outlined.

1. Introduction The process e^+e^-–annihilation into hadrons is one of the most informative process in elementary particle physics. Over the past few decades special attention has been paid to the detailed theoretical and experimental study of its basic characteristics, and in particular, of the ratio $R^{e^+e^-}(s) = \sigma_{tot}(e^+e^- \to hadrons)/\sigma(e^+e^- \to \mu^+\mu^-)$. As a result, important information about the properties of hadrons and of their constuents (quarks and gluons) was obtained. For example, e^+e^- collisions enabled discovery in Novovosibirsk of the first direct evidence for the ρ^0-meson 1. The J/Ψ resonance 2 to find in the e^+e^--collider SPEAR (SLAC) was simultaneous discovered by the e^+e^--collider SPEAR at SLAC, and at BNL as a result of study of the process $p + p \to e^+e^- + X$ 3). Rapid confirmation came from a slight increase of the beam of energy of the ADONE e^+e^- collider 4.

The observation of $\Psi^{'}$, $\Psi^{''}$, particles and their as the $\bar{c}c$ bound states of quarks (se ee.g. the review 5) has surved as an incitement to the development of the theory of strong interactions and QCD in particular. It brought up the question of the possibility of finding the signal from the fifth quark in e^+e^--annihilation. Moreover, an indirect determination of the mass of the sixth t-quark was made from the detailed fits of the experimental data of high-energy e^+e^--colliders LEP and SLC at the Z^0-pole taking into account the effects of its virtual propagation (for a review see 6). Impressively, the extracted mass of the t-quark turned out to be in agreement its direct "measurement", resulting from subsequent discovery of the 6th quark at the with the Tevatron.

Among present theoretical studies of data from e^+e^--colliders are attempts to find the phenomenologically allowed window for the mass of the Standard Model Higgs boson. These studies are based on combined fits of data from the high-energy colliders LEP and SLC (for a review see7) taking ino account the effect of running of the inverse electomagnetic coupling constant from its low energy value $\alpha^{-1}(0) \approx 137.0356...$ to M_Z. At this reference scale its value was determined using the compilation of the available e^+e^--data 8. The result of Ref8 $\alpha^{-1}(M_Z) = 128.896(90)$ was recently updated to give $\alpha^{-1}(M_Z) = 128.913(35)$ 9 (for a discussion of the fastly developing situation in this area see the review of Ref.10 and other related works on the subject

11). Futher estimates of experimental and theoretical uncertainties in this important quantity are on the agenda.

Table 1: Classification of constructed and planned e^+e^--colliding machines

Group	Machine	Location	Start Data	Status in 1999 June	Beam Energy Region E + E [GeV]
	AdA	Frascati	1960	-	
		ORSAY	1961	-	0.2 + 0.2
	VEPP-2	Novosibirsk	1966	-	0.2-0.55 + 0.2-0.55
I	ACO	ORSAY	1966	-	0.2-0.55 + 0.2-0.55
	ADONE	Frascati	1969	-	0.7-1.55 + 0.7-1.55
	VEPP-2M	Novosibirsk	1974	working	0.2-0.67 + 0.2-0.67
	DCI	ORSAY	1976	-	0.5-1.7 +0.5-1.77
	ϕ-factory DAΦNE	Frascatti	1999	launched	0.51+ 0.51
	CEA	Cambridge (USA)	1971	-	1.5-3.5 + 1.5-3.5
	SPEAR	SLAC	1972	-	1.2-4.2 + 1.2-4.2
	DORIS	Hamburg	1974	-	1-5.1 + 1-5.1
II	VEPP-4	Novosibirsk	1979	planned to restart	1.5-5 + 1.5-5
	CESR	Cornell	1979	working	3-8 + 3-8
	BEPC	Bejing	1991	working	1-2.5 + 1-2.5
	c-τ- factory	Bejing	>1999	planned	1.5-3 + 1.5-3
	B-factory			assymetric colliders	
III	PEP-II	SLAC	1999	launched	9 + 3.1
	B-factory	KEK	1999	launched	8 + 3.5
	PETRA	Hamburg	1978	-	5-19 + 5-19
IV	PEP	Stanford	1980	-	5-18 + 5-18
	TRISTAN	KEK	1987	-	25-30 + 25-30
	SLC	SLAC	1989	working	45-50 + 45-50
V	LEP-I	CERN	1989	-	45-47 + 45-47
	LEP-II	CERN	1995	working	65-102 + 65 -102
	TESLA	DESY	> 2005	linear colliders	250-500 + 250-500
VI	NLC	SLAC	> 2005	(projects under	250-500 + 250-500
	JLC	KEK	> 2005	discussions)	250-500 + 250-500

2. Electron-postron annihilation: experiment vs QCD predictions. From the perspective of scanned energy regions, and the physical problems under investigation, all past, present and proposed e^+e^--colliders can be devided into six groups. We present this classification at Table 1, updating the material given in Ref.12 by the new information, gained in part from the materials of Ref.13.

These colliders provide complementary experimental information about the behaviour of $e^+e^- \to hadrons$ total cross-section, at different energies, from machines of different luminosities. Moreover, some important physical problems under investigation necessitate more precise experimental data, not only at high energies, but also in low and intermediate energy regions. Indeed, the study of the letter regions, both by experimental and theoretical methods, may provide better estimates of

$$\Delta\alpha_{had}(q^2) = -\frac{\alpha q^2}{3\pi} Re \int_{4m_\pi^2}^{\infty} ds \frac{R^{e^+e^-}(s)}{s(s-q^2-i\epsilon)} \tag{1}$$

which is the hadronic vacuum-polarization contribution to the value of the effective fine structure constant.

Another important characteristic of the process e^+e^--hadrons was introduced in Ref.14. It concerns the Euclidian Adler D-function

$$D(Q^2) = Q^2 \int_{4m_\pi^2}^{\infty} \frac{R^{e^+e^-}(s)}{(s+Q^2)^2} ds \tag{2}$$

which can be related to Eq.(1) as follows:

$$D(-s) = \frac{3\pi}{\alpha} s \frac{d}{ds} \Delta\alpha_{had}(q^2) \tag{3}$$

The study of this quantity has a number of attractive features. Its behaviour was first analyzed from experimental points of view some times ago 14, 15. In the recnt

work of Ref.16 this problem was reconsidered using a compilation of the available at present most precise e^+e^- data 8[a]. The results are depicted in Fig.1 and Fig.2 where the shaded areas represent the $\pm 1\sigma$ band obtained from the data.

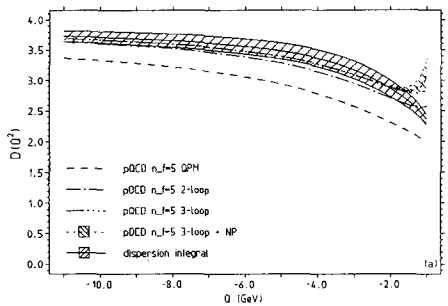

Figure 1: The "experimental" curve for the Adler function together with QCD predictions

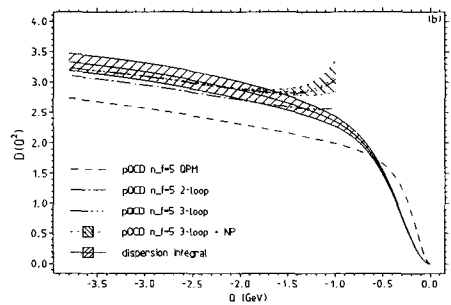

Figure 2: The low energy "experimental" and QCD behaviour of the Adler function

It is interesting to compare the "experimental" behaviour for the D-function with its QCD theoretical expression. One can express it in the following form

$$D^{QCD}(Q^2) = D^{PT}(Q^2) + D^{NP}(Q^2) \tag{4}$$

where the first part is describing the perturbative QCD contributions, while the second term takes account of higher-twist effects, which are related to the vacuum condensates of quarks and gluon fields 18. In the work of Ref.16 we considering the α_s^2 massive dependent expression for $D^{PT}(Q^2)$, namely

$$D^{PT}(Q^2) = D^{(0)}(Q^2) + D^{(1)}(Q^2)\frac{\alpha_s(Q^2)}{\pi} + D^{(2)}(Q^2)(\frac{\alpha_s(Q^2)}{\pi})^2 \tag{5}$$

The Born term expression is well known and has the following form

$$D^{(0)}(Q^2) = 3\sum_f Q_f^2\left(1 - 6x + \frac{12x^2}{\sqrt{1+4x^2}} ln\left[\frac{\sqrt{1+4x}+1}{\sqrt{1+4x}-1}\right]\right) \tag{6}$$

[a]It would be interesting to include in this related analysis the new measurements of $R^{e^+e^-}(s)$ at $\sqrt{s}$ values of 2.6, 3.2, 3.4, 3.55, 4.6 and 5 GeV from BEPC 17

where $x = m_f^2/Q^2$, while m_f is the pole quark mass. The analytic mass-dependent expression for $D^{(1)}$ can be obtained from the calculations of Ref.19, which are in agreement with the results of Ref.20. Since the mass dependence of the 3-loop term $D^{(2)}$ is not yet known analytically, detailed information about its small-mass 21, 22 and heavy-mass 23 expansion was used in Ref.16 to approximate the behaviour of $D^{(2)}$ in the Eucledian region, with high presision using conformal mapping and Padé improvement 24. However, the theoretical expression for mass dependence of the double-bubble three-loop vacuum polarization diagram was not included into the theoretical expression for $D^{(2)}$-term in Ref.16. There are the arguments, based on the calculations of the $(m^2/Q^2)\alpha_s^2$-corrections 21, that this contribution is small.

Table 2: The origin of uncertainties for the "experimental" Adler function at $Q = 2.5\ GeV$ and M_Z

	$D(2.5\ GeV)$	rel. err.	abs. err.	$D(M_Z)$	rel. err.	abs. err
Resonances	.688 (.025)	3.6 %	0.8 %	.004 (.000)	5.2 %	0.0 %
$E < M_{J/\Psi}$	1.068 (.127)	11.9 %	4.2 %	.002 (.000)	14.9 %	0.0 %
$M_{J/\Psi} < E < 3.6\ GeV$	.178 (.035)	19.9 %	1.2 %	.001 (.000)	19.8 %	0.0 %
$3.6\ GeV < E < M_\Upsilon$	.850 (.055)	6.4 %	1.8 %	.032 (.002)	7.0 %	0.1 %
$M_\Upsilon < E < 12\ GeV$	.088 (.008)	8.7 %	0.3 %	.024 (.002)	9.0 %	0.1 %
$E < 12\ GeV$ data	2.871 (.146)	5.1 %	4.8 %	.063 (.003)	4.9 %	0.1 %
$12\ GeV < E$ QCD	.162 (.001)	0.3 %	0.0 %	3.755 (.006)	0.2 %	0.2 %
total	3.033 (.146)	4.8 %	4.8 %	3.818 (.007)	0.2 %	0.2 %

Let us consider the non-perturbative contributions to $D^{NP}(Q^2)$. In Ref.16 the following expression was used

$$
\begin{aligned}
D^{NP}(Q^2) &= 3\sum_f Q_f^2(8\pi^2) \\
&\times \left[\frac{1}{12}\left(1-\frac{11}{18}\frac{\alpha_s(\mu^2)}{\pi}\right)\frac{<\frac{\alpha_s}{\pi}G^2>}{Q^2}\right. \\
&+ 2\left(1+\frac{\alpha_s(\mu^2)}{3\pi}+O(\alpha_s^2)\right)\frac{<m_q\bar{q}q>}{Q^4} \\
&+ \left(\frac{4}{27}\frac{\alpha_s(\mu^2)}{\pi}+O(\alpha_s^2)\right)\sum_{q'}\frac{<m_{q'}\bar{q'}q'>}{Q^4}
\end{aligned}
\tag{7}
$$

The terms beyond leading order in α_s, calculated in the works of Ref.25, turned out to be not so important at the moment, because the curent experimental data for the D-function gives only rough constraints on the contributions of dimension-four condensates, which were varied in Ref.16 within following intervals $<\frac{\alpha_s}{\pi}G^2> \approx (0.336-0.442\ GeV)^4$, $<m_u\bar{u}u> = <m_d\bar{d}d> = -(0.086-0.111\ GeV)^4$, $<m_s\bar{s}s> = -(0.192-0.245\ GeV)^4$. Nevertheless, in Fig.1 and Fig.2 one can see the region, where the addition of the nonperturbative QCD corrections to the three-loop perturbative QCD expression leads to the deviation from the experimentally allowed region for the D-function at low Euclidian momentum transfer, Q^2. It is possible, that taking into account higher-order power corrections 26 might improve the agreement with "experi-

mental data" at low energies, shown in Fig.2. Moreover, it is of real interest to update the previous analysis of the low-energy e^+e^- experimental data (see Refs27, 28) with the help of the QCD Borel sum rule method 18

$$\int_0^\infty R^{th}(s)e^{-s/M^2}ds = \int_0^\infty R^{e^+e^-}(s)e^{-s/M^2}ds \tag{8}$$

In the process of such an analysis, new low-energy experimental data, obtained in part in Novosibirsk, can be used. In the theoretical part of Eq.(8) one should also include perturbative contributions to the coefficients function of quark and gluon condensateseffects of dimension four 25, available from the results of Ref26 higher-dimension condensates, and information about massless α_s^3 contributions to $R^{th}(s)$29. As to the sum-rule analysis of high-energy e^+e^- experimental data, one can update the studies of Ref30, performed with the help of the finite energy sum rules approach

$$\int_0^{s_0} R^{th}(s)ds = \int_0^{s_0} R^{e^+e^-}(s)ds \quad . \tag{9}$$

Concerning the curves for the D-function extracted from the experimental data (see Figs.1,2 of Ref.16), it is worth noting that the theoretical analysis of the recent works 31, 32 result in a description of the low-energy tail of Fig.2 by completely different ideas, related to the concept of "freezing" of the QCD coupling constant at small energies33, 34. These ideas have realizations, distinct from conclusions in Ref35, based on application of the PMS approach36 to the four-loop massless theoretical expresion for $R^{e^+e^-}(s)$. Indeed, it was argued in Ref37, that the observed "perturbative" freezing can be spurious, indicating breakdown of a next-to-next-to-leading PMS expression, around the scale of ρ-meson mass. Note, however, that the low-energy results for the fit of the e^+e^- data on $R^{e^+e^-}(s)$, performed in Ref35 with the help of the proposed in Ref38 sum rule

$$\overline{R}(s,\Delta) = \frac{\Delta}{\pi}\int_0^\infty \frac{R^{e^+e^-}(s')}{(s'-s)^2+\Delta^2}ds' \tag{10}$$

merited serious attention. It should be stressed that the low-energy Novosibirsk data of Ref39 turned out to be essential in this analysis. For example, they served as an ingradient in the phenomenological part of the considerations of Ref40, devoted to the analysis of "analytical" freezing of the QCD coupling constant α_s in the Minkowskian region, and also in Ref41, devoted to the consideration of the Crewther relation 42 and its $\overline{MS}$-scheme QCD generalization 43 using the "commensurate scale relations" 44 (for reviews see 45, 46). It should be recalled that the α_s^3-generalization of the Crewther relation connects a massless α_s^3 theoretical expression for the e^+e^--annihilation D-function 29 with the massless theoretical expressions for the Gross-Llewellyn Smith sum rule of the νN deep-inelastic scattering and Bjorken sum rule of the polarized deep-inelastic scattering, which were calculated at the α_s^3-level in Ref47. This connection involves the first and second terms of the two-loop approximation to the QCD β-function. We will consider this problem in more detail in the next Section.

We now return to the results of Ref.16. Before discussing the comparision of the three-loop massive theoretical QCD predictions for the D-function with the "experimental" behaviour of the D-function at higher transfered momentum it is worth mentioning, that in the process of extracting the "experimental" behaviour of the D-function not all e^+e^- data up to 40 GeV were applied. Indeed, in Ref.16 a con-

servative attitude was adopted: the real data were replaced by perturbative QCD results in certain regions, but only where it is obviously safe to do so. Thus, in the regions from 4.5 GeV to M_Υ and above 12 GeV perturbative QCD results were used, including massive three-loop results 22 and a massless four-loop QCD contributions 29.

The origins of the uncertainties of the "experimental" curves for the D-function were analysed in Ref.16 (see Table 2). The main sources come from the region $E < M_{J/\Psi}$, **accessible for more detailed experimental inspection at VEPP-2M and BEPC**, and the region $M_{J/\Psi} < E < 3.6\ GeV$, **which is privilege of BEPC, VEPP-4** and a possible future $c-\tau$ factory. However, as was shown in Ref.16, even at the current level of experimental precision one can already obtain new information, namely a demonstration of the importance of two-loop heavy-quark mass -dependent effects for the description of the "experimental" behaviour of the D-function at moderate and high Euclidian transfered momentum transfers. Indeed, after including mass effects, both in the three-loop perturbative part of the D-function and also in the two-loop running of the QCD coupling constant α_s from the value of $\alpha_{s,\overline{MS}}(M_Z) = 0.120 \pm 0.003$ to lower energy scales via the proposed in Ref48 variant of momentum subtractions scheme[b] one can observe the appearence of real agreement of the three-loop massive theoretical expression for the D-function with the experimentally-motivated Eucledian curves of Fig.1 and Fig.2. It should be stressed, that if we had not included the three-loop massive term, a discrepancy with the "experimental" behaviour of the D-function might have been interpreted as requiring non-perurbative power corrections from Eq.(7). While the addition of the twist-4 power corrections can be of real importance, the deviation of the two-loop curves from the "experimental" corridor for the D-function at high momentum transfere (see Fig.1) can be associated with the omission of perturbative QCD contributions only. Another interesting observation is that the cuves of Fig.1 and Fig.2 turned out to be rather smooth 16, lacking the resonance enhancements and "threshold steps", typical of the Minkowskian region. In view of this we think that possible future applications and improvements of the results obtained in Ref.16 can be useful for more detailed tests of perturbative and non-perturbative theoretical QCD predictions in the Euclidian region. One such application in presented in the next Section.

3. New tests of the generalized Crewther relation The Crewther relation 42 connects the amplitude of $\pi^0 \to \gamma\gamma$ decay with the product of the e^+e^- annihilation D-finction and deep-inelastic scattering sum rules, namely with Bjorken sum rule of polarized lepton-nucleon scattering

$$\begin{aligned} Bjp(Q^2) &= \frac{1}{6}|\frac{g_A}{g_V}|C_{Bjp}(Q^2) \\ &= \int_0^1 [g_1^{ep}(x,Q^2) - g_1^{en}(x,Q^2)]dx \end{aligned} \tag{11}$$

or with the Gros-Llewellyn Smith sum rule of νN deep-inelastic scattering

$$GLS(Q^2) = 3C_{GLS}(Q^2) = \int_0^1 F_3(x,Q^2)dx \tag{12}$$

[b]For earlier discussions of the advantages of MOM-type schemes, taking into account threshold effects, see Ref49

where the analytical massless perturbative theory expression for the $D(Q^2)$-function is known at the α_s^3-level29, while the massless analytical perturbative theory expressions for $C_{Bjp}(Q^2)$ and $C_{GLS}(Q^2)$ up to α_s^3-corrections are known from the calcultaions of Ref47. It should be stressed that all the quantities we will be interested in are defined in the Euclidian region and all the results were obtained in the $\overline{MS}$-scheme. In this scheme the α_s^3 generalization of the Crewther relation, discovered in Ref43, has the following form:

$$C_{Bjp}(\alpha_s(Q^2))C_D(\alpha_s(Q^2)) = 1 + \frac{\beta^{(2)}(\alpha_s)}{\alpha_s}P(\alpha_s) \tag{13}$$

where $C_D(\alpha_s(Q^2))$ is coefficient function for the Adler D-function, normalized to unity, $\beta^{(2)}(\alpha_s)$ is the two-loop approximation of the QCD β-function and $P(\alpha_s)$ is a polynomial, which starts from α_s and contains two terms. It was suggested in Refs43, 50 that the factorization of the β-function will persist generally, to all perturbative orders, and can be related to the effects of violation of the conformal symmetry in massless QCD. This fact was later proved in Ref51. The theoretical properties of the generalized relation, written down in the $\overline{MS}$-scheme, were discussed in detail in Refs43, 45, 51 and we will avoid their description in this work. However, we will consentrate on some phenomenological applications. It is rather useful to use for this purpose the "commensurate scale relations" 44, which combine the concepte of the effective-charges 52 (or scheme-invariant perturbation theory 53) with variants of the BLM approach 54, 55 allowing one to write the following generalization of the Crewther relation 41 in the region where the heavy-quark masses can be neglected:

$$\frac{1}{3\sum_f Q_f^2}D(Q^2)C_{GLS}(Q_*^2) \approx 1 \tag{14}$$

$$\frac{1}{3\sum_f Q_f^2}D(Q^2)C_{Bjp}(Q_*^2) \approx 1$$

where

$$\begin{aligned} ln\frac{Q_*^2}{Q^2} &= -\frac{7}{2} + 4\zeta_3 \\ &+ \left(\frac{\alpha_{GLS}}{4\pi}\right)\left[\left(\frac{11}{12} + \frac{56}{3}\zeta_3 - 16\zeta_3^2\right)\beta_0 \right. \\ &\left. - \frac{56}{27} - \frac{808}{9}\zeta_3 + \frac{320}{3}\zeta_5\right] \end{aligned} \tag{15}$$

As spiceman physical input we will first use the recently obtained value of the Gross-Llewellyn Smith sum rule 56

$$GLS(12.59\ GeV^2) = 2.80 \pm 0.13 \pm 0.17 \tag{16}$$

which does not contradict to the less presise similar results, obtained using the extrapolation of the data 57. Using the results of Ref58 we conclude, that at this energy region $f = 4$ numbers of flavours are manifesting themselves. Moreover, at momentum transfer $Q_*^2 = 12.59\ GeV^2$ we will neglect c-quark mass effects, which are suppressed by a factor $m_c^2/Q_*^2 < 0.19$. Thus we conclude that the value of the corresponding effective charge is

$$\begin{aligned} \frac{\alpha_{GLS}(Q_*^2)}{\pi} &= 1 - \frac{GLS(Q_*^2)}{3} \\ &= 0.067 \pm 0.043 \pm 0.06 \end{aligned} \tag{17}$$

where the first (second) error is related to the statistical (systematical) uncertainty of the experimental result of Eq.(16). Using Eqs.(14)-(17) one can get the following estimate

$$D(Q \approx 1.8\ GeV) \approx 3.57 \pm 0.3 \tag{18}$$

which crosses the upper part of "experimentally" motivated curve of Fig.2 at this reference scale. A similar conclusion emerges in the case of the analogous treatement of the experimental result of SMC collaboration for the polarized Bjorken sum rule 59, which is

$$\begin{aligned} Bjp(Q^2 = 10\ GeV^2) &= 0.195 \pm 0.029 \\ &= \frac{1}{6}\left|\frac{g_A}{g_V}\right|\left(1 - \frac{\alpha_{Bjp}(Q_*^2)}{\pi}\right) \end{aligned} \tag{19}$$

As a result of application of a discusions of Ref.60 and considerations presented above, we obtain the following estimate for the D-function

$$D(Q \approx 1.6\ GeV) \approx 3.59^{+0.35}_{-0.45} \tag{20}$$

which is in rough agreement with the "experimentally" motivated Euclidian result of Ref.16, though with larger errors.

Of course, our considerations are not so detailed, as the ones, given in Ref.61, where an expression for the coupling constant α_s was extracted from the Bjorken sum rule data (for earlier discussion of this problem see Ref.62). However, we believe, that even approximate tests of the generalized Crewther relation, written down in the form of commensurate scale relations of Ref.41 **directly in the Euclidian region**, giving one the feeling, that the estimates obtained from deep-inelastic sum rule are less precise than direct extraction of the behaviour of D-function in the Euclidian region. This might suggest a need for adding higher-twist terms to the perturbative generalizations of the Crewther relation.

Acknowledgements

It is the pleasure to thank S.I. Eidelman, F. Jegerlehner and O.L. Veretin for the fruitful and plesant collaboration, which resulted in studies of the experimentally motivated and theoretical behaviour of the D-function and S.J. Brodsky, G.T. Gabadadze, H.J. Lu and especially D.J. Broadhurst for sharing their insight during the common derivations of the various forms of the generalized Crewther relation. I am also grateful to D.J. Broadhurst for making some style corrections in the previous draft of this work. I would like to thank I.A. Savin and D.V. Peshekhonov for discussions on the possibility of different applications of the polarized Bjorken sum rules data of the SMC Collaboration.

References

[1] V.L.Auslender, G.I. Budker et al., *Phys.Lett.* **25B** (1967) 433.
[2] J.E. Augustin et al., *Phys. Rev. Lett.* **33** (1974)1406.
[3] J.J. Aubert et al., *Phys. Rev. Lett.* **33** (1974) 1404.
[4] C. Bacci et al., *Phys. Rev. Lett.* **33** (1974) 1408.
[5] P.N. Bogolyubov, N.V. Krasnikov, V.A. Kuzmin and K.G. Chetyrkin, *Fiz. Elem. Chast. Atom. Yadra* **7** (1976) 816.

[6] M.I. Vysotsky, V.A. Novikov, L.B. Okun and A.N. Rozanov, *Phys. Usp.* **39** (1996) 503.
[7] W.J. Marciano, hep-ph/9902332.
[8] S.I. Eidelman and F. Jegerlehner, *Z. Phys.* **C67** (1995) 585; see also: H. Burkhart and B. Pietrzyk, *Phys. Lett.* **B356** (1995) 398.
[9] S.I. Eidelman and F. Jegerlehner, work in progress (1999).
[10] F. Jegerlehner, preprint DESY 99-007 (hep-ph/9901386).
[11] M. Davier and A. Höcker, *Phys. Lett.* **B419** (1998) 419; J.H. Kühn and M. Steinhauser, *Phys. Lett.* **B437** (1998) 425; J.G. Körner, A.A. Pivovarov and K. Schilcher, preprint MZ-TH-98-59 (1998) (hep-ph/9812465); M. Steinhauser, Report BUTP-99/06 (hep-ph/9904373); S. Groote, Report MZ-TH/99-18 (hep-ph/9905373).
[12] S.G. Gorishny, A.L. Kataev and S.A. Larin, Proceedings of the Seminar "Physics of e^+e^- Interactions", Dubna 8-9 December 1987; E2-88-363, p.33.
[13] Talks at the Workshop "Bruno Toschek and the birth of e^+e^- physics", Frascati, November 16, 1998.
[14] S. Adler, *Phys. Rev.* **D10** (1973) 3714.
[15] A. De Rujula and H. Georgi, *Phys. Rev.* **D13** (1976) 1296.
[16] S. Eidelman, F. Jegerlehner, A.L. Kataev and O. Veretin, *Phys. Lett.* **B454** (1999) 369.
[17] BES Collaboration, J.Z. Bai et al, hep-ex/9908046.
[18] M.A. Shifman, A.I. Vainshtein and V.I. Zakharov, *Nucl. Phys.* **B147** (1979) 385.
[19] F. Jegerlenher, *Prog. Part. Nucl. Phys.* **71** (1991) 1, Sec. 4.5.
[20] B.A. Kniehl, *Nucl. Phys.* **B347** (1990) 86.
[21] S.G. Gorishny, A.L. Kataev and S.A. Larin, *Nuov. Cim.* **92A** (1986) 119.
[22] K.G. Chetyrkin, R. Harlander, J.H. Kühn and M. Steinhauser, *Nucl. Phys.* **B503** (1997) 339.
[23] K.G. Chetyrkin, J.H. Kühn and M. Steinhauser, *Nucl. Phys.* **B482** (1996) 213.
[24] J. Fleischer and O.V. Tarasov, *Z. Phys.* **C64** (1994) 413.
[25] K.G. Chetyrkin, S.G. Gorishny and V.P. Spiridonov, *Phys. Lett.* **160B** (1985) 149; V.P. Spiridonov and K.G. Chetyrkin, *Sov. J. Nucl. Phys.* **47** (1988) 522; L.R. Surguladze and F.V. Tkachov, *Theor. Math. Phys.* **75** (1988) 502; *Nucl. Phys.* **B331** (1990) 35.
[26] S.G. Generalis and D.J. Broadhurst, *Phys. Lett.* **139B** (1984) 85; D.J. Broadhurst and S.G. Generalis, *Phys. Lett.* **165B** (1985) 175; A.G. Grozin and Yu. F. Pinelis, *Phys. Lett.* **166B** (1986) 429; *Zeit. Phys.* **C33** (1987) 419; L.V. Lanin, V.P. Spiridonov and K.G. Chetyrkin, *Yad. Fiz.* **44** (1986) 1372.
[27] S.I. Eidelman, L.M. Kurdadze and A.I. Vainshtein, *Phys. Lett.* **82B** (1979) 278.
[28] A.G. Grozin and Yu. F. Pinelis, *Mod. Phys. Lett.* **A3** (1988) 725.
[29] S.G. Gorishny, A.L. Kataev and S.A. Larin, *Phys. Lett.* **B259** (1991) 144; *JETP Lett.* **53** (1991) 127; L.R. Surguladze and M.A. Samuel, *Phys. Rev. Lett.* **66** (1991) 560; ibid. 2416 (Err.); K.G. Chetyrkin, *Phys. Lett.* **B391**

(1997) 402.
[30] V.A. Kuzmin, A.N. Tavkhelidze and K.G. Chetyrkin, *Pisma Zh. Eksp. Teor. Fiz.* **25** (1977) 456; K. G. Chetyrkin, A.N. Tavkhelidze and N.V. Krasnikov, *Phys. Lett.* **76B** (1978) 83.
[31] D.V. Shirkov and I.L. Solovtsov, talk at this Workhop (hep-ph/9906495).
[32] B.V. Geshkenbein and B.L. Ioffe, hep-ph/9906406.
[33] D.V. Shirkov and I.L. Solovtsov, *Phys. Rev. Lett.* **79** (1997) 1209.
[34] Yu.L. Dokshitzer, G. Marchesini and B.R. Webber, *Nucl. Phys.* **B469** (1996) 93.
[35] A.C. Mattingly and P.M. Stevenson, *Phys. Rev.* **D49** (1994).
[36] P.M. Stevenson, *Phys. Rev.* **D23** (1981) 2916.
[37] J. Chýla, A.L. Kataev and S.A. Larin, *Phys. Lett.* **B267** (1991) 269.
[38] H. Poggio, H. Quinn and S. Weinberg, *Phys. Rev.* **D13** (1976) 1958.
[39] OLYA/CMD Collab., L.M. Barkov et al., *Nucl. Phys.* **B256** (1985) 365.
[40] I.L. Solovtsov and D.V. Shirkov, *Phys. Lett.* **B442** (1998) 344.
[41] S.J. Brodsky, G.T. Gabadadze, A.L. Kataev and H.J. Lu, *Phys. Lett.* **B372** (1996) 133.
[42] R.J. Crewther, *Phys. Rev. Lett.* **28** (1972) 1421.
[43] D. J. Broadhurst and A.L. Kataev, *Phys. Lett.* **B315** (1993) 179.
[44] S.J. Brodsky and H.J. Lu, *Phys. Rev.* **D51** (1995) 3652.
[45] A.L. Kataev, Proc. II Workshop "Contenuous Advances in QCD", Minneapolis, March 1996, WorldScientific 1996, p. 107 (hep-ph/9607426).
[46] S.J. Brodsky and J. Rathsman, preprint SLAC-PUB-8176 (1999) (hep-ph/9906339).
[47] S.A. Larin and J.A.M. Vermaseren, *Phys. Lett.* **B259** (1991) 345.
[48] F. Jegerlehner and O.V. Tarasov, *Nucl. Phys.* **B549** (1999) 481.
[49] D.V. Shirkov, *Theor. Math. Phys.* **93** (1992) 1403; D.V. Shirkov and S.V. Mikhailov, *Z. Phys.* **C63** (1994) 463.
[50] G.T. Gabadadze and A.L. Kataev, *JETP Lett.* **61** (1995) 448;
[51] R.J. Crewther, *Phys. Lett.* **B397** (1997) 137.
[52] G. Grunberg, *Phys. Lett.* **B95** (1980) 70; *Phys. Rev.* **D29** (1984) 2315.
[53] A. Dhar and V. Gupta, *Phys. Rev.* **D29** (1984) 2822; V. Gupta, D.V. Shirkov and O.V. Tarasov, *Int. J. Mod. Phys.* **A6** (1991) 3381.
[54] S.J. Brodsky, G.P. Lepage and P.B. Mackenzie, *Phys. Rev.* **D28** (1983) 228.
[55] G. Grunberg and A.L. Kataev, *Phys. Lett.* **B279** (1992) 352.
[56] CCFR-NuTeV Collab., J.H. Kim, D.A. Harris et al., *Phys. Rev. Lett.* **81** (1998) 3595.
[57] A.L. Kataev and A.V. Sidorov, *Phys. Lett.* **B331** (1994) 179.
[58] J. Chýla nad A.L. Kataev, *Phys. Lett.* **B297** (1992) 385.
[59] SMC Collab., B. Adeva et al., *Phys. Lett.* **B412** (1997) 414.
[60] K.A. Milton, I.L. Solovtsov and O.P. Solovtsova, *Phys. Lett.* **B439** (1998) 421.
[61] G. Altarelli, R.D. Ball, S. Forte and G. Ridolfi, *Nucl. Phys.* **B496** (1997) 337.
[62] J. Ellis, E. Gardi, M. Karliner and M.A. Samuel, *Phys. Rev.* **D54** (1996) 6986.

PERTURBATION THEORY WITH CONVERGENT SERIES FOR LARGE VALUES OF COUPLING CONSTANT: A CALCULATION OF β-FUNCTION IN φ^4 MODEL

V. V. Belokurov[a], E. T. Shavgulidze[b], Yu. P. Solov'yov[c], I. L. Yudin[d]
Physics Faculty of Moscow State University, 119899 Moscow, Russia

Abstract. A new perturbation theory with convergent series is used to calculate quantities given by a finite number of terms of the traditional perturbation theory. As examples of such a problem, the zero-dimensional analog of a functional integral and β-function in $g\varphi^4$ model in four-dimensional space-time are considered. The results obtained demonstrate high accuracy of the calculation in a wide region of coupling constant values.

Introduction

It is well known that perturbation series used in quantum physics are nothing but asymptotic expansions in powers of some parameter (i. g. coupling constant) and therefore are well-defined for sufficiently small values of the parameter only.

A new approach has been developed in 1-8 to the problem of summation of divergent series and evaluation of functional integrals. In this approach, the quantity under investigation can be approximated with any given accuracy by an absolutely convergent series.

It is a notable feature of this method that if the coefficients of asymptotic expansion and the expanded function $f(g)$ itself satisfy certain conditions (see below), the value of $f(g)$ can be restored with high precision for all values of the expansion parameter, even if only a few terms of traditional perturbation theory are known.

1 The Method

Consider a class of divergent series of the form

$$\sum_{n=0}^{\infty} f_n(-g)^n \ . \tag{1}$$

We assume this class posessing the following three properties (A)-(C):

(A) The coefficients f_n satisfy the condition

$$f_n \sim C\, n! a^n n^b \ , \qquad n > N_0 \ ,$$

where a, b and C are some positive constants.

(B) The series (1) is the Taylor expansion of the function $f(g)$ at the point $g = 0$. The function $f(g)$ is continuously differentiable for $g \geq 0$ and has an analytical

[a]e-mail: belokur@rector.msu.ru
[b]e-mail: shav@
[c]e-mail: solo@
[d]e-mail: elieyudin@mail.ru

continuation to the right half-plane $\mathrm{Re}\, g > 0$. *The following estimation is also holds even in* $g \in G$, $G = \{g : \mathrm{Re}\, g > 0\}$:

$$|f(g) - \sum_{n=0}^{N-1} f_n g^n| < C_1^N N! N^\alpha g^N .$$

(C) Represent $f(g)$ *in the form*

$$f(g) = \int_0^\infty e^{-gt} F(t)\, dt , \tag{2}$$

where $F(t)$ *is a distribution. The following inequality should hold:*

$$\int_0^\infty x^n |F(x)|\, dx \leq \mathrm{const} \left| \int_0^\infty x^n F(x)\, dx \right| , \qquad n \geq 0 .$$

Introduce the function

$$\tilde{\varphi}_m(\rho) = \frac{1}{2\pi} \int_{-\infty}^{+\infty} \exp\{-i\rho r\} \exp\{-r^{2m}\}\, dr , \tag{3}$$

where m is some positive integer number.

Now represent the exponent in (2) as the inverse Fourier transformation of the functon $\tilde{\varphi}(\rho)$:

$$e^{-gt} = \int_{-\infty}^{+\infty} \tilde{\varphi}(\rho) \exp\{i\rho g^{1/2m} t^{1/2m}\}\, d\rho . \tag{4}$$

Introducing a cut-off parameter R in the integral in ρ and expanding the exponent $\exp\{-i\rho g^{1/2m} t^{1/2m}\}$, one can obtain instead of (2) an absolutely convergent series for a regularized function $f(g, R)$,

$$f(g, R) = \sum_{n=0}^{\infty} \frac{(-1)^n}{(2n)!} g^{\frac{n}{m}} B_{\frac{n}{m}} A_{2n}(R) , \tag{5}$$

where we denote

$$A_{2n}(R) = \frac{1}{\pi} \int_{-R}^{+R} \tilde{\varphi}(\rho) \rho^{2n}\, d\rho ,$$

$$B_\alpha = \int_0^\infty x^\alpha F(x)\, dx .$$

Obviously, $f(g, R)|_{R\to\infty} \to f(g)$.

To decrease the number of the coefficients f_k of the original perturbation theory series (1) effectively used to evaluate the value of $f(g)$ in case of $g \geq 1$, one may re-expand the regularized function $f(g, R)$ in inverse powers of g. With this goal, substitute $\rho \to g^{-1/2m} \rho$ and expand the exponent in the integrand of (3), that yields

$$f(g, R) = \frac{1}{4\pi m} \sum_{n=0}^{\infty} \frac{(-1)^n}{(2n)!} g^{-\frac{2n+1}{2m}} E_{2n}(m, R) , \tag{6}$$

where

$$E_{2n}(m,R) = \frac{1}{2\pi m}\sum_{k=0}^{\infty}\frac{(-1)^k}{(2k)!}\Gamma\left(\frac{2k+1}{2m}\right)\frac{2R^{2n+2k+1}}{2n+2k+1}B_{\frac{k}{m}} .$$

Since the formula (6) is nothing but re-expansion of the original formula, it is no wonder that the values of $f(g)$ obtained with (5) and (6) coincide. Naturally, the values of R differ in this two cases.

The function $f(g)$ now can be approximated with any given accuracy by the function $f(g,R,N)$, which is a sum of the first N terms in (5) and (6) for g small, $(g<1)$, and g large, $(g \geq 1)$, respectively.

The coefficients $B_{k/m}$ with integer indices $k/m = n$ are nothing but the coefficients f_n of the original series (1). An evaluation of the coefficients with non-integer indices raises a separate problem within this approach. A method has been proposed in 5, 8, allowing to calculate the coefficients B_α with noninteger α as a solution of a system of approximative nonlinear algebraic equations. For the case $m = 4$, it looks like

$$\left(B_{\frac{n-1}{4}}\right)^{9/16}\left(B_{\frac{n}{4}}\right)^{9/16}\left(B_{\frac{n-2}{4}}\right)^{-1/16}\left(B_{\frac{n+1}{4}}\right)^{-1/16} \approx$$

$$C(n)\sum_{k=0}^{4N-1}\frac{(-1)^k}{(2k)!}\frac{a^{2k-2n+1}}{2k-2n+1}B_{\frac{k}{4}} , \tag{7}$$

where

$$C(n) = \frac{(-1)^n\, 2\,(2n-1)!}{\pi} ,$$

and a is a free parameter which has to be choosen to minimize the error of (7).

The following considerations allow to obtain an appropriate value of the parameter R. When g is fixed and $R, N \to \infty$, the regularized finite sum $f(g,R,N) \to f(g)$. If N is fixed also, $f(g,R,N)$ is a polynomial in R of degree $4mN+1$ and there is $\varepsilon = \varepsilon(g,N)$, such that within an interval Δ_R of the values of R function $f(g,R,N)$ approximates $f(g)$ within an error not exceeding ε. According to our numerical analysis, with $N = 4, 5$ and $0 \leq g \leq 20$ an interval Δ_R such that the error of the approximation $\delta_f \leq 0.1$, does exist. As an approximative value of $f(g)$ one may take the quantity

$$\bar{f}(g) = 1/2|\max_{\Delta_R} f(g,R,N) + \min_{\Delta_R} f(g,R,N)| .$$

An error obviously is

$$\delta_f = 1/2|\max_{\Delta_R} f(g,R,N) - \min_{\Delta_R} f(g,R,N)| .$$

Such a method can be applied in case of g small as well as in case of g large.

2 Examples

2.1 *Zero-dimensional analog of a functional integral*

Consider a zero-dimensional analog of the functional integral which appears in the $g\varphi^4$ quantum field theory:

$$I(g) = \int_{-\infty}^{+\infty} e^{-x^2 - gx^4}\, dx = \exp\left\{\frac{1}{8g}\right\} K_{\frac{1}{4}}\left(\frac{1}{8g}\right) \frac{1}{\sqrt{4g}} \,.$$

The corresponding asymptotic series diverges:

$$I(g) = \sum_{k=0}^{\infty} a_k (-g)^k, \qquad a_k = \frac{1}{k!}\frac{1}{2^{4k}}\frac{(4k)!}{(2k)!} \,. \tag{8}$$

In this case, for the coefficients $B_{k/m}$ of (5) (and (6)) an analytical expression can be obtained,

$$B_{\frac{k}{m}} = \Gamma\left(\frac{4k+2}{2m}\right) \,. \tag{15}$$

Making use of this fact we have compared the exact values of $B_{k/4}$ and approximative ones $\tilde{B}_{k/4}$ obtained by the method mentioned above . The results are shown in the Table 1.

Table 1

k	$B_{k/4}$	$\tilde{B}_{k/4}$	$\frac{\lvert B_{k/4}-\tilde{B}_{k/4}\rvert}{B_{k/4}}$
5	2	1.957	0.0214
6	3.323	3.281	0.01269
7	6	5.89	0.0184
9	24	24.494	0.0206
10	52.343	54.175	0.035
11	120	123.804	0.03817
13	720	693.432	0.0369

The result of the comparison between the exact values of the integral and approximative ones, calculated in the region $0 < g \leq 20$ is shown in the Fig. 2. The values of m and N was choosen 4 and 5 respectively, and the approximative values of $B_{k/4}$ was used. Within the whole region of the values of g considered, the error of the approximation $\delta_f \leq 0.01$ in the whole region.

2.2 *β-function of $g\varphi^4$ model in four-dimensional space-time*

The first five terms of the series for the β-function in $g(\varphi^a\varphi^a)^2$, $(a = 1, 2)$ model, being calculated in the MS-scheme, are the following 10, 9:

$$\beta^{MS}(g) \simeq \frac{5}{3}g^2 - \frac{10}{3}g^3 + 20.043\, g^4 - 175.257\, g^5 + 1922.33\, g^6 \,.$$

The method described above can be applied to the function $f(g) = \exp\{-\beta(g)/g\}$. Expanding $f(g)$ and leaving the first six terms, we obtain

$$f(g) = 1 - 1.6667\, g + 4.7222\, g^2 - 26.3705\, g^3 + 219.17\, g^4 - 2321.02\, g^5 \,.$$

Table 2 shows the coefficients $B_{k/4}$ obtained by solving the system (7).

Table 2

α	B_α	α	B_α	α	B_α
1/4	1.0	7/4	5.445	14/4	858.3
2/4	1.1	9/4	17.532	15/4	2097.9
3/4	1.31	10/4	34.609	17/4	13526
5/4	2.273	11/4	72.21	18/4	36010
6/4	3.380	12/4	361.8	19/4	98800

The result of the calculation of β-function for $0 \leq g \leq 20$ is presented in the Fig. 3. The error $\delta_f \leq 0.1$ for all g considered.

References

[1] V. V. Belokurov, E. T. Shavgulidze, Yu. P. Solovyev, *Mod. Phys. Lett.* **A10**, 39, 3033, (1995).

[2] V. V. Belokurov, V. V. Kamchatny, E. T. Shavgulidze, Yu. P. Solovyev, *Mod. Phys. Lett.* **A12**, 10, 661, (1997).

[3] V. V. Belokurov, Yu. P. Solovyev, E. T. Shavgulidze, *Teor. Mat. Fiz.*, **109**, 51, (1996).

[4] V. V. Belokurov, Yu. P. Solovyev, E. T. Shavgulidze, *Fund. Pricl. Mat.*, **3**, 3, 693, (1997).

[5] V. V. Belokurov, Yu. P. Solovyev, E. T. Shavgulidze, *Fund. Pricl. Mat.*, **5**, 2, 363, (1999).

[6] V. V. Belokurov, Yu. P. Solovyev, E. T. Shavgulidze, *Uspechi. Mat. Nauk*, **52**, 2, 153, (1997).

[7] V. V. Belokurov, Yu. P. Solovyev, E. T. Shavgulidze, *Uspechi. Mat. Nauk*, **53**, 3, 153, (1999).

[8] V. V. Belokurov, E. T. Shavgulidze, Yu. P. Solovyev, *Teor. Mat. Fiz.*, **123**, 3, 452, (2000).

[9] S. G. Gorishny et al., *Phys. Lett.* **B132**, 351, (1983).

[10] D. I. Kazakov, *Phys. Lett.* **B133**, 406, (1983).

[11] D. V. Shirkov//KEK Report 91–13, (1992).

TWO-DIMENSIONAL QCD AND INSTANTON CONTRIBUTION

A. BASSETTO, F. VIAN
Dipartimento di Fisica "G. Galilei", INFN, Sezione di Padova,
Via Marzolo 8, 35131 Padua, Italy
L. GRIGUOLO
Dipartimento di Fisica "M. Melloni", INFN, Gruppo Collegato di Parma,
Viale delle Scienze, 43100 Parma, Italy

*Abstract.*In these notes Yang-Mills theories in $1+1$ dimensions are reviewed. Instantons on a sphere prove to be —in the decompactification limit— the key issue to clarify an old controversy between equal-time and light-front quantization.

1 INTRODUCTION

In the past few years a large amount of efforts has been devoted to two-dimensional gauge theories (YM_2), mainly motivated by the possibility of exact solutions which are believed to share features with the real four-dimensional world.

Although YM_2 seems trivial when quantized in the light-cone gauge, still topological degrees of freedom occur if the theory is put on a (partially or totally) compact manifold, whereas the simpler behaviour enforced by the light-cone gauge condition on the plane entails a severe worsening in its infrared structure. One can say that, in light-cone gauge, dynamics gets hidden in the very singular nature of correlators at large distances (IR singularities).

The first quantity that comes to mind is the two-point correlator. If the theory is quantized in the gauge $A_- = 0$ at *equal-times*, the free propagator has the following causal expression (WML prescription) in two dimensions

$$D^{WML}_{++}(x) = \frac{1}{2\pi}\frac{x^-}{-x^+ + i\epsilon x^-}, \qquad x^\pm = \frac{x^0 \pm x^1}{\sqrt{2}}, \tag{1}$$

first proposed by T.T. Wu [1]. In turn this propagator is nothing but the restriction in two dimensions of the expression proposed by S. Mandelstam and G. Leibbrandt [2] in four dimensions and derived by means of a canonical quantization in ref. [3].

In dimensions higher than two, where "physical" degrees of freedom are switched on (transverse "gluons"), causality is mandatory in order to get correct analyticity properties, which in turn are the basis of any consistent renormalization program, and to obtain agreement with Feynman gauge results [4].

The situation is somewhat different in exactly two dimensions. Here the theory can be quantized on the *light-front* (at equal x^+); with such a choice, no dynamical degrees of freedom occur as the non-vanishing component of the vector field does not propagate

$$D^P_{++}(x) = -\frac{i}{2}|x^-|\,\delta(x^+), \tag{2}$$

but rather gives rise to an instantaneous (in x^+) Coulomb-like potential.

A formulation based essentially on the potential in Eq. (2) was originally proposed by G. 't Hooft in 1974 [5], to derive beautiful solutions for the $q\bar{q}$-bound state problem under the form of rising Regge trajectories. On the other hand, when Wu's prescription is adopted, the bound state equation at large-N turns out to be very difficult,

and Regge trajectories disappear. A suitable tool to clarify the origin of this discrepancy is the Wilson loop, owing to its gauge invariance and to its reasonable infrared properties.

2 WILSON LOOP ON THE PLANE

When inserted in perturbative Wilson loop calculations, expressions Eqs. (1) and (2) lead to completely different results. In two dimensions pure-area exponentiation is expected. This is due to the invariance of the theory under area-preserving diffeomorphisms, which suggests that the Wilson loop is a function of the dimensionless quantity $g^2\mathcal{A}$, with $\mathcal{A}$ the encircled area, and to unitary evolution.

If a rectangle with light-like sides is chosen as a contour, with 't Hooft potential only planar diagrams can be built, for any value of N. Therefore the perturbative series is easily resummed leading to the expected result [a]

$$W[\mathcal{A}] = \exp\left(-\frac{1}{2}C_F g^2 \mathcal{A}\right) , \tag{3}$$

where C_F is the quadratic Casimir operator for the fundamental representation, *i.e.* $\frac{N^2-1}{2N}$, $\frac{N}{2}$ for $SU(N)$, $U(N)$, respectively. Confinement holds and, in the 't Hooft limit $N \to \infty$, $g^2 N$ fixed, Eq. (3) exhibits a finite string tension.

When the propagator is endowed with the causal prescription Eq. (1), instead, disagreement with the result Eq. (3) already shows up at order $\mathcal{O}(g^4)$, and is due to graphs with crossed vector propagators which produce a contribution proportional to $C_F C_A$, C_A being the Casimir of the adjoint representation. Although non-trivial, resummation of the perturbative series at all orders in the coupling constant g is still possible. This was performed in [6]: once a circular contour is chosen, geometry factorizes out and the task of determining the Wilson loop reduces to the purely combinatorial problem of finding the group factors corresponding to the Wick contractions. Fortunately these factors are generated by a matrix integral in the space of hermitian (traceless) $N \times N$ matrices for $U(N)$ ($SU(N)$). The result for $U(N)$ reads

$$\mathcal{W} = \frac{1}{N}\exp\left[-\frac{g^2\mathcal{A}}{4}\right] L^{(1)}_{N-1}(g^2\mathcal{A}/2) , \tag{4}$$

the function $L^{(1)}_{N-1}$ being a generalized Laguerre polynomial. In addition to the extra polynomial appearing in Eq. (4), the string tension turns out to be different from the one in Eq. (3). More dramatically, Eq. (4) in the 't Hooft limit becomes

$$\lim_{N\to\infty} \mathcal{W} = \sqrt{\frac{2}{\hat{g}^2\mathcal{A}}} J_1\left(\sqrt{2\hat{g}^2\mathcal{A}}\right) , \tag{5}$$

where $\hat{g}^2 = g^2 N$, and confinement is lost, thereby explaining the failure of Wu's spectrum.

We are now standing before two different scenarios and there is apparently no motivation to prefer one to the other, since both 't Hooft's and Wu's results are analytic in g^2. The need for reconciliation becomes urgent.

[a] in the Euclidean formulation

3 THE INSTANTON EXPANSION

In order to gain a deeper insight, it is worthwhile to study the problem on a compact two-dimensional manifold [7]. Let it be the sphere for simplicity. Therein the procedure is purely geometrical and group-theoretical, so that no gauge-fixing has to be adopted and infra-red problems are absent.

The starting point are the well-known expressions [8] of the exact partition function and of a Wilson loop for a pure $U(N)$ Yang-Mills theory on a sphere S^2 with area A

$$\mathcal{Z}(A) = \sum_R (d_R)^2 \exp\left[-\frac{g^2 A}{4} C_2(R)\right], \tag{6}$$

$$\begin{aligned} \mathcal{W}(A-\mathcal{A},\mathcal{A}) &= \frac{1}{\mathcal{Z}N}\sum_{R,S} d_R\, d_S \int dU \mathrm{Tr}\,[U]\,\chi_R(U)\chi_S^\dagger(U) \\ &\times \exp\left[-\frac{g^2(A-\mathcal{A})}{4}C_2(R) - \frac{g^2\mathcal{A}}{4}C_2(S)\right], \end{aligned} \tag{7}$$

$d_{R(S)}$ being the dimension of the irreducible representation $R(S)$ of $U(N)$; $C_2(R)$ ($C_2(S)$) is the quadratic Casimir, $A-\mathcal{A},\mathcal{A}$ are the areas singled out by the loop, the integral in Eq. (7) is over the $U(N)$ group manifold and $\chi_{R(S)}$ is the character of the group element U in the $R(S)$ representation. In order to evaluate $\mathcal{W}(\mathcal{A}-\mathcal{A},\mathcal{A})$ in the decompactification limit, for $N>1$ Eqs. (6), (7) can be explicitly written in the form

$$\begin{aligned} \mathcal{Z}(A) = \frac{1}{N!}\exp\left[-\frac{g^2 A}{48}N(N^2-1)\right] \sum_{m_i=-\infty}^{+\infty} \Delta^2(m_1,...,m_N) \\ \times \exp\left[-\frac{g^2 A}{4}\sum_{i=1}^{N}\left(m_i - \frac{N-1}{2}\right)^2\right], \end{aligned} \tag{8}$$

$$\begin{aligned} \mathcal{W}(A-\mathcal{A},\mathcal{A}) &= \frac{1}{\mathcal{Z}NN!}\exp\left[-\frac{g^2 A}{48}N(N^2-1)\right] \\ &\times \sum_{k=1}^{N}\sum_{m_i=-\infty}^{+\infty} \Delta(m_1,...,m_N)\Delta(m_1+\delta_{1,k},...,m_N+\delta_{N,k}) \\ &\times \exp\left[-\frac{g^2(A-\mathcal{A})}{4}\sum_{i=1}^{N}\left(m_i-\frac{N-1}{2}\right)^2\right. \\ &\left. -\frac{g^2\mathcal{A}}{4}\sum_{i=1}^{N}\left(m_i-\frac{N-1}{2}+\delta_{i,k}\right)^2\right]. \end{aligned} \tag{9}$$

In the previous formulae the generic irreducible representation has been described by means of the set of integers $m_i = (m_1,...,m_N)$, related to the Young tableaux, in terms of which one gets

$$C_2(R) = \frac{N}{12}(N^2-1) + \sum_{i=1}^{N}\left(m_i - \frac{N-1}{2}\right)^2,$$

$$d_R = \Delta(m_1, ..., m_N). \tag{10}$$

Δ is the Vandermonde determinant and the integration in Eq. (7) has been performed explicitly, using the well-known formula for the characters in terms of the set m_i.

Now, as first noted by Witten[9], it is possible to represent $\mathcal{Z}(A)$ —and consequently $\mathcal{W}(A-\mathcal{A},\mathcal{A})$— as a sum over instable instantons, each instanton contribution being associated to a finite, non-trivial, perturbative expansion. One can observe that in the sum over $\{m_i\}$ the dependence on the area is through the dimensionless quantity g^2A, whereas an instanton action typically depends on $\frac{1}{g^2A}$. Therefore a duality transformation is required to turn the fraction upside down. The mathematical tool to carry out such a task is provided by a Poisson resummation [10] over $\{m_i\}$

$$\sum_{m_i=-\infty}^{+\infty} F(m_1, ..., m_N) = \sum_{n_i=-\infty}^{+\infty} \tilde{F}(n_1, ..., n_N), \tag{11}$$

$$\tilde{F}(n_1, ..., n_N) = \int_{-\infty}^{+\infty} dz_1 ... dz_N e^{[2\pi i(z_1 n_1 + ... + z_N n_N)]} F(z_1, ..., z_N).$$

When performed in Eqs. (8), (9), it gives

$$\mathcal{Z}(A) = C(g^2A, N) \sum_{n_i=-\infty}^{+\infty} \exp\left[-S_{inst}(n_i)\right] Z(n_1, ..., n_N),$$

$$\mathcal{W}(A-\mathcal{A},\mathcal{A}) = \frac{1}{\mathcal{Z}N} C(g^2A, N) \exp\left[-g^2 \frac{A(A-\mathcal{A})}{4A}\right] \tag{12}$$

$$\times \sum_{n_i=-\infty}^{+\infty} \exp\left[-S_{inst}(n_i)\right] \sum_{k=1}^{N} \exp\left[-2\pi i n_k \frac{A-\mathcal{A}}{A}\right] W_k(n_1, ..., n_N),$$

where

$$S_{inst}(n_i) = \frac{4\pi^2}{g^2A} \sum_{i=1}^{N} n_i^2. \tag{13}$$

Finally, $S_{inst}(n_i)$ is interpreted as an instanton action [b], while $Z(n_1, ..., n_N)$ and $W_k(n_1, ..., n_N)$ are the quantum corrections around the classical solutions [11].

From the above representations it is rather clear why the decompactification limit $A \to \infty$ should not be performed too early. As a matter of fact, on the plane fluctuations around the instanton solutions are undistinguishable from Gaussian fluctuations around the trivial field configuration, since $S_{inst}(n_i)$ goes to zero for any finite set n_i when $A \to \infty$. For finite A and finite n_i instead, in the limit $g \to 0$, only the zero-instanton sector can survive in the Wilson loop expression.

4 RELATION WITH PERTURBATION THEORY

In principle the zero-instanton contribution should be obtainable by means of perturbative calculations. If in Eqs. (12), (13) only the zero-instanton sector, *i.e.* $n_i = 0$, is

[b] Indeed, on S^2 there are non-trivial solutions of the Yang-Mills equation, labelled by the set of integers $\{n_i\} = (n_1, \ldots, n_N)$ (see [11]).

retained, after some technicalities the following result is found [11]

$$\mathcal{W}^{(0)} = \frac{1}{N} \exp\left[-g^2 \frac{\mathcal{A}(A-\mathcal{A})}{4A}\right] L^1_{N-1}\left(g^2 \frac{\mathcal{A}(A-\mathcal{A})}{2A}\right) . \tag{14}$$

At this point a remark is in order: in the decompactification limit $A \to \infty$, $\mathcal{A}$ fixed, the quantity in the equation above *exactly* coincides, for any value of N, with Eq. (4), which was derived from a matrix model. Hence, the zero-instanton contribution corresponds in a sense to "integrating over the group algebra".

5 THE WILSON LOOP WITH WINDING NUMBER n

Disagreement of Eq. (14) with the pure-area exponentiation is at this stage no longer surprising since $\mathcal{W}^{(0)}$ does not contain any genuine non-perturbative contribution, *viz* instantons. For any value of N the pure-area exponentiation follows, after decompactification, from resummation of all instanton sectors, changing completely the zero-sector behaviour and, in particular, the value of the string tension.

What might instead be unexpected in this context is the fact that, using the instantaneous 't Hooft potential and just resumming at all orders the related perturbative series, one still ends up with the correct pure-area exponentiation.

This is true also in more general instances, such as Wilson loops winding n times on a closed contour [12]. For a pure $U(N)$ Yang-Mills theory on a sphere S^2 with area A it holds

$$\mathcal{W}_n(A-\mathcal{A},\mathcal{A}) = \frac{1}{\mathcal{Z}N} \sum_{R,S} d_R\, d_S \int dU \mathrm{Tr}[U^n] \chi_R(U) \chi^\dagger_S(U)$$
$$\times \exp\left[-\frac{g^2(A-\mathcal{A})}{4} C_2(R) - \frac{g^2\mathcal{A}}{4} C_2(S)\right] , \tag{15}$$

the notation being as in Eq. (7). It can be shown that in the decompactification limit $A \to \infty$, $\mathcal{A}$ fixed, the following expression is recovered

$$\mathcal{W}_n(\mathcal{A};N) = \frac{1}{nN} \exp\left[-\frac{g^2\mathcal{A}}{4} n(N+n-1)\right] \tag{16}$$
$$\times \sum_{k=0}^{+\infty} \frac{(-1)^k}{k!} \frac{\Gamma(N+n-k)}{\Gamma(N-k)\Gamma(n-k)} \exp\left[\frac{g^2\mathcal{A}}{2} n\, k\right] .$$

The series is actually a finite sum, stopping at $k = n-1$ or $k = N-1$, depending on the smaller one. As happened for $n = 1$, Eq. (16) is expected to come out from the resummation of 't Hooft perturbative series, that corresponds to a light-front quantization of the theory. Some comments are now in order. First of all notice that when $n > 1$ the simple abelian-like exponentiation is lost. In other words the theory starts to feel its non-abelian nature and the combinatorial coefficients in Eq. (16) signal that the light-front vacuum, though simpler than its analog in the equal-time quantization, cannot be considered trivial. Actually, from the sphere point of view, Eq. (16) can be understood as coming from an instantons' resummation. The procedure to see this is exactly the one outlined above for the case $n = 1$. On the

other hand to neglect instantons, and then to send the area of the sphere to infinity, is likely to reproduce the WML computation. In fact the perturbative analysis have confirmed these claims. Furthermore, Eq. (16) exhibits an intriguing duality

$$\mathcal{W}_n(\mathcal{A};N) = \mathcal{W}_N\left(\frac{n}{N}\mathcal{A};n\right) , \tag{17}$$

a relation that is far from being trivial, involving an unexpected interplay between the geometrical and the algebraic structure of the theory. Looking at Eq. (17), the abelian-like exponentiation for $U(N)$ when $n = 1$ appears to be connected to the $U(1)$ loop with N windings, the "genuine" triviality of Maxwell theory providing the expected behaviour for the string tension. Finally, one should observe that the large-N limit (with n fixed) is equivalent to the limit in which an infinite number of windings is considered with vanishing rescaled loop area. Alternatively, this rescaling could be thought to affect the coupling constant $g^2 \to \frac{n}{N}g^2$. In detail, the former limit ($N \to \infty$, $\hat{g}^2 = g^2 N$ fixed) coincides with the Kazakov-Kostov result [13]

$$\mathcal{W}_n(\mathcal{A};\infty) = \frac{1}{n}L^{(1)}_{n-1}\left(\hat{g}^2\mathcal{A}\,n/2\right)\,\exp\left[-\frac{\hat{g}^2\mathcal{A}\,n}{4}\right] . \tag{18}$$

Next, using Eq. (17) one is able to perform the latter limit, namely $n \to \infty$ with fixed $n^2\,\mathcal{A}$

$$\lim_{n\to\infty}\mathcal{W}_n(\mathcal{A};N) = \frac{1}{N}\,L^{(1)}_{N-1}\left(g^2\mathcal{A}\,n^2/2\right)\,\exp\left[-\frac{g^2\mathcal{A}\,n^2}{4}\right] . \tag{19}$$

Eq. (19) turns out to be *exactly* the zero-instanton contribution $\mathcal{W}^{(0)}_n$ in $\mathcal{W}_n(A - \mathcal{A},\mathcal{A})$ after decompactification [12]. Such a coincidence can be explained by observing that, having the instantons a finite size, small loops are essentially blind to them. Again, this is not the end of the story: as expected, Eq. (19) can be derived through resummation of the perturbative series defined via WML prescription (matrix model).

The conclusion to be drawn is that the interpretation of both the equal-time and the light-front vacua in the case of a simple Wilson loop can be extended to the more general case of a loop with winding number n. In the light of the considerations above, WML, even resummed, appears to be truly perturbative since it provides only the expression of the zero-instanton contribution to Wilson loops $\mathcal{W}^{(0)}$. As opposed to this, 't Hooft is non-perturbative, in the sense that a "perturbative" series in a "static" potential reproduces a complex instanton expansion. This emerges also in the case of loops in the adjoint representation with non trivial θ-vacua (when the theory is based on the group $SU(N)/\mathbb{Z}_N$). Again $\mathcal{W}^{(0)}$ corresponds to a matrix model after decompactification and is insensitive to the choice of the vacuum sector. This topic has been addressed in [14].

References

[1] T.T. Wu, Phys. Lett. **71B**, 142 (1977).

[2] S. Mandelstam, Nucl. Phys. **B213**, 149 (1983); G. Leibbrandt, Phys. Rev. **D29**, 1699 (1984).

[3] A. Bassetto, M. Dalbosco, I. Lazzizzera and R. Soldati, Phys. Rev. **D31**, 2012 (1985).

[4] A. Bassetto, G. Nardelli and R. Soldati, *Yang-Mills Theories in Algebraic Non-Covariant Gauges*, World Scientific, Singapore 1991; A. Bassetto, I.A. Korchemskaya, G.P. Korchemsky and G. Nardelli, Nucl. Phys. **B408**, 62 (1993); A. Bassetto and M. Ryskin, Phys. Lett. **B316**, (1993); C. Acerbi and A. Bassetto, Phys. Rev. **D49**, 1067 (1994); A. Bassetto, Nucl. Phys. Proc. Suppl. **51C**, 281 (1996); A. Bassetto, G. Heinrich, Z. Kunszt and W. Vogelsang, Phys. Rev. **D58**, 094020 (1998).

[5] G. 't Hooft, Nucl. Phys. **B75**, 461 (1974).

[6] M. Staudacher and W. Krauth, Phys. Rev. **D57**, 2456 (1998).

[7] D. J. Gross and A. Matytsin, Nucl. Phys. **B437**, 541 (1997).

[8] A.A. Migdal, Sov. Phys. JETP **42**, 413 (1975); B.E. Rusakov, Mod. Phys. Lett. **A5**, 693 (1990).

[9] E. Witten, Commun. Math. Phys. **141**, 153 (1991) and J. Geom. Phys. **9**, 303 (1992).

[10] M. Caselle, A. D'Adda, L. Magnea and S. Panzeri, *Two dimensional QCD on the sphere and on the cylinder*, in Proceedings of Workshop on High Energy Physics and Cosmology, (Trieste 1993) eds. E.Gava, A.Masiero, K.S.Narain, S.Randjbar-Daemi and Q.Shafi, World Scientific, Singapore, 1994.

[11] A. Bassetto and L. Griguolo, Phys. Lett. **B443**, 325 (1998).

[12] A. Bassetto, L. Griguolo and F. Vian, Nucl. Phys. **B559**, 563 (1999).

[13] V.A. Kazakov and I.K. Kostov, Nucl. Phys. **B176**, 199 (1980); V.A. Kazakov, *ibid.* **179**, 283 (1981).

[14] A. Bassetto, L. Griguolo and F. Vian, *Wilson loops in the adjoint representation and multiple vacua in two-dimensional Yang-Mills theory*, hep-th/0002093.

COLOR RECONNECTION AND BOSE-EINSTEIN CORRELATIONS AT LEP2

Th. Ziegler [a]

Institut für Physik, Johannes Gutenberg Universität, Staudingerweg 7, 55099 Mainz, Germany

Abstract. Recent investigations of final state interactions of W^+W^- events in e^+e^- collisions up to center of mass energies $\sqrt{s} = 189\ GeV$ at LEP2 are reviewed. The data were used to look for color reconnection and Bose-Einstein correlations between the two color singlets of fully hadronic W events.

1 Motivation

In high energy e^+e^- collisions at LEP the W bosons are produced in pairs. As the hadronisation scale is much larger than the distance of the W bosons at their primary decay vertices, the decay products have a significant space-time overlap and the two systems may interfere during the hadronisation phase. One important consequence is a possible shift in the invariant mass of the reconstructed W bosons in the fully hadronic channel. Two types of final state interactions are investigated and will be reviewed seperately: color reconnection and Bose-Einstein correlations.
The results are based on $\approx 55\ pb^{-1}$ at $\sqrt{s} = 183\ GeV$ and $\approx 173\ pb^{-1}$ at $\sqrt{s} = 189\ GeV$ per LEP collaboration.

2 Color Reconnection (CRC)

Color reconnection (CRC) leads to a rearrangement of the color flow between the hadronic decay products of the W bosons. That this may cause a possibly significant shift in the W mass measurement was first suggested by Sjöstrand and Khoze [11]. In the perturbative case the color flow of the primary quarks is rearranged and possible effects can be estimated by perturbative QCD. The shift of the W mass is predicted to $\Delta M_W \leq \mathcal{O}(5MeV)$ and thus negligible. The effect due to the rearrangement of the color flow of the secondary decay products has to be investigated by MC studies and non-perturbative QCD models have to be used. The consequence for the W mass shift is estimated to be of the order of $\Delta M_W \leq \mathcal{O}(50MeV)$. The following review concentrates on the latter case.

2.1 *Inclusive Mean Charged Particle Multiplicity*

To investigate effects of CRC simple observables like the inclusive charged multiplicity N_{ch} are obvious candidates. There have been models [13] which predict a $\approx 10\%$ effect of CRC on the mean charged multiplicity $\langle N_{ch}^{4q} \rangle$ in the $W^+W^- \rightarrow q\bar{q}q\bar{q}$ channel which were excluded in earlier analysis [4, a.o.] but encouraged the interest in these kind of studies.
As a reference for $\langle N_{ch}^{4q} \rangle$ the mean charged multiplicity $\langle N_{ch}^{qq\ell\nu} \rangle$ of the hadronic part of the semileptonic channel is used. Typically the difference $\Delta\langle N_{ch} \rangle = \langle N_{ch}^{4q} \rangle - 2 \cdot \langle N_{ch}^{qq\ell\nu} \rangle$

[a] e-mail: Thomas.Ziegler@cern.ch

	$\Delta\langle N_{ch}\rangle = \langle N_{ch}^{4q}\rangle - 2\langle N_{ch}^{qq\ell\nu}\rangle$
ALEPH	0.47 ± 0.44 ± 0.26
L3	-0.23 ± 0.40 ± 0.52
OPAL	0.7 ± 0.8 ± 0.6 [b]
DELPHI	-0.92 ± 0.66 [c]
	$\langle N_{ch}^{4q}\rangle/2 \cdot \langle N_{ch}^{qq\ell\nu}\rangle$
DELPHI	0.977 ± 0.017 ± 0.027

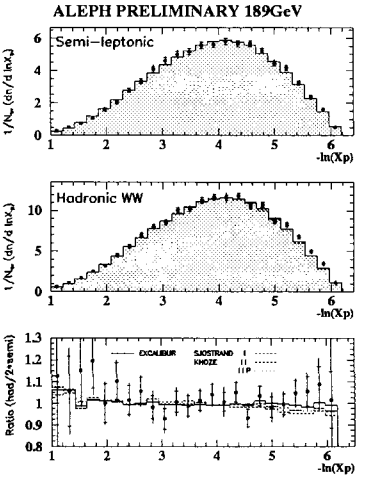

Figure 1:
a) Studies of the mean charged particle multiplicity of the LEP collaborations at $\sqrt{s} = 189\ GeV$ (table above).
b) Inclusive charged particle momentum distributions and comparison with MC predictions with and without CRC models (figure on the right)

is chosen as an observable and should be 0 for no observed effect. The results of the four collaborations [6 - 9] in figure 1a should not be compared directly with each other due to different unfolding and correction procedures. MC studies with physically reasonable CRC models predict a shift in the mean charged multiplicity of the fully hadronic channel of $|\Delta\langle N_{ch}\rangle^{MC}| \leq 0.3$. Therefore all the results are still compatible with standard model predictions.

2.2 Inclusive Charged Particle Momentum Distributions

From MC studies an effect of CRC [12], especially in the low momentum region of the hadronic WW events, is expected. ALEPH [1], DELPHI [2] and OPAL [4] performed similar analysis on momentum distributions. However no evidence for CRC within the statistical significance could be found. As an example the ξ distribution of ALEPH is shown in figure 1b where ξ is the transformed normalized momentum of the charged particles: $\xi = -ln(x_p) = -ln(\frac{p}{\sqrt{s}/2})$. A comparison of the hadronic and the semileptonic channel shows no evidence for color reconnection. Even more low momentum particles are observed whereas less are expected by the 3 shown CRC models of Sjöstrand and Khoze. Further MC studies claimed [12], that the effect should be enlarged for low momentum heavy particles in the context of Sjöstrands CRC models. DELPHI [2] and OPAL [5] performed analyses on the low momentum distributions of charged Kaons and Protons. The result of OPAL is shown in figure 2. In both channels some discrepancies between the data and the KORALW standard MC are found. Nevertheless the ratio $R = N_{K,p}^{4q}/(2 \cdot N_{K,p}^{qq\ell\nu})$ prefers the MC without CRC. For comparison 2 ARIADNE CRC models are shown. The ratio of the production rates in the momentum region $0.002 \leq x_p \leq 0.012$ was found to be

[b] result for $\sqrt{s} = 183\ GeV$
[c] extracted from the numbers given in the DELPHI paper

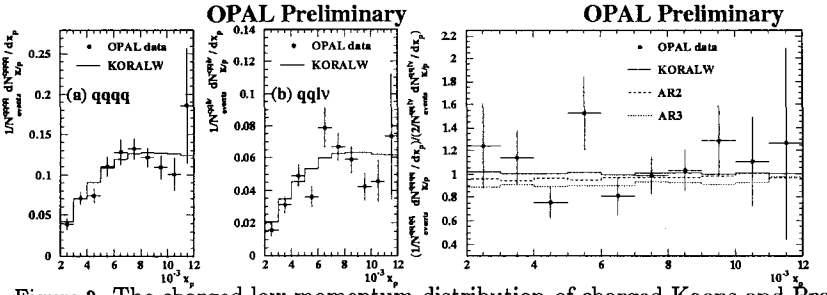

Figure 2: The charged low momentum distribution of charged Kaons and Protons and their ratio compared to MC predictions with and without CRC models.

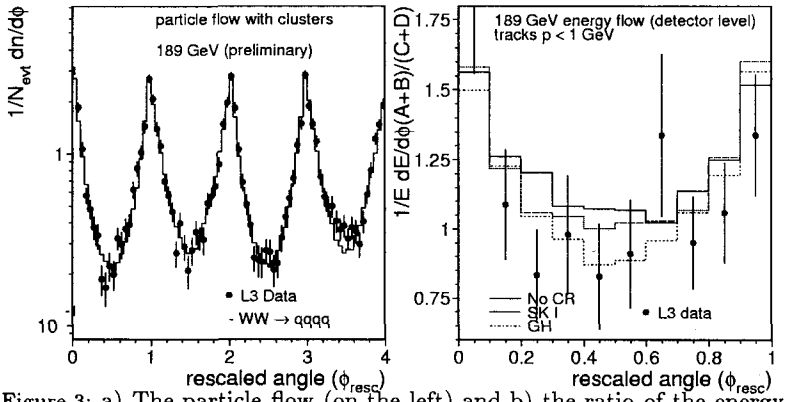

Figure 3: a) The particle flow (on the left) and b) the ratio of the energy flow distribution (on the right)

$$R(183\ GeV) = 0.91 \pm 0.13 \pm 0.08$$
$$R(189\ GeV) = 1.11 \pm 0.08 \pm 0.06$$

For both energies the result is consistent with the expectation of standard QCD models without CRC.

2.3 Particle and Energy Flow Distributions between Jets

In the context of the string fragmentation model CRC should change the particle production between different jets. This can be investigated via particle and energy flow distributions. The particle flow describes the number of particles produced per angular unit between 2 adjacent jets. In the energy flow histogram the entries are weighted with the energy of the particles. The analysis of the L3 collaboration [3] uses a topological event selection, afterwards the jets coming from one W boson are identified and sorted. The angle between the jets is rescaled to be one. Angles from 0 to 1 (A) and from 2 to 3 (B) in figure 3a describe the region between the jets from the same W boson, angles from 1 to 2 (C) and from 3 to 4 (D) describe the region between jets from different W bosons. The data show no significant deviation from the MC

without CRC. The ratio between the particle production of jets coming from the same and from different W bosons $\frac{particleflow(regionA+B)}{particleflow(regionC+D)}$ can be used as a more sensitive variable to CRC. In figure 3b this ratio is shown for the energy flow distribution of the low momentum particles ($p < 1\ GeV$) in comparison with one of the Sjöstrand/Khoze models (SK I) as well as the somewhat extreme Gustafson/Häkkinen model (GH) [14]. Although the errors are still quite large it seems that most of the data points are systematically slightly lower than the standard MC prediction without CRC. Nevertheless no evidence for CRC can be claimed within the statistical significance.

3 Bose-Einstein Correlations (BEC)

From quantum mechanics it is known that the wave function of a pair of identical bosons must be symmetric. As a consequence the number of identical bosons, produced close in phase space, is enhanced. The so called Bose-Einstein correlations (BEC) are well established for pions in Z^o decays. However it is not clear to what extent BEC are induced from the space-time overlap of the decay products of the pair-produced W bosons. From MC studies the shift in the W mass in the hadronic channel is estimated to the order of $\Delta M_W \leq \mathcal{O}(50\ MeV)$.

3.1 BEC Studies at ALEPH

The ALEPH collaboration uses the following double ratio [6]:

$$R^*(Q) = \left(\frac{N_\pi^{++,--}(Q)}{N_\pi^{+-}(Q)}\right)^{data} \Big/ \left(\frac{N_\pi^{++,--}(Q)}{N_\pi^{+-}(Q)}\right)^{MC}_{noBEC}$$

The ratio of the number of 'like-sign pion pairs' to 'unlike-sign pion pairs' of the data is compared with a MC sample without BEC. This ratio is parametrized with $R^*(Q) = \kappa(1+\epsilon Q)(1+\lambda e^{-\sigma^2 Q^2})$. Q is the Lorentz-invariant momentum distance of 2 bosons, κ defines the strength of the correlations and σ the source size of the boson emitter. The double ratio and the fit to the data are shown in figure 4a. The data points are compared to MC with and without BEC which is tuned and corrected at the Z^o peak. BEC between pions from different W bosons are disfavoured by the MC.

3.2 BEC Studies at DELPHI

The DELPHI collaboration uses an event mixing technique [7] where they compare the number of 'like-sign pion pairs' in the hadronic channel with the number of 'like-sign pion pairs' of a hadronic event, which is built of the hadronic part of 2 semileptonic events:

$$g'(Q) = \left(\frac{N_{4q}(Q)}{N_{mix}(Q)}\right)^{data} \Big/ \left(\frac{N_{4q}(Q)}{N_{mix}(Q)}\right)^{MC}_{noBEC}$$

By definition there are no correlations between the pions of different W bosons. The double ratio is parametrized as $g'(Q) = 1 + \Delta e^{-k^2 Q^2}$. The fit results in $\Delta = (7.3 \pm 2.5_{stat} \pm 1.8_{syst})\%$. If there are no BEC between pions from different W bosons the expectation would be $\Delta = 0$. Therefore the BEC between the W bosons are preferred by this analysis.

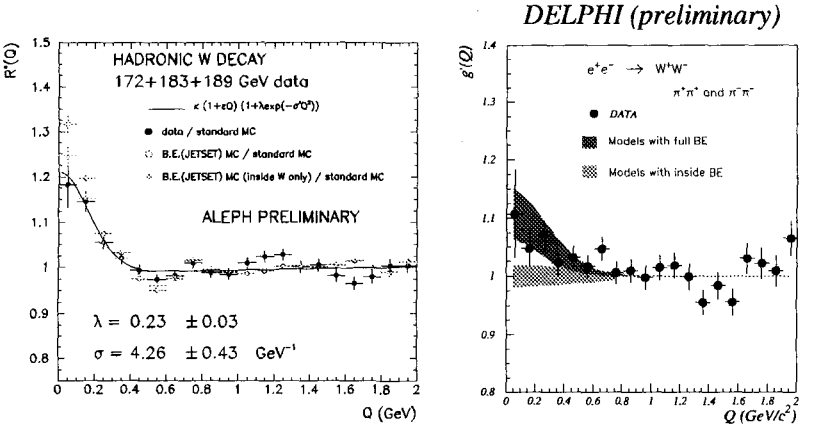

Figure 4: a) The pion pair correlation function of ALEPH (left) and b) of DELPHI (right) with MC predictions with and without BEC.

Parameter	R(fm)	λ
same W	$1.07 \pm 0.07 \pm 0.12$	$0.69 \pm 0.12 \pm 0.06$
diff W	$1.51 \pm 0.05 \pm 0.35$	$0.05 \pm 0.67 \pm 0.35$
$(Z^o/\gamma)^*$	$1.01 \pm 0.08 \pm 0.14$	$0.43 \pm 0.06 \pm 0.08$

Table 1: The fit results of the OPAL collaboration

3.3 BEC Studies at L3

In the subtraction method of the L3 collaboration [8] a 2 particle density function is defined as $\rho(p_1, p_2) = \frac{1}{N_{evt}} \frac{dn_{pairs}}{dQ}$.
The overall 2 particle density can be written as:

$$\rho^{WW} = 2\rho^{W} + 2\rho^{WW}_{mix} \qquad \rightarrow \qquad \Delta\rho = \rho^{WW} + 2\rho^{W} + 2\rho^{WW}_{mix}$$

with $\Delta\rho = 0$ for no BEC between pion pairs from different W bosons. The $\Delta\rho$ distributions for the like-sign and unlike-sign charged pions are investigated as well as $\delta\rho = \Delta\rho(\pm,\pm) - \Delta\rho(+,-)$ which should only depend on BEC. No excess is observed in the distributions and BEC between pions from different W bosons are disfavoured.

3.4 BEC Studies at OPAL

The OPAL collaboration uses the same double ratio as ALEPH but performs a simultanous fit [9] to the following event classes:
hadronic WW, semileptonic WW and $e^+e^- \rightarrow q\bar{q}$ events. In table 1 the fit result of the source size R and the strength of the correlations λ are shown.
With $\lambda = 0.05 \pm 0.67 \pm 0.35$ BEC between pions coming from different W bosons cannot be established with the current level of precision.

4 Summary

Studies of final state interactions are an interesting field in itself and may help to obtain a deeper understanding of the space-time development of the fragmentation process.
The analyses on color reconnection show that all the investigated distributions are compatible with standard MC predictions. Nevertheless they are still limited by the statistics. The particle and energy flow analysis of the L3 collaboration looks promising as the statistics will be increased by at least a factor of 3. With similar analyses of the other LEP collaborations the statistical errors could be decreased by almost a factor of 4 with the final statistics.
The BEC analyses for the LEP collaborations use different methods and the results are not yet conclusive. More experimental effort is needed in this sector to understand BEC resulting from the interference of the hadronic decay products of different W bosons.
One should be aware that an interference between CRC and BEC may reduce or enhance the overall effect.
The present experimental status of the W mass [10] is

$$M_W(q\bar{q}q\bar{q}) - M_W(q\bar{q}\ell\nu_\ell) = 152 \pm 74\ MeV/c^2$$

As the actual systematic error on final state interaction is given with 58 MeV/c^2 [10] it is important to understand color reconnection and Bose-Einstein correlations because they are an important systematic uncertainty on the W mass measurement in the hadronic channel.

Acknowledgments

I would like to thank all colleagues in the LEP collaborations who performed the analyses and helped in preparing the talk.

References

[1] ALEPH Collaboration, *Charged particle multiplicity and momenta in $e^+e^- \to$ W-pair decays at 189 GeV*, Contribution to EPS HEP 99, Tampere, Finland, 15-21 July 1999.

[2] DELPHI Collaboration, *Charged and Identified Particles from the Hadronic Decay of W Bosons and in $e^+e^- \to q\bar{q}$ at 183 and 189 GeV*, DELPHI 99-21 CONF 220.

[3] L3 Collaboration, *Colour Reconnection Studies in $e^+e^- \to W^+W^-$ Events at $\sqrt{s} = 189$ GeV*, L3 Note 2406, submitted to EPS HEP 99, Tampere, Finland, 15-21 July 1999.

[4] OPAL Collaboration, *Colour reconnection studies in $e^+e^- \to W^+W^-$ at $\sqrt{s} =$ 183 GeV*, CERN-EP/98-196, Paper submitted to Physics Letters B.

[5] OPAL Collaboration, *Investigation of colour reconnection via heavy particle production in W^+W^-*, OPAL Physics Note, PN412.

[6] ALEPH Collaboration, *Bose-Einstein correlations in W-pair decays* ALEPH 99-061, Contribution to EPS-HEP 99, Tampere, Finland, 15-21 July 1999.

[7] DELPHI Collaboration, *Bose-Einstein Correlation Between Particles from Different Ws in $e^+e^- \to W^+W^-$ Events*, DELPHI 99-22 CONF 221.

[8] L3 Collaboration, *Study of Bose-Einstein Correlations in W-Pair Production at $\sqrt{s} = 189$ GeV*, L3 Note 2405, Submitted to EPS HEP 99, Tampere, Finland, 15-21 July 1999.

[9] OPAL Collaboration, *Bose-Einstein Correlations in $e^+e^- \to W^+W^-$ at 172 and 183 GeV*, CERN-EP/98-174, Submitted to Euro. Phys. Jour. C.

[10] The LEP WW Working Group, *LEP WW cross-section and W mass (up to 189 GeV) for '99 summer conferences*, LEPEWWG/WW/99-02

[11] T. Sjöstrand, V. A. Khoze, *On Colour Rearrangement in Hadronic W^+W^- Events*, CERN-TH 7011/93.

[12] V.A. Khoze, T. Sjöstrand, *Soft-Particle Spectra as a Probe of Interconnection Effects in Hadronic W^+W^- Events*, HEP-PH/9804202

[13] J. Ellis and K. Geiger, Phys. Rev. D54(1996) 1967; Phys. Lett. B504 (1997) 230.

[14] G. Gustafson and J. Häkkinen, Z. Phys. C64(1994) 659.

Analytic approach to QCD and the interquark potential

A.V. Nesterenko[a]

Physical Department, Moscow State University, Moscow, 119899, Russia

Abstract. The quark-antiquark potential is constructed by making use of a new analytic running coupling in QCD. This running coupling arises under analytization of the renormalization group equation. The rising behavior of the quark-antiquark potential at large distances, which provides the quark confinement is shown explicitly. At small distances the standard behavior of this potential originated in the QCD asymptotic freedom is revealed. The Λ estimation is obtained.

1 Introduction

The description of quark dynamics inside hadrons remains an actual problem of the elementary particle theory. The asymptotic freedom in the Quantum Chromodynamics (QCD) enables one to investigate the quarks interaction at small distances by making use of the standard perturbation theory. The quark dynamics at large distances (the confinement region) lies out of such calculation scope. For this purpose another approaches are used: the phenomenological potential models [1], the string models [2], the bags models [3], the lattice calculations [4], the explicit account of non-trivial QCD vacuum structure [5], the variational perturbation theory [6].

The analytic approach to QCD has been proposed recently [7]. It's basic idea is to combine the renormalization group (RG) summation with the analyticity requirement. The analytic approach has been applied to the RG equation solution in the work [8]. The analyticity requirement was imposed on the RG equation itself, before its solution. Solving the RG equation analytized by above-mentioned way, at one-loop level one gets the new analytic running coupling [8]

$$^{\mathrm{N}}\alpha^{(1)}_{\mathrm{an}}(q^2) = \frac{4\pi}{\beta_0}\frac{z-1}{z\ln z}, \qquad z = \frac{q^2}{\Lambda^2}. \tag{1}$$

It has been shown that this running coupling possesses practically the same remarkable features as the Shirkov-Solovtsov running coupling [7] does. An essential distinction between these couplings, which plays a crucial role in the framework of this paper, is that new analytic running coupling (1) has the singularity at $q^2 = 0$.

Using the running coupling $\alpha(q^2)$, one can obtain the quark-antiquark ($q\bar{q}$) potential by simple Fourier transformation [5], [9]. However, perturbative running coupling $\alpha_{\mathrm{s}}(q^2)$ doesn't enable one to obtain the rising $q\bar{q}$ potential without invoking additional assumptions [9].

The objective of this paper is to construct the quark-antiquark potential by making use of the new analytic running coupling (1). The certain advantage of the current approach is the following. On this way one has succeed to obtain the $q\bar{q}$ potential growing at large distances (that is providing quark confinement), and corresponding to asymptotic freedom at small distances at the same time. It is essential that for this purpose *there is no any additional assumptions* lying beyond the frameworks of the standard RG method in the Quantum Field Theory and the analyticity requirement.

[a]E-mail: nesterav@thsun1.jinr.ru

2 Quark-antiquark potential generated by the new analytic running coupling

Let us proceed to the construction of the quark-antiquark potential ${}^{N}V(r)$ by making use of the new analytic running coupling ${}^{\mathrm{N}}\alpha_{\mathrm{an}}(q^2)$ (1). As it has been mentioned above, we shall use the standard expression for the $q\bar{q}$ potential

$$V(r) = -\frac{16\pi}{3}\int_0^\infty \frac{\alpha(q^2)}{q^2}\frac{e^{i\mathbf{q}\mathbf{r}}}{(2\pi)^3}\,d\mathbf{q}. \tag{2}$$

For the construction of the potential ${}^{N}V(r)$ we shall use the new analytic running coupling (see work [8])

$${}^{\mathrm{N}}\alpha_{\mathrm{an}}^{(1)}(Q^2) = \frac{4\pi}{\beta_0}\frac{z-1}{z\ln z}, \qquad z = \frac{Q^2}{\Lambda^2}, \tag{3}$$

where $\beta_0 = 11 - 2\,n_f/3$ – first coefficient of the β-function. After the integration over the angular variables and changing of variables $q/\Lambda \to q$, $r\Lambda \to R$ in the expression (2) one gets

$${}^{N}V(r) = -\frac{32}{3\beta_0}\Lambda\cdot\widetilde{V}(R), \quad R = \Lambda r, \tag{4}$$

where

$$\widetilde{V}(R) = \int_0^\infty \frac{q^2-1}{q^2\ln q^2}\frac{\sin(qR)}{qR}\,dq. \tag{5}$$

For the calculation of the dimensionless $q\bar{q}$ potential $\widetilde{V}(R)$ (5) lets consider the auxiliary function

$$I(n,R) = \lim_{a\to 0+}\int_0^\infty \frac{q^{n-1}}{\ln(a+q^2)}\sin(qR)\,dq. \tag{6}$$

The parameter a is introduced here just for the shifting the origin of the cut along the imaginary axis $\Im m\ q$. It is obvious that

$$\widetilde{V}(R) = \frac{1}{R}\left[I(0,R) - I(-2,R)\right]. \tag{7}$$

For even n the integrand in (6) is the even function of q. Therefore

$$I(n,R) = \frac{1}{2}\Im m\lim_{a\to 0+}\mathcal{P}\!\int_{-\infty}^{\infty} F(q)\,dq, \quad F(q) = \frac{q^{n-1}e^{iqR}}{\ln(a+q^2)}. \tag{8}$$

Here, the $\mathcal{P}$ sign means the principle value of the integral. In the further calculations we shall suppose $0 \le a < 1$.

The function $F(q)$ (8) has both cuts $(-i\infty, -i\sqrt{a}]$, $[i\sqrt{a}, i\infty)$ and first order poles at $p_{1,2} = \mp\sqrt{1-a}$. Let us consider the integral of the function F along the contour Γ presented on Fig. 1. Since function $F(q,n,a,R)$ has no singularities inside contour Γ then $\oint_\Gamma F\,dq = 0$. Performing the integration along two semicircles c_- and c_+ of the

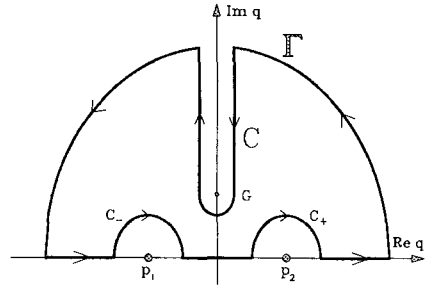

Figure 1: The integration contour in the complex q-plane. The notations are: $p_1 = -\sqrt{1-a}$, $p_2 = \sqrt{1-a}$, G$= i\sqrt{a}$.

vanishing radius and along the cut C on the imaginary axis, we obtain that function $I(n,R)$ (6) (for even n) takes the form

$$I(n,R) = \pi\left[\frac{1}{2}\cos R - (-1)^{n/2}\mathcal{N}(R,n)\right], \tag{9}$$

where

$$\mathcal{N}(R,n) = \int_0^\infty \frac{x^{n-1}e^{-Rx}}{\ln^2(x^2)+\pi^2}\,dx. \tag{10}$$

It is rather complicated to perform the integration in (10) over dx explicitly. First of all, we are interested in the question whether the $q\bar{q}$ potential ${}^NV(r)$ (4) provides the quark confinement. For the investigation of the potential ${}^NV(r)$ (4) behavior at large distances it is quite enough to consider the asymptotic of function $\mathcal{N}(R,n)$ (10) at $R\to\infty$. Let us represent this function in the following way

$$\mathcal{N}(R,n) = (-1)^n\frac{\partial^n}{\partial R^n}\int_0^\infty \frac{e^{-Rx}}{x\left[\ln^2(x^2)+\pi^2\right]}\,dx. \tag{11}$$

Using the formula (4.361.2) from [10]

$$\int_0^\infty \frac{e^{-\mu x}}{x(\ln^2 x+\pi^2)}dx = e^\mu - \nu(\mu), \quad \nu(\mu) = \int_0^\infty \frac{\mu^t dt}{\Gamma(t+1)}, \tag{12}$$

(here $\nu(\mu)$ is so-called transcendental ν-function [11]) one can obtain (at large R) for function $\mathcal{N}(R,n)$

$$\mathcal{N}(R,n) = \frac{(-1)^n}{4}\left[e^R - \nu(R) + \int_0^{-n}\frac{R^t dt}{\Gamma(t+1)}\right]. \tag{13}$$

Taking into account the relationships (7), (9) and (13) one can present the $q\bar{q}$ potential ${}^NV(r)$ (4) in the form

$${}^NV(r) = \frac{8\pi}{3\beta_0}\frac{\Lambda}{R}\left[2\left(e^R - \nu(R)\right) + \int_0^2 \frac{R^t dt}{\Gamma(t+1)}\right], \quad R = \Lambda r. \tag{14}$$

It should be pointed out here that relationship (14) is valid for the large R. The behavior of the potential ${}^{N}V(r)$ at $r \to \infty$ is determined by the last term in (14).[b] It's integration by parts gives

$$\int_0^2 \frac{R^t dt}{\Gamma(t+1)} = \frac{R^2}{2\ln R}\left[1 + 2\sum_{k=1}^{\infty}\frac{f_k(2)}{\ln^k R}\right] - \frac{1}{\ln R}\left[1 + \sum_{j=1}^{\infty}\frac{f_j(0)}{\ln^j R}\right], \tag{15}$$

where

$$f_n(t) = \frac{d^n}{ds^n}\frac{(-1)^n}{\Gamma(s+1)}\bigg|_{s=t}. \tag{16}$$

Expression (15) takes the form in the limit $R \to \infty$

$$\int_0^2 \frac{R^t dt}{\Gamma(t+1)} = \frac{R^2}{2\ln R}. \tag{17}$$

Thus, the quark-antiquark potential ${}^{N}V(r)$ (4) is rising at large distances

$${}^{N}V(r) \xrightarrow{r\to\infty} \frac{8\pi}{3\beta_0}\Lambda \cdot \frac{1}{2}\frac{\Lambda r}{\ln(\Lambda r)}. \tag{18}$$

Therefore the new analytic running coupling $\alpha_{\rm an}(q^2)$ (1), as it follows explicitly from the asymptotic (18) provides the growing behavior of the quark-antiquark potential ${}^{N}V(r)$ (4) at $r \to \infty$. Hence it describes quark confinement. It is important to point out that behavior of the potential ${}^{N}V(r)$ at $r \to 0$ has the standard form, prescribing by the asymptotic freedom (e.g., see [9])

$${}^{N}V(r) \xrightarrow{r\to 0} \frac{8\pi}{3\beta_0}\Lambda \cdot \frac{1}{\Lambda r \ln(\Lambda r)}. \tag{19}$$

Unfortunately, it is impossible to obtain the explicit dependence ${}^{N}V(r)$ for the whole region $0 < r < \infty$. The simple interpolating formula, which can be applied for the practical purposes will be given in the next section.

3 Discussion

One can try to construct the $q\bar{q}$ potential (2) on the base of perturbative $\widetilde{\alpha}_{\rm s}(q^2) = 1/\ln(z)$ and analytized [7] $\widetilde{\alpha}_{\rm an}(q^2) = 1/\ln(z) + 1/(1-z)$ running couplings. This leads to the following obvious result. In the first case the interquark potential can be represented at large distances in the form

$$V_{\rm s}(r) = \frac{8\pi}{3\beta_0}\frac{\Lambda}{R}\left[e^R - \nu(R) - 2\cos R\right], \quad R = \Lambda r. \tag{20}$$

[b] It follows explicitly from the asymptotic of $\nu(R)$ (see [11]), and from the quite simple considerations. Thus, one can say about the term $f(R) = e^R - \nu(R)$ that (at $R > 0$) $f(R) \geq 0$, $f'(R) \leq 0$. Hence, $f(R) \to$ const at $R \to \infty$, and its contribution to ${}^{N}V(r)$ at large R is of the $1/R$-order.

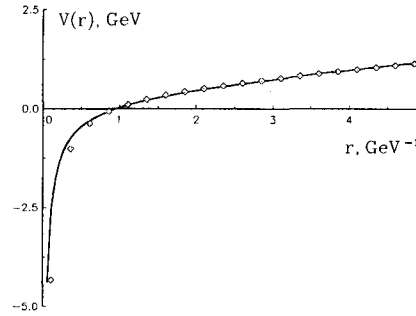

Figure 2: Comparison of the potential $U(r)$ given by Eq. (22) (solid curve) with the phenomenological Cornell potential ($\diamond$), Eq. (23). The values of the parameters are: $a = 0.39$, $\sigma = 0.182$ GeV^2 [5], $\Lambda = 530$MeV, $n_f = 5$.

The $q\bar{q}$ potential calculated by making use of $\alpha_{\rm an}$ at large r is

$$V_{\rm an}(r) = \frac{8\pi}{3\beta_0}\frac{\Lambda}{R}\left[e^R - \nu(R) - 2\right], \quad R = \Lambda r. \tag{21}$$

As it has been shown in the previous section, at large R one has $(e^R - \nu(R))/R \to 0$. Thus it is follows from (20) and (21) that $q\bar{q}$ potential constructed on the base of both perturbative α_s and analytized [7] $\alpha_{\rm an}$ running couplings is not growing at large distances, i.e. it doesn't describe quark confinement.

For the practical use of the constructed potential it is interesting to obtain the simple explicit expression, which approximate it's behavior good enough. For this purpose one can use for instance the next approximating function:

$$\begin{aligned} U(r) &= \frac{8\pi}{3\beta_0}\Lambda\left[\frac{1}{\ln R}\left(\frac{1}{R}+\frac{R}{2}\right)+\frac{1}{1-R}\left(\frac{3}{2}+Rf_1(2)\right)\right. \\ &\left. +Rf_1(2)\left(\frac{1}{\ln^2 R}-\frac{1}{(R-1)^2}+\frac{11}{12}\right)\right], \end{aligned} \tag{22}$$

which doesn't contain any unphysical singularities and it has asymptotics (18) and (19). The formula (22) retains explicitly the second leading term of the expansion (15), $f_1(2) = 0.461$. Some terms have been introduced into (22) just for the singularity elimination at $R = 1$. It should be mentioned here that next expansion terms (15) practically don't affect on the shape $U(r)$ (22). Of course, (22) is not a unique interpolation between asymptotics (18) and (19). Nevertheless, the comparison of the $U(r)$ (22) with phenomenological potential

$${}^{C}V(r) = -\frac{4}{3}\frac{a}{r} + \sigma r + \text{const} \tag{23}$$

(so-called Cornell potential [1]) has shown their almost complete coincidence (see Fig. 2). The fit has been performed with use of the least square method on the physical-meaning distances region $r \in [0.1 \div 1]$ fm [5]. The varied parameter in (22)

is Λ. The opportunity to shift the potential ${}^{C}V(r)$ (23) by a constant was used also. A rough estimation of Λ in the course of this fitting gives $\Lambda \simeq 500$ MeV. This is in agreement with the values obtained earlier in the framework of the analytic approach to QCD [7].

Acknowledgments

The author is grateful to academician D. V. Shirkov and to Dr. I. L. Solovtsov for the valuable discussions and useful comments. The partial support of RFBR (Grant No. 99-01-00091) is appreciated.

References

[1] E. Eichten *et al.*, Phys. Rev. D **17**, 3090 (1978); A. Martin, Phys. Lett. B **93**, 338 (1980); C. Quigg and J. L. Rosner, Phys. Lett. B **71**, 153 (1977).

[2] B. M. Barbashov and V. V. Nesterenko, *Introduction to the relativistic string theory* (World Scientific, 1990).

[3] P. Hasenfratz and J. Kuti, Phys. Rep. C **40**, 75 (1978). S. Adler and T. Piran, Rev. Mod. Phys. **56**, 1 (1984).

[4] G. S. Bali, C. Schlichter, and K. Schilling, Phys. Rev. D **51**, 5165 (1995).

[5] N. Brambilla and A. Vairo, hep-ph/9904330.

[6] I. L. Solovtsov, Phys. Lett. B **327**, 335 (1994).

[7] D. V. Shirkov and I. L. Solovtsov, Phys. Rev. Lett. **79**, 1209 (1997); hep-ph/9704333; D. V. Shirkov and I. L. Solovtsov, Theor. Math. Phys. **120**, 482 (1999); hep-ph/9909305.

[8] A. V. Nesterenko, Diploma thesis, Moscow State University, 1998.

[9] J. L. Richardson, Phys. Lett. B **82**, 272 (1979); R. Levine and Y. Tomozawa, Phys. Rev. D **19**, 1572 (1979).

[10] I. S. Gradshteijn and I. M. Ryzhik, *Table of Integrals, Series and Products* (Academic, New York, 1994).

[11] H. Bateman and A. Erdelyi, *Higher transcendental functions* (McGraw-Hill, New York, 1953-55), Vol. 3.

A NLO QCD ANALYSIS OF THE SPIN STRUCTURE FUNCTION g_1 AND HIGHER TWIST CORRECTIONS

E. LEADER [a]
Birkbeck College, University of London, England
A. S. SIDOROV [b]
Bogoliubov Theoretical Laboratory, JINR, Dubna, Russia
D. B. STAMENOV [c]
Institute for Nuclear Research and Nuclear Energy, Sofia, Bulgaria

Abstract. We present a concise description of our present knowledge of the polarized parton densities extracted from the world data on inclusive deep inelastic lepton-nucleon scattering. The role of the higher twist effects is discussed.

Deep inelastic scattering (DIS) of leptons on nucleons has remained the prime source of our understanding of the internal partonic structure of the nucleon and one of the key areas for the testing of perturbative QCD. Decades of experiments on unpolarized targets have led to a rather precise determination of the unpolarized parton densities. Spurred on by the famous EMC experiment [1] at CERN in 1988, there has been a huge growth of interest in polarized DIS experiments which yield more refined information about the partonic structure. Many experiments have been carried out at SLAC, CERN and DESY. In this talk we present a next-to-leading order (NLO) QCD analysis of the world data [1, 2] on inclusive polarized DIS and the polarized parton densities determined from the data.

The spin-dependent structure function of interest, $g_1^N(x, Q^2)$, is a linear combination of the asymmetries $A_\parallel^N$ and $A_\perp^N$ (or the related virtual photon-nucleon asymmetries $A_{1,2}^N$) measured with the target polarized longitudinally or perpendicular to the lepton beam, respectively. Neglecting as usual the subdominant contributions $A_1^N(x, Q^2)$ can be expressed via the polarized structure function $g_1^N(x, Q^2)$ as

$$A_1^N(x, Q^2) \cong (1 + \gamma^2) \frac{g_1^N(x, Q^2)}{F_1^N(x, Q^2)} , \tag{1}$$

where F_1^N is the unpolarized structure function and γ^2 is a kinematic factor given by

$$\gamma^2 = \frac{4M_N^2 x^2}{Q^2} . \tag{2}$$

In the NLO QCD approximation the quark-parton decomposition of $g_1(x, Q^2)$ has the following form:

$$\begin{aligned} g_1(x, Q^2) &= \frac{1}{2} \sum_q^{N_f} e_q^2 [(\Delta q + \Delta \bar{q}) \otimes (1 + \frac{\alpha_s(Q^2)}{2\pi} \delta C_q) \\ &+ \frac{\alpha_s(Q^2)}{2\pi} \Delta G \otimes \delta C_G], \end{aligned} \tag{3}$$

[a] e-mail: leader@physics.bbk.ac.uk
[b] e-mail:sidorov@thsun1.jinr.ru
[c] e-mail:stamenov@inrne.bas.bg

where $\Delta q(x,Q^2), \Delta\bar{q}(x,Q^2)$ and $\Delta G(x,Q^2)$ are quark, anti-quark and gluon polarized densities which evolve in Q^2 according to the spin-dependent NLO DGLAP equations [5]. In (3) $\delta C_{q,G}$ are the NLO terms in the spin-dependent Wilson coefficient functions and the symbol $\otimes$ denotes the usual convolution in Bjorken x space. N_f is the number of flavours.

All details of our approach are given in [3,4]. Here we would like to mention only that according to this approach the NLO QCD predictions have been confronted to the data on the spin asymmetry $A_1^N(x,Q^2)$, rather than on the $g_1^N(x,Q^2)$. The choice of A_1^N should minimize the higher twist contributions which are expected to partly cancel in the ratio (1), allowing use of data at lower Q^2 (in polarized DIS most of the small x experimental data points are at low Q^2). We will demonstrate further that the higher twist corrections to A_1^N are indeed negligible and consistent with zero.

We carry out our analysis in three different factorization schemes: $\overline{\mathrm{MS}}$, AB (Adler-Bardeen) [6] and JET (see [4] and references therein) and test the independence of the physical results on the choice of the factorization convention.

As was shown in [3] the inclusive polarized DIS determine in principle the individual parton densities

$$(\Delta u + \Delta\bar{u})(x,Q^2),\ (\Delta d + \Delta\bar{d})(x,Q^2),\ (\Delta s + \Delta\bar{s})(x,Q^2),\ \Delta G(x,Q^2) \qquad (4)$$

i.e., the data fix uniquely only the sum of the polarized quark and antiquark densities for each flavour, but not allow a decomposition of Δu and Δd quarks into sea and valence parts. In order to extract them from the data (the success of the parton model is based on the universality of the parton densities and they are needed to make predictions for other processes, like polarized pp reactions, etc.), additional assumptions about the flavor decomposition of the sea are necessary. Conventionally, the assumption $\Delta\bar{u} = \Delta\bar{d} = \lambda\Delta\bar{s}$, where λ is a parameter, has been used in most of the analyses.

We check the stability of our results when we vary the parameter λ and confirm that the quark densities $\Delta u + \Delta\bar{u}, \Delta d + \Delta\bar{d}, \Delta s + \Delta\bar{s}$, as well as the gluon density ΔG are invariant (do *not* change as λ is varied). Of course, the valence quark densities Δu_v and Δd_v are sensitive to the different assumptions about the sea.

For the input polarized parton densities at $Q_0^2 = 1\ GeV^2$ we have adopted a very simple parametrization

$$\begin{aligned}
x\Delta u_v(x,Q_0^2) &= \eta_u A_u x^{a_u} x u_v(x,Q_0^2),\\
x\Delta d_v(x,Q_0^2) &= \eta_d A_d x^{a_d} x d_v(x,Q_0^2),\\
x\Delta Sea(x,Q_0^2) &= \eta_S A_S x^{a_S} x Sea(x,Q_0^2),\\
x\Delta G(x,Q_0^2) &= \eta_g A_g x^{a_g} x G(x,Q_0^2),
\end{aligned} \qquad (5)$$

where on RHS of (5) we have used the MRST unpolarized densities [7]. The normalization factors A_f in (5) are fixed such that η_f are the first moments of the polarized densities. In the case of SU(3) flavour symmetry the first moments of the valence quark densities η_u and η_d are fixed by the octet nucleon and hyperon β decay constants [8].

The rest of the parameters in (5), $\{a_u,\ a_d,\ \eta_S,\ a_S\ ,\ \eta_g\ ,\ a_g\}$, have been determined from the fits to the world data on $A_1^N(x,Q^2)$ [1,2]. The total (statistical and

systematic) errors are taken into account. The results presented below correspond to an SU(3) symmetric sea.

What follows from our analysis is that the NLO QCD predictions are in a very good agreement with the presently available data on A_1^N (g_1^N) in all the schemes, JET, AB and $\overline{\mathrm{MS}}$, with the essentially the same $\chi^2 \approx 128.5$ for 155 DOF. An example of the quality of the fits is shown in Fig. 1.

Let us now comment briefly upon the state of our knowledge about the individual polarized parton densities. The extracted quark (valence and sea) and gluon densities are shown in Fig. 2 and Fig. 3.

$\mathbf{\Delta u_v(x, Q^2)}$ and $\mathbf{\Delta d_v(x, Q^2)}$

i) Δu_v and Δd_v in the JET, AB and $\overline{\mathrm{MS}}$ schemes coincide within the errors, in excellent agreement with what follows from the theory (they should be the same in the factorization schemes under consideration).

ii) Δu_v is very well determined once an assumption about the flavour decomposition of the sea is made.

iii) Although the first moment of $\Delta d_v(x, Q_0^2)$, η_d, has been kept fixed in the analysis, Δd_v is not well determined from the present inclusive data.

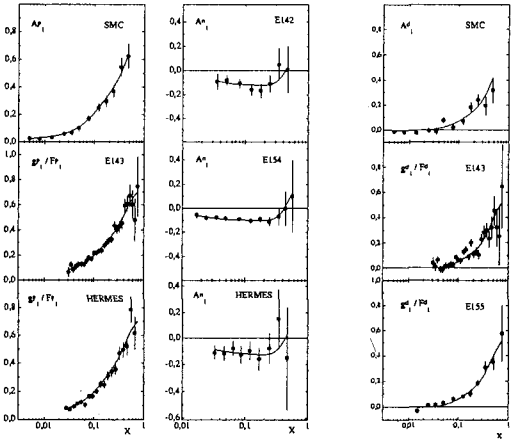

Figure 1: Comparison of our NLO results (JET scheme) for $A_1^p(x, Q^2)$ and $A_1^N(x, Q^2)$ with the experimental data at the measured x and Q^2 values. Errors bars represent the total error.

$\mathbf{\Delta\bar{s}(x, Q^2)}$ and $\mathbf{\Delta\Sigma(x, Q^2)}$

Note that these quantities are scheme dependent.

We recall here the remarkable relation between the first moments of the singlet density $\Delta\Sigma(x, Q^2), \Delta\Sigma$, given in the $\overline{\mathrm{MS}}$ and JET(AB) schemes

$$a_0(Q^2) = \Delta\Sigma(Q^2)_{\overline{\mathrm{MS}}} = \Delta\Sigma_{\mathrm{JET(AB)}} - N_f \frac{\alpha_s(Q^2)}{2\pi} \Delta G(Q^2), \tag{6}$$

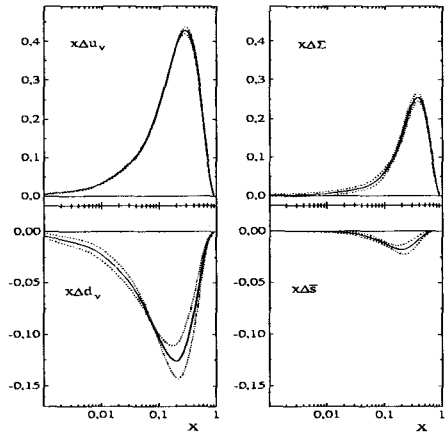

Figure 2: Polarized valence, strange and singlet quark distributions at $Q^2 = 1\ GeV^2$ with their error bands (JET scheme). The systematic errors are added quadratically.

where $a_0(Q^2)$ is the singlet axial charge and $\Delta G(Q^2) = \eta_g(Q^2)$ is the first moment of the polarized gluon density. Note that the gluons do not change in the factorization schemes under consideration.

It follows from our analysis that:

i) $\Delta\bar{s}$ and $\Delta\Sigma$ are well determined from the data (see Fig. 2) if the non-singlet axial charge a_8 is fixed from the hyperon β-decays data.

ii) The first moment of $\Delta\bar{s}$ in the $\overline{\mathrm{MS}}$ scheme, $(\eta_{\bar{s}})_{\overline{\mathrm{MS}}}$, is almost twice as big as it is in the JET(AB) schemes, $(\eta_{\bar{s}})_{\mathrm{JET(AB)}}$:

$$\begin{aligned} (\eta_{\bar{s}})_{\overline{MS}} &= -0.051 \pm 0.006, \\ (\eta_{\bar{s}})_{JET} &= -0.032 \pm 0.005. \end{aligned} \tag{7}$$

The polarized strange quark density is significantly different from zero independently of the factorization schemes used in the analysis. The result (7) demonstrates the extent to which the strange quark densities in different schemes can differ in the polarized case.

Gluons $\Delta G(x, Q^2)$

Unlike the quark densities $(\Delta q + \Delta\bar{q})$, the gluons contribute to the spin structure function g_1 in NLO. That is why, the extraction of the polarized gluon density from DIS data is much more difficult and strongly depends on the accuracy and the kinematic (x, Q^2) region of the data. Although the progress in determining of the gluon

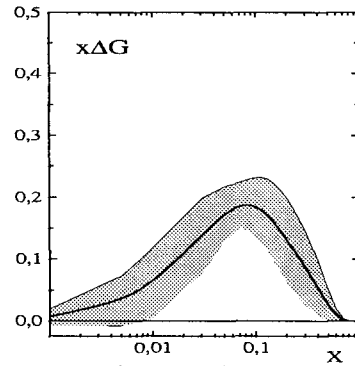

Figure 3: Polarized gluon density at $Q^2 = 1\ GeV^2$. The error band accounts for the statistical and systematic uncertainties.

density due to the new set of SMC data [2] at small x is obvious (see Fig. 3), the gluons are still poorly constrained. An independent and direct measurements of the gluon polarization (COMPASS, RHIC) are very important for the better understanding of the partonic spin content of the nucleon.

The nucleon spin

In the JET and AB schemes $\Delta\Sigma$ does *not* depend on Q^2 and is it meaningful to directly interpret $\Delta\Sigma$ as the contribution of the quark spins to the nucleon spin and to confront its value obtained from the high energy region with predictions from low energy models like constituent quark, chiral quarks models, etc. Our value of $\Delta\Sigma = 0.40 \pm 0.04$ at $Q^2 = 1\ GeV^2$ is not far from the value 0.6 expected in certain quark models [9].

We have also investigated (JET scheme) the sensitivity of χ^2 to the alternative possibilities of explanation of the spin of the nucleon via the spins of its constituents (a large negative strange sea or a large positive gluon polarization).

We have found that the present inclusive DIS data prefer small strange sea and small gluon polarized densities at $Q^2 = 1\ GeV^2$:

$$\eta_{\bar{s}} = -0.032 \pm 0.005, \quad \eta_g = 0.57 \pm 0.14. \tag{8}$$

Then for the spin contribution from both quarks and gluons we have:

$$\frac{1}{2}\Delta\Sigma(1) + \eta_g = 0.76 \pm 0.14 \tag{9}$$

This value is consistent with 1/2 in two standard deviations. The more accurate determination of $\Delta\Sigma$ and η_g will determine whether it is necessary to have any contri-

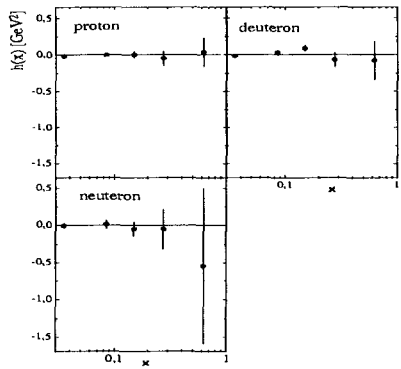

Figure 4: Twist-4 contributions $h^N(x)$ to the spin asymmetry $A_1^N(x, Q^2)$ extracted from the data.

bution from orbital angular momentum $L_z(Q^2)$ at this scale. At larger Q^2, however, the strong rise of η_g have to be compensated by a large negative $L_z(Q^2)$.

Higher twist effects

Finally, we present our results (Fig. 4) on the twist-4 contributions $\mathcal{O}(1/Q^2)$ to the spin asymmetry A_1^{QCD} (Eq. (1))

$$A_1^{(N)}(x, Q^2) = A_1^{(N)\mathrm{QCD}}(x, Q^2) + h^{(N)}(x)/Q^2. \tag{10}$$

The unknown functions $h^{(N)}(x)$ (N=p, n, d) are parametrized at different x_i-points and then the free parameters $h_i^N = h^N(x_i)$ are fixed from the fit to the data. It is seen from Fig. 4 that the higher twist $\mathcal{O}(1/Q^2)$ terms are negligible and consistent with zero within the errors. This result clearly demonstrate the advantage of the approach in which the QCD predictions are confronted with the data on A_1, rather than with g_1.

Acknowledgments

This research was partly supported by a UK Royal Society Collaborative Grant, by the Russian Foundation for Basic Research, Grant No 00-02-16696 and by the JINR-Bulgaria Collaborative Grant.

References

[1] EMC, J. Ashman et al., *Phys.Lett.* **B** 206, 364 (1988); *Nucl.Phys.* **B** 328, 1 (1989).

[2] SLAC E142 Collaboration, P.L. Anthony et al., *Phys.Rev.* **D** 54, 6620 (1996); SLAC/E154 Collaboration, K. Abe et al., *Phys.Rev.Lett.* **79**, 26 (1997); SLAC E143 Collaboration, K. Abe et al., *Phys.Rev.* **D** 58, 112003 (1998); SLAC/E155 Collaboration, P.L. Anthony et al., *Phys.Lett.* **B** 463, 339 (1999); SMC, D. Adeva et al., *Phys.Rev.* **D** 58, 112001 (1998); HERMES Collaboration, K. Ackerstaff et al., *Phys.Lett.* **B** 404, 383 (1997); HERMES Collaboration, A. Airapetian et al., *Phys.Lett.* **B** 442, 484 (1998).

[3] E. Leader, A.V. Sidorov and D.B. Stamenov, *Phys.Rev.* **D** 58, 114028 (1998).

[4] E. Leader, A.V. Sidorov and D.B. Stamenov, *Phys.Lett.* **B** 445, 232 (1998).

[5] V.N. Gribov and L.N. Lipatov, *Sov.J.Nucl.Phys.* **15**, 438 (1972); Yu.L. Dokshitzer, *Sov.Phys.JETP* **46**, 641 (1977); G. Altarelli and G. Parisi, *Nucl.Phys.* **B**126, 298 (1977); R. Mertig and W.L. van Neerven, *Z.Phys.* **C** 70, 637 (1996); W. Vogelsang, *Phys.Rev.* **D** 54, 2023 (1996).

[6] R.D. Ball, S. Forte and G. Ridolfi, *Phys.Lett.* **B** 378, 255 (1996).

[7] A.D. Martin, R.G. Roberts, W.J. Stirling and R.S. Torn, *Eur.Phys.J.* **C** 4, 463 (1998).

[8] Particle Data Group, L. Montanet et al., *Phys.Rev.* **D** 50, 1173 (1994); F.E. Close and R.G. Roberts, *Phys.Lett.* **B** 313, 165 (1993).

[9] R.D. Jaffe and A. Manohar, *Nucl.Phys.* **B** 337, 509 (1990).

Leptonic decays of D_s

John Putz [a], The Aleph Collaboration
Physics Department, University of Washington, Seattle, Washington, 98195, USA

Abstract. The branching ratios for the leptonic decays $D_s \to \mu\nu$ and $D_s \to \tau\nu$ have been measured in the ALEPH experiment at LEP. The results are preliminary.

1 Leptonic decay of D_s

The D_s is a second generation analog of the charged pion and can undergo a Cabibbo-allowed leptonic decay into any of the charged leptons and a neutrino. The rate into lighter charged leptons is helicity-suppressed. The decay rate is given by

$$\Gamma(D_s \to \ell\nu) = \frac{G_F^2}{8\pi} f_{D_s}^2 |V_{cs}|^2 M_{D_s} M_\ell^2 \left(1 - \frac{M_\ell^2}{M_{D_s}^2}\right)^2$$

where the poorest known quantity is the decay constant f_{D_s}. The decay constants (f_D, f_{D_s}, f_B, $f_{B_s}, \ldots$) can be predicted theoretically (e.g., Lattice QCD). While f_B and f_{B_s} are needed for interpretation of $B\bar{B}$ mixing they are experimentally inaccessible due to a very low branching ratio. Measurements of f_{D_s} would allow checks of the theoretical predictions and give confidence in calculations of f_B.

For a typical value of $f_{D_s} = 260\,\mathrm{MeV}$, we expect

$$\begin{aligned} B(D_s \to \tau\nu) &= 5.2\% \\ B(D_s \to \mu\nu) &= 0.54\% \\ B(D_s \to e\nu) &= 1.3 \times 10^{-7}\ . \end{aligned}$$

1.1 Previous results

$D_s \to \tau\nu$ L3 at CERN.

L3 analyzed about 1.5×10^6 $Z \to q\bar{q}$ at LEP. The technique used was to find the energy and direction of D_s from the sum of all energies and momenta (except the lepton). A 3-5 GeV photon from $D_s^* \to \gamma D_s$ was observed and $M(\gamma D_s)$ was reconstructed. The signal efficiency was $\approx 2\%$. In the expected mass region: 47 events were observed of which ≈ 27 were background. For f_{D_s} they obtained 1
$f_{D_s} = [309 \pm 58(\mathrm{stat}) \pm 33(\mathrm{syst}) \pm 38(\mathrm{norm})]\,\mathrm{MeV}$

$D_s \to \mu\nu$ CLEO-II at Cornell.

A large sample (5×10^6) of $c\bar{c}$ was analyzed. The missing neutrino momentum was found taking advantage of the hermiticity of the detector and the D_s^* photon (> 150 MeV) was observed. $\Delta M = M(\gamma\mu\nu) - M(\mu\nu)$ was calculated and was used to identify signal events. The signal efficiency was about 4.2%. The normalization was obtained from $D_s^* \to \gamma D_s$, $D_s \to \phi\pi$ which gave an additional uncertainty (BR). Background was due to random photons together with $D_s \to \mu\nu$ or $D \to \mu\nu$. The D_s electron

[a] e-mail: putz@phys.washington.edu

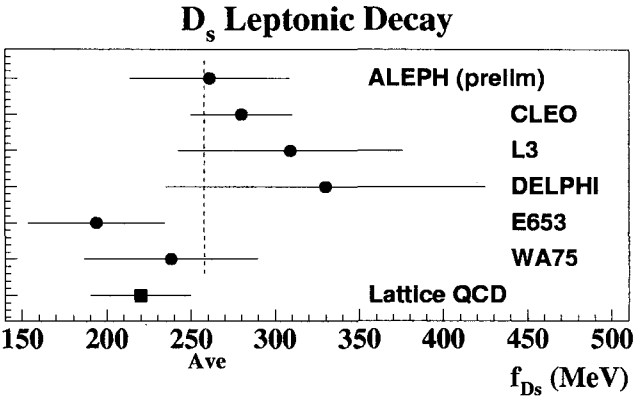

Errors are Statistical and Systematic

$D_s \to \phi\pi$ branching ratio error not included

decay mode was used to study the background. In the expected ΔM region 182 ± 22 events were seen above background. For the decay constant they obtained 2
$f_{D_s} = [280 \pm 17(\text{stat}) \pm 25(\text{syst}) \pm 34(\text{BR})]\,\text{MeV}$

1.2 The ALEPH *measurements*

$D_s \to \mu\nu$.

The D_s mesons are produced from $e^+e^- \to c\bar{c}$ at the Z resonance. The event selection, giving high signal efficiency, is optimized for $c\bar{c}$ events with a muon in one hemisphere. The other tracks in the muon hemisphere should be fragmentation tracks originating at the interaction point. A constrained kinematic fit improves the resolution on the missing momentum (the neutrino from $D_s \to \mu\nu$) and the D_s invariant mass $M(\mu\nu)$, is computed.

The leptonic branching fractions are found using a fitting procedure designed to distinguish the signal from the two principal background components which are semileptonic b decays and semileptonic c decays. Two linear discriminant variables U_b and U_c, which are combinations of many physical variables, distinguish the signal events from the two types of background. The sample of signal events includes a small contribution from tau final states and from D^+ leptonic decays. Appropriate assumptions are made about the decay rates for these channels.

The fitted number of signal events is 747 ± 93 while the number of background events is 5496. The important systematic uncertainties are due to uncertainties in the physics input parameters to the Monte Carlo simulation. Estimates of the systematic errors were determined by varying each of the input parameters around the nominal value3. The overall uncertainty is dominated by the systematic error and by the uncertainty of the $D_s \to \phi\pi$ branching ratio.

$D_s \to \tau\nu$.

Charged leptons from the tau decay leptonic final states $\tau \to \mu\bar{\nu}\nu$ and $\tau \to e\bar{\nu}\nu$ are observed.

Two discriminating variables, U_c and U_b, distinguish the signal from uds, $c\bar{c}$, and $b\bar{b}$ backgrounds for each of the tau decay final states. The input variables with the greatest discriminating power include the fitted D_s momentum, the angle between the lepton and the D_s direction, several b-tag variables, and the total momentum of the reconstructed particles in the lepton hemisphere. The total number of fitted signal events in both tau decay channels is 652 with a background of 8586 events giving a ratio of signal to square-root of background $\text{Sig}/\sqrt{\text{Bkg}} \approx 7$. The systematic uncertainties are dominated by input parameters to the Monte Carlo simulation and detector resolution as well as the $D_s \to \phi\pi$ branching ratio.

Results

The uncertainty on $\mathcal{B}(D_s \to \phi\pi)$ is common to most experiments and contributes the largest systematic uncertainty (BR) on the D_s leptonic branching ratios. The present value4 is
$\mathcal{B}(D_s \to \phi\pi) = [3.6 \pm 0.9]\%$

The ALEPH results for $\mathcal{B}(D_s \to \tau\nu)$ are:
$[4.9 \pm 1.4(\text{stat}) \pm 2.0(\text{syst}) \pm 1.6(\text{BR})]\%$ e mode
$[4.9 \pm 0.9(\text{stat}) \pm 1.6(\text{syst}) \pm 1.4(\text{BR})]\%$ μ mode

The results for both D_s decay modes are
$\mathcal{B}(D_s \to \tau\nu)$
$= [4.9 \pm 0.9(\text{stat}) \pm 1.6(\text{syst}) \pm 1.4(\text{BR})]\%$
$\mathcal{B}(D_s \to \mu\nu)$
$= [0.64 \pm 0.08(\text{stat}) \pm 0.21(\text{syst}) \pm 0.15(\text{BR})]\%$

The combined result for the decay constant is
$f_{D_s} = [261 \pm 20(\text{stat}) \pm 43(\text{syst}) \pm 35(\text{BR})]\,\text{MeV}$

The figure shows the decay constant obtained by ALEPH along with previous results from CLEO2, L31, DELPHI5, FNAL E653[6], and CERN WA75[7]. The statistical and systematic errors have been combined but the normalization error has not been included. The normalization uncertainty is typically about 35 MeV. Also shown is an average of results of lattice QCD calculations.

References

[1] Acciarri M et al 1997 *Physics Lett.* **B396** 327
[2] Chadha M et al 1998 *Phys. Rev.* **D58** 32002
[3] The LEP Heavy Flavour Working Group reports. LEPHF/94-001, LEPHF/98-01.
[4] Caso C et al. (Particle Data Group) 1998 *Eur. Phys. J.* **C3** 1.
1999 update `http://pdg.lbl.gov`
[5] Parodi F et al 1997 International Europhysics Conference on High Energy Physics
[6] Kodama K et al 1996 *Physics Lett.* **B382** 299
[7] Aoki S 1993 et al *Prog. Theor. Phys.* **89** 131
[8] DELPHI Collaboration 1999 CERN-EP/99-67
OPAL Collaboration 1999 *Eur. Phys. J.* **C8** 573

HEAVY QUARK ASYMMETRIES

A. TRICOMI [a]

Dipartimento di Fisica and INFN Catania, I-95129 Catania, Italy [b]

Abstract. The electroweak properties of the heavy-quark production have been measured both at LEP and SLD. Progress in the flavour separation technique has significantly improved the accuracy of the measurements. We review recent measurements of the Forward-Backward asymmetries at LEP and of the Left-Right Forward-Backward asymmetries at SLD, and their comparison with the Standard Model expectations.

1 Introduction

The ALEPH, DELPHI, L3, and OPAL experiments [1] at the LEP and the SLD experiment [2] at the SLC have completed extremely successful data runs at the Z pole and have produced a great number of electroweak measurements: e.g., the Z lineshape parameters, the hadronic and leptonic cross-sections and their forward-backward and polarization asymmetries. These measurements constitute the building blocks of electroweak physics at the Z and a stringent test of the Standard Model of electroweak interactions by overcostraining its parameters. In particular, the measurements of the couplings for the process $Z \to f\bar{f}$ provide predictions for the unknown parameters of the Standard Model, and test of the model itself. Currently the best limits on the mass of the Higgs boson are derived from the radiative corrections to this process. Among the electroweak asymmetries measured both at LEP and SLD, there are four that involve the production of bottom and charm quarks: the *Forward/Backward asymmetries*, A^b_{FB} and A^c_{FB}, and the *Left-Right Forward-Backward Asymmetries*, A^b_{LRFB} and A^c_{LRFB} (measurable only at SLD due to the electron beam polarization), which are defined as:

$$A^f_{FB} = \frac{\sigma_F - \sigma_B}{\sigma_F + \sigma_B} = \frac{3}{4} A_e A_f \tag{1}$$

$$A^f_{LRFB} = \frac{(\sigma^L_F - \sigma^L_B) - (\sigma^R_F - \sigma^R_B)}{(\sigma^L_F + \sigma^L_B) + (\sigma^R_F + \sigma^R_B)} = P_e A_f \frac{2\cos\theta}{1+\cos^2\theta} \tag{2}$$

where σ is the differential cross-section of the process $e^+e^- \to Z \to f\bar{f}$, θ is the polar angle, P_e is the initial state longitudinal polarization ($P_e \neq 0$ only at SLD), and A_e (A_f) is the initial (final) state coupling asymmetry defined in terms of the chiral couplings as:

$$A_f = \frac{2c^f_V c^A_V}{(c^f_V)^2 + (c^f_A)^2} = \frac{(c^f_L)^2 - (c^f_R)^2}{(c^f_L)^2 + (c^f_R)^2}. \tag{3}$$

The coupling of the Z to leptons has been measured to a very high precision [3], and a similar precision is needed in the quark sector to test the universality of the coupling constants. The measurements reported here concern the heavy quark sector,

[a] e-mail: alessia.tricomi@cern.ch

[b] Also at INFN Sezione di Bari, I-70126 Bari, Italy

where the mass and lifetime of the associated hadron offer a variety of experimental signatures and the possibility of developing efficient tagging techniques.

2 Asymmetries Measurements

As can be inferred from equation (1, 2), measurements of the Forward-Backward asymmetries involve not only tagging the final state but also a method must be devised to sign the quark charge. Several techniques are used to identify $Z \to b\bar{b}$ and $Z \to c\bar{c}$ decays: lepton tags, kaon tags, vertex charge, D meson tags. Several new measurements have been presented this summer: new preliminary results from ALEPH on A^b_{FB} and A^c_{FB} using a lepton tag, and four new SLD results on A_b and A_c using vertex charge, kaon tag and reconstructed D mesons. A schematic summary of the different techniques used for the asymmetry measurements is shown in Tab. 1.

	Analysis	Tag	Quark Sign	Exp
A_b	Jet/Vtx Charge	Lifetime	Jet/Vtx Charge	ADLOS
	Kaon Tag	High M_{VTX}	Kaon	S
	Lepton tag	e, μ	e, μ	DLS
	+ NN			AO
A_c	Lepton tag	e, μ	e, μ	DLS
	+ NN			AO
	Inclusive Charm	Low M_{VTX}	Kaon or Vertex	S
		High P_{VTX}	Charge	
	Inclusive Slow	Veto	Slow pion	S
	Pion			
	Exclusive Charm	D	D^{*+}, D^+, D^0	ADOS

Table 1: The different techniques used for the asymmetry measurements by the four LEP Collaborations and SLD Collaboration.

2.1 A^b_{FB} *and* A^c_{FB} *Forward-Backward asymmetries using leptons*

A new preliminary result has been presented this summer by the ALEPH Collaboration [4] using the full sample of hadronic Z decays collected in the years 1991/1995. The analysis benefits from the upgraded track reconstruction and improved particle identification achieved in the recent reprocessing of the LEP1 data set.

In this analysis the quark's electric charge is tagged by means of the electron and muon charges produced in b and c semileptonic decays. The signal events are $b \to \ell$ and $c \to \ell$ respectively for A^b_{FB} and A^c_{FB}. The relevant point for the b and c asymmetry measurements is the isolation of this processes. This is achieved by means of two multivariate quantities (denoted N_b and N_{uds}), optimized to provide the flavour separation within the lepton candidate sample. The variable used to form multivariate quantities are described in detail in Ref. [4]. In addition, special attention has been directed towards the separation of the process $b \to \ell$ and $b \to c \to \ell$, the latter being the major source of dilution of the statistical significance of the measurement. A dedicated multivariate analysis is used also for this purpose.

The A^b_{FB} and A^c_{FB} are extracted simultaneously in a fit to the polar angle distribution of event containing at least one identified lepton candidate in the parameter space of the three variables controlling the flavour and the processes separation. The b and c asymmetries at peak energy are measured to be:

$$A^b_{FB} = 0.0949 \pm 0.0040\,(stat.) \pm 0.0023\,(syst.),$$

$$A^c_{FB} = 0.0562 \pm 0.0053\,(stat.) \pm 0.0036\,(syst.),$$

which result in the following measurement of the electroweak mixing angle:

$$\sin^2\theta_W^{eff} = 0.23228 \pm 0.00076.$$

2.2 *New* A_b *and* A_c *results from* SLD

Two new results have been presented by the SLD Collaboration for the A_b measurement: a new analysis using a vertex-charge technique and an update of the measurement using charged kaons. Also for the A_c measurements they reported two new results: one using inclusive charm tagging and the other one using reconstructed charmed mesons.

New measurement of A_b using a vertex charge technique

A preliminary direct measurement of A_b from data collected in the SLC Large Detector (SLD) during its 1996-1998 run has been realized using an inclusive vertex mass tag to select a sample of $Z \to b\bar{b}$ events [5]. Events containing two vertices well separated from the interaction point were selected, with at least one vertex (the "tag" vertex) with invariant mass $M_{VTX} > 2.0\,\mathrm{Gev}/c^2$.
The quark/antiquark direction is determined by the charge of the reconstructed vertex. To estimate the accuracy of the quark assignment, a self-calibration technique was used. This reduces the model dependence of the result. The value of A_b is extracted via a fit to a maximum likelihood function based on the differential cross-section, which gives

$$A_b = 0.897 \pm 0.027\,(stat)^{+0.036}_{-0.034}\,(syst).$$

Measurement of A_b using charged kaons

The data collected by SLD during the 1997-98 period have been used to update a previous measurement using charged kaons [6]. This measurement uses a vertex tag technique, where the selection of b hemisphere is based on the reconstructed mass of the bottom hadron decay vertex. The method benefits from the 3D vertexing capabilities of SLD's CCD vertex detector to obtain a high b purity and efficiency. Charged kaons associated with separated topological vertices are used to sign the quark direction, exploiting the dominant $b \to c \to s$ decay chain, with the analyzing power calibrated on data. A maximum likelihood fit to the total cross section gives:

$$A_b = 0.997 \pm 0.044 \pm 0.067.$$

Measurement of A_c using inclusive charm tagging

A new measurement of A_c has been realized using the 1993-98 SLD dataset [7]. This measurement uses a vertex tag technique, similar to the one used for the A_b measurement. The method takes advantage of the 3D vertexing capabilities of SLD's CCD vertex detector and the small and stable SLC beams: the selection of c hemispheres is based on the reconstructed mass of the charm hadron decay vertex. A high c-event tagging efficiency and purity (28% and 82% respectively) has been obtained. The determination of the quark/antiquark direction is done in two ways: the first is the vertex charge, the second is the kaon charge, with about 50% and 25% efficiency respectively. The probability to correctly discriminate between quark/antiquark for this tag has been calibrated from the data.
A maximum likelihood fit of all tagged events gives

$$A_c = 0.603 \pm 0.028 \pm 0.023.$$

Measurement of A_c using reconstructed charmed mesons

Approximately 550K Z decay collected by the SLD detector during the 1993-98 data period have been analyzed to extract the parity-violation parameter A_c [8]. The tagging of $Z \to c\bar{c}$ events was performed using two different methods: the exclusive reconstruction of D^{*+}, D^+, and D^0 mesons, and the inclusive p_T spectrum of soft-pions (π_s) in the decay chain of $D^{*+} \to D^0 \pi_s^+$. The charge of the primary quark is determined by the sign of the $D^{(*)+}$, or K^- (in the D^0 case). The direction of the primary quark is estimated from the direction of reconstructed D meson. To extract A_c, in both cases, an unbinned maximum likelihood fit, based on the Born-level cross section for fermion production in Z decay, was used.
The combined results of this two methods gives the preliminary result:

$$A_c = 0.688 \pm 0.035\,(stat.) \pm 0.025\,(syst.).$$

3 Combined LEP and SLD results

All LEP and SLD heavy flavour electroweak results were combined by the LEP Electroweak Working Group and the SLD Heavy Flavour Group. Tab. 2 shows all the measurements of A_b and A_c from Z samples collected by the LEP experiments and SLD. For the purpose of comparison, the LEP $A_{FB}^{b,c}$ values are scaled to $A_{b,c}$ using $A_e = 0.1496 \pm 0.016$, which is obtained combining the LEP lepton data with the SLD A_{LR} measurements.

All these measurements are combined taking into account the common systematics. For the Z pole asymmetries, data from all $\sqrt{s}$ points are combined, corrected for $\sqrt{s} = m_Z$, for QED initial state radiation and for small photon exchange contribution. The LEP averages are $A_{FB}^b = 0.0988 \pm 0.0020$ and $A_{FB}^c = 0.0692 \pm 0.0037$. In the SM these are equivalent to $\sin^2\theta_W^{eff} = 0.23228 \pm 0.00036$ and $\sin^2\theta_W^{eff} = 0.23255 \pm 0.00086$ respectively. The fit performed on the full set of LEP and SLD electroweak measurements, described in detail in reference [9] gives the following results for the heavy quark asymmetries and coupling parameters:

$$A_{FB}^{0,b} = 0.0988 \pm 0.0020$$

	Technique	Exp.	$A_{b,c} \pm$ stat $\pm$ syst
A_b	jetcharge	ALEPH	$0.950 \pm 0.037 \pm 0.029$
		DELPHI	$0.892 \pm 0.042 \pm 0.020$
		L3	$0.803 \pm 0.105 \pm 0.051$
		OPAL	$0.897 \pm 0.048 \pm 0.036$
		SLD	$0.882 \pm 0.020 \pm 0.029$
	vtx charge	SLD	$0.897 \pm 0.027 \pm 0.034$
	lepton	ALEPH	$0.889 \pm 0.036 \pm 0.023$
		DELPHI	$0.917 \pm 0.057 \pm 0.026$
		L3	$0.871 \pm 0.055 \pm 0.030$
		OPAL	$0.852 \pm 0.038 \pm 0.021$
		SLD	$0.924 \pm 0.032 \pm 0.026$
	$K^{\pm}$	SLD	$0.960 \pm 0.040 \pm 0.069$
A_c	D^*	ALEPH	$0.63 \pm 0.08 \pm 0.02$
		DELPHI	$0.64 \pm 0.08 \pm 0.04$
		OPAL	$0.64 \pm 0.10 \pm 0.05$
	D^*, D^+	SLD	$0.690 \pm 0.042 \pm 0.050$
	soft π	SLD	$0.683 \pm 0.052 \pm 0.050$
	lepton	ALEPH	$0.59 \pm 0.05 \pm 0.03$
		DELPHI	$0.73 \pm 0.10 \pm 0.11$
		L3	$0.82 \pm 0.29 \pm 0.19$
		OPAL	$0.58 \pm 0.06 \pm 0.04$
		SLD	$0.567 \pm 0.051 \pm 0.064$
	$K^{\pm}$	SLD	$0.603 \pm 0.028 \pm 0.023$

Table 2: SLD and LEP measurements of A_b, A_c. LEP measurements are derived from $A_{b,c} = 4A_{FB}^{b,c}/3A_e$.

$$A_{FB}^{0,c} = 0.0692 \pm 0.0037$$

$$A_b = 0.911 \pm 0.025$$

$$A_c = 0.630 \pm 0.026$$

Fig. 1 shows all the measurements of $\sin^2\theta_W^{eff}$ from Z data from SLD and LEP. The combined average is $\sin^2\theta_W^{eff}$=0.23151±0.00017, in agreement with the direct m_t measurement.

Fig. 2 (left panel) compares the results on A_{FB}^b and A_b with the Standard Model predictions, as a function of the leptonic coupling asymmetry A_l. The horizontal band shows the SLD A_b result, while the LEP A_{FB}^b results is shown on the diagonal band and the vertical band represents the combined LEP and SLD A_l results. The Standard Model prediction is displayed as a solid line. A slight disagreement can be seen between the Standard Model expectation and the intersection of experimental bands, even if it is not statistically significant with the current dataset. A similar trend can be seen also for the c asymmetry (right panel).

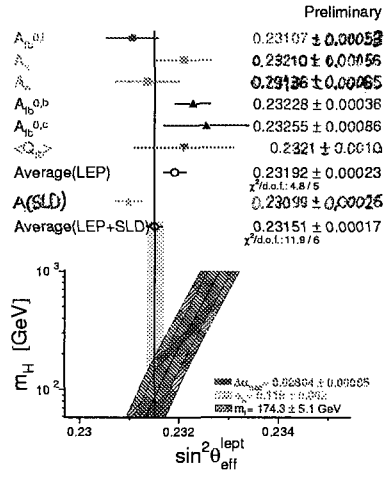

Figure 1: SLD and LEP weak mixing angle measurements.

4 Conclusions

The four LEP Collaborations and SLD Collaboration have made precise measurements of the b and c asymmetries, which are generally in good agreement with the Standard Model expectation.
Several new analyses have been reported this summer, which, thank to improved tagging techniques, have increased the sensitivity of these measurements. No new data at the Z are expected, however new multivariate analysis seem promising for further improve the b and c asymmetry estimation.

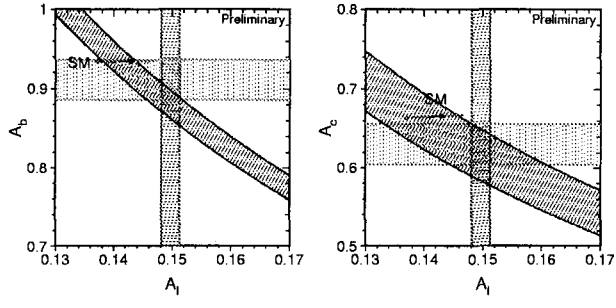

Figure 2: Standard Model expectation vs experimental SLD $A_{b,c}$, LEP $A_{FB}^{b,c}$ results in the $A_{b,c}, A_l$ plane. For explanation see the text.

Acknowledgments

I am very grateful to the LEP and SLD Collaborations and the LEP Electroweak Working Group, especially D. Abbaneo and S. Fahey. I thank also the conference organizers for their hospitality.

References

[1] The LEP Experiments: ALEPH, DELPHI, L3, and OPAL, *Nucl. Inst. Meth. A* **378**, 101 (1996).
[2] K. Abe et al., *Phys.Rev. D* **53**, 1023 (1996).
[3] J. Brau, to appear in *Proceedings of HEP-EPS Conference*, July 1999, Tampere, Finland.
[4] R. Barate at al., *"Measurements of the b and c Forward-Backward Asymmetries Using Leptons"*, ALEPH 99-076, CONF 99-048, contributed paper to the HEP-EPS Conference, July 1999, Tampere, Finland.
[5] K. Abe et al., *Measurement of A_b at the Z^0 using a Vertex Charge Techinique*, SLAC-PUB-8201, 1999.
[6] K. Abe et al., *Measurement of A_b using charged Kaons at SLD*, SLAC-PUB-8200, 1999.
[7] K. Abe et al., *Direct Measurement of A_c using Inclusive Charm Tagging at th SLD Detector*, SLAC-PUB-, 1999.
[8] K. Abe et al., *Measurement of A_c with charmed mesons at SLD*, SLAC-PUB-8195, 1999.
[9] The LEP Electroweak Working Group, CERN-EP/99-15.

Experimental signature of a fermiophobic Higgs boson

L. BRÜCHER [a], R. SANTOS [b]

Centro de Física Nuclear da Universidade de Lisboa, Av. Prof. Gama Pinto 2, 1649-003 Lisboa, Portugal

Abstract. The most general Two Higgs Doublet Model potential without explicit CP violation depends on 10 real independent parameters . Excluding spontaneous CP violation results in two 7 parameter models. Although both models give rise to 5 scalar particles and 2 mixing angles, the resulting phenomenology of the scalar sectors is different. If flavour changing neutral currents at tree level are to be avoided, one has four alternative ways of introducing the fermion couplings in both cases. In one of these models the mixing angle of the CP even sector can be chosen in such a way that the fermion couplings to the lightest scalar Higgs boson vanishes. At the same time it is possible to suppress the fermion couplings to the charged and pseudo-scalar Higgs boson by appropriately choosing the mixing angle of the CP odd sector. We investigate the phenomenology of both models in the fermiophobic limit and present the different branching ratios for the decays of the scalar particles. We use the present experimental results from the LEP collider to constrain the models.

1 Introduction

Despite the great success of the Standard model (SM) the mechanism to generate the vector boson masses, the so called Higgs mechanism, still awaits experimental confirmation. Current limits at LEP yield a mass of $m_h > 91.0\ GeV$ 1 for a minnimal Higgs boson. Thus it is appropriate to investigate models with an extended Higgs sector, which allow a light Higgs boson not restricted by the current SM Higgs mass limit. A class of these models are the Two Higgs Doublets models (2HDM) with type I coupling to the fermions 2. In the following we will discuss these models in the so-called fermiophobic limit. We start our discussion with summarizing the 2HDM potentials and defining the fermiophobic limit. Thereafter we will restrict the physical parameters by theoretical constraints. Then we will discuss the branching ratios of the light scalar Higgs particle. Finally we will constrain the model by using recent experimental data.

2 The potentials

The most general 2HDM potential invariant under $SU(2) \times U(1)$ has fourteen independent real parameters. If one imposes that the potential neither explicit nor spontaneously violates CP one has two different possibilities to restrict the potential 3. First, the potential can be made invariant under a Z_2 transformation $\phi_1 \to \phi_1$ and $\phi_2 \to -\phi_2$. The resulting potential, which is known as V_A, is:

$$V_A = -\mu_1^2 x_1 - \mu_2^2 x_2 + \lambda_1 x_1^2 + \lambda_2 x_2^2 + \lambda_3 x_3^2 + \lambda_4 x_4^2 + \lambda_5 x_1 x_2 \ , \tag{1}$$

where we used the abbriviations $x_1 = \phi_1^\dagger \phi_1$, $x_2 = \phi_2^\dagger \phi_2$, $x_3 = \Re\{\phi_1^\dagger \phi_2\}$ and $x_4 = \Im\{\phi_1^\dagger \phi_2\}$. Second, it is possible to make the potential invariant under the global $U(1)$

[a] e-mail: bruecher@alf1.cii.fc.ul.pt

[b] e-mail: rsantos@alf1.cii.fc.ul.pt

transformation $\phi_2 \to e^{i\theta}\phi_2$. The potential then reads:

$$V_B = -\mu_1^2 x_1 - \mu_2^2 x_2 - \mu_{12}^2 x_3 + \lambda_1 x_1^2 + \lambda_2 x_2^2 + \lambda_3 \left(x_3^2 + x_4^2\right) + \lambda_5 x_1 x_2 \ . \qquad (2)$$

Note that the term $-\mu_{12}^2 x_3$ breaks the global symmetry softly. Both V_A and V_B have seven degrees of freedom, the four particle masses, the two rotation angles (α,β) and the term providing the masses for the gauge bosons. The major difference of the potentials is in the scalar self couplings. This leads to a different phenomenology not only in the cases where the Higgs particles interact among themselves, but also when loop effect play a dominant role in particle decays.

3 The fermiophobic limit

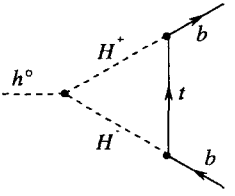

Figure 1: Feynman diagram of the largest contribution to $h^0 \to b\bar{b}$

Although potential V_A and V_B give rise to different scalar self-couplings, the couplings of the scalars to the fermions and the vector bosons are the same. Avoiding flavour changing neutral currents induced by Higgs exchange one has four different ways to couple the fermions to the Higgs sector. This is done most naturally by extending the global symmetry to the Yukawa Lagrangian. The resulting for different models are usually denoted as as model I, II, III and IV (cf. e.g. 2).

In model I all fermions couple to just one Higgs doublet. Thus, by choosing $\alpha = \pi/2$, one obtains a complete fermiophobic light CP-even scalar Higgs particle, h^0, in this model. However, h^0 can still decay to a fermion pair via $h^0 \to W^*W(Z^*Z) \to 2\,\bar{f}f$ or $h^0 \to W^*W^*(Z^*Z^*) \to 2\,\bar{f}f$. We will include these decays in our analysis. Moreover, decays of h^0 to two fermions can also be induced by scalar and gauge boson loops (see e.g. fig. 1). But fortunately it turns out that the only relevant one-loop decay is $h^0 \to b\bar{b}$ due to a large contribution of the Feynman diagram shown in fig. 1 to the total decay width.[c] Thus, on one hand, h^0 is not completely fermiophobic at $\alpha = \pi/2$, and on the other hand, all decays $h^0 \to f\bar{f}$ but $h^0 \to b\bar{b}$ are almost zero even at one-loop level. The coupling of the h^0 to the vector bosons is proportional to the sine of $\delta \equiv \alpha - \beta$. If we let β tend to α ($\beta \to \alpha = \pi/2$), then h^0 is not only fermiophobic but also bosophobic and "ghostphobic" – It always needs another scalar particle to be able to decay. The differences between potential A and B can be extremely important in this limit since h^0 will have different signatures in each model. In contrast, the heaviest CP-even scalar, H^0, acquires the Higgs standard

[c]The coupling $[H^+\bar{t}b]$ is proportional to the t-quark mass.

model couplings to the fermions in this limit. We will relax the limit $\beta \approx \pi/2$ and analyze the decays as a function of δ and of the Higgs masses.

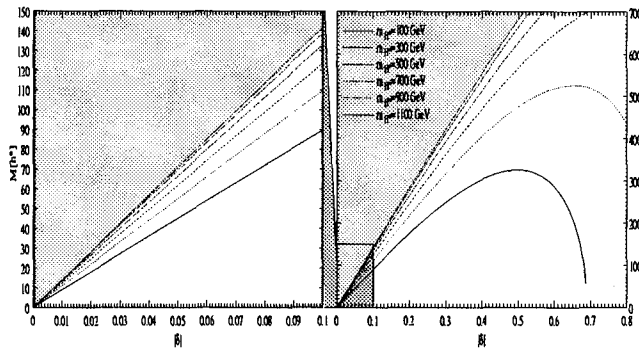

Figure 2: Limit on m_{h^0} as a function of δ in potential$A$.

Before we start our analysis we have to ensure, that by choosing a set of values for $(m_{h^0}, m_{H^0}, m_A, m_{H^+}, \alpha, \beta)$ we do not leave the perturbative regime. In general, the bounds ensuring this, are the so-called tree-level unitarity bounds 4. For potential V_A they yield:

$$m_{h^0} \leq \sqrt{\frac{16\pi\sqrt{2}}{3\,G_F}\cos^2\beta \;-\; m_{H^0}^2\cot^2\beta} \;, \tag{3}$$

where $G_F = 1.166\ GeV^{-2}$ denotes Fermis constant. We have plotted this equation in fig. 2. One easily verifies that in the limit $\delta \to 0$ h^0 becomes massless, which is also clear from eq. 3. Unfortunately no tree-level unitarity bounds are avalaible for potential V_B. Nevertheless, we know that in the fermiophobic limit 5:

$$m_{h^0}^2 = m_A^2 - 2\,(\lambda_+ - \lambda_1)\,v^2\cos^2\beta \;, \tag{4}$$

with $\lambda_+ = \frac{1}{2}(\lambda_3 + \lambda_5)$ and $v = 246\ GeV/c^2$ denoting the vacuum expectation value. The equation shows, that in the limit $\delta \to 0$ the masses of h^0 and A^0 will be degenerated, which is also illustrated in fig. 3.

The overall picture given by all branching ratios led us to distinguish between three different regions for δ. We define these regions now for the following qualitative analysis:

- the *tiny* δ region where $|\delta| \leq 0.05$,
- the *small* δ region with $0.05 < |\delta| \leq 0.1$ and
- finally the medium and *large* δ region when $|\delta| > 0.1$.

4 The lightest scalar Higgs boson

As already pointed out, the lightest scalar Higgs boson (h^0) has no tree level couplings to the fermions for $\alpha = \pi/2$. Thus the following tree level decays have to be

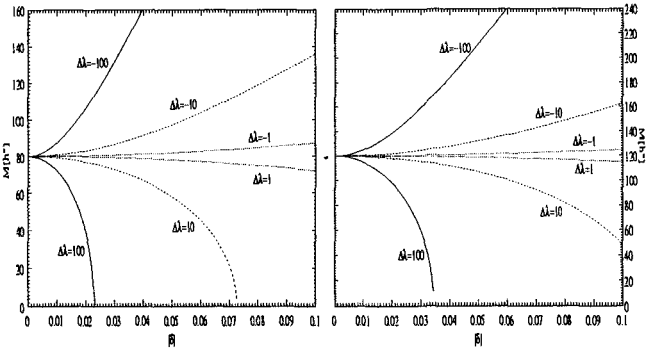

Figure 3: Limit m_{h^0} as a function of δ for $m_A = 80\ GeV$ and $m_A = 120\ GeV$.

considered:

$$h^0 \to W^+W^- \quad ; \quad h^0 \to ZZ \quad ; \quad h^0 \to ZA^0 \quad ;$$
$$h^0 \to W^\pm H^\mp \quad ; \quad h^0 \to A^0A^0 \quad ; \quad h^0 \to H^+H^- \quad .$$

Additionally the following one-loop induced decays are important:

$$h^0 \to \gamma\gamma \quad ; \quad h^0 \to Z\gamma \quad ; \quad h^0 \to b\bar{b} \quad .$$

Moreover, decays to fermions via virtual vector bosons have to be taken into account, namely:

$$h^0 \to W^*W^* \to f\bar{f}f\bar{f} \quad ; \quad h^0 \to W^*W \to f\bar{f}W \quad ;$$
$$h^0 \to Z^*Z^* \to f\bar{f}f\bar{f} \quad ; \quad h^0 \to Z^*Z \to f\bar{f}Z \quad .$$

The partial tree-level decay widths are listed in 6, where also results for the other Higgs particles A, $H^\pm$ and H^0 can be found. The one-loop induced decays have been calculated with *xloops* 7. Decays via virtual particles have been calculated in ref. 8. We have taken these formulas and changed them appropriately.

As stated earlier, the only significant decay mode to fermions, via vector boson and scalar loops, is $h^0 \to b\bar{b}$. For all the other fermionic decays the Feynman graphs are suppressed either by the Cabbibo-Kobayashi-Maskawa matrix or by the small mass of the fermions in the loop. However, the diagram shown in fig. 1 is suppressed by a $\tan^2\delta$ factor when compared with the corresponding diagram in $h^0 \to \gamma\gamma$. Thus, as will be seen below, the decay $h^0 \to b\bar{b}$ is of minor importance in the tiny and small δ region.

In potential A the upper bound for the mass of the lightest scalar Higgs boson is approximately the W mass in the tiny δ region. Thus h^0 has only two possible decay modes. Either it decays into A^0A^0, if the mass of the lightest scalar is twice as large as the mass of the pseudo-scalar Higgs boson, or it decays into two photons.[d] In the

[d]The third possible decay, $h^0 \to H^+H^-$ is already ruled out by the experimental lower limit on the mass of the charged Higgs boson (cf. section 5).

small δ region the growth of the upper mass limit for m_{h^0} gives rise to more decay modes, as can be seen in fig. 4. For small h^0 masses the situation is the same as in the tiny δ region. Depending on the mass of the pseudo-scalar, the dominant decay is again either $h^0 \to A^0 A^0$ or $h^0 \to \gamma\gamma$. As soon as $m_{h^0} > m_W$, decays via virtual vector bosons overtake the decay to $\gamma\gamma$ and give rise to a fermionic signature of h^0. Of course the value of m_{h^0}, for which the branching ratio of $h^0 \to W^* W^*$ becomes bigger than 50% depends on δ. At the lower end of the small δ region this happens approximately at $m_{h^0} = 110\ GeV$, whereas at the upper end it is close to the W mass. At first, in the large δ region the branching ratio does not change much. Of course the upper bound for m_{h^0} looses importance and all decays become kinematically allowed, as can be seen in fig. 5. As δ increases, the decay $h^0 \to b\bar{b}$ becomes more and more significant for small masses of m_{h^0}. If e.g. $m_{h^0} = 20\ GeV$ we get a branching ratio for $h^0 \to b\bar{b}$ of the order of 30% at $\delta = 0.5$ and of 75% at $\delta = 1.0$. This reflects the already mentioned $\tan^2\delta$ suppression of this decay mode.

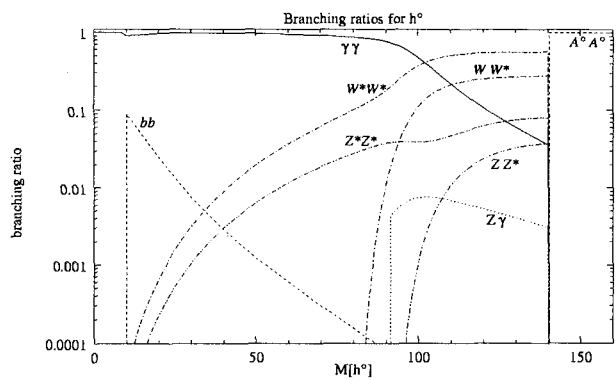

Figure 4: Branching ratios of h^0 at $m_{A^0} = 70\ GeV$, $m_{H^+} = 140\ GeV$, $m_{H^0} = 300\ GeV$ and $\delta = 0.1$ in potential A.

In potential B the masses of h^0 and A^0 are almost degenerated in the tiny δ region. Thus for small masses ($< m_W$) h^0 decays mainly into two photons. On the other hand, no upper bound on m_{h^0} exists in potential B. As a consequence a heavy h^0 can also decay via virtual vector bosons into fermions in the tiny δ region (cf. fig. 6). In the small δ region the branching ratio strongly depends on the parameters m_A and m_{H^+}. It can either resemble the plot for potential A (see fig. 4), or, due to strong cancellation between the H^+- and the W-loops in the $h^0 \to \gamma\gamma$ decay, it can be as shown in fig. 7. In this figure we see that $h^0 \to \gamma\gamma$ only dominates until $m_{h^0} \approx 30\ GeV$. Then, decays via virtual vector bosons are the major decays of h^0. Note that $h^0 \to b\bar{b}$ is suppressed in a similar way to $h^0 \to \gamma\gamma$, because both decays depend on the same couplings of h^0 to the vector bosons and to the scalars. In the large δ region this behaviour is almost the same. Of course, as in potential A, for some value of δ the decay $h^0 \to b\bar{b}$ will dominate over $h^0 \to \gamma\gamma$ for small values of m_{h^0}.

Finally we show the total decay width of h^0 as function of m_{h^0} for different values

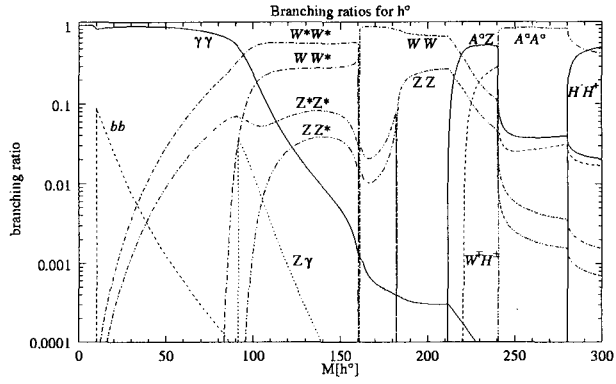

Figure 5: Branching ratios of h^0 at $m_{A^0} = 120\ GeV$, $m_{H^+} = 140\ GeV$, $m_{H^0} = 300\ GeV$ and $\delta = 0.2$ in potential A.

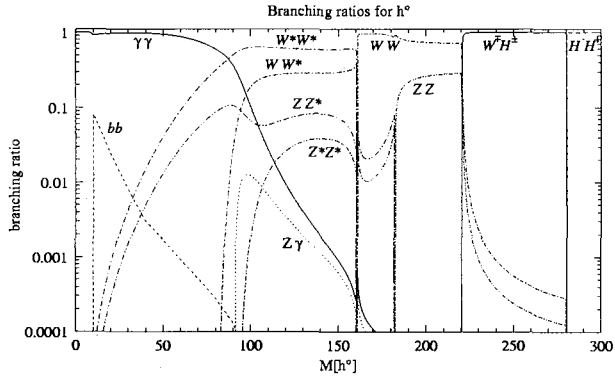

Figure 6: Branching ratios of h^0 at $m_{A^0} = m_{h^0}$, $m_{H^+} = 140\ GeV$, $m_{H^0} = 300\ GeV$ and $\delta = 0.01$ in potential B.

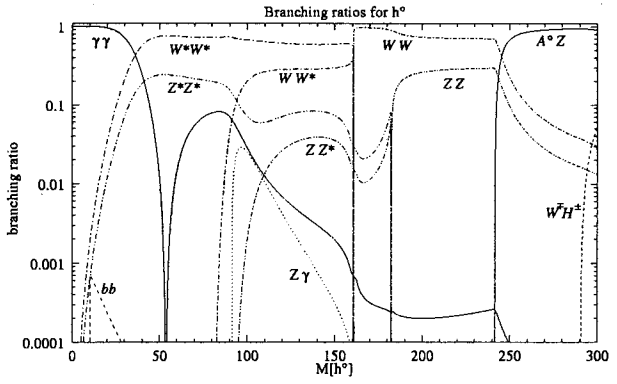

Figure 7: Branching ratios of h^0 at $m_{A^0} = 150\ GeV$, $m_{H^+} = 210\ GeV$, $m_{H^0} = 300\ GeV$ and $\delta = 0.1$ in potential B.

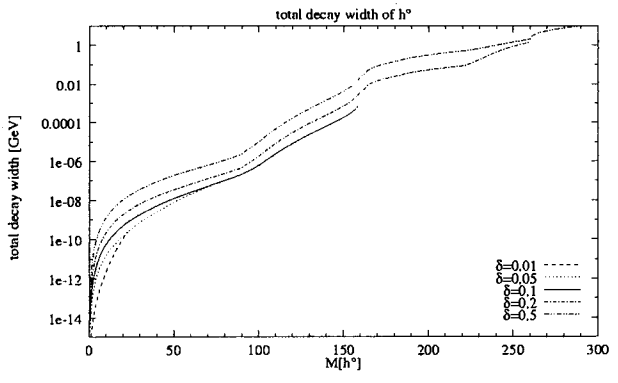

Figure 8: Total decay width of h^0 with $m_{A^0} = 130\ GeV$, $m_{H^+} = 150\ GeV$, $m_{H^0} = 300\ GeV$ for different values of δ potential A.

of δ in fig. 8. As expected, the total decay width grows with m_{h^0} and δ. We do not show the total decay width for potential B because the overall behaviour is the same as for potential A.

5 Constraints on the models

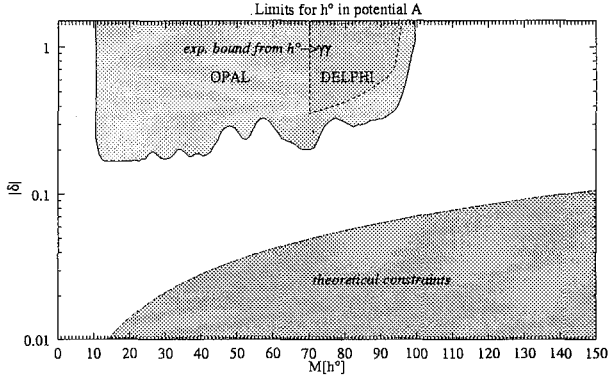

Figure 9: Bounds in the m_{h^0}-δ plane for potential A.

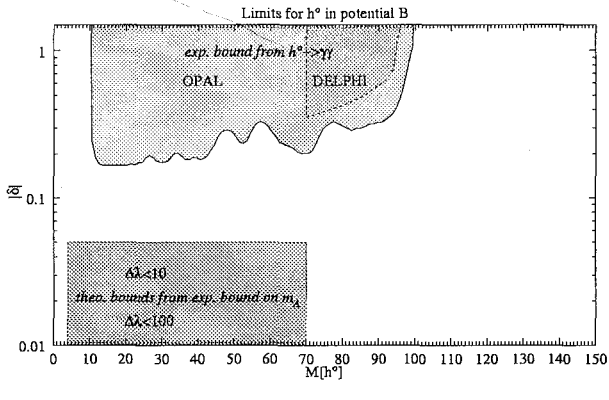

Figure 10: Bounds in the m_{h^0}-δ plane for potential B.

In this section we use the available experimental data and the bounds derived in section 3 to constrain the models.

Most production modes of the pseudo-scalar Higgs boson at LEP are suppressed in the fermiophobic limit. An exception is the associated production $Z^* \to h^0 A^0$ when kinematically allowed. The more δ tends to zero the larger becomes the cross section for this production mode. However, the obtained limit for m_A is not independent of

the mass of the lightest scalar Higgs boson. This production mechanism has recently been measured by the DELPHI coll. 9, where more detailed results can be found. For this associated production we roughly summarize their result in the following inequation:

$$\sqrt{m_{h^0}^2 + m_A^2} \geq 80\ GeV \tag{5}$$

For the lightest scalar Higgs boson mass the most stringent bounds can be derived from the experimental measurement of massive di-photon resonances. The most recent data have been published in refs. 10, 9. We have used this data to exclude some regions in the m_{h^0}-δ plane. We have plotted the results in fig. 9 for potential A and in fig. 10 for potential B. Moreover we have inserted the theoretical constraints shown in fig. 2. In fig. 9 (potential A) this can be seen as the lower limit on δ for a given h^0 mass. For potential B the experimental bound on m_A can be used to derive a lower limit on δ for a given m_{h^0}. In fig. 10 we have plotted this area for different values of $\Delta\lambda$.[e]

6 Conclusion and outlook

We have shown the branching ratios for the lightest CP-even scalar Higgs particles of fermiophobic 2HDMs as a function of the Higgs masses and δ. We have shown that the two different scalar sectors, potential A and B, give rise to different signatures for some regions of the parameter space. Most of the mass bounds based on a general 2HDM or on the MSSM do not apply in the fermiophobic case. We have used the available experimental data and tree-level unitarity bounds to constrain the models. It turns out, that there is still a wide region of this parameter space not yet excluded by experimental data and still accessible at the LEP collider. So, one should keep an open mind for surprises in the Higgs sector.

Acknowledgements

We like to thank our experimental colleagues at LIP for the inspiring discussions. L.B. is partially supported by JNICT contract No. BPD.16372.

References

[1] The OPAL coll. *Search for Neutral Higgs bosons in e^+e^- Collisions at $\sqrt{s} \approx$ 189 GeV. OPAL PN382* (1999).
[2] R. Santos and A. Barroso. *Phys. Rev.* **D 56** (1997) 5366–5385.
[3] J. Velhinho, R. Santos and A. Barroso. *Phys. Lett.* **B 322** (1994) 213–218.
[4] S. Kanemura, T. Kubota and E. Takasugi. *Phys. Lett.* **B 313** (1993) 155–160.
[5] A. Barroso, L. Brücher and R. Santos. *Phys. Rev.* **D 60** (1999) 0035005.
[6] L. Brücher and R. Santos, Eur. Phys. J. **C12** (2000) 87.
[7] L. Brücher, J. Franzkowski and D. Kreimer. *Nucl. Instrum. Meth.* **A 389** (1997) 323–342; L. Brücher, J. Franzkowski and D. Kreimer. *hep-ph* **9710484**;

[e] c.f. section 3.

L. Brücher, J. Franzkowski and D. Kreimer. *Comp. Phys. Comm.* **115** (1998) 140–160.

[8] Jorge C. Romao and Sofia Andringa. *Eur. Phys. J.* **C7** (1999) 631.

[9] DELPHI coll.. *Search for non fermionic neutral Higgs couplings at LEP 2. Conference contribution to HEP Conference in Helsinki* (1999).

[10] OPAL coll.. *Eur. Phys. J.* **C 1** (1998) 31–43.

s-channel Higgs Physics beyond the Standard model

G.G.Boyarkina [a]
Department of Physics, Minsk State Pedagogical University,
Soviet Street 18 , Minsk, 220050, Belarus

Abstract. The model with the $SU(2)_L \times SU(2)_R \times U(1)_{B-L}$ gauge group, containing one bidublet and two triplets in the Higgs sector, is considered. It is shown that the observation of the ultrahigh-energy neutrinos with the help of the processes

$$e^-\nu_e \to W^-Z, \qquad e^-\nu_e \to \mu^-\nu_\mu,$$

give us information about the singly charged Higgs bosons.

1 Introduction

It is quite possible that the actual Higgs sector in nature has more than one doublet of Higgs bosons or has Higgs bosons in other multiplets. This is expected in many theories that go beyond the SM. Attractive motivation for extending the Higgs sector is to generate the small masses of the left-handed neutrinos whose existence is hinted at by present solar and atmospheric neutrinos data, as well as cosmological observations of the large scale structure and the possible explaining of the hot dark matter picture in the universe. Amongst the extensions of the SM having the massive neutrino the left right models (LRM's) based on the gauge group $SU(2)_L \times SU(2)_R \times U(1)_{B-L}$ [1] are of special interest because the LRM's also offer a dynamical solution to the parity violation of weak interaction. Let us consider the asymmetric LRM ($g_L \neq g_R$) [2] with the bidoublet and two triplets. After spontaneous symmetry violation we are left with the following physical Higgs bosons: 4 doubly charged scalars $\Delta^{(\pm\pm)}_{L,R}$, 4 singly charged scalars $h^{(\pm)}$ and $\tilde{\delta}^{(\pm)}$, 4 neutral scalars S_i ($i = 1,2,3,4$) and 2 neutral pseudoscalars $P_{1,2}$. Masses of these bosons are the functions on the vacuum expectation values (VEV's) of the neutral components of the Higgs fields

$$< \delta^0_{L,R} >= \frac{v_{L,R}}{\sqrt{2}}, \qquad < \Phi^0_1 >= k_1, \qquad < \Phi^0_2 >= k_2,$$

where $v_L << max(k_1, k_2) << v_R$, and on a big number of self-coupling constants entering the Higgs potential. The subject of our investigation will be the phenomenology of the singly charged Higgs bosons. The Lagrangians describing the interaction of the singly charged Higgs bosons with leptons and gauge bosons are given by the expressions

$$\mathcal{L}_l = \sum_{a,b}\{[\frac{h'_{ab}k_2 - h_{ab}k_1}{2k_+}\overline{\nu}_a(1-\gamma_5)l_b - \frac{h_{ab}k_2 - h'_{ab}k_1}{2k_+}\overline{N}_a(1+$$

$$+\gamma_5)l_b]h^{(+)} + \frac{f_{ab}}{\sqrt{2}}\overline{l^c_a}(1+\gamma_5)\nu_b[\left(\frac{\beta k_0^2}{(\alpha+\rho_1-\rho_3/2)v_R^2}h^{(+)} - \tilde{\delta}^{(+)}\right) +$$

$$+\overline{l_a^c}(1-\gamma_5)N_b\left(\frac{k_0}{v_R}h^{(+)}+\frac{\beta k_0}{(\alpha+\rho_1-\rho_3/2)v_R}\tilde{\delta}^{(+)}\right)]+conj.\}, \qquad (1)$$

$$\mathcal{L}_V=\{-\frac{g_L g_R c_W c_\Phi b k_-^2}{\sqrt{2}k_+}h^{(+)}-\frac{g_L g_R g' s_W(g'^{-1}s_W c_\Phi+g_R^{-1}s_\Phi)}{c_W}[k_0 h^{(+)}+$$

$$\frac{\beta k_0}{(\alpha+\rho_1-\frac{\rho_3}{2})}\tilde{\delta}^{(+)}]\}W_{R\mu}Z_{1\mu}-$$

$$-\frac{e g_L s_\Phi v_L(g' g_R^{-1}+g_R g'^{-1})}{c_W}\left(\frac{\beta k_0^2}{(\alpha+\rho_1-\frac{\rho_3}{2})v_R^2}h^{(+)}-\tilde{\delta}^{(+)}\right)W_{L\mu}Z_{1\mu}. \qquad (2)$$

where $W_{R\mu}=-s_\xi W_{1\mu}+c_\xi W_{2\mu}$, $W_{L\mu}=c_\xi W_{1\mu}+s_\xi W_{2\mu}$, Φ and ξ are the mixing angles of the neutral and the charged gauge bosons, respectively, g' is the gauge coupling of the $U(1)_{B-L}$ subgroup,

$$k_\pm=\sqrt{k_1^2\pm k_2^2}, \qquad k_0=\frac{k_-^2}{\sqrt{2}k_+}, \qquad \alpha=\frac{\alpha_3 k_+^2}{2k_-^2},$$

$$\beta=\frac{k_+^2(\beta_1 k_1+2\beta_3 k_2)}{2k_-^2 k_0},$$

α_i, ρ_i and β_i are the constants entering the Higgs potential, h_{ab}, h'_{ab} and f_{ab} are the bidoublet and the triplet Yukava coupling constants (YCC's), respectively. In Ref. [3] was shown that in the LRM it is possible two possibilities: i) the mixing angles inside the neutrino generation φ_l are small ($10^{-5}-10^{-6}$), which takes place at both $v_L=0$ and $v_L\neq 0$; ii) at non-zero values v_L, the values of the angles φ_l can be as large as $few\times 10^{-2}$. Since in the LRM, as in any gauge theory where the neutrino acquires mass through the Higgs mechanism, there are the connection between the YCC's and the neutrino oscillation parameters, then the YCC's could have both the big and the small values. We also recall that the LRM structure allows to obtain the sizable values of the bidoublet nondiagonal constants at the degeneracy of the bidoublet VEV's (DBVEV) $k_1=k_2$ as well [3].

At present the most powerful neutrino accelerators are the cosmic accelerators in the outer space. It is known some sources of the ultrahigh- energy (UHE) cosmic ray neutrinos. One of them exploits neutrinos produced when UHE protons inelastically scatter off the cosmic microwave background radiation (CBR) in processes such as $\gamma p\to n\pi^+$ where the produced pion subsequently decays. The CBR neutrino energy can be as large as 1 EeV. Another sources of the UHE neutrinos are the Active Galactic Nuclei (AGN). Within AGN, protons accelerated to very high energy interact whith matter or ambient radiation and produce pions whose decay products include photons and neutrinos. The maximum energy of AGN neutrinos is of order 1 PeV. Let us discuss two processes with the UHE cosmic neutrinos which could be studied with the help of such the neutrino telescopes as BAIKAL NT-200, NESTOR and AMANDA. The first one is

$$e^-\nu_e\to W_1^- Z_1, \qquad (3)$$

In Fig.1 the Feynman diagrams corresponding to the process (3) in the second order of perturbation theory are shown. Since for the right polarized neutrino beam there are no diagrams with the virtual Higgs bosons and there are no resonance peaks we shall not discuss this case. In the case of the left polarized neutrino beam the contributions to the cross section of the reaction (3) come from the diagrams shown on Fig.1c, Fig.1d. As analysis shows the cross section σ_{LL} increases at moving away k_1 from $k_1 = k_2 = k_g \simeq 122.9537$ GeV. σ_{LL} does not practically depend on the values of both v_L and φ_l. Note, that $\Gamma_{\tilde{\delta}^{(-)} \to W_1^- Z_1}$ is of order $few \times 10^{-2}$ MeV and grows very slowly with the increase of $m_{\tilde{\delta}}$. So, the value of $f_{\tau\tau}$ is getting very important when the $\tilde{\delta}^{(-)}$ decay channels with the such heavy particles as W_2, Z_2, N_e, N_μ etc. are closed. Really, let us consider the case of the DBVEV. Then, the total cross section in the non-resonance region is very small. Notwithstanding this fact, the $\tilde{\delta}^{(-)}$- resonance could be detected. For example, at

$$c_Y = \frac{da\beta}{\alpha + \rho_1 - \rho_3/2} = 3, \qquad f_{ee} = 0.2,$$

$v_L = 1.7$ GeV and $m_{\tilde{\delta}} = 200$ GeV, the resonance peak height $(\sigma_{LL})_{\tilde{\delta}}$ is 3.6, 24, 15×10^3 fb. for $f_{\tau\tau}$ equals to 0.8, 0.5, 0.1, respectively. Special attention must be given to the Higgs potential parameters $\alpha + \rho_1 - \rho_3/2$ since they have potent effects on $(\sigma_{LL})_{\tilde{\delta}}$. There are no reasons that would forbid this combination to be very small. Recall, that the sole constraint on the parameters follows from the arguments of vacuum stability which demand [4]

$$\rho_1 - \rho_3/2 < 0.$$

Then, assuming $\alpha + \rho_1 - \rho_3/2 = 10^{-2}$ we, for the case of the small mixing angles, get

$$(\sigma_{LL})_{\tilde{\delta}} = 3.6 \times 10^3 \ pb.$$

Now we pass on to the case when the target electrons are right polarized. The cross section does not equal to zero for the right polarized neutrino only. The contributions to it come from the diagrams shown in Fig.1c and Fig.1e. It is pertinent to note, that in the Two Higgs Doublet Model we also have the same diagrams. The analysis shows that the sole chance for the observation of σ_{RR} is to operate in the $h^{(-)}$-resonance region. However the resonance peak height $(\sigma_{RR})_h$ mainly depends on the fact whether the interaction between the $h^{(\pm)}$ Higgs boson and quarks takes place or not. Let us assume that this interaction is absent. Then the situation is as follows. In the case of the DBVEV and in the case of the large values of the angle φ_e we always can detect the resonance peak connected with the $h^{(-)}$-boson. For example, when $m_h = 300$ GeV, $\varphi_e = 2 \times 10^{-2}$ and $k_1 = 140$ GeV, $(\sigma_{RR})_h$ is of order 3.5×10^3 pb. When the angle φ_e is very small then our possibilities for detecting the $h^{(-)}$ resonance peak crucially depend on the values k_1 ($(\sigma_{RR})_h$ increases or decreases when k_1 approaches to or moves off k_g). For example, at $m_h = 250$ GeV and $\varphi_e = 10^{-5}$ we have $(\sigma_{RR})_h = 2 \times 10^{-4}, 6 \times 10^{-2}, 1.6, 14$ pb. for k_1 equals to $10, 70, 100, 110$ GeV, respectively.

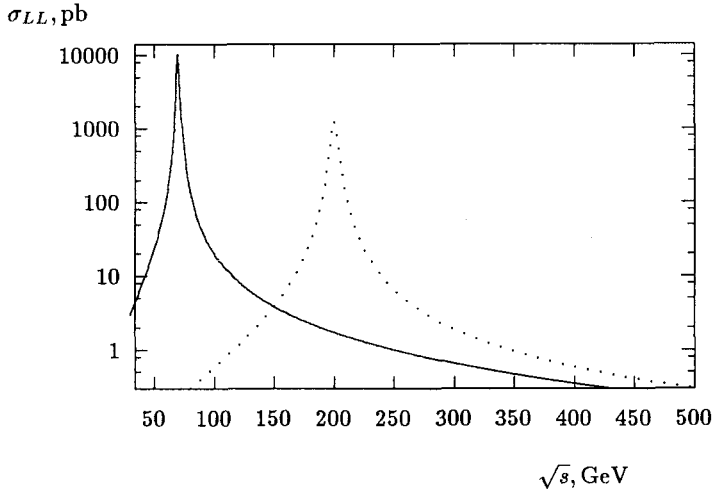

Fig. 1. The σ_{LL} as a function of $\sqrt{s}$ when $f_{\tau\tau} = 0.5$, $f_{\mu\mu} = 7.5 \times 10^{-2}$, $f_{ee} = 5.5 \times 10^{-2}$ and $k_1 = 90$ Gev for the cases (a) $m_{\tilde{\delta}} = 70$ GeV (solid line); (b) $m_{\tilde{\delta}} = 200$ GeV (dotted line).

Now we consider one more the process with the UHE neutrinos, namely

$$e^- \nu_e \to \mu^- \nu_\mu. \tag{4}$$

For the left polarized electrons and the right polarized neutrino the deviations from the SM predictions are very small. For example, at $f_{e\mu} = 3 \times 10^{-2}$ they are of order 0.1%. Recall that in this case there is the W-resonance peak (Glashow resonance) and its heihgt (σ_W) reaches the values of order 10^4 pb. The analysis shows that the initial $e_L^- \nu_{eL}$ and $e_R^- \nu_{eR}$ are of more direct interest to us. In Fig.2 we desplay the total cross section for the former case.

It is well to bear in mind that the following possibility could take place. The cross section on the singly charged Higgs boson resonances $(\sigma_{e^-\nu_e \to \mu^-\nu_\mu})_{\tilde{\delta},h}$ turns out to be bigger than σ_W. For example, when $f_{\tau\tau} = 0.6$, $f_{\mu\mu} = 0.75$, $f_{ee} = 0.09$ and $m_{\tilde{\delta}} = 70$ GeV, then we have $(\sigma_{e^-\nu_e \to \mu^-\nu_\mu})_{\tilde{\delta}} \sim 10^5$ pb.

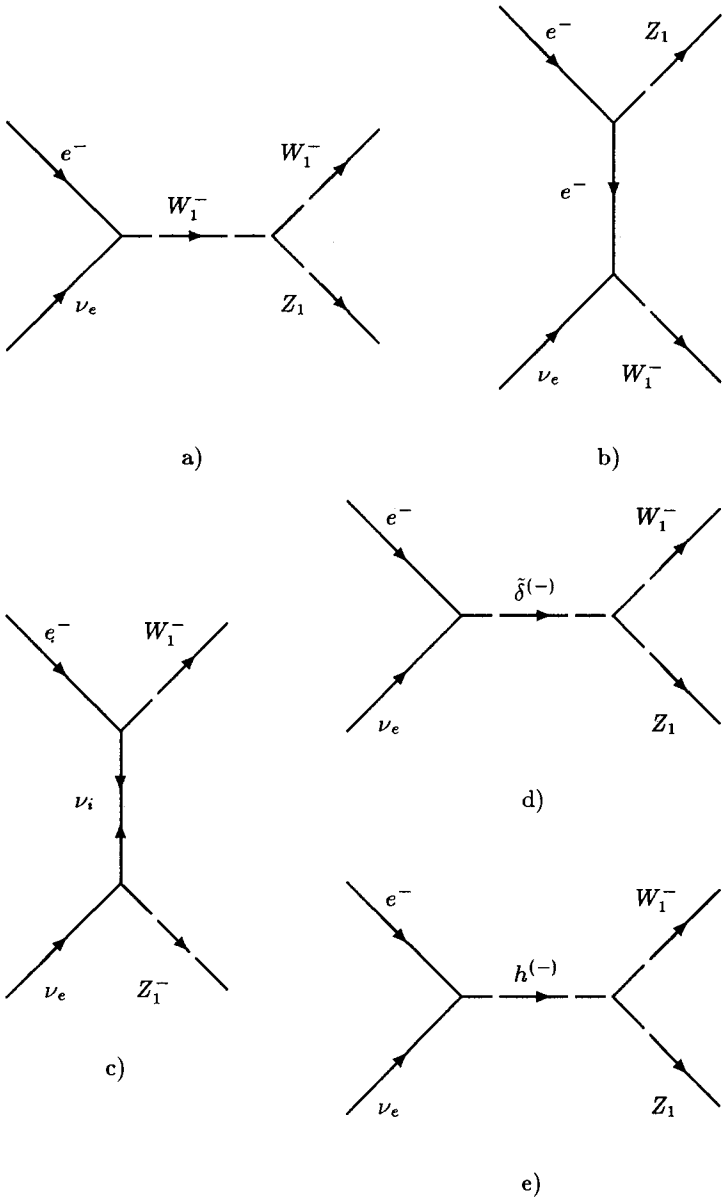

Fig.2 The Feynman diagrams giving the contributions to the reaction $e^-\nu_e \to W_1^- Z_1$.

In conclusion, we have considered two reactions

$$e^-\nu_e \to W_1^- Z_1, \qquad e^-\nu_e \to \mu^-\nu_\mu.$$

For the former within the SM any resonances are absent while the LRM predicts the existence of the $\tilde{\delta}^{(-)}$- and $h^{(-)}$- resonances whose heights could reach the values of order $few \times 10^3$ pb. For the latter, at $\sqrt{s} = m_W$, there is so called the Glashow resonance predicted both by the SM and the LRM. However, the LRM total cross section also has two resonance peaks related to the $\tilde{\delta}^{(-)}$- and $h^{(-)}$-Higgs bosons. At the corresponding values of the YC's and the Higgs potential parameters the height of these peaks could exceed that of the Glashow resonance. The UHE cosmic neutrino could be used for studying these two reactions at such the neutrino telescopes as BAIKAL NT-200, NESTOR and AMANDA. Then, the observation of the heavy muon showers connected with the resonance splashes in the cross sections will be definitely certifying both the existence of the singly charged Higgs bosons and the character of their interaction with quarks and leptons.

References

[1] J.C.Pati and A.Salam, *Phys. Rev.* **D**10, 275 (1974); G.Senjanovich and R.N.Mohapatra, *Phys. Rev.* **D**12, 1502 (1975).

[2] O.M.Boyarkin, *Phys. Rev.* **D**50, 2247 (1994).

[3] G.G.Boyarkina and O.M.Boyarkin, *Yad. Fiz.* 60, 683 (1997).

[4] N.G.Deshpande et al., *Phys. Rev.* **D**44, 837 (1991).

QUANTUM FIELD of NONSTATIONARY POLARON

O.A.KHRUSTALEV [a], M.V. TCHITCHIKINA [b] E.Yu.SPIRINA [c]
Physics Faculty of Moscow State University, 119899 Moscow, Russia

Abstract. Polaron problem is considered. Bogoliubov group variables for the space-time translations group are defined. The scheme of secondary quantization for the scalar field interacting with charged quantum field is proposed. Scalar field is assumes to have nonzero classical component. Polaron is treated as a result of interaction of charged particle and neutral field classical component. The system state space is constructed. Expressions for integrals of motion in zero-point order with respect to inverted powers of coupling constant are given as a derivatives with respect to symmetry group generators.

1 Introduction

The problem of accurate account of conservation lows in quantum theory when methods of approximate calculations are used has been solved by N.N.Bogoliubov. He considered the motion of classical particle in quantum field. In present work we come back to polaron problem and treat it as a problem of quantum field theory.

2 Bogoliubov Group Variables

Let's consider $(1+1)D$ system of charged and neutral scalar fields. Operators $\hat{\Psi}, \hat{\Psi}^*$ correspond to charged field and ϕ is neutral field.

Field interactions leads to appearance of classical component of neutral field. Bogoliubov transformation permits to separate this component:

$$\xi(x) = gv(x^{'}) + u(x^{'}), \tag{1}$$

where $g \gg 1$,

$$x^{'\alpha} = x^{\alpha} - \tau^{\alpha}, \quad \alpha = 1, 2,$$

τ^{α}-new variables connected with space-time translations. τ^{α} are considered as independent, so the right part of eq(1) contains on 2 variables more than the left part, and it is necessary to equalize the number of variables. To that end to additional conditions are imposed on $u(x^{'})$ function:

$$w(N^a, u) = \int (N_n^a(x^{'})u(x^{'}) - N^a(x^{'})u_n(x^{'}))dl = 0. \tag{2}$$

Symbol f_n denote the normal derivative of function f alone the integration line C which is defined as a straight line with a normal $n = (n^{\alpha}), n^2 = 1$ for simplicity. Equation of the line C

$$x^{\alpha} = e^{\alpha} l$$

[a] e-mail: khrust@goa.bog.msu.su
[b] e-mail: CHICH@srdlan.npi.msu.su
[c] e-mail: spirina@hep.phys.msu.su

is determined by vector n $e = (e^\alpha), e^2 = -1$ orthogonal to n. Using substitution (1) for $\xi(x)$ in (2) one can obtain functional dependence τ^α with respect to ξ, ξ_n in differential form:

$$\frac{\delta\tau^c}{\delta\xi(x)} = -\frac{1}{g}Q^c_b N^b_n(x'), \quad \frac{\delta\tau^c}{\delta\xi_n(x)} = \frac{1}{g}Q^c_b N^b(x'),$$

$Q^a_b = \delta^a_b - \frac{1}{g}R^a_c Q^c_b, R^c_\alpha = -w(N^c_\alpha, u)$. From now onwards $w(N^a, v_\beta) = \delta^a_\beta$, it is possible to satisfy by appropriate N^a choice.

Varying $\xi(x)$ and $\xi_n(x)$ we have:

$$\frac{\delta}{\delta\xi(x)} = \frac{\delta}{\delta u(x')} + \frac{\delta\tau^\alpha}{\delta\xi(x)}\left(S_\alpha + \frac{\partial}{\partial\tau^\alpha}\right), \qquad \frac{\delta}{\delta\xi_n(x)} = \frac{\delta}{\delta u_n(x')} + \frac{\delta\tau^\alpha}{\delta\xi_n(x)}\left(S_\alpha + \frac{\partial}{\partial\tau^\alpha}\right),$$

where

$$S_\alpha = \int\left(u_\alpha(x')\frac{\delta}{\delta u(x')} + u_{\alpha n}(x')\frac{\delta}{\delta u_n(x')}\right)dl.$$

Here the following equation is used:

$$\int\left(v_\alpha(x')\frac{\delta}{\delta u(x')} + v_{\alpha n}(x')\frac{\delta}{\delta u_n(x')}\right)dl = 0. \tag{3}$$

This equation is the immediate consequence of additional conditions (2) and relationship $w(N^a, v_\beta) = \delta^a_\beta$.

Let's define operators:

$$\hat{q}(x) = \frac{1}{\sqrt{2}}\left(\xi(x) + i\frac{\delta}{\delta\xi_n(x)}\right), \qquad \hat{p}(x) = \frac{1}{\sqrt{2}}\left(\xi_n(x) - i\frac{\delta}{\delta\xi(x)}\right). \tag{4}$$

They are selfconjugated and satisfy commutation relations

$$[\hat{q}(x'), \hat{p}(x'')] = i\delta(x' - x''),$$

so in is possible it treat them as coordinate and momentum operators of field oscillators.

However there is another pair of selfconjugated operators which is satisfy the same commutation relations. So the number of possible field states turns out to be doubled. Field state number reduction is possible to carry out using holomorphic representation for example, see [8].

In the terms of new variables operators $\hat{q}(x)$ and $\hat{p}(x)$ looks like:

$$\hat{q}(x) = gF(x') + Q(x') + \frac{1}{g}A(x'), \qquad \hat{p}(x) = gF_n(x') + P(x') + \frac{1}{g}A_n(x'),$$

$$F(x') = \frac{1}{\sqrt{2}}(v(x') + N^b(x')\Phi_b), \qquad A(x') = \frac{1}{\sqrt{2}}N^b(x')Q_b^c T_c,$$

$$Q(x') = \frac{1}{\sqrt{2}}\Big(u(x') + i\frac{\delta}{\delta u_n(x')} - N^b(x')r_b\Big),$$

$$P(x') = \frac{1}{\sqrt{2}}\Big(u_n(x') - i\frac{\delta}{\delta u(x')} - N_n^b(x')r_b\Big),$$

$$T_\gamma = K_\gamma + R_\gamma^a r_a, \qquad r_\alpha = R_\alpha^c \Phi_c, \qquad K_\alpha = iS_\alpha + i\frac{\partial}{\partial \tau^\alpha}.$$

$\frac{\partial}{\partial \tau^\alpha}$ enter in integrals of motion in the order $\frac{1}{g}$ only. In order to take into account all interaction effects earlier the canonical transformation is made: $i\frac{\partial}{\partial \tau^\alpha} \to g^2\Phi_\alpha + i\frac{\partial}{\partial \tau^\alpha}$, and then K_α becomes to be $K_\alpha + g^2\Phi_\alpha$.

3 Scheme of Perturbation Theory

The dynamic of the system is determined by Lagrangian (function arguments are omitted):

$$L = 1ø2\int(\phi_n^2 - \phi_l^2 - \mu^2\phi^2)dl +$$

$$+g^2\int(\Psi_n^*\Psi_n - \Psi_l^*\Psi_l - m^2\Psi^*\Psi)dl - -g\int\Psi^*\Psi\phi dl. \tag{5}$$

Action is invariant with respect to space-time translations, so energy and momentum are to integrals of motion. Now it is possible to quantize via substitution

$$\phi \longrightarrow \hat{q}, \qquad \phi_n \longrightarrow \hat{p}, \qquad \phi_\lambda \longrightarrow \hat{q}_\lambda,$$

and we have the following expressions of the integrals of motion as series with respect to inverted powers on coupling constant g:

$$O = g^2 O_{-2} + gO_{-1} + O_0 + \cdots,$$

Let's take notice that H_{-2}, P_{-2} don't depend from neutral field operators.

In prospect we will consider only one-particle conditions of charged field

$$|1> = \int\hat{\Psi}^*(x)f(x)dl|0>, \qquad <1| = <0|\int\hat{\Psi}(x)f^*(x)dl$$

and

$$[\hat{\Psi}(x), \hat{\Psi}^*(x')] = -iD(x - x')$$

. If state vectors is $\Psi = \Psi_{ch} \otimes \Psi_n$, in the first approximation, then averages of $< H_{-1} >_{ch}$, $< P_{-1} >_{ch}$ are reduced to linear forms with respect to neutral field operators. There is no normalizible eigenvectors of operators O_{-1}, so perturbation theory is applicable only is this operators are equal zero.

If the following boundary condition is performed $F_l Q\,|_{\partial c} = 0$, than

$$H_{-1} = 1\emptyset\sqrt{2}\int\left(F_n(u_n - i\frac{\delta}{\delta u} - r_b N_n^b) + B(u + i\frac{\delta}{\delta u_n} - r_b N^b)\right)dl,$$

where $B = -F_{ll} + \mu^2 F + < \hat{\Psi}^*\hat{\Psi} >= -F_{ll}(x^{'}) + \mu^2 F(x^{'}) + V(x^{'})$.

Let's suppose the following equality to be true:

$$F_n = c^\alpha v_\alpha, \quad B = -c^\alpha v_{\alpha n}, \tag{6}$$

than the first order of Hamiltonian tuns out to be (3), and condition of perturbation theory application is accomplished. As a consequence of (6) we obtain equation for the classical component of neutral scalar field:

$$F_{nn} - F_{ll} + \mu^2 F + V = 0.$$

Further $F(x^{'})$ is considered as a solution of the equation

$$F_{tt}(x^{'}) - F_{xx}(x^{'}) + \mu^2 F(x^{'}) + V(x') = 0 \tag{7}$$

with given boundary conditions on ' (Caushy problem), here

$$V(x) = -\int\int f^*(x_1)D(x_1 - x)D(x - x_2)f(x_2)dl_1 dl_2.$$

It is easy to show that $H_{-1} = 0$ if $v_\alpha = N_\alpha^c \Phi_c$ it means that $F = cN^c\Phi_c$. From $F = 1\emptyset\sqrt{2}(v + N^c\Phi_c) = \sqrt{2}v$ immediately follows that $c = \sqrt{2}$.

Analogously one can show that $P_{-1} = 0$, if the following boundary conditions are accomplished $F_l Q\,|_{\partial c} = 0$.

It is possible to obtain equation for the function $f(x)$ describing one-particle charged field state. $\hat{\Psi}(x)$ satisfy the following equation (due to variational principle):

$$\hat{\Psi}_{tt} - \hat{\Psi}_{xx} + m^2\hat{\Psi} + v\hat{\Psi} = 0.$$

Than it is possible to represent $\hat{\Psi}(x)$ as a following:

$$\hat{\Psi}(x) = \hat{\Psi}_0(x) + \int D_c(x - y)\, v(y)\, \hat{\Psi}(y)\, dy, \tag{8}$$

where $\hat{\Psi}_0(x)$ - is a solution of the homogeneous equation.

One-particle state is:

$$|\,1\rangle = \int f(x)\,\hat{\Psi}^*(x)\,|\,0\rangle dx.$$

Denote

$$\langle 0\,|\,\hat{\Psi}(x)\,|\,1\rangle = \int \langle 0\,|\,\hat{\Psi}(x)\, f(y)\,\hat{\Psi}^*(y)\,|\,0\rangle dy = \bar{f}(x),$$

$$f(x) = ([] + m^2)\bar{f}(x).$$

From (8) we have:

$$\bar{f}(x) = \langle 0 \mid \hat{\Psi}_0(x) \mid 1 \rangle + \int D_c(x-y)\, v(y)\, \bar{f}(y)\, dy.$$

$\bar{f}(x)$ satisfies to the equation

$$\left(\Box + m^2\right) \bar{f}(x) + v(x)\, \bar{f}(x) = 0.$$

In nonrelativistic limits $\bar{f}(x)$ could be represented as

$$\bar{f}(x) = e^{-imt} \bar{\xi}(x,t),$$

and it $\bar{\xi}(x,t)$ changes slowly in process of time, it means $\bar{\xi}_{tt}(x,t) = 0$, and for $\bar{\xi}(x,t)$ we have:

$$i\frac{\partial \bar{\xi}(x,t)}{\partial t} + \frac{1}{2m}\nabla_r \bar{\xi}(x,t) - \frac{1}{2m} v(x) \bar{\xi}(x,t) = 0.$$

4 System State Space Construction

Neutral field dynamic properties in zero-point order with respect to inverted powers of coupling constant g are determined by operators H_0 and P_0. It is possible to show that after system state space construction those operators reduces to the derivatives with respect to symmetry group generators.

If $AF_l\,|_{\partial c} = 0$, where $A = \frac{1}{\sqrt{2}} N^b T_b$, then

$$H_0 = in^\alpha \frac{\partial}{\partial \tau^\alpha} + 1\emptyset 2 \int (P^2 + Q_l^2 + \mu^2 Q^2) dl +$$

$$+ i \int \left(u_n \frac{\delta}{\delta u} + + u_{nn} \frac{\delta}{\delta u_n} \right) dl + \int (N_n^c u_n - N_{nn}^c u) dl r_c. \tag{3}$$

If coordinate and momentum operators of field oscillators looks like (4), then the number of possible neutral scalar field states is doubled over against real situation. That is why states number reduction is necessary.

Primarily let's analyze the number of independent variables. Original number of independent variables was ∞. After defining of Bogoliubov group variables (they are considered to be independent) the number became $\infty + 2$. This number was doubled due to determination of creation-annihilation operators: $(\infty + 2) * 2 = 2 * \infty + 4$. Additional conditions reduced the number of independent variables on 2, that is at present time the number of possible field states is $2 * \infty + 2$. Let's separate from field variables $u(x')$ two variables r_a which has no any physical sense and are connected with the method of perturbation scheme realization. Then the state number is $2 * \infty$, and field is described via $w(x')$ variables which are determined as the following:

$$u = w + N^a r_a, \quad u_n = w_n + N_n^a r_a,$$

$$\frac{\delta}{\delta u} = \frac{\delta}{\delta w} + \frac{\delta r_a}{\delta u}\frac{\partial}{\partial r_a}, \quad \frac{\delta}{\delta u_n} = \frac{\delta}{\delta w_n} + \frac{\delta r_a}{\delta u_n}\frac{\partial}{\partial r_a}.$$

In this case operators Q and P are:

$$Q = \hat{Q} + q, \quad P = \hat{P} + p,$$

where

$$\hat{Q} = \frac{1}{\sqrt{2}}\left(w + i\frac{\delta}{\delta w_n}\right), \quad \hat{P} = \frac{1}{\sqrt{2}}\left(w_n - i\frac{\delta}{\delta w}\right),$$

$$q = \frac{i}{\sqrt{2}}\frac{\delta r_a}{\delta u_n}\frac{\partial}{\partial r_a}, \quad p = -\frac{i}{\sqrt{2}}\frac{\delta r_a}{\delta u}\frac{\partial}{\partial r_a}.$$

Using variables w and w_n one can reduce of state number by the following way: let's describe the field states by the functionals in which $\delta\phi\delta w$ $\frac{\delta}{\delta w_n}$ reduces to the operators:

$$\frac{\delta}{\delta w} \to \frac{\delta}{\delta w} - iw_n, \quad \frac{\delta}{\delta w_n} \to -iw.$$

Then

$$\hat{Q} \to \sqrt{2}w, \quad \hat{P} \to -i\frac{1}{\sqrt{2}}\frac{\delta}{\delta w},$$

and if $\frac{\partial r_a}{\partial u_n} w_\lambda|_{\partial c} = 0$,

after states number reduction Hamiltonian H_0 in zero-point order with respect to coupling constant depends on extra variables r_a and derivatives with respect to translation group generators only.

$$H_0 = in^\alpha \frac{\partial}{\partial \tau^\alpha} + h_0, \qquad P_0 = ie^\alpha \frac{\partial}{\partial \tau^\alpha} + p_0,$$

where h_0 and p_0 are the quadratic forms with respect to r_a and canonical momenta.

Commutator of h_0 and p_0 is equal zero on the state vector which looks like

$$\Phi(\xi, \eta) = Cexp(\hat{\alpha}(\xi^2 - \eta^2)),$$

here ξ and η are linear combinations of r_a. So h_0 and p_0 can be removed from dynamical scheme.

Hence

$$H_0 = in^\alpha \frac{\partial}{\partial \tau^\alpha} = i\frac{\partial}{\partial \tau^1} \qquad Psi(x) = \Psi(x - \tau^2).$$

So energy and momentum conservation lows are accomplished.

5 Conclusion

Formalism proposed above permits to consider arbitrary motions of charged particle, for example periodic motion or particle motion in external field (group variables not cyclic in this case but this is not important for the formalism development).

References

[1] N.N.Bogoliubov *Ukrainian Mathematical Journal.* 1950. v.2. P.3-24.

[2] E.P.Solodovnikova, A.N.Tavkhelidze, O.A.Khrustalev *Teor.Mat.Fiz.* 1972. T.10.

[3] O.A.Khrustalev, M.V.Tchitchikina *Teor.Mat.Fiz.* 1997. T. 111. N2.p. 242-251; 14 pt 1997. T. 111. N3. p. 413-422.

Dirac's Equation, $SU(2)$ Model and Octanions

S.V.Kopylov
STE "Brainstorm", 26-9 Konstantinov St., Moscow 129278, Russia

Abstract. A presentation of Dirac, Weyl's equations and $SU(2)_l$ models is considered in terms of quaternion and octanion algebras.

1 Quaternions

For quaternion algebra q, with elements: $q = A_0 1 + A_1 J_1 + A_2 J_2 + A_3 J_3$, and algebras on the base σ-matrices of Pauli isomorphism is known 1:
$\{1; J_\alpha\} \to \{I; (-i\sigma_\alpha)\}$.
Thus the quaternion$q$ is presentable in the form:

$$q = A_0 I + A_1(-i\sigma_1) + A_2(-i\sigma_2) + A_3(-i\sigma_3).$$

This allows the Weyl equations for left and right spinors $i\hbar\partial_t(L) = +c\hat{P}_\alpha\sigma_\alpha(L)$, $i\hbar\partial_t(R) = -c\hat{P}_\alpha\sigma_\alpha(R)$ to be presented in the form: $(\hbar\partial_t - c\hat{P}_\alpha J_\alpha)L = 0$, $(\hbar\partial_t + c\hat{P}_\alpha J_\alpha)R = 0$.

In such a representation right - R and left - L Weyl spinors must also be written in the form of quaternion functions. In the σ-matrix presentation this is identical to writing R and L in the form of matrices 2×2. A quaternion representation of wave functions was considered repeatedly, a conclusion herewith was made about existence of two independent Hilbert solution space 2. In the σ-matrix presentation this is obvious since each of the columns of the matrix 2×2 is an independent solution. There arises a question about connection (interaction) between these spaces 3.

We shall consider, as an example, the Weinberg-Salam models for the sector of left spinors. Write for bispinors $\Psi^{1,2}$:

$$\left[\left(\partial_\mu - iA_\mu - iB^\alpha_\mu\sigma^\alpha\right)\gamma_\mu\right]\begin{pmatrix}\Psi^1\\ \Psi^2\end{pmatrix}. \tag{1}$$

Multiplying this expression from the left on $(1+\gamma_5)$, we get for left spinors a scheme $SU(2)\otimes U(1)$ of the model:

$$\left[\left(\partial_\mu - iA_\mu - iB^\alpha_\mu\sigma^\alpha\right)\tilde{\sigma}_\mu\right]\begin{pmatrix}\psi^1_L\\ \psi^2_L\end{pmatrix}. \tag{2}$$

Here $\mu = 1,2,3,4$; $\alpha = 1,2,3$; $\tilde{\sigma}_\mu$: $\{I; -i\sigma_\alpha\}$; σ_μ: $\{I; +i\sigma_\alpha\}$.

Transpose the matrices relating to $SU(2)$ the sector:

$$\tilde{\sigma}_\mu\left(\psi^1_L; \psi^2_L\right)\left(\partial_\mu - iA_\mu - iB^\alpha_\mu\overbrace{\sigma^\alpha}^{\tau}\right). \tag{3}$$

Here $\overbrace{\sigma^\alpha}^{\tau}$ the transposed matrices (the matrices σ_μ are not transposed , as not relating to the sector $SU(2)$. It is clear that (2) and (3) differ only by a form of writing, which

is checked directly, in (2) relations are written in the form of a system, but in (3) "sequentially". If one multiplies (3) from the right by $(1-\sigma_3)/2$ or by $(1+\sigma_3)/2$, the first or the second from the relations of the system will be obtained (2). In the expression (3) $\left(\psi_L^1;\psi_L^2\right)$ is a sought for matrix 2×2 (quaternion), whose columns are two left spinors. The relation (3) is an equation of motion for two earlier linear independent columns(of the linear independent Hilbert spaces mentionned above) "interacting" now via a field B_μ^α. In fact, before the transposition we had in an expression of the type:

$$\left[(iB_\mu^\alpha\sigma^\alpha)\otimes\tilde{\sigma}_\mu\right]\left\{\begin{pmatrix}1\\0\end{pmatrix}\otimes\psi_L^1+\begin{pmatrix}0\\1\end{pmatrix}\otimes\psi_L^2\right\}. \tag{4}$$

Realizing the scheme of transposition of the left side of the direct product:

$$(\sigma^\alpha\otimes\tilde{\sigma}_\mu)\left\{\begin{pmatrix}1\\0\end{pmatrix}\otimes\psi_L^1\right\}=\sigma^\alpha\begin{pmatrix}1\\0\end{pmatrix}\otimes\tilde{\sigma}_\mu\psi_L^1\xrightarrow{\tau}\{1;0\}(\sigma^\alpha)^\tau\otimes\tilde{\sigma}_\mu\psi_L^1=$$

$$=\{\tilde{\sigma}_\mu\psi_L^1;0\}(\sigma^\alpha)^\tau \tag{5}$$

we obtain (3). Thus the quaternion form of writing for the model $SU(2)$ turns out to be natural, as a product of σ_μ-matrices of the relativistic sector by the quaternion wave function $\left(\psi_L^1;\psi_L^2\right)$ and by the σ-matrices of interaction sector $SU(2)$. However, a disadvantage of such a presentation is seen: the operator in the presence of $SU(2)$ interaction is not separated from the wave function. It should be noted that the spinors in the matrices are ideals with respect to action on them from the left of matrices of the relativistic sector σ_μ. But they are already not such with respect to the action on them from the right of matrices σ^α of the "interaction" sector $SU(2)$ which do not transpose them (in what, strictly speaking, the "interaction" is expressed).

2 Octanions

Separation of an operator from the wave function in some cases turns out to be possible. Consider an octanion algebra. The latter is an extension of the quaternion algebra due to introducing, in addition to σ^α-matrices, one more operator anticommutating with them $\hat{k}$. The products $(\hat{k}\sigma^\alpha)$ are assumed to be anticommuted as well as with $\hat{k}$ and σ^α. These requirements allow one to introduce an octanion norm for real octanions, but make the octanion algebra (Cayley's algebra) be nonassociated. Thus $\hat{k}$ is not presentable in a matrix form, otherwise we had a matrix algebra, but they are associative. For the octanion Q we have:

$$Q=A_0 1+A_1J_1+A_2J_2+A_3J_3++B_0\hat{k}+B_1(J_1\hat{k})+B_2(J_2\hat{k})+B_3(J_3\hat{k}),$$

Or in the σ-matrix presentation:

$$Q=A_0I+A_1(-i\sigma_1)+A_2(-i\sigma_2)+A_3(-i\sigma_3)+$$

$$+B_0\hat{k}+B_1((-i\sigma_1)\hat{k})+B_2((-i\sigma_2)\hat{k})+B_3((-i\sigma_3)\hat{k}).$$

Physically, the anticommutating operator $\hat{k}$, this is just that fourth operator which was lacking for constructing the massive Weyl equations i.e. the Dirac equation. We

shall realize constructing the Dirac equation in terms of the octanion algebra in a inverse order. Multiply directly I by the Dirac equation : $\left(\gamma_\mu\partial_\mu - \frac{mc}{\hbar}\right)\Phi = 0$, we get: $[I \otimes \left(\gamma_\mu\partial_\mu - \frac{mc}{\hbar}\right)]\binom{\Phi}{\Phi} = 0$. Hereinafter we multiply successively the expression obtained by unitary matrices-constants: A; B; C, transforming conventionally, the operator and wave function, while multiplying by A and B. Here:

$$A = \{1/2(I + \sigma_3) \otimes \exp(i\gamma_5\kappa/2) + 1/2(I - \sigma_3) \otimes \gamma_5 \exp(-i\gamma_5\kappa/2)\},$$

$$B = \{\exp[i\xi/2(\sigma_1 \cos\lambda + \sigma_2 \sin\lambda)] \otimes J\}, \qquad C = \{\sigma_3 \otimes J\},$$

where J is a unit matrix 4×4.

As a result, we obtain the expression:

$$\{(I \otimes \gamma_\mu\partial_\mu) + m[i(I \otimes \gamma_5)\alpha + (\sigma_3 \otimes J)\beta +$$

$$+(\sigma_2 \otimes J)\gamma + (\sigma_1 \otimes J)\delta]\}\begin{pmatrix}\phi^1\\ \phi^2\end{pmatrix} = 0.$$

here $\alpha = \sin\kappa$, $\beta = \cos\kappa\cos\xi$, $\gamma = \cos\kappa\sin\xi\cos\lambda$, $\delta = \cos\kappa\sin\xi\sin\lambda$; and thus $\alpha^2 + \beta^2 + \gamma^2 + \delta^2 = 1$.

Multiplying the expression obtained by $(I \otimes (1 + \gamma_5))$, from the left we get:

$$\{(I \otimes \tilde{\sigma}_\mu\partial_\mu)\}\begin{pmatrix}\phi_1^L\\ \phi_2^L\end{pmatrix} + m[+i(I \otimes I)\alpha + (\sigma_3 \otimes I)\beta +$$

$$+(\sigma_2 \otimes I)\gamma + (\sigma_1 \otimes I)\delta]\}\begin{pmatrix}\phi_1^R\\ \phi_2^R\end{pmatrix} = 0.$$

Multiplying by $(I \otimes (1 - \gamma_5))$, we get:

$$\{(I \otimes \sigma_\mu\partial_\mu)\}\begin{pmatrix}\phi_1^R\\ \phi_2^R\end{pmatrix} + m[-i(I \otimes I)\alpha + (\sigma_3 \otimes I)\beta +$$

$$+(\sigma_2 \otimes I)\gamma + (\sigma_1 \otimes I)\delta]\}\begin{pmatrix}\phi_1^L\\ \phi_2^L\end{pmatrix} = 0.$$

Transposing the left sides of the direct product and denoting the matrix wave functions $(\phi_1^L; \phi_2^L) = L$, but $(\phi_1^R; \phi_2^R) = R$, we obtain:

$$\{(\tilde{\sigma}_\mu\partial_\mu)\}(L) + (R)\{m[+i(I)\alpha + (\sigma_3^\tau)\beta + (\sigma_2^\tau)\gamma + (\sigma_1^\tau)\delta]\} = 0,$$

$$\{(\sigma_\mu\partial_\mu)\}(R) + (L)\{m[-i(I)\alpha + (\sigma_3^\tau)\beta + (\sigma_2^\tau)\gamma + (\sigma_1^\tau)\delta]\} = 0.$$

It is not difficult to show that for the case of reflected space: $R(x) = L(-x), L(x) = R(-x)$. (It should be taken into account that the sign before the member containing mi changes in the reflection, since this member appears, while multiplying the equation by a matrix- constant containing γ_5 and contains it, but after the reflection, while carrying γ_0 through the sign changes s.) Using the relations obtained and the operator $\hat{k}$, one may write:

$$\{\tilde{\sigma}_\mu\partial_\mu + \hat{k}m[-i(I)\alpha + (\sigma_3^\tau)\beta + (\sigma_2^\tau)\gamma + (\sigma_1^\tau)\delta]\}(L(x) + \hat{k}L(-x)) = 0,$$

or in another form:

$$\{\sigma_\mu \partial_\mu + \hat{k}m[+i(I)\alpha + (\sigma_3^\tau)\beta + (\sigma_2^\tau)\gamma + (\sigma_1^\tau)\delta]\}(R(x) + \hat{k}R(-x)) = 0.$$

As a result of "opening" the last relation, we shall obtain the same result as in the "opening" of the previous one, namely, - two equations for functions L and R being a result of transformations of the Dirac equation. Thus any of the relaticus presented is a representation of the Dirac equation in terms of Keyley's algebra or, that is the same, an octanions algebra (the octet).

References

[1] D. K. Faddeev, *Lectures on Algebra*, (Nauka, Moscow), 1984.

[2] E. V .Gaponov, *Preprint IAE*, 2181 (1972).

[3] S. V. Kopylov, in *"Elementary Particle Physics"*, ed. by A.Studenikin, Interregional Centre for Advanced Studies, (Proceedings of the 8th Lomonosov Conference on Elementary Particle Physics), 145, 1999.

Irreducible Darboux Transformations

Vladislav G. Bagrov [a] and Boris F. Samsonov [b]
Physics Department of Tomsk State University, 634050 Tomsk, Russia

Abstract. Detailed analysis of second order Darboux transformations for a growing potential of the Schrödinger equation is given. It is shown, that except for the known annihilation of two levels from a discrete spectrum other possibilities can be released as well: a) the transformed spectrum remains identical to the initial one; b) one level is deleted from a spectrum; c) one additional level is created; d) two additional levels are created.

Introduction

Recently an interest to Darboux transformation in quantum mechanics and mathematical physics has appreciably increased. This is stimulated, in particular, by discovering a number of its new properties and opportunities of application. In 1–2 one can find a detailed analysis of Darboux transformation operator method together with some possible applications. The main historical stages of development of this approach are published recently in an electronic archive 3.

The Darboux transformation is based on two key moments 2. The first one is so called intertwining relation of two different Hamiltonians by the Darboux transformation operator. This relation underlies a more general method – method of transformation (or transmutation) operators (see e.g. 4). For the stationary one-dimensional Schrödinger equation it is defined as follows.

Let us have all solutions of the Schrödinger equation with the Hamiltonian h_0 (called initial Schrödinger equation)

$$h_0\psi_E(x) = E\psi_E(x), \quad h_0 = -\partial_x^2 + V_0(x), \quad x \in (a,b) \tag{1}$$

with an arbitrary value of the parameter $E \in \mathbb{C}$. If the problem is to find the solutions of this equation with another Hamiltonian $h_1 = -\partial_x^2 + V_1(x)$ $x \in (a,b)$, this problem can easily be solved if the operator L, which is defined by the intertwining relation $Lh_0 = h_1 L$, is known. Nontrivial solutions of the equation

$$h_1\varphi_E(x) = E\varphi_E(x), \tag{2}$$

with $\psi_E \notin \ker L$ are functions $\varphi_E = L\psi_E$.

The second key moment consists in a special choice of the operator L. If L is the Nth order differential operator, it is called *Darboux transformation operator of order* N 2. When $N = 1$ it is simply called Darboux transformation operator.

Potential $V_1(x)$ of the transformed Schrödinger equations (2) is defined by the initial potential $V_0(x)$, which can be any. Therefore, it is possible to take $V_1(x)$ as the initial potential for the second transformation. In such a way we come to a concept of a chain of transformations.

Any Nth order Darboux transformation is equivalent to some chain of $n(\leq N)$ transformations of the first order 2. However, it can appear that some section of

[a] e-mail: bagrov@phys.tsu.ru
[b] e-mail: samsonov@phys.tsu.ru

such a chain "is bad determined" 2. This means, that some intermediate potential is complex-valued or has singularities (poles) on the interval (a, b), while resulting potential of the whole chain remains "good", that is real and regular. The possibility for intermediate potentials to be complex-valued was mentioned for the first time in 1 and subsequently independently in 5. The possibility to use the discrete spectrum eigenfunctions as transformation functions for the Nth order Darboux transformation, which leads to singular intermediate potentials, has been first established by M.G. Krein 6. Such chains of transformations result in supersymmetric models with an unusual manifestation of supersymmetry breakdown at the quantum level 2.

The Nth order Darboux transformation ($N > 1$) refers to as reducible if it is equivalent to a chain of first order transformations with the real-valued and regular on the interval (a, b) potentials. Otherwise it refers to as irreducible 2.

An elementary irreducible Darboux transformation is a second order transformation. It is possible to show that any Nth order Darboux transformation creating a real and regular on (a, b) potential can be presented as a superposition of "good" transformations of order less or equal two. In this connection it is sufficiently to investigate the transformations of the first and second orders. A large number of papers is devoted to transformation of the first order. Second order transformations are not explored in the same details.

In the present paper a detailed analysis of second order irreducible Transformations, for which the intermediate potential has poles on the interval (a, b) is given. As the interval (a, b) we consider all real axis $(-\infty, \infty)$. We shall also consider such initial potentials that satisfy the condition $V_0(x) \to \infty$ as $|x| \to \infty$ and we shall consider only real values of the parameter E.

It is established in this paper that in addition to the known case of deletion of two discrete spectrum levels other possibilities can be realized also: a) the transformed spectrum remains identical to the initial one; b) one level is deleted from a spectrum; c) one additional level is created; d) two additional levels are created. These results have been previously partly announced in 7. We give only the formulation of the theorem and skip all the proofs.

1 First and second order Darboux transformation operators

In this section we describe known properties of the Darboux transformation operators of the first and second orders (see, for example, 2), which are necessary for the subsequent analysis.

The more elementary Darboux transformation operator is a first order operator. Its action on some differentiable function is given by the following expression: $\varphi = L\psi = -\psi u'_\alpha/u_\alpha + \psi' = W(u_\alpha, \psi)/u_\alpha$, where $W(u_\alpha, \psi) = u_\alpha\psi' - u'_\alpha\psi$ is the Wronskian of the functions ψ and u_α and u_α is a solution of the differential equation $h_0 u_\alpha = \alpha u_\alpha$. The function u_α is called *transformation function.* Potential V_1 of the transformed Schrödinger equation is defined by the initials potential V_0 and the transformation function u_α: $V_1 = V_0 - 2(\ln u_\alpha)''$.

From here it is clear, that if we require, that the potential difference $A = V_1 - V_0$ is a regular function on the interval (a, b), it is necessary to take as transformation

functions only these, which do not vanish on this interval. (In our case $(a,b) = \mathbb{R}$).

If the Schrödinger equation (1) has a discrete spectrum $E_0 < E_1 < \dots$ with the eigen-functions $\psi = \psi_n$, $n = 0, 1, 2, \dots$, the functions ψ_n belong to the space $L_2(\mathbb{R})$. Then at $E > E_0$ any solution of the equation (1) vanishes at some $x = x_0 \in \mathbb{R}$ and this point is a pole for the potential V_1. (This assertion is a direct implication of the known Sturm oscillator theorem for the solutions of a differential equation (1) see, for example, 8.) It is known 9, that at $E \leq E_0$ any solution of the equation (1) either has one zero or is everywhere different from zero at $x \in \mathbb{R}$. Therefore, only these functions are suitable as transformation functions whose eigenvalues are subject to the condition $\alpha \leq E_0$.

The second order Darboux transformation operator is defined with the help of two transformation functions u_1 and u_2, $h_0 u_{1,2} = \alpha_{1,2} u_{1,2}$: $\varphi = L\psi = W(u_1, u_2, \psi)/$ $/W(u_1, u_2)$ where $W(u_1, u_2, \psi)$ is the Wronskian of the functions u_1, u_2, ψ. For the potential V_1 we have in this case the expression

$$V_1 = V_0 - 2[\ln W(u_1, u_2)]''.$$

It is clear from the above relation that for regularity of the potential difference $A = V_1 - V_0$ it is not necessary to impose restrictions on the transformation functions u_1 and u_2. It is sufficiently to require, that the Wronskian of these functions $W(u_1, u_2)$ does not vanish $\forall x \in \mathbb{R}$. The functions u_1 and u_2 can vanish.

Every second order transformation is equivalent to the following chain of transformations of the first order. The first transformation is made with the help of the transformation function u_1 and the second one with the help of the function Lu_2. Clearly, that if the function $u_1(x)$ vanishes, intermediate potential will have a singularity (pole). If the Wronskian $W(u_1, u_2)$ differs from the zero everywhere, resulting potential is "good" and we have an irreducible Darboux transformation. In case when the functions u_1 and u_2 correspond to two consecutive points of the discrete spectrum, this statement is established by M.G. Krein 6. In the following section for growing potential we shall establish other conservation sign conditions for the Wronskian $W(u_1, u_2)$.

2 Operator with a growing potential

Let the function $V_0(x)$ be such that $V_0(x) \to +\infty$ as $|x| \to +\infty$. We assume also, that it is differentiable (for simplicity infinitely differentiable) for all $x \in \mathbb{R}$. Obviously, the potential $V_0(x)$ is bounded from below and the operator h_0 considered on a set of infinitely differentiable functions with a compact support, is self-adjoint in essential, that is it has a self-adjoint extension in the Hilbert space $L_2(\mathbb{R})$. This extension we shall denote by the same symbol h_0. In this case the operator h_0 has a discrete spectrum $E = E_k$. Its eigen-functions $\psi = \psi_k$, $k = 0, 1, 2, \dots$ belong to the space $L_2(\mathbb{R})$ and form a basis in this space (see e.g. 8).

Our analysis of conservation sign conditions for the Wronskian $W(u_1, u_2)$ is based on the following statements.

Proposition 1. *If $E_{k+1} > E > E_k$, where E_k is a point of a discrete spectrum of the operator h_0, $k = 0, 1, 2, \dots$, the solutions of the equation (1), ψ_E, have either $k+1$ zeros or $k+2$ zeros. If ψ_E has $k+2$ zeros then $|\psi_E(x)| \to \infty$ as $|x| \to \infty$. If ψ_E*

has $k+1$ zeros then two types of the solutions are possible: a) Solution with a zero asymptotic, $\psi_E \to 0$ as $x \to \infty$ and b) solution with infinitely growing asymptotic, $|\psi_E| \to \infty$ as $|x| \to \infty$. Any solution ψ_E with the zero asymptotic has $k+1$ zeros.

Proposition 2. *Let u_1 and u_2 be such solutions of the equation (1) With a continuous potential $V_0(x)$ that have alternating zeros (that is between each two zeros of one function there is exactly one zero of the other function). Let x_0 be the coordinate which is minimal among all the zeros of the functions u_1 and u_2, and x_m be the maximal one. Then the Wronskian $W(u_1, u_2)$, considered as a function of x, $W(u_1, u_2) = W(x)$, does not vanish for all x from the interval $[x_0, x_m]$.*

We want to emphasize the following obvious consequence of this statement. For u_1 and u_2 satisfying conditions of the Proposition 2, the equation $W(x) = 0$ can have the solutions only for $x < x_0$ or $x > x_m$.

Now we formulate conditions when $W(x) \neq 0$ for all $x \in \mathbb{R}$.

Proposition 3. *If $E_{k+1} \geq \alpha_2 > \alpha_1 > E_k$ and the function u_1 has $k+2$ zeros and u_2 has $k+1$ zeros, $h_0 u_{1,2} = \alpha_{1,2} u_{1,2}$ then the Wronskian $W(u_1, u_2) = W(x)$ conserves the sign $\forall x \in \mathbb{R}$.*

It is clear from just now indicated reasons that if on the contrary the function $u_1(x)$ has $k+1$ zeros and the function $u_2(x)$ has $k+2$ zeros, then at the same assumptions, the function $W(x)$ at the points x_0 and x_{2k+2} is positive and reaches maxima. Besides, even if $\alpha_2 = E_{k+1}$, the function u_2 is not square integrable (as it has $k+2$ zeros), and by virtue of the condition $\alpha_1 < \alpha_2$, the function u_1 also those is not. This means that $|u_1(x)|$ should tends to infinity on one of the infinities at least and $|u_2(x)|$ tends to infinity as $|x| \to \infty$. As a result $|W(x)|$ tends to infinity on the one of the infinities at least and $W(x)$ has one zero at least.

The last condition can be avoided if the function $|W(x)|$ did not grow but decreased as $|x| \to \infty$. For this purpose it is necessary that u_1 is square integrable. (The case when u_2 is square integrable is covered by the Proposition 3.) Besides, to analyse the asymptotic of the Wronskian $W(x)$ it is necessary to know the asymptotic of the solutions of the equation (1). This asymptotic is known under additional conditions on the potential of this equation 8.

Let us require that the potential $V_0(x)$ satisfies to following conditions:

$$\int_{x_0}^{\infty} \left| \frac{V_0'}{V_0^{5/4}} \right|^2 dx < \infty, \quad \int_{x_0}^{\infty} \frac{|V_0''|}{|V_0|^{3/2}} dx < \infty. \tag{3}$$

Now we can establish conservation sign conditions for the Wronskan $W(x)$ additional to these established in the Propositron 3.

Proposition 4. *If potential $V_0(x)$ satisfies the conditions (3), $E_{k+1} \geq \alpha_2 > \alpha_1 = E_k$ and $u_1 = \psi_k$, and u_2 has $k+1$ zeros ($h_0 u_{1,2} = \alpha_{1,2} u_{1,2}$), then Wronskian $W(u_1, u_2) = W(x)$ conserves the sign $\forall x \in \mathbb{R}$.*

The Propositions 3 and 4 give conditions when the second order Darboux transformation with transformation functions possessing zeros is "good", that is irreducible.

Conclusion

The existence of new types of irreducible second order Darboux transformations, established in this paper, considerably enlarges an opportunity of application of the

Darboux transformation operator method to generation of new exact solutions of the Schrödinger equation. The detailed analysis of conservation sign conditions of the Wronskian $W(u_1, u_2)$ given in this paper establishes conditions on transformation functions u_1 and u_2. A similar analysis is possible for potentials with other asymptotic behaviour. Note, that the possibility to use transformation functions u_α with the eigenvalues α higher then the ground state E_0 of the Hamiltonian h_0 has recently been noted in 11 without any analysis.

Acknowledgements

The work is partially supported by the grants of RFBR and the ministry of education of Russia.

References

[1] A.A. Andrianov, M.V. Ioffe, V. Spiridonov *Phys. Lett.* **A174**, 273, (1993); A.A. Andrianov, M.V. Ioffe, D.N. Nishnianidze, *Theor. Math. Phys.* **104**, 463, (1995); A.A. Andrianov, M.V. Ioffe, F. Cannata, J.-P. Dedonder, *Int. J. Mod. Phys.* **A10**, 26, (1995); A.A. Andrianov, M.V. Ioffe, F. Cannata, *Mod. Phys. Lett.* **A11**, 1417, (1996).

[2] B.F. Samsonov, *Mod. Phys. Lett.* **A11**, 1563, (1996); V.G. Bagrov, B.F. Samsonov, L.A. Shekoyan, *Russ. Phys. J.* No 7, 59, (1995); V.G. Bagrov, B.F. Samsonov, *Phys. Lett.* **A210**, 60, (1996); V.G. Bagrov, B.F. Samsonov, *JETP.* **109**, 1105, (1996); B.F. Samsonov, *Nucl. Phys.* **59**. 753, (1996); B.F. Samsonov, *J. Math. Phys.* **39**, 967, (1998); V.G. Bagrov, B.F. Samsonov, *J. Phys. A: Math. Gen.* **29**, 1011, (1996). B.F. Samsonov, *JETP.* **114**, 1930, (1998); V.G. Bagrov, B.F. Samsonov, *Phys. Element. Particle Nucl.* **28**, 951, (1997);

[3] H.C. Rosu, *Short survey of Darboux transformations.* E-reprint quant-ph/9809056. URL: http://xxx.lanl.gov

[4] B.M. Levitan, *"Inverse Sturm-Liouville Problems"*, (Nauka, Moscow), 1984.

[5] V.G. Bagrov, I.N. Ovcharov, B.F. Samsonov *J. Moscow Phys. Soc.* **5**, 191, (1995).

[6] M.G. Krein, *DAN.* **113**, 970, (1957).

[7] B.F. Samsonov, *Phys. Lett.* **A263**, 274, (1999).

[8] F.A. Berezin, M.A. Shubin, *"The Schrödinger Equation"*. (University Press, Moscow), (1983).

[9] C.V. Sukumar, *J.Phys. A: Math. Gen.* **19**, 2297, (1986).

[10] A.G. Kostuchenko, I.C. Saregsyan, *"Distributions of Eigenvalues"*. (Nauka, Moscow). 1979.

[11] D.J.C. Fernandez, V. Hussin, B. Mielnik *Phys. Lett.* **A244**, 309, (1998).

THE AMS EXPERIMENT : FIRST RESULTS AND PHYSICS PROSPECTS

J.P. VIALLE [a]
LAPP-IN2P3/CNRS/University of Savoie
BP. 110, F-74941 Annecy-le-Vieux Cedex
AMS Collaboration

Abstract. The main physics goal of the AMS experiment is the search for primordial antimatter, non-baryonic dark matter, and the measurement with high statistics and high accuracy of the electrically charged cosmic ray particles and light nuclei in the extraterrestrial space beyond the atmosphere. AMS is the first magnetic spectrometer which will be flown in space. It will be installed for 3 years on the international space station (ISS) in 2003. A precursor flight with the space shuttle DISCOVERY took place in June 1998 with a first version of the detector. 100 millions particles were recorded during the test flight and unexpected physics results were observed on fluxes of protons, electrons, positrons, and helium nuclei. These results are described below, and the physics prospects for the second phase of the experiment on the space station as well.

1 Introduction

In the early age of the cosmic ray physics, most of the experiments where looking at charged particles, and at the showers in the atmosphere produced by the interaction of these particles. When it became possible to launch detectors in the outer space beyond the atmosphere the new generation of experiments looked at high energy gamma rays, and many discoveries were done. Gamma rays propagation in the intergalactic and interstellar medium is not affected by magnetic fields, and thus it was possible to point at sources of gamma rays and to identify it.

On the contrary, the information of direction of the sources of charged particles is washed out by the propagation in the galactic and intergalactic magnetic field. Near the earth, the fluxes of charged cosmic rays are disturbed by the solar activity which produces the solar wind, a plasma made mainly of protons and electrons which acts like a shielding for the earth. Furthermore, the earth magnetic field bends the trajectories of particles coming from the outer space and sends them back to space when the energy is below a threshold that depends on the impinging angle and the geomagnetic latitude of the particle. The earth magnetic field is in first approximation a dipole inclined of about 11° with respect to the earth rotation axis, with the dipole axis shifted by about 400 kms from the center of the earth, and the south magnetic pole near the north geographic pole. Near the magnetic pole the kinetic energy threshold is as low as 10 MeV while at the magnetic equator it raises to 10 GeV. Despite these effects, charged cosmic rays contain physics information on the dynamics of galaxies (cosmic wind, confinement, origin of charged cosmic rays) and on primordial universe that cannnot be found elsewhere.

Due to the difficulty to build a magnetic spectrometer and operate it in space, former experiments on charged cosmic rays in space were only measuring particles by range, and therefore they could not distinguish positive from negative charge

[a] e-mail: vialle@lapp.in2p3.fr

particles. Several balloon borne experiments aimed at measuring electrically charged cosmic rays, but they suffer from two drawbacks : i) balloons are limited in altitude to about 40 Kms, and there is still 4 g/cm^2 of atmosphere above, thus inducing interactions of primary cosmic rays which give a lot of background particles ii) The duration of balloon flights is so far limited to 2 to 3 weeks, hence these experiments cannot get high statistics, which limits the sensitivity reachable even with an ideal detector. For the study of rare phenomena, it is mandatory to be in the outer space beyond the atmosphere, to have a detector with a large acceptance, and to gather data for a long time

AMS will be the first magnetic spectrometer in space for a long duration, 3 to 5 years. The main goal of the experiment is the search for primordial antimatter, for non-baryonic dark matter, and the high precision and high statistics measurement of electrically charged cosmic ray particles and light nuclei in a very wide range of energy, from a few hundred MeV up to a few TeV in momentum.

2 The physics of AMS

2.1 The primordial antimatter

It was demonstrated by A. Zacharov [1] that to generate an asymmetric universe made of matter only, starting from a symmetric universe, i.e. an universe in which there is the same amount of matter and of antimatter, as it is in the big-bang theory at the very beginning of the universe, 4 conditions must be fulfilled : i) Violation of the baryonic number ii) Violation of the charge conjugation C iii) large CP violation iv) Baryogenesis out of the thermal equilibrium. These conditions are in contradiction with the experimental observations. The first condition means that the proton should be unstable; the experimental limit on the lifetime proton is very high [2], around 10^{33} years, which almost exclude the first condition. The CP violation observed in the K system are too small to account for the condition iii). Furthermore, in the Minimal SuperSymmetric Model, from the condition iii) one can derive an upper limit of about 60 GeV for the mass of the lightest Higgs boson [3] , while the recent LEP results put a lower limit of 88.3 GeV on this mass[b]. The theoretical attempts to find a way to make the antimatter disappearing like in the inflation model have not yet found a natural way. On the other hand, the absence of observation of gamma ray peaks from matter-antimatter annihilation excludes the presence of large quantity of antimatter within a distance of the order of 10 Mpc from the earth.

A clear signature of the existence of islands of antimatter in the universe would be the observation of antinuclei of Helium or Carbon, since such nuclei cannot be produced by interaction of cosmic rays with the interstellar medium. They can only be produced in the furnace of a star of antimatter, and be ejected in the outer space in a supernova explosion. Balloon borne experiments have searched for such antinuclei

[b]The limit on $M - h$, mass of the lightest boson in the MSSM model published by the L3 Collaboration [4] is $M_h > 77.1 GeV$ at 95% confidence level using the data with an energy in the center of mass up to 189 GeV. Quite recently, the new preliminary value of $M_h > 88.3 GeV$ was obtained by combining the data of the 4 experiments at LEP, with the data at 192, 196, 200, and 202 GeV in the center of mass from year 1999 (A. Quadt, talk at the XXXV Rencontres de Moriond, Electroweak session, March 2000)

for more than 20 years with negative results [5, 6, 7]. AMS is designed to reach a sensitivity of 10^{-9} on the ratio antihelium/helium, better by 3 to 4 order of magnitude than the existing experiments.

2.2 The Dark matter

From the motion of the spiral arms of galaxies and of the cluster of galaxies it can be deduced that about 90% of the mass of the universe is non-radiating, and therefore is invisible to classical astrophysics experiments. The nature of this so-called dark matter is not yet known. This missing matter could have been due to brown dwarfs, stars with a mass too small to ignite the nuclear reaction, and several [8] experiments search for such object by using gravitational lensing, but from the spectrum of microwave background one can put a limit of about 20the fraction of the dark matter which is baryonic (the so-called cold dark matter). Therefore most of the dark matter is of non baryonic origin. These objects are called WIMP's. In supersymmetric theories, a good candidate for WIMP's is the neutralino χ, lightest supersymmetric particle. This particle could have accumulated in the halo of galaxies and be observed through the annihilation with its antiparticle from which particles like antiprotons, positrons, and gammas are produced and can be observed above the flux of the same particles produced in the interaction of cosmic rays of high energy with the interstellar medium [9]. AMS will measure with high statistics and high resolution the fluxes of antiprotons, positrons, and gamma rays from .5 GeV/c to 1 TeV/c.

2.3 And the ordinary matter

A big amount of information on the mechanisms of galaxies is buried in the abundance and in the spectra of ordinary charged particles and nuclei. The spectra of charged cosmic rays at high energy falls off according to a power law, and the slope contains information about the source of such cosmic rays, either primary or secondary. Unexpected phenomena could show up as a distortion of such spectra, but this implies a high precision and high statistics measurement on a broad range of energy. For light nuclei it is of chief importance to disentangle the isotopic content, which contains information on the confinement of cosmic rays in the galaxy. The unstable isotopes act like a clock which gives the time spent in the galaxy by the nuclei between their production and the measurement. This is especially the case for the Be^9 and Be^{10}, of which the ratio of abundance gives a direct measurement of the confinement time. To have a complete information in order to test theoretical model, this ratio must be measured as a function of the energy of the nucleus, on a range of kinetic energy from low energies few tens of MeV/N up to around 15 GeV/N.

The experimental measurements on nuclei done up to now by satellites have very limited range in energy since they are using the range of nuclei in matter to disentangle the various isotopes, and they suffer from low statistics: at the time of the AMS proposal, there was only 14 Be^{10} nuclei measured world wide in 40 years, while AMS was expected to measure 400 per day. High statistics, high precision, good identification power, and broad energy range are the key parameter to reach the physics content in this area, and these are the parameters by which the design of the AMS experiment is driven.

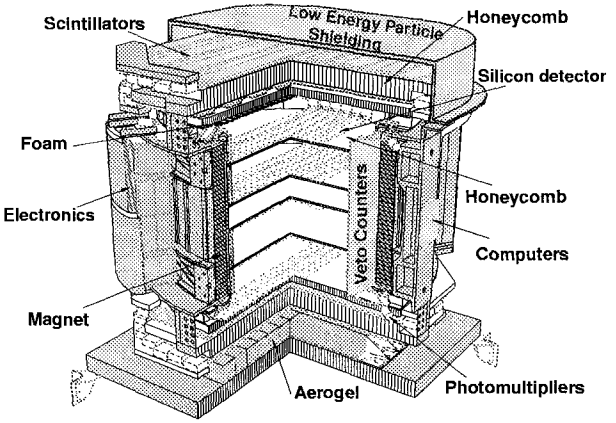

Figure 1: The AMS01 detector

3 AMS precursor flight on shuttle DISCOVERY

3.1 The AMS01 detector

Since it was the first time that a magnetic spectrometer was to be flown in space for a long time, it was decided to have a precursor flight of a few days on board the space shuttle DISCOVERY in order to test the detector behavior and performances under actual space flight conditions, to gather data on the background sources, and to study the operating parameters of the experiment. The detector was flown in June 1998, in the mission STS-91 of the shuttle DISCOVERY with an orbit inclined of 51.6° on the geographic equator, at an altitude varying between 320 kms and 390 kms. More than 100 millions triggers were gathered during the data taking. Most of the data were collected with the shuttle attitude such that AMS z-axis was pointing toward the zenith, within an angle of 45 degrees. However 4 hours of data taking were done with the axis pointing toward the center of the earth in order to have measurement of the fluxes of upward moving particles.

For this precursor flight, AMS consisted mainly of a permanent magnet, a silicon tracker, time of flight hodoscopes, anticoincidence counters, and an aerogel threshold Cerenkov counter. The acceptance was about 0.3 m^2sr. The permanent magnet was made of 1.9 tons of Nd-Fe-B in the shape of a cylindrical shell of inner diameter 1115 mm and length 800 mm. The Nd-Fe-B was magnetized to 46 MGOe with the direction varying in order to provide a dipole field in the x direction perpendicular to the cylinder axes, with a value of 0.14 Tesla in the center of the magnet and an analysis power BL^2, parallel to the magnet axis z of 0.14 Tm^2. The trajectory of particles traversing the magnet bore was measured by six planes of double sided silicon microstrip detector put inside the magnet perpendicular to the axis, the outer layers being just outside the magnet cylinder, above and below. From the deflection the rigidity $R = pc/|Z|e$ (GV) was measured. The tracker had an accuracy of about 10 microns in the bending plane and 30 microns in the other one. The tracker provided also a determination of the charge $|Z|$ through multiple measurements of energy loss.

The total amount of material of the tracker as seen by a particle parallel to the axis of the magnet was only 3multiple scattering.

The particle velocity and direction of motion were measured by a time-of-flight system made of four layers of scintillation counters, 2 above and 2 below the magnet. Each layer consisted of 14 paddles of 10 mm thickness and 110 mm width overlapping in such a way to provide a hermetic coverage. The typical accuracy on the time measurement was 120 psec for particles of unit charge, and 105 psec for charge $|Z| = 2$, allowing to separate electrons from protons up to 1.5 GeV/c. The pulse height information from each plane provided additional determination of the charge $|Z|$. The velocity measurement was complemented by a threshold Cerenkov counter with an aerogel radiator of refractive index n=1.035, giving a separation between electrons and protons up to 3.7 GeV/c. A layer of anticoincidence scintillation counters lined the inner surface of the magnet to get rid of the background caused by particles passing through or interacting in the magnet walls and support structure. Finally, the detector was also shielded from low energy (a few MeV) particles by thin carbon fiber walls.

During the construction, the detector components went successfully through extensive space qualification tests (acceleration, vibration, thermal vacuum, electromagnetic interference, and radiation).

The basic trigger was made of the coincidence of signals in 3 out of 4 of the TOF planes, with a veto on a signal in the anticoincidence counters. During the flight, the detector performances as well as temperature and magnetic field were monitored continuously, and the alignment of the tracker was also continuously monitored with an infrared laser system. After the flight, the detector was checked and calibrated again first in an ion beam of Helium and Carbon at GSI-Darmstadt, then with an high energy pion and proton beam at CERN-PS, confirming that the detector performances remained the same before, during, and after the flight.

4 First physics results

At the time of this conference, the analysis of the data gathered by AMS was not yet finished. However, results were already available on antimatter search, on fluxes of protons, of electrons and positrons, and on flux and mass spectrum of helium. For the analysis, the data gathered above the area of the South Atlantic Anomaly were excluded. Apart from results on antihelium and proton spectra, the results presented below are preliminary.

4.1 Search for antihelium

For this search, the sample was restricted to data taken with the shuttle attitude such that the z-axis of AMS was pointing toward the zenith within an angle of 45 degrees. Events were selected after full reconstruction (momentum, sign, velocity, direction upward or downward, energy loss in the tracker and in the TOF) and were required to give hits in at least 4 tracker planes out of 6, and to have an energy loss in tracker and in TOF compatible with Z=2 charge. The latter criteria rejected the background of electrons with wrongly measured charge, since the combined charge confusion probability was found to be less than 10^{-7} (fig 2). The possibility of

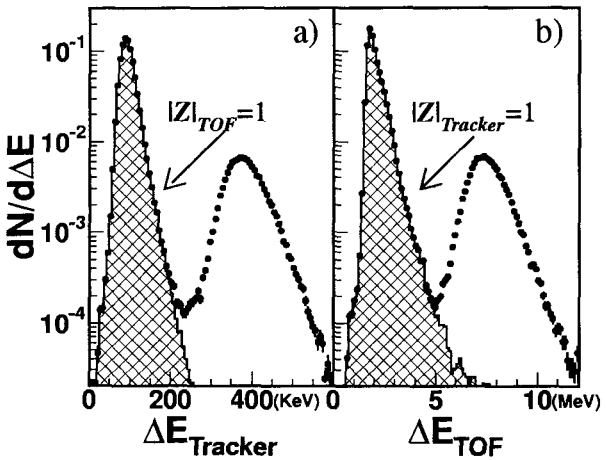

Figure 2: Energy loss measurements in tracker and TOF

misidentifying the direction upward or downward of the cosmic ray was found to be negligible from a control sample. To get rid of large angle nuclear scattering on one of the tracker plane, it was also requested that the parameters of the track reconstructed with the first 3 hits, the last 3 hits, and using all the hits in the tracker be compatible. To remove events with colinear delta rays which could disturb the reconstruction a last cut was applied on events with an excess of energy within $\pm$ 5 mm of the track. Finally a probability function was constructed from the measurement of velocity, rigidity, and energy loss to to check the compatibility of the track with the passage of an helium or antihelium nuclei with A=3 or 4. While this last cut removed the 4 last remaining antihelium candidates, the Helium sample was very little affected. A total of $2.8 \cdot 10^6$ He was obtained in a rigidity range of up to 140 GV while there was not antihelium at any rigidity(fig 3). The limit on antihelium is : N(antihelium)/N(helium)$< 1.1 \cdot 10^{-6}$ over the range 1 to 140 GV in rigidity. The same study applied to nuclei with $|Z| > 2$ gave $1.56 \cdot 10^5$ events in the same rigidity range and no antinucleus candidate. Eventually, after the flight AMS was put in an ion beam at GSI Darmstadt to confirm that the performances on charge separation and mass reconstruction were thoroughly understood.

4.2 Systematic measurement of proton spectra

Protons are easy to study since they are the most abundant singly charged particles, all other ones being orders of magnitude lower in flux. The huge statistics gathered by AMS allowed to study the proton energy spectrum as a function of the latitude and the high accuracy of the measurement allowed to trace backward the particles recorded in AMS. The sample was restricted to the period in which the z-axis was pointing within 1 of the zenith to measure the downward going particles and to the period in which the z-axis was pointing within 1 of the Nadir to measure the upward going particles. After reconstruction, tracks were selected with at least 4 hits in the

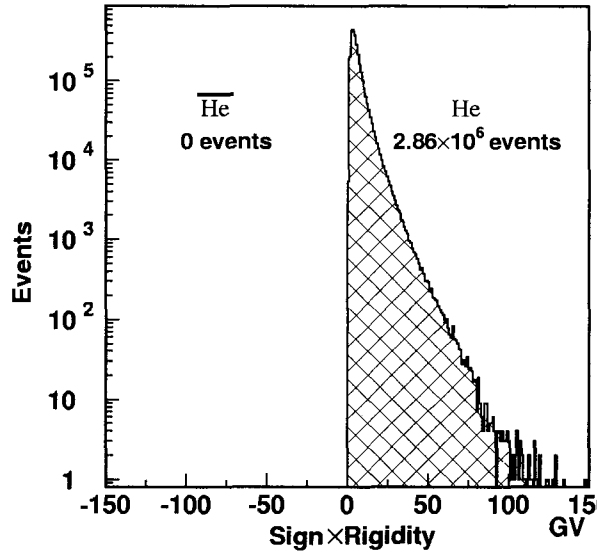

Figure 3: Measured rigidity times the charge sign for selected $|Z| = 2$ events

tracker in the bending plane and a measured charge from energy loss compatible with Z = 1. The remaining background events from pions produced in the top part of AMS was found to be less than 0.5% below 1 GeV and vanishing rapidly with energy, while the contamination of deuterons was reduced to a negligible level by requiring the measured mass to be within 3 standard deviations of the proton mass. The measured spectra were corrected for the differential acceptance estimated from Monte-Carlo simulation, giving a contribution to the total systematic error of 5%, then the effect of detector resolution was unfolded using resolution functions obtained from the simulation and checked at several energy from test beam measurement (fig 4). The effect of geomagnetic cutoff shows up very neatly as a function of geomagnetic latitude, and at high energy all the spectra have the same behavior. Surprisingly, a second (secondary) spectrum starts below the geomagnetic cutoff with a rate about an order of magnitude below. Near the equator the secondary spectrum has a distinct structure. In this region near the equator, the spectrum extend from the lowest measured energy, 0.1 GeV to about 6 GeV, with a rate of $70m^{-2}.sec^{-1}.sr^{-1}$. In all the bins in latitude up to $\Theta_M = 0.7$ the secondary spectrum of downward particle has a flux equal to the one of upward particles measured with the detector pointing toward the earth (fig 5). By tracing back 105 protons of the secondary flux in the earth magnetic field and stopping the extrapolation either when the particle reach the top of atmosphere defined at 40 kms, or when the flight time reached 10 seconds, it was found that all the protons from the secondary spectrum originate in the atmosphere. 30% of the protons flew for less than 0.3 seconds and their origin in the atmosphere is uniformly distributed around the globe reflecting the shuttle orbits, while the remaining 70% flew for more than 0.3 sec and originate from a restricted geographic zone, which

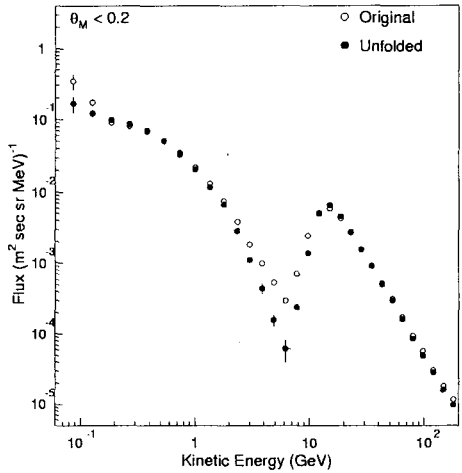

Figure 4: Original and unfolded proton spectrum near the geomagnetic equator

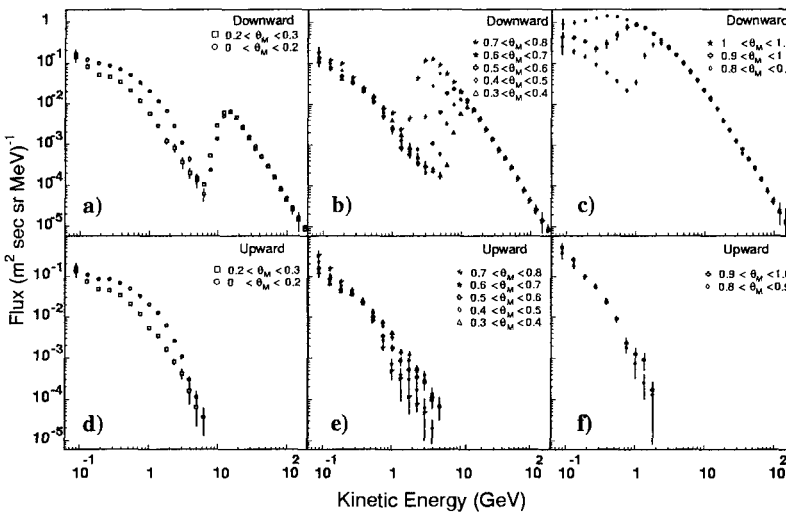

Figure 5: Fluxes of proton upward and downward in bins of geomagnetic latitude

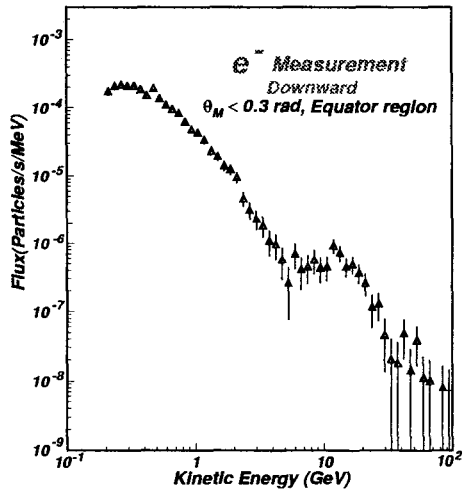

Figure 6: Flux of electrons in the geomagnetic equator region

could be related to the South Atlantic Anomaly.

Above the geomagnetic threshold, the proton spectrum follows a power law in rigidity $\Phi_0 \cdot R^{-\gamma}$. Fitting the parameters on the rapidity range 10 to 200 GV yields :

$$\gamma = 2.79 \pm 0.012(fit) \pm 0.019(sys)$$

$$\Phi_0 = 16.9 \pm 0.2(fit) \pm 1.3(sys) \pm 1.5(\gamma) GV^{2.79}/(m^2.sec.sr.MV)$$

To check these results, a calibration of the AMS detector was done at CERN after the flight with 100 millions of protons and pions of energy 2,3,4,10, 14 GeV. From the beam of 10 $\pm$ 0.1 GeV protons, the tracks reconstructed gave a mean value of 10.04 GeV with a width of 0.92 GeV, showing that there is no bias in the reconstruction.

4.3 Electron and Positron measurements

AMS was also able to measure electrons and positrons. The electrons thanks to their negative sign have clear identification and very small background, hence AMS was able to measure their spectra with limited statistics up to energies of 100 GeV. For a geomagnetic latitude of $\Theta_M < 0.3$, it was found that the electron spectrum has the same behaviour as the proton one, with a secondary flux below the geomagnetic cutoff extending up to 3 GeV (fig 6) and the same amount of electrons moving downward and upward, uniformly spread around the globe. For positrons, the high flux of protons with a rate about thousand time higher gives a lot of background at high energy, hence the study was done only below 2 GeV, an energy range where time of flight of the particle and the signal in the aerogel counter allows to reduce the proton misidentification to a negligible level. As a consistency check, the positron fraction over the sum of positron and electron rate was compared in the polar region ($\Theta_M > 1.0$) to the previous measurement by balloon borne experiments and was found in excellent agreement.

The electron and positron spectra in the geomagnetic equator region $\Theta_M < 0.3$

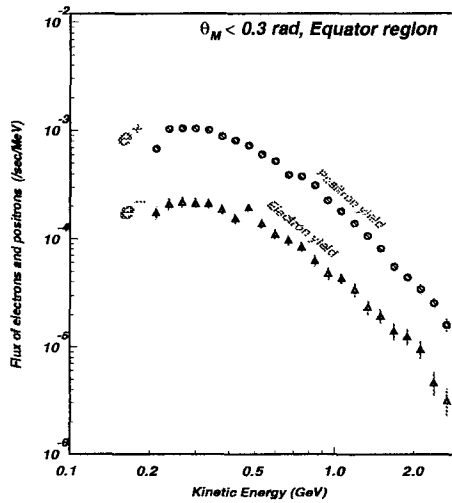

Figure 7: Relative electron and positron yield around the equator

rad in the energy range 0.1 to 2.5 GeV exhibit exactly the same behavior, but the flux of positrons is 3 to 4 times higher than the electron one (fig 7), which again was never observed before.

4.4 Measurement of Helium fluxes and mass spectrum

From the helium nuclei sample selected as explained above, it was possible to derive the helium spectra for various bins of geomagnetic latitude (fig 8). Above the geomagnetic threshold, the helium spectrum follows a power law in rigidity $\Phi_0 \cdot R^{-\gamma}$. Fitting the parameters on the rapidity range 10 to 140 GV yields :

$$\gamma = 2.65 \pm 0.014(fit) \pm 0.03(sys)$$
$$\Phi_0 = 1.45 \pm 0.06(fit) \pm 0.12(sys) \pm 0.15(\gamma) GV^{2.65}/(m^2.sec.sr.MeV)$$

Below the energy threshold after the fall of the primary spectrum a secondary spectrum shows up, 2 to 3 order of magnitude smaller in flux, in the equatorial region $|\Theta_M| < 0.4$ rad. Fitting the mass of helium nuclei above the threshold one gets M = 3.64 ± 0.01 GeV/c^2 in the polar region $|\Theta_M| > 0.4$ rad, and M = 3.65 ± 0.09 GeV/c^2 in the equatorial region $|\Theta_M| < 0.4$ rad. Comparing with the He^4 mass of 3.727 GeV/c^2, it shows that the content is mostly He^4. However, the same mass fitting applied to Helium nuclei below the threshold in the equatorial region gives a mass of 2.86 ± 0.04 GeV (fig 9 a and b), close to the He^3 mass of 2.809 GeV/c^2 which implies that these nuclei are mostly He^3.

4.5 Conclusion on physics of AMS01.

These results on cosmic rays below threshold were not observed previously since nobody had made measurements in these conditions, and it was not expected from models. From preliminary studies of the trajectory of high energy cosmic rays in

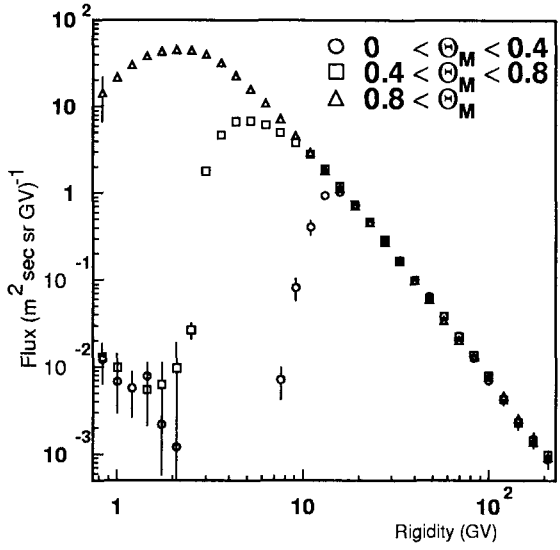

Figure 8: Spectra of Helium nuclei in bins of geomagnetic latitude

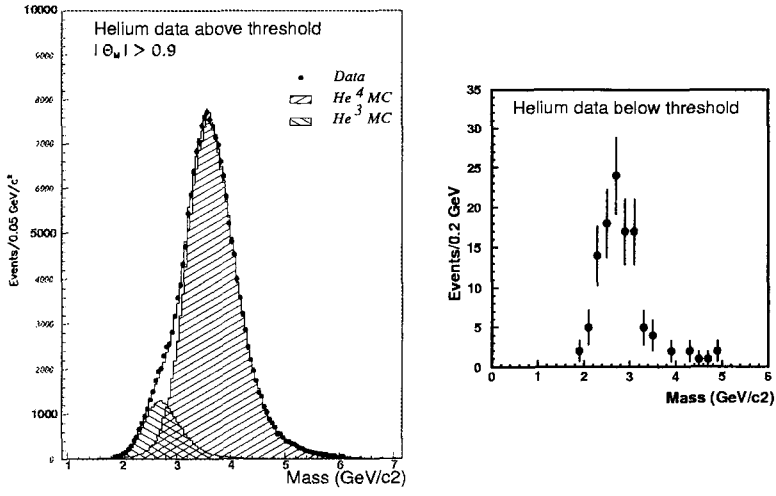

Figure 9: Helium mass spectra above and below threshold

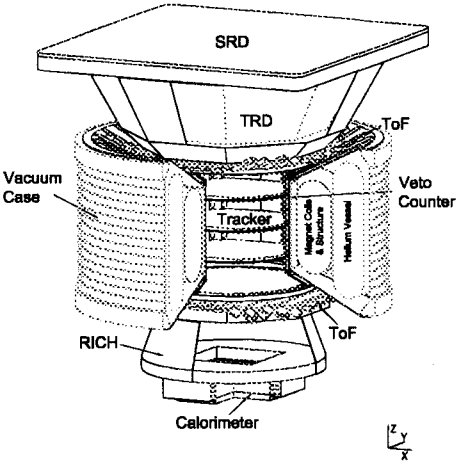

Figure 10: The AMS02 detector for the ISS

the earth magnetic field, it appears that these particles trapped at high altitude in the magnetic field are secondaries of the interaction of primary cosmic rays with the atmosphere, forming a kind of belt. The detailed analysis is underway. It must also be remarked that, though it was only a technological test flight, the limit put on the antimatter/ matter ratio was better than any other published results, which demonstrates the quality of the instrument.

5 AMS on the international space station ISS

AMS is scheduled to fly to the international space station ISS in September 2003, and to take data for 3 to 5 years. In order to fulfill the program of physics, specially for the high energy part of the cosmic rays up to a few TeV, the instrument will be modified and completed with new detectors (fig 10) to improve measurement accuracy and particle identification.

The permanent magnet will be replaced by a superconducting one with the same inner volume, the same configuration of field, and a bending power 6 times higher $BL^2 = 0.86Tm^2$. This will allow to measure particle momentum with a resolution better than 2% up to 100 GeV and to have a excellent determination of the sign of electric charge up to several TeV. The tracker will be upgraded from 6 to 8 double-sided planes of silicon detector.

A transition radiation detector placed above the Time of Flight detector, made of 20 planes of straw tubes and foam, will give a separation power of nearly 200 between hadrons and electrons up to 500 GeV, and will give additional points on the trajectory of particles. Below the magnet, a RICH cerenkov counter with a double radiator of aerogel and Sodium fluoride will allow to identify nuclei up to Aluminium, and to disentangle the isotopic content up to Oxygen for nuclei with an energy per nucleon below 15 GeV. Underneath the RICH, an imaging electromagnetic calorimeter made of a sandwich of lead and scintillating fibers of depth 16.5 X_0 will

measure the electromagnetic showers with an accuracy of a few percent. Thanks to its very fine granularity (18 sampling in depth, and a transverse granularity of 0.5 Mollier radius in both direction) the calorimeter will allow to achieve a rejection power hadrons/electron close to 10^4, which combined with the TRD will achieve the identification power necessary for the study of the charged cosmic rays up to TeV range. Eventually, a Synchrotron Radiation Detector will detect the synchrotron radiation produced by electrons/positrons of energy above 500 GeV in the earth magnetic field before traversing the detector and will allow to increase the range of energy covered by AMS for electrons and positrons to 3 TeV. 20000 such particles are expected between 500 GeV and 3 TeV during the 3 to 5 years of data taking.

6 Conclusion

The AMS02 experiment on the international space station will open a domain of physics yet largely unexplored. The precursor flight dedicated to test the technology and the conditions in space gave numerous original and f unexpected physics results, which demonstrates the capability of the detector to fulfill its physics program.

Acknowledgments

I am very indebted to Professor Samuel C.C. Ting for giving me the opportunity to present the results of AMS at this conference. I would like also to thank all my colleagues of the AMS experiment for many fruitful discussions and specially J. Berdugo for the help. I would like also to thank the IN2P3/CNRS, the "Conseil Regional Rhone-Alpes", and the "Conseil General de Haute-Savoie" for their financial support that was a great help for contributing to the experiment.

References

[1] A. D. Sacharov, *JETP Lett.* 5, 24, (1967).
[2] B. Viren, *Current status of the nucleon decay search with SuperKamiokande*, (Proceedings of the DPF99 Conference) 1999.
[3] See discussion in *The Alpha Magnetic Spectrometer.* Proposal of experiment.
[4] M. Acciari et al., L3 Collaboration, *Phyis. Lett.* **B** 471, 177, (2000)
[5] R.L. Golden et al, *ApJ* 479, 992, (1997).
[6] J.F.Ormes et al., *ApJ Letters* 482, L187, (1997).
[7] T. Saeki et al., *Phys. Lett.* **B** 422, 319, (1998).
[8] M. Spiro, in *XXIX International Conference on High Energy Physics*, ed. by A. Astbury et al., World Scientific Press, (Proceedings of the XXIX ICHEP Conference), 1999
[9] E. Diehl et al., *Phys.Rev.* **D** 52, 7 (1995).
[10] J. Alcazar et al., AMS Collaboration, *Phys.Let.* **B** 461, 387 (1999).
[11] J. Alcazar et al., AMS Collaboration, *Phys.Let.* **B** 472, 215 (2000).

POSSIBLE OBSERVATIONAL EVIDENCES OF NON-COMPACT (NON-BARYONIC) MICROLENSES ("NEUTRALINO STARS")

A.F. ZAKHAROV [a]

Institute of Theoretical and Experimental Physics, B. Cheremushkinskaya, 25, 117259, Moscow, Russia

Abstract. Microlensing distant stars by non-compact objects such as neutralino stars is considered. Recently Gurevich and Zybin considered the objects as microlenses. Using the non-singular density distribution we analyse microlensing by non-compact objects. We obtain the analytical solutions of the gravitational lens equation and the analytical expression for the amplification factor of the gravitational lens. We show that using the model of microlensing by non-compact objects it is possible to interpret event candidates having two typical maximums of light curves which are usually interpreted as binary microlenses.

The first results of observations of microlensing which were presented in the papers [1 – 3] have discovered a phenomenon, predicted in the papers [4, 5]. The basics of microlensing theory and observational data are given in the reviews [6 – 9] and in the book [10]. A matter of the gravitational microlens is unknown till now, although the most widespread hypothesis assumes that they are compact dark objects as brown dwarfs. Nevertheless, they could be presented by another objects, in particular, an existence of the dark objects consisting of the supersymmetrical weakly interacting particles (neutralino) has been recently discussed in the papers [11, 12]. The authors showed that the stars could be formed on the early stages of the Universe evolution and to be stable during cosmological timescale. Using the singular model distribution microlensing by non-compact lenses were analysed in the papers [13 – 17].

We approximate the density of distribution mass of a neutralino star in the following form

$$\rho_{NeS}(r) = 2\rho_0 \frac{{r_c}^2}{r^2 + r_c^2}, \tag{1}$$

where r is the current value of a distant from stellar center, ρ_0 is a mass density of a neutralino star for a boundary of a core (or for a distance r_c from a center), r_c is a radius of a core. So we use the nonsingular isothermal sphere model (or the model of an isothermal sphere with a core). The dependence is approximation of the dependence which has been considered in the paper [8], where the authors considered the model of non-compact object with a core. It is clear that the singular (degenerate) dependence is the limiting dependence of (1) for $r_c \to 0$.

So, it is not difficult to obtain surface density mass, according to expression (1)

$$\Sigma(\vec{\xi}) = 4\rho_0 r_c^2 \int_0^{\sqrt{{R_x}^2 - \xi^2}} \frac{{a_0}^2}{\xi^2 + h^2 + r_c^2} dh =$$

$$4\rho_0 \frac{{r_c}^2}{\sqrt{\xi^2 + r_c^2}} \quad \arctan \frac{\sqrt{{R_x}^2 - \xi^2}}{\sqrt{\xi^2 + r_c^2}}.$$

[a] e-mail: zakharov@vitep5.itep.ru

In the case, if $R_0 \gg \xi$, then $\Sigma(\vec{\xi}) \longrightarrow 2\pi\rho_0 \frac{r_c{}^2}{\sqrt{\xi^2+r_c^2}}$. In that case the lens equation has the following form

$$\vec{\eta} = \frac{D_s}{D_d}\vec{\xi} - D_{ds}\vec{\alpha}_{NeS}(\vec{\xi}), \tag{2}$$

where D_s is a distance from the source to the observer, D_d is a distance from the gravitational lens to the observer, D_{ds} ia a distance from the source to the gravitational lens, vectors $(\vec{\eta}, \vec{\xi})$ define a deflection on the plane of the source and the lens, respectively

$$\vec{\alpha}_{NeS}(\vec{\xi}) = \int_{R^2} d^2\xi' \frac{4G\Sigma(\vec{\xi}')}{c^2} \frac{\vec{\xi} - \vec{\xi}'}{|\vec{\xi} - \vec{\xi}'|^2}. \tag{3}$$

We calculate the microlens mass

$$M_x = 8\pi\rho_0 r_c^2 \int_0^{R_x} \frac{r^2 dr}{r^2 + r_c^2} \approx 8\pi\rho_0 r_c^2 R_x.$$

We use characteristic value of a radius r_c, corresponding the microlens "mass" $M_x = 8\pi\rho_0 r_c^2 R_x$, thus we obtain lens equation in the dimensionless form. We introduce the dimensionless variables by the following way

$$\vec{x} = \frac{\vec{\xi}}{r_c}, \quad \vec{y} = \frac{\vec{\eta}}{\eta_0}, \quad \eta_0 = r_c \frac{D_s}{D_d}, \quad \Sigma_{\rm cr} = \frac{c^2 D_s}{4\pi G D_d D_{ds}},$$

$$k(\vec{x}) = \frac{\Sigma(a_0\vec{x})}{\Sigma_{\rm cr}}, \quad \vec{\alpha}(\vec{x}) = \frac{1}{\pi}\int_{R^2} d^2x' k(\vec{x}') \frac{\vec{x} - \vec{x}'}{|\vec{x} - \vec{x}'|^2}.$$

As we supposed that surface density is an axial symmetric function then the equation of the gravitational lens may be written in the scalar form [10]

$$y = x - \alpha(x) = x - \frac{m(x)}{x}, \quad m(x) = 2\int_0^x x' dx' k(x').$$

We remind, that we have the following expression for the function $k(x)$

$$k(x) = \frac{k_0}{\sqrt{1+x^2}},$$

$$k_0 = \frac{2\pi\rho_0 r_0}{\Sigma_{\rm cr}} = \frac{\pi}{4 r_c R_x} \frac{4GM_x}{c^2} \frac{D_d D_{ds}}{D_s} = \frac{\pi}{4} \frac{R_E^2}{r_c R_x}.$$

Hence, the lens equation has the following form [10]

$$y = x - D\frac{\sqrt{x^2+1} - 1}{x}, \tag{4}$$

where $D = 2k_0$.

We will show that gravitational lens equation has only one solution if $D < 2$ and have three solutions if $D > 2$ and $y > y_{\rm cr}$ (we consider gravitational lens equation for $y > 0$), where $y_{\rm cr}$ is a local maximal value of right hand of Eq. (4). It is possible to show that we determine the value $x_{\rm cr}$ which corresponds to $y_{\rm cr}$ using the following expression

$$x_{\rm cr}^2 = \frac{2D - 1 - \sqrt{4D+1}}{2}, \tag{5}$$

It is easy to see that according to (5) $x_{\rm cr}^2 > 0$ if and only if $D > 2$ and

$$y_{\rm cr} = x_{\rm cr} - D\frac{\sqrt{1 + x_{\rm cr}^2} - 1}{x_{\rm cr}}, \tag{6}$$

If we choose $x_{\rm cr} < 0$ then $y_{\rm cr} > 0$. So, if $D \leq 2$ then gravitational lens equation has only one solution for $(y > 0)$, if $D > 2$ then gravitational lens equation has one solution (if $y > y_{\rm cr}$), three distinct solutions (if $y < y_{\rm cr}$), one single solution and one double solution (if $y = y_{\rm cr}$).

It is possible to show that gravitational lens equation is equivalent to the following equation

$$x^3 - 2yx^2 - (D^2 - y^2 - 2D)x - 2yD = 0, \tag{7}$$

jointly with the inequality

$$x^2 - yx + D > 0. \tag{8}$$

Thus it is possible to obtain the analytical solutions of gravitational lens equation by the well-known way. We perform $z = x - 2y/3$ and obtain incomplete equation of third degree

$$z^3 + pz + q = 0, \tag{9}$$

where $p = 2D - D^2 - \frac{y^2}{3}$ and $q = \frac{2y}{3}\left(\frac{y^2}{9} - D(D+1)\right)$, so we have the following expression for the discriminant

$$Q = \left(\frac{p}{3}\right)^3 + \left(\frac{q}{2}\right)^2 =$$

$$\frac{D^2}{27}\left[-y^4 + y^2(2D^2 + 10D - 1) + D(2 - D)^3\right].$$

If $Q \geq 0$ then Eq. (9) has unique real solution (therefore the gravitational lens equation (4) has unique real solution). We use Cardan expression for the solution

$$x = \sqrt[3]{-q/2 + \sqrt{Q}} + \sqrt[3]{-q/2 - \sqrt{Q}} + 2y/3. \tag{10}$$

We suppose the case $D > 2$. If $y > y_{\rm cr}$ then the gravitational lens equation has unique solution. If $Q \geq 0$ then we use the expression (10) for the solution. If $Q < 0$ then we have the following expression

$$x = 2\sqrt{-\frac{p}{3}}\cos\frac{\alpha + 2k\pi}{3} + 2y/3, \quad (k = 0, 1, 2) \tag{11}$$

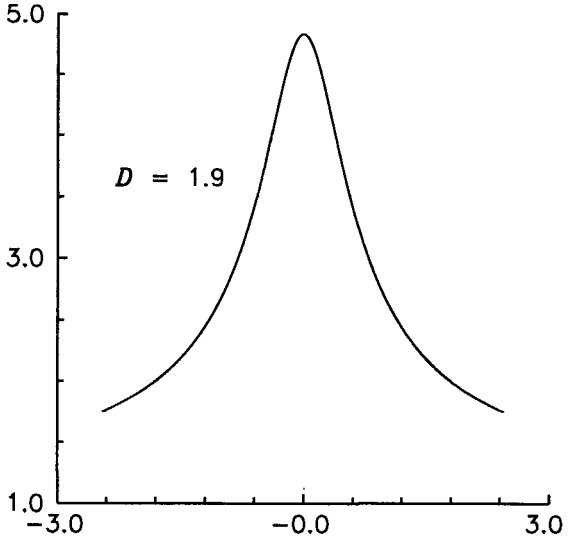

Figure 1: The light curve which corresponds to microlensing by a non-compact object (a neutralino star) for $D = 1.9$. The light curve resembles the standard light curve for microlensing by a compact object.

where

$$\cos\alpha = -\frac{q}{2\sqrt{-(p/3)^3}}, \tag{12}$$

and we select only one solution which corresponds to the inequality (8) which corresponds to $k = 0$ in (11) because if the gravitational lens equation has only one solution then we have a positive solution x for a positive value of impact parameter y therefore there is the inequality $x > y$ which is easy to see from (6). It is possible to check that maximal solution of (7) corresponds to $k = 0$ therefore the solution is the solution of (6).

If $y < y_{\rm cr}$ then the gravitational lens equation has three distinct solutions and we use the Eqs. (11-12) to obtain the solutions.

We consider now the case $D < 2$. We know that the gravitational lens equation has unique solution for the case. If $Q \geq 0$ then we use the expression (10) for the solution. If $Q < 0$ then we have the following expressions (11-12) and we select only one solution which corresponds to the inequality (8) which also corresponds to $k = 0$ as in the previous case.

It is known that magnification for gravitational lens solution x_k is defined by the following expression

$$\mu_k = \left|\left(1 - \frac{D(\sqrt{1+x^2}-1)}{x}\right)\left(1 + D\frac{\sqrt{1+x^2}-1}{x^2} - \frac{D}{\sqrt{1+x^2}}\right)\right|,$$

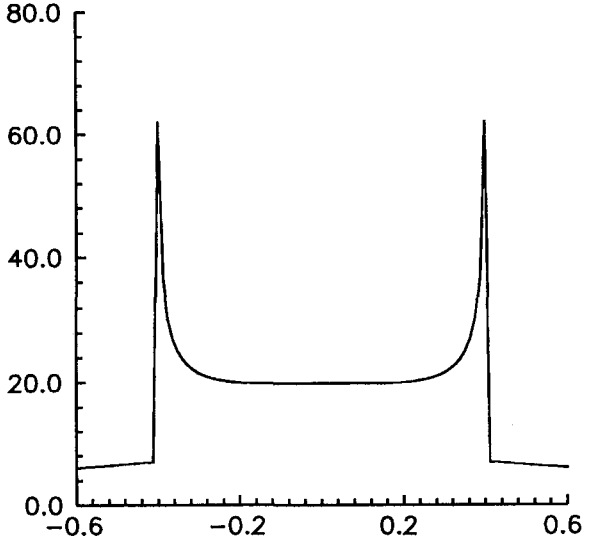

Figure 2: The light curve corresponds microlensing by non-compact object for $D = 4$. The light curve resembles the light curve for OGLE #7 event.

so the total magnification is equal

$$A_{\rm tot}(y) = \sum \mu_k, \tag{13}$$

where the summation is taken over all solutions of gravitational lens equation for a fixed value y.

The light curve corresponding to non-compact microlens is shown in Fig. 1 (for $D = 1.9$). The light curve resembles the light curves which are interpreted usually by the simple Schwarzschild microlens model [9]. The light curve corresponding to non-compact microlens is shown in Fig. 2 (for $D = 4$). The finite maximal value of the amplification in Fig. 2 is connected with a calculation of amplification for a finite set of times and if we consider the amplification on the all interval then the maximal value of the amplification must be infinite. It is easy to see that the light curves resemble the light curve for OGLE # 7 event candidate that is usually interpreted by binary lens model [18]. We recall that the appearance of two types of light curves for a toy density distribution model for noncompact object was discussed by Ossipov and Kurian [19]. More detailed analysis of the nonsingular model and its consequences are presented in the paper [20]. Using the singular and non-singular models polarization during microlensing was analysed and degenerate properties of the singular model are discussed in the paper [9].

I appreciate M.V. Sazhin for useful and stimulating discussions of different aspects of microlensing.

References

[1] C. Alcock *et al.*, *Nature* **365**, 621 (1993).
[2] E. Aubourg *et al.*, *Nature* **365**, 623 (1993).
[3] A. Udalski *et al.*, *Astrophys. J.* **426**, L69 (1994).
[4] A.V. Byalko, *Astron. Zhurn.* **46**, 998 (1969).
[5] B. Paczynski, *Astrophys. J.* **304**, 1 (1986).
[6] B. Paczynski, astro-ph/9604011.
[7] E. Roulet and S. Mollerach, astro-ph/9603119.
[8] A. V. Gurevich, K.P. Zybin and V.A. Sirota, *Uspekhi Phys. Nauk* **167**, 913 (1997).
[9] A. F. Zakharov and M.V. Sazhin, *Uspekhi Phys. Nauk* **168**, 1041 (1998).
[10] A.F. Zakharov, *"Gravitational Lenses and Microlenses"*, (Moscow: Janus, 1997).
[11] A. V. Gurevich and K.P. Zybin, *Phys. Lett. A* **208**, 276 (1995).
[12] A.V. Gurevich, K.P. Zybin, and V.A. Sirota, *Phys. Lett. A* **214**, 232 (1995).
[13] A.F. Zakharov and M.V. Sazhin, *Journ. Exper. Theor. Phys.* **110**, 1921 (1996).
[14] A.F. Zakharov and M.V. Sazhin, *Journ. Exper. Theor. Phys. Lett.* **63**, 894 (1996).
[15] A.F. Zakharov and M.V. Sazhin, *Pis'ma v Astron. Zhurn.* **23**, 403 (1997).
[16] A.F. Zakharov and M.V. Sazhin, *Phys. Atom. Nucl.* **61**, 1120 (1998).
[17] A.F. Zakharov and M.V. Sazhin, *Phys. Atom. Nucl.* **61**, 1126 (1998).
[18] A. Udalski *et al.*, *Astrophys. J.* **436**, L103 (1994).
[19] D.L. Ossipov and V.E. Kurian, *Phys. Lett. A* **223**, 157 (1996).
[20] A.F. Zakharov, *Astron. Zhurn.* **76**, 423 (1999).
[21] A.F. Zakharov, *Phys. Lett. A* **250**, 67 (1998).

Neutrino Conversions in Active Galactic Nuclei[a]

Athar Husain[b]
Department of Physics, Tokyo Metropolitan University, Minami-Osawa 1-1, Hachioji-Shi, Tokyo 192-0397, Japan

Abstract. I discuss the possibility of production of high energy cosmic neutrinos ($E \geq 10^6$ GeV) in cores of active galactic nuclei and study some of the effects of neutrino mixing on their subsequent propagation. I also discuss the prospects for observations of these high energy cosmic neutrinos in new km^2 surface area underwater/ice neutrino telescopes.

1 Introduction

In this contribution I discuss the possibility of production of high energy cosmic neutrinos ($E \geq 10^6$ GeV) in cores of Active Galactic Nuclei (AGN) originating from proton acceleration, the effects of three flavour neutrino mixing on these high energy cosmic neutrino fluxes and the prospects for their observations in new km^2 surface area underwater/ice neutrino telescopes.

In addition to AGNs, high energy cosmic neutrinos may also be produced in several currently envisaged other cosmologically distant astrophysical sources. These sources may include, for instance, Gamma Ray Burst fireballs and Topological Defects 1. For some possible effects of neutrino mixing other than the flavour one on high energy cosmic neutrino fluxes, see 2. The present study is particularly useful as several high energy neutrino telescopes are now at their rather advanced stage of development and deployment 3.

I start in Section 2 with a brief description of possibility of production of high energy cosmic neutrinos and discuss in some detail the effects of three flavour neutrino mixing on their subsequent propagation and further discuss the prospects for their detection. In Section 3, I summarize the results.

2 High Energy Neutrinos from AGNs

2.1 Production

High energy cosmic neutrinos may mainly be produced either in $p\gamma$ or in pp collisions in a cosmologically distant environment.

In $p\gamma$ collisions, high energy ν_e and ν_μ are mainly produced through $p + \gamma \to \Delta^+ \to n + \pi^+$ (typically with $\nu_e/\nu_\mu \sim 1/2$). The same collisions will give rise to a greatly suppressed high energy ν_τ flux ($\nu_\tau/\nu_{e,\mu} < 10^{-5}$) mainly through $p + \gamma \to D_S^+ + \Lambda^0 + \bar{D}^0$. In pp collisions, the ν_τ flux may be obtained through $p + p \to D_S^+ + X$. The relatively small cross-section for D_S^+ production together with the low branching ratio into ν_τ implies that the ν_τ flux in pp collisions is also suppressed up to 5 orders of magnitude relative to ν_e and/or ν_μ fluxes (which are mainly produced through $\pi^\pm$) 4.

---

[a]Talk given at 9th Lomonosov Conference on Elementary Particle Physics, 20-26 September, 1999, Moscow, Russia.

[b]E-Mail: athar@phys.metro-u.ac.jp

2.2 Propagation

Matter effects on vacuum neutrino oscillations are relevant if $G_F\rho/m_N \sim \delta m^2/2E$. Using ρ from Ref. 5 as an example, it turns out that matter effects are absent for $\delta m^2 \geq \mathcal{O}(10^{-10})$ eV^2. Matter effects are not expected to be important in the neutrino production regions around AGN and will not be further discuss here.

In the framework of three flavour analysis, the flavour precession probability from α to β neutrino flavour is 6

$$\begin{aligned} P(\nu_\alpha \to \nu_\beta) \equiv P_{\alpha\beta} &= \sum_{i=1}^{3} |U_{\alpha i}|^2 |U_{\beta i}|^2 \\ &+ \sum_{i\neq j} U_{\alpha i} U^*_{\beta i} U^*_{\alpha j} U_{\beta j} \cos\left(\frac{2\pi L}{l_{ij}}\right), \end{aligned} \tag{1}$$

where $\alpha, \beta = e, \mu$, or τ. U is the 3×3 MNS mixing matrix and can be obtained in usual notation through

$$\begin{aligned} U &\equiv R_{23}(\theta_1)\mathrm{diag}(e^{-i\delta/2}, 1, e^{i\delta/2}) \\ &\cdot R_{31}(\theta_2)\mathrm{diag}(e^{i\delta/2}, 1, e^{-i\delta/2}) R_{12}(\theta_3), \end{aligned} \tag{2}$$

thus coinciding with the standard form given by the Particle Data Group 7. In Eq. (1), $l_{ij} \simeq 4\pi E/\delta m^2_{ij}$ with $\delta m^2_{ij} \equiv |m_i^2 - m_j^2|$ and L is the distance between the source and the detector. For simplicity, I assume here a vanishing value for CP violating phase δ and θ_{31} in U.

At present, the atmospheric muon and solar electron neutrino deficits can be explained with oscillations among three active neutrinos 8. For this, typically, $\delta m^2 \sim \mathcal{O}(10^{-3})$ eV^2 and $\sin^2 2\theta \sim \mathcal{O}(1)$ for the explanation of atmospheric muon neutrino deficit, whereas for the explanation of solar electron neutrino deficit, we may have $\delta m^2 \sim \mathcal{O}(10^{-10})$ eV^2 and $\sin^2 2\theta \sim \mathcal{O}(1)$ [just so] or $\delta m^2 \sim \mathcal{O}(10^{-5})$ eV^2 and $\sin^2 2\theta \sim \mathcal{O}(10^{-2})$ [SMA (MSW)] or $\delta m^2 \sim \mathcal{O}(10^{-5})$ eV^2 and $\sin^2 2\theta \sim \mathcal{O}(1)$ [LMA (MSW)]. The present status of data thus permits multiple oscillation solutions to solar neutrino deficit. I intend to discuss here implications of these mixings for high energy cosmic neutrino propagation.

In the above explanations, the total range of δm^2 is $10^{-10} \leq \delta m^2/\text{ eV}^2 \leq 10^{-3}$ irrespective of neutrino flavour. The typical energy span relevant for possible flavour identification for high energy cosmic neutrinos is $2 \cdot 10^6 \leq E/\text{GeV} \leq 2 \cdot 10^7$ in which currently the neutrino flux from cores of AGNs dominate. Taking a typical distance between the AGN and our galaxy as $L \sim 100$ Mpc (where 1 pc $\sim 3 \cdot 10^{16}$ m), note that cos term in Eq. (1) vanishes and so Eq. (1) reduces to

$$\langle P_{\alpha\beta}\rangle \simeq \sum_{i=1}^{3} |U_{\alpha i}|^2 |U_{\beta i}|^2. \tag{3}$$

It is assumed here that no relatively dense objects exist between the AGN and the earth so as to effect significantly this oscillations pattern. Note also that since $\langle P_{\alpha\beta}\rangle$

in above Eq. is symmetric under the exchange of indices α and β implying that no T (or CP) violation effects arise in neutrino vacuum flavour oscillations for high energy cosmic neutrinos 9.

Let me denote by F^0_α, the intrinsic neutrino fluxes. From the discussion in the previous Subsection, it follows that $F^0_e : F^0_\mu : F^0_\tau = 1 : 2 :< 10^{-5}$. For simplicity, I take these ratios as $1 : 2 : 0$. In order to estimate the final (downward going) flux ratios of high energy cosmic neutrinos reaching on earth, let me introduce a 3×3 matrix of vacuum flavour precession probabilities such that

$$F_\alpha = \sum_\beta \langle P_{\alpha\beta}\rangle F^0_\beta, \tag{4}$$

where the unitarity conditions for $\langle P_{\alpha\beta}\rangle$ read as

$$\begin{aligned} \langle P_{ee}\rangle + \langle P_{e\mu}\rangle + \langle P_{e\tau}\rangle &= 1, \\ \langle P_{e\mu}\rangle + \langle P_{\mu\mu}\rangle + \langle P_{\mu\tau}\rangle &= 1, \\ \langle P_{e\tau}\rangle + \langle P_{\mu\tau}\rangle + \langle P_{\tau\tau}\rangle &= 1. \end{aligned} \tag{5}$$

The explicit form for the matrix $\langle P\rangle$ in case of just so flavour oscillations as solution to solar neutrino problem along with the solution to atmospheric neutrino deficit in terms of ν_μ to ν_τ oscillations with maximal mixing is

$$\langle P\rangle = \begin{pmatrix} 1/2 & 1/4 & 1/4 \\ 1/4 & 3/8 & 3/8 \\ 1/4 & 3/8 & 3/8 \end{pmatrix}. \tag{6}$$

Using Eq. (6) and Eq. (4), it follows that $F_e : F_\mu : F_\tau = 1 : 1 : 1$ at the level of F^0_e. Also, Eq. (5) is satisfied. The same flux ratio is obtained in the remaining two cases for which the corresponding $\langle P\rangle$ matrics are: [for SMA (MSW)]

$$\langle P\rangle = \begin{pmatrix} 1 & 0 & 0 \\ 0 & 1/2 & 1/2 \\ 0 & 1/2 & 1/2 \end{pmatrix}, \tag{7}$$

whereas in case of LMA (MSW),

$$\langle P\rangle = \begin{pmatrix} 5/8 & 3/16 & 3/16 \\ 3/16 & 13/32 & 13/32 \\ 3/16 & 13/32 & 13/32 \end{pmatrix}. \tag{8}$$

Thus, essentially independent of the oscillation solutions for solar neutrino problem, it follows that $F_e : F_\mu : F_\tau = 1 : 1 : 1$. The deviations from these ratios are estimated to be small 10.

Summarizing, although intrinsically the downward going high energy cosmic tau neutrino flux is negligibally small however because of vacuum flavour oscillations it becomes comparable to ν_e flux thus providing some prospects for its possible detection.

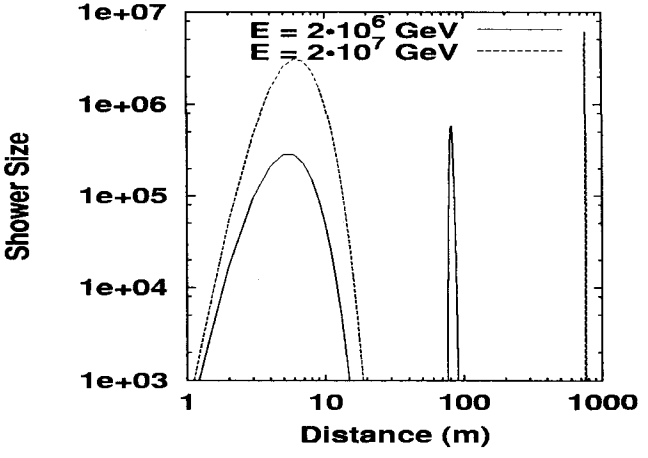

Figure 1: Typical longitudinal development of a double shower produced by the deep inelastic charged current interaction of the tau neutrino in water/ice.

2.3 Prospects for detection

I briefly mention here the prospects for detection of downward going high energy cosmic tau neutrinos through double shower technique 11. For prospects of observations of high energy cosmic tau neutrinos other than double shower technique, see 12, whereas for possibility of detection of non tau neutrinos, see 13.

The downward going tau neutrinos reaching close to the surface of the detector may undergo a charged current deep inelastic scattering with nuclei inside/near the detector and produce a tau lepton in addition to a hadronic shower. This tau lepton traverses a distance, on average proportional to its energy, before it decays back into a tau neutrino and a second shower most often induced by decay hadrons. The second shower is expected to carry about twice as much energy as the first and such double shower signals are commonly referred to as a double bangs. As tau leptons are not expected to have further relevant interactions (with high energy loss) in their decay timescale, the two showers should be separated by a clean μ-like track.

The calculation of downward going contained but separable double shower event rate can be carried out by replacing the muon range expression with the tau range expression and then subtracting it from the linear size of a typical high energy neutrino telescope in the event rate formula while using the expected ν_τ flux spectrum given by Eq. (4). This ensures that the two separate showers are contained within km of the underwater/ice detector. Here, I restrict myself by mentioning that the expected number of contained but separable double showers induced by downward going high energy tau neutrinos for $E \sim 2 \cdot 10^6$ GeV may be $\sim \mathcal{O}(10)$/yr·sr irrespective of the oscillation solutions of solar neutrino problem, if one uses the F_e^0 from Ref. 5 as an example. At this energy, the two showers initiated by the downward going high energy cosmic tau neutrinos are well separated ($\geq$ 70 m) such that the size of the second

shower is essentially 2 times the first shower and the two showers are connected by a μ−like track (see Fig. 1). This identification, if empirically realized, may provide a possibility to isolate ν_τ flavour from the rest of neutrino flavors. The chance of having double shower events induced by non tau neutrinos is negligibly small for relevant energies.

3 Conclusions

1. Intrinsically, the flux of high energy cosmic tau neutrinos is quite small, relative to non tau flavour neutrinos, typically being $F^0_\tau/F^0_{e,\mu} < 10^{-5}$ (whereas $F^0_e/F^0_\mu \sim 1/2$) from cosmologically distant astrophysical sources, namely, for instance, cores of Active Galactic Nuclei.

2. Because of neutrino oscillations, this ratio can be greatly enhanced. In the context of three flavour neutrino mixing scheme which can accommodate the oscillation solutions to solar and atmospheric neutrino deficits in terms of oscillations between three active neutrinos, the final ratio of fluxes of downward going high energy cosmic neutrinos on earth is $F_e \sim F_\mu \sim F_\tau \sim F^0_e$, essentially irrespective of the oscillation solutions to solar neutrino problem.

3. This enhancement in high energy cosmic tau neutrino flux may lead to the possibility of its detection in km^2 surface area high energy neutrino telescopes. For $2 \cdot 10^6 \leq E/\mathrm{GeV} \leq 2 \cdot 10^7$, the downward going high energy cosmic tau neutrinos may produce a double shower signature because of charged current deep inelastic scattering followed by a subsequent hadronic decay of the associated tau lepton.

Acknowledgements

I thank Japan Society for the Promotion of Science (JSPS) for financial support.

References

[1] See, for instance, R. J. Protheroe, *Nucl. Phys.* **B** (Proc. Suppl.) 77, 465 (1999).
[2] Athar Husain, *Nucl. Phys.* **B** (Proc. Suppl.) 76, 419 (1999).
[3] L. Moscoso, in *Sixth International Workshop on Topics in Astroparticle and Underground Physcis* (TAUP 99), Paris, France, ed. by M. Froissart, J. Dumarchez and D. Vignaud (to appear).
[4] A somewhat detailed numerical study supports this oder of magnitude estimate; H. Athar, R. A. Vázquez and E. Zas (in preparation).
[5] A. P. Szabo and R. J. Protheroe, *Astropart. Phys.* 2, 375 (1994).
[6] Ta-Pei Cheng and Ling-Fong Li, Gauge theory of elementary particle physics (Clarendon Press, Oxford, 1984) p. 411.
[7] C. Caso et al., *The Euro. Phys. J.* **C** 3, 103 (1998).
[8] See, for instance, E. Lisi, in *New Era in Neutrino Physics*, ed. by H. Minakata and O. Yasuda, Universal Academy Press, Inc., Tokyo, Japan (Proceedings of Satellite Symposium after Neutrino 98) June 1998, p. 153.
[9] N. Cabibbo, *Phys. Lett.* **B** 72, 333 (1978).

[10] H. Athar, M. Jezabek and O. Yasuda (in preparation).
[11] J. G. Learned and S. Pakvasa, *Astropart. Phys.* 3, 267 (1995). See also scanned transparencies by Athar Husain at URL http://taup99.in2p3.fr/TAUP99/Thursday/thursday.html.
[12] For a recent discussion, see, S. Iyer, M. H. Reno and I. Sarcevic, hep-ph/9909393 and references cited therein.
[13] R. Gandhi, C. Quigg, M. H. Reno and I. Sarcevic, *Astropart. Phys.* 5, 81 (1996); *Phys. Rev.* **D** 58, 093009 (1998).

LEPTON PRODUCTION BY NEUTRINOS IN AN EXTERNAL ELECTROMAGNETIC FIELD

A.V. BORISOV [a] and N.B. ZAMORIN

Physics Faculty of Moscow State University, 119899 Moscow, Russia

Abstract. We study two processes of lepton production by high-energy neutrinos in an external electromagnetic field: (*i*) the decay of a massive neutrino into an electron-positron pair and a light neutrino in the framework of the theory with neutrino mixing; (*ii*) the annihilation of a muon neutrino and an electron antineutrino into a muon and a positron. The asymptotic behavior of the lepton production rates as the functions of the kinematic and field parameters are investigated. We discuss the possibility of observing of the external field effects and some astrophysical applications.

1 Introduction

The problem of the neutrino mass has yet to be solved [1, 2]. For the masses of the neutrinos of three flavors, the upper limits obtained so far are the following [1]:

$$m_{\nu_e} < 3 \text{ eV}, \quad m_{\nu_\mu} < 0.19 \text{ MeV}, \quad m_{\nu_\tau} < 18.2 \text{ MeV} . \tag{1}$$

If the neutrinos are massive particles, the neutrinos of a specific flavor ν_l ($l = e, \mu, \tau$) that appear in a weak current generally represent a superposition of the neutrinos ν_i ($i = 1, 2, 3$) with definite masses m_i [2, 3]:

$$\nu_l = \sum_i U_{li}\nu_i \ , \tag{2}$$

where U_{li} is a unitary matrix similar to the quark mixing matrix in the Standard Model [4]. We can always order the neutrino mass states in such a way that $m_1 \leq m_2 \leq m_3$. Under the assumption that lepton mixing obeys a hierarchy similar to the well-known quark-mixing hierarchy – i.e., $|U_{jj}|^2 \gg |U_{jk}|^2$ for $j \neq k$ (which means that the matrix U is close to a diagonal matrix) – the constraints (1) can be interpreted as those on the masses m_i.

Neutrino mixing leads to observable fundamental effects [2, 3] such as neutrino oscillations $\nu_l \longleftrightarrow \nu_{l'}$ ($l \neq l'$) and radiative massive-neutrino decays caused by transitions between various mass states, $\nu_i \to \nu_j + \gamma$ and $\nu_i \to \nu_j + \gamma + \gamma$ (provided that $m_i > m_j$). The "invisible" neutrino decay $\nu_i \to \nu_j + \nu_k + \overline{\nu}_k$ is also possible. If the neutrino ν_3 is sufficiently heavy, $m_3 > 2m_e = 1.022$ MeV, the channel feauturing the emission of an electron-positron pair is open [3]:

$$\nu_3 \to \nu_j + e^+ + e^- \quad (j = 1, 2) \ . \tag{3}$$

In relation to the decay channel (3), which is described by a tree diagram involving the exchange of a W boson, the radiative decay channels are suppressed since they are allowed only in approximations not lower than the one-loop level [3]. Experimental searches for the process (3) at the nuclear reactor [5] resulted in the most stringent

[a] E-mail: borisov@ave.phys.msu.su

constraint on $|U_{e3}|^2$ for the mass range 1 MeV $< m_3 <$ 5 MeV (see [5] for references to original studies).

The reaction (3) is considered as one of decay channels for relic neutrinos in the universe [2]. This process for ultrahigh-energy neutrinos might be a source of relativistic lepton pairs in our galaxy. Another source of this kind we consider below is the annihilation of a neutrino pair into a lepton pair:

$$\nu_\mu + \overline{\nu}_e \to \mu^- + e^+ \ . \tag{4}$$

We note that various processes of inelastic scattering of ultrahigh-energy cosmic (anti)neutrinos on low-energy relic (anti)neutrinos in our galaxy are discussed as probable sources of high-energy cosmic rays (see, e.g., [6]).

For astrophysical and cosmological applications, it is of interest to take into account the effect of strong external magnetic fields on neutrino-lepton reactions. The radiative decay $\nu_i \to \nu_j + \gamma$ in a constant external field was studied in [7,8]. The inverse muon decay $\nu_\mu + e^- \to \mu^- + \nu_e$ in a magnetic field was investigated in [9,10]. In these Refs. it was proven that the external field considerably increases the rates of the processes.

In the present study, we consider the processes (3) and (4) in a constant external electromagnetic field using the crossed field as a model: $|\mathbf{E}| = |\mathbf{H}| = F =$ const, $\mathbf{E} \perp \mathbf{H}$. It is well known [11] that the expression for the rate of the process in the crossed field approximately describes the process in an arbitrary constant field of strength $F \ll H_0 = m^2c^3/e\hbar$ for relativistic particles ($\varepsilon \gg mc^2$), provided that the angles between the momentum $\mathbf{p}$ and the vectors $\mathbf{E}$ and $\mathbf{H}$ are not overly small (much greater than mc^2/ε).

For calculating rates we use the general procedure proposed in [11].

2 Decay of a massive neutrino $\nu_3 \to \nu_j e^+ e^-$ ($j = 1, 2$)

The Lagrangian for the interaction of a weak charged leptonic current with W bosons has the form [4]

$$\mathcal{L} = \frac{g}{\sqrt{2}} \sum_l \bar{l}\gamma^\mu \frac{1+\gamma^5}{2} \nu_l W_\mu + \text{h.c.} \tag{5}$$

Here g is the dimensionless coupling constant, $\gamma^5 = -i\gamma^0\gamma^1\gamma^2\gamma^3$, and the current neutrinos ν_l appear to be the superpositions (2) of the massive neutrinos ν_i , which are assumed to be Dirac particles. We use the metric with signature $(+---)$ and the system of units in which $\hbar = c = 1$.

By using Eqs. (2), (5) and the explicit expression ¿from [11] for the electron wave functions in the crossed field, we find, after rather tedious calculations, the spectral representation of the decay rate in the four-fermion approximation:

$$w = \frac{\sqrt{\pi} K_U G_F^2}{6\,(2\pi)^4} \frac{m_e^6}{\omega} \int_0^1 du \int_0^1 dv [\left(B_{-1}^{(0)} + B_{-1}^{(1)} \kappa^2\right) \Phi_1(z)$$
$$+ \kappa^{4/3} B_0 \Phi(z) + \kappa^{2/3} B_1 \Phi'(z)]. \tag{6}$$

Here G_F is the Fermi constant; $K_U = |U_{ei}^* U_{e3}|^2$;

$$\Phi(z) = \pi^{-1/2} \int_0^\infty dt \cos\left(zt + t^3/3\right)$$

is the Airy function of the argument $z = (\kappa s)^{-2/3}(1 - s/\lambda)$;

$$\Phi'(z) = d\Phi(z)/dz \ , \quad \Phi_1(z) = \int_z^\infty dt \Phi(t) \ ;$$

B's are the rational functions of λ, u, v. The dynamical parameter κ and the mass one λ are defined as

$$\kappa = \frac{e}{m_e^3}\left[-(F^{\mu\nu}k_\nu)^2\right]^{1/2} ; \quad \lambda = (m_e/m_\nu)^2 \ , \tag{7}$$

where m_e is the electron mass, $k = (\omega, \mathbf{k})$ is the 4-momentum of the initial neutrino with mass $m_3 = m_\nu$, while the final neutrino can be thought to be massless by virtue of the constraints (1); $F^{\mu\nu}$ is the field strength tensor.

We will consider below the extremes of small and large values of the dynamical parameter κ (see (7)).

For $\kappa \ll 1$ and $\lambda < 1/4\,(m_\nu > 2m_e)$ the decay width $\Gamma = (\omega/m_\nu)\,w$ (the rate in the neutrino rest frame) we obtain

$$\Gamma = K_U G_F^2 \frac{m_\nu^5}{192\pi^3}\left[f_0(\lambda) + \kappa^2 f_1(\lambda)\right] \ , \tag{8}$$

where

$$f_0(\lambda) = \mu\left(1 - 14\lambda - 2\lambda^2 - 12\lambda^3\right) + 24\lambda^2\left(1 - \lambda^2\right)L(\mu) \, ,$$
$$f_1(\lambda) = \tfrac{16}{9}\lambda^3\left[-\mu\left(13 + 2\lambda + 12\lambda^2\right) + \tfrac{3}{2}\left(1 - 16\lambda^3\right)L(\mu)\right] \, ,$$
$$\mu = \sqrt{1 - 4\lambda} \ , \quad L(\mu) = \ln\frac{1+\mu}{1-\mu} \ .$$

The function f_0 corresponds to the decay in the absence of the external field (i.e., at $\kappa = 0$) and f_1 – to the field-induced correction ($\sim \kappa^2$) to the free process.

We note that, for $\lambda > 1/4\,(m_\nu < 2m_e)$, the free decay (3) is forbidden and its rate (6) in the weak field is exponentially small,

$$w \sim \kappa^4 \exp\left[-\frac{8}{3\kappa}\left(1 - \frac{1}{4\lambda}\right)^{3/2}\right] \ ,$$

in accordance with general theory [11].

Let us now consider the case of a strong external field: $\kappa \gg 1$. We obtain from (7) the asymptotic formula

$$w = \frac{K_U G_F^2}{(3\pi)^3}\frac{m_e^6}{\omega}\kappa^2\left(\ln\kappa + C\right), \quad C = -\gamma_E - \frac{1}{2}\ln 3 - \frac{29}{24} \ , \tag{9}$$

where $\gamma_E = 0.577...$ is the Euler constant. This result is consistent with the corresponding formulas from [12, 13], where the case of a massless neutrino ($m_\nu = 0$, i.e., $\lambda \to \infty$) without mixing was considered (the emission of a lepton pair by a massless neutrino, $\nu_l \to \nu_l e^+ e^-$, is forbidden in the absence of an external field).

3 Neutrino annihilation $\nu_\mu + \overline{\nu}_e \to \mu^- + e^+$

For astrophysical applications it is of interest the case of collision of a high-energy neutrino (antineutrino) with a low-energy antineutrino (neutrino). The cross section for the process (4) in the four-fermion approximation is given by

$$\begin{pmatrix} \sigma^{(+)} \\ \sigma^{(-)} \end{pmatrix} = \frac{4G_F^2}{\pi^{3/2}} m_\mu^2 \int_0^1 dv \begin{pmatrix} \overline{v}/v \\ v/\overline{v} \end{pmatrix}$$

$$\times [\begin{pmatrix} -(v/2)(1-\nu\overline{v}) \\ (\overline{v}/2)(1+\nu v) \end{pmatrix} \Phi_1(y) - (\chi v \overline{v})^{2/3} \begin{pmatrix} 1 \\ 1 \end{pmatrix} \Phi'(y)] \,. \tag{10}$$

Here

$$y = (\chi v \overline{v})^{-2/3} v (1 - \nu \overline{v}) \;;\; \chi = \frac{e}{m_\mu^3} \left[-\left(F_{\alpha\beta} q^\beta\right)^2 \right]^{1/2} ,\; \nu = \frac{q^2}{m_\mu^2} \;; \tag{11}$$

v is a fraction of the total energy carried by the positron; $q = k + k'$, k (k') is the 4-momentum of the neutrino (antineutrino); $\sigma^{(+)}$ ($\sigma^{(-)}$) corresponds to the kinematical condition $\omega \gg \omega'$ ($\omega' \gg \omega$). Neutrinos are assumed to be massless: $k^2 = k'^2 = 0$. In addition, we have neglected the small mass parameter $\delta = m_e/m_\mu \simeq 5 \times 10^{-3}$ because its value is of order of radiative corrections.

Let us consider the asymptotics of the cross section (10).

For $\chi \ll 1$ and $\nu > 1$ the effect of a weak field $\sim \kappa^2$:

$$\begin{pmatrix} \sigma^{(+)} \\ \sigma^{(-)} \end{pmatrix} = \frac{G_F^2}{4\pi} m_\mu^2 [F_0(\nu) \begin{pmatrix} 1 \\ 1 \end{pmatrix} + \left(\frac{\chi}{\nu - 1}\right)^2 \begin{pmatrix} F_+(\nu) \\ F_-(\nu), \end{pmatrix}], \tag{12}$$

where

$$F_0(\nu) = \frac{1}{3}(2\nu + 1)\left(1 - \frac{1}{\nu}\right)^2 , \quad F_+(\nu) = -\frac{8}{3}\left(1 + \frac{3}{\nu^2} - \frac{2}{\nu^3}\right),$$

$$F_-(\nu) = -\frac{8}{3}\left(1 - \frac{2}{\nu}\right)\left(1 - \frac{1}{\nu}\right)^2 .$$

For $\nu < 1$ the free process (at $\chi = 0$) is forbidden and the cross section in a weak field is exponentially small,

$$\sigma \sim \chi \exp\left(-\sqrt{3}\delta \frac{1-\nu}{\chi}\right) .$$

The effect of a strong field, $\chi \gg 1$, comes to be dominant:

$$\sigma^{(\pm)} = \frac{15}{56\pi^3} \Gamma^4 \left(\frac{2}{3}\right) G_F^2 m_\mu^2 (3\chi)^{2/3} . \tag{13}$$

4 Discussion

In the above analysis, we have used the four-fermion approximation of electroweak theory. It is applicable if the square of the 4-momentum transfer satisfies the condition

$\left|q^2\right| \ll m_W^2$, where m_W is the W-boson mass. It follows that for the process (3) the dynamical field parameter κ (see (8)) must obey the constraint

$$\kappa \ll (m_W/m_e)^2 \simeq 2.5 \times 10^{10} \ . \tag{14}$$

For the process (4) we obtain the kinematical and dynamical constraints (see (11)):

$$\nu \ll (m_W/m_\mu)^2 \simeq 6 \times 10^5; \quad \chi \ll (m_W/m_\mu)^3 \simeq 4.4 \times 10^8 \ . \tag{15}$$

The last one expresses the smallness of the variation of the particle momentum over the formation length of the process in an external field [11] in comparison with m_W.

Let us consider the possibility of observing the effect of an external field on the processes in question under astrophysical conditions [14, 15].

A magnetic field can abruptly increase the probability of the process (3) for neutrinos of ultrahigh energies ($\kappa \gg 1$) owing to the factor $D(\kappa) = \kappa^2 \ln \kappa$ (cf. (9)). If we set, e.g., $H/H_0 = 0.1$ and $\omega = 5 \times 10^6$ GeV, then $\kappa = 10^9$ (see (15)), which yields $D(\kappa) \simeq 2 \times 10^{19}$.

For the process (4) at $\chi \gg 1$ the amplification is $A(\chi) = (3\chi)^{2/3}$ (see (13)). Assuming the annihilation of cosmic ray neutrinos of ultra-high energies ω with massless relic ones of the low energy $\omega' \sim 2$ K $\simeq 1.7 \times 10^{-4}$ eV we can apply our result (12) in the energy range

$$m_\mu \ll \omega \lesssim m_\mu^2/\omega' \lesssim 10^{20} \text{ eV}$$

because $\nu \lesssim 1$ in the semiclassical approximation for the cross section (10). Hence, the field parameter

$$\chi \simeq eH\omega/m_\mu^3 \lesssim 10^{-7} \, (H/1 \text{ G}) \ . \tag{16}$$

Dipole fields of neutron stars $H \lesssim 10^{13}$ G [14]. In this case it follows from (17) that $\chi \lesssim 10^6$ and $A(\chi) \lesssim 10^4$.

Thus, the process (4) could be a sufficiently effective source of high-energy charged leptons. We note that, in spite of a relatively small size of neutron stars, they may have appreciable influence on the cosmic ray energy spectra due to the large-scale pulsar wind effect (see, e.g., [16]).

5 Conclusion

In summary, the analyzed processes (3) and (4) could have astrophysical applications as effective sources of high-energy leptons in the vicinity of compact objects possessing strong magnetic fields.

References

[1] Particle Data Group: D. Groom et al., *Eur. Phys. J.* **C 15**, 1 (2000).

[2] K. Zuber, *Phys. Rep.* **305**, 295 (1998).

[3] F. Boehm, P. Vogel, *"Physics of Massive Neutrinos"*, (Cambridge Univ. Press, Cambridge, 1992).

[4] T.-P. Cheng, L.-F. Li, *"Gauge Theory of Elementary Particle Physics"*, (Clarendon Press, Oxford), 1984.

[5] C. Hagner et al., *Phys. Rev.* **D 52**, 1343 (1995).

[6] D. Fargion, B. Mele, E-print astro-ph/9902024; J. Blanco-Pillado, R. Vázquez, E. Zas, E-print astro-ph/9902266.
[7] A. Gvozdev, N. Mikheev, L. Vassilevskaya, *Phys. Lett.* **B 289**, 103 (1992); L. Vassilevskaya, A. Gvozdev, N. Mikheev, *Phys. At. Nucl.* **57**, 117 (1994).
[8] V. Zhukovsky, P. Eminov, A. Grigoruk, *Mod. Phys. Lett.* **A 11** 3119 (1996).
[9] A. Borisov, V. Guseinov, *Phys. At. Nucl.* **57**, 466 (1994).
[10] A. Borisov, V. Guseinov, O. Pavlova, *Phys. At. Nucl.* **61**, 94 (1998).
[11] A. Nikishov, V. Ritus, *Zh. Eksp. Teor. Fiz.* **46**, 776, 1768 (1964); V. Ritus, *Tr. FIAN* **111**, 5 (1979).
[12] A. Borisov, A. Ternov, V. Zhukovsky, *Phys. Lett.* **B 318**, 489 (1993).
[13] A. Kuznetsov, N. Mikheev, *Phys. At. Nucl.* **60**, 1865 (1997).
[14] V. Lipunov, *"Astrophysics of Neutron Stars"*, (Nauka, Moscow), 1987.
[15] G. Raffelt, *"Stars as Laboratories for Fundamental Physics"*, (Univ. of Chicago Press, Chicago), 1996.
[16] M. Giller, W. Michalak, in *"Relativistic Jets in AGNs"*, ed. by M. Ostrowski et al., Obserwatorium Astronomiczne, Uniwersytet Jagiellonski, (Proc. Int. Conf., Cracow, 27 - 30 May 1997), p. 189, Kraków, 1997.

PROPAGATION OF AXIONS IN A STRONGLY MAGNETIZED MEDIUM

A.V. BORISOV [a] and P.E. SIZIN

Physics Faculty of Moscow State University, 119899 Moscow, Russia

Abstract. The polarization operator of an axion in a degenerate gas of electrons occupying the ground-state Landau level in a superstrong magnetic field $H \gg H_0 = m_e^2 c^3/e\hbar = 4.41 \times 10^{13}$ G is investigated in a model with a tree-level axion-electron coupling. It is shown that a dynamic axion mass, which can fall within the allowed range of values (10^{-5} eV $\lesssim m_a \lesssim 10^{-2}$ eV), is generated under the conditions of strongly magnetized neutron stars. As a result, the dispersion relation for axions is appreciably different from that in a vacuum.

1 Introduction

The *a priori* strong nonconservation of CP parity in the standard model can be eliminated in a natural manner by introducing axions — pseudo-Goldstone bosons associated with the spontaneous breaking of the additional Peccei–Quinn global symmetry $U(1)_{PQ}$ [1, 2]. According to the experimental data [3], the energy scale v_a for the $U(1)_{PQ}$ symmetry breaking is much greater than the electroweak scale — $v_a \gtrsim 10^{10}$ GeV, and the constants of the possible couplings of an axion to the standard particles ($\sim 1/v_a$) are very small (the "invisible" axion: see [4] for a review of various axion models).

Axion effects can be appreciable under the astrophysical conditions of high matter densities, high temperatures, and strong magnetic fields (for example, in neutron stars [5]). Axion production processes, which result in additional energy losses by stars, and the limits obtained by astrophysical methods on the parameters of axion models are examined in [4]. In so doing, the influence of electromagnetic fields was neglected.

The investigation of axion processes in strong magnetic fields commenced comparatively recently. The Compton and Primakoff mechanisms of axion photoproduction on electrons ($\gamma + e \to e + a$) in the presence of an external electromagnetic field are studied in [6] – [9]. A new axion production mechanism — synchrotron emission of axions ($e \to e + a$) by relativistic electrons — was proposed in [10] and its contribution to the energy losses by a neutron star was calculated. In [6] – [10] it was assumed that the external field strength $F \ll H_0 = m_e^2 c^3/e\hbar \simeq 4.41 \times 10^{13}$ G. In [11] numerical methods were used to extend the results of [10] to superstrong magnetic fields $H \gtrsim H_0$. The axion synchrotron luminosity of neutron stars and white dwarfs was also investigated in [11].

In [8] – [11] a model with a derivative axion-electron coupling eae, described by the interaction Lagrangian [4]

$$\mathcal{L}_{ae} = \frac{g_{ae}}{2m_e} \left(\overline{\psi}\gamma^\mu\gamma^5\psi\right) \partial_\mu a, \tag{1}$$

was used. Here m_e is the electron mass and $\gamma^5 = -i\gamma^0\gamma^1\gamma^2\gamma^3$; the system of units such that $\hbar = c = 1$ is used; the signature of the metric is $(+ - - -)$; and $g_{ae} = c_e m_e/v_a$

[a] E-mail: borisov@ave.phys.msu.su

is a dimensionless coupling constant, where the numerical factor c_e depends on the choice of the specific axion model [4].

In models where axions are coupled only to heavy fermions by a tree-level coupling there arises an effective direct low-energy axion–photon interaction of the type $\gamma a \gamma$ [4]. This interaction is the basis of the Primakoff axion photoproduction mechanism employed in [6, 7]. The synchrotron process $e \to ea$ in the absence of a tree-level axion–electron coupling was considered in [12]. This process is due to resonant conversion of a longitudinal plasmon (a photon in a medium), emitted by a relativistic electron in a magnetic field, into an axion.

Decay of an axion in a strong magnetic field into a fermion pair ($a \to f\bar{f}$) [13] and two photons ($a \to \gamma\gamma$) [14] are also of interest for astrophysics and cosmology.

In the present report the model (1) is used to calculate the polarization operator of an axion moving in a strongly magnetized degenerate electron gas and the change in the dispersion relation of an axion in a medium is investigated using this operator.

2 Polarization operator of an axion

Taking account of the contribution of the electrons only (see Eq. (1)) and the translational invariance (the constant uniform magnetic field $\mathbf{H} \parallel \hat{\mathbf{z}}$, homogeneous isotropic medium) we obtain, using the real-time formalism of the finite-temperature quantum field theory (see, e.g., [15]), the diagonal momentum representation for the one-loop polarization operator of an axion:

$$\Pi(k, k') = (2\pi)^4 \delta^{(4)}(k - k')\Pi(k) \ , \tag{2}$$

where k (k') is the final (initial) 4-momentum of an axion. Here $\Pi(k)$ determines the axion propagator $D(k)$ in the momentum representation according to the Dyson equation

$$D(k) = \left[k^2 - m_a^2 - \Pi(k)\right]^{-1} , \tag{3}$$

where m_a is the free-axion mass (in the absence of a field and a medium), which is generated by the chiral anomaly of QCD [2]: $m_a \sim \Lambda_{QCD}^2/v_a$. The renormalized value $\Pi_R(k)$ (see below) gives the dispersion relation

$$k^2 = m_a^2 + \Pi_R(k) \ . \tag{4}$$

In the present report we confine our attention to superstrong magnetic fields and comparatively low temperatures,

$$H \gg H_0 \ , \quad T \ll \mu - m_e \ , \tag{5}$$

and we require the chemical potential to satisfy

$$\mu^2 - m_e^2 < 2h \ . \tag{6}$$

Here $h = eH$; the electron charge $-e < 0$. It follows from Eqs. (5) and (6) that in this case the contribution of positrons in the time-dependent single-particle Green's function of an ideal electron-positron gas with temperature T and chemical potential μ in a constant magnetic field [15] can be neglected (it is suppressed by the factor

$\exp[-(\mu - m_e)/T]$ [15]) and the medium is a degenerate gas of electrons occupying the ground-state Landau level (the principal quantum number $n = 0$). We also limit the range of the axion 4-momentum:

$$|k_0^2 - k_z^2| \ll h \ . \tag{7}$$

Then the main contribution of virtual (vacuum) electrons and positrons is likewise formed by states with $n = 0$. As a result, we can use an approximate expression for the Green's function in a superstrong magnetic field (in the absence of a medium this function is reduced to the well-known, effectively two-dimensional, electron propagator used in the theory of electrodynamic processes in superstrong magnetic fields and, specifically, for investigation of the photon polarization operator [16]).

This gives the following representation of the polarization operator (2):

$$\Pi(k) = \alpha_a \frac{H}{H_0} \exp\left(-\frac{k_\perp^2}{2h}\right) [F(\tau) + M(\tau)] \ . \tag{8}$$

Here $\alpha_a = g_{ae}^2/4\pi$, $\tau = l^2/4m_e^2$, $l = (k_0, 0, 0, k_z)$. In Eq. (8) the function F corresponds to the purely field contribution, M describes the influence of the medium and does not renormalize [15]. The renormalized value F_R can be obtained from the dispersion relation with one subtraction (as well as it was done for the photon polarization operator in [16])

$$\frac{1}{\tau} F_R(\tau) = \frac{1}{\pi} \int\limits_0^\infty \frac{dt \, \mathrm{Im}\, F(t)}{t(t - \tau - i0)} \ . \tag{9}$$

For $\tau < 0$ we obtain from Eq. (9) the renormalized field contribution

$$\Pi_R^{(F)} = -\frac{\alpha_a}{\pi} m_e^2 \frac{H}{H_0} \exp\left(-\frac{k_\perp^2}{2h}\right) \frac{1-\xi}{1+\xi} \ln \xi \tag{10}$$

to the axion polarization operator. Here the standard variable [17] ξ is introduced as $\tau = -(1-\xi)^2/4\xi$, which is convenient for analytical continuation in $l^2 = 4m_e^2\tau$.

For $\tau > 1$, a channel is open for axion decay into an electron-positron pair ($a \to e^- e^+$) in a magnetic field. Its rate w for a real axion is related with the imaginary part of the polarization operator on the mass shell by the well-known relation

$$w = -\frac{1}{\omega} \mathrm{Im}\, \Pi_R^{(F)} = \alpha_a \frac{m_e^2}{\omega} \frac{H}{H_0} \exp\left(-\frac{k_\perp^2}{2h}\right) \theta(\tau - 1) \left(1 - \frac{1}{\tau}\right)^{-1/2} \ , \tag{11}$$

where ω is the axion energy.

This result is identical to the result obtained in [13] on the basis of a calculation of the elastic scattering amplitude of an axion in a magnetic field.

Let us consider the contribution M of the medium to the axion polarization operator. For the imaginary part on the mass shell we obtain the representation

$$\mathrm{Im}\, M = \frac{m_e^2}{2} \theta(\tau - 1) [\theta(\mu - \varepsilon_+) + \theta(\mu - \varepsilon_-)] ,$$
$$\varepsilon_\pm = \frac{\omega}{2} \pm \frac{k_z}{2} \left(1 - \frac{1}{\tau}\right)^{1/2} \ . \tag{12}$$

Here ε is the energy of electrons in the medium.

¿From Eqs. (8), (11), and (12) we find the rate

$$w_M = \frac{1}{2}\left[\theta(\varepsilon_+ - \mu) + \theta(\varepsilon_- - \mu)\right] w \ , \tag{13}$$

where w is the decay rate (11) in the absence of a medium, for the axion decay into an e^-e^+ pair in the presence of a magnetized degenerate electron gas. We underscore that the blocking Pauli factors $\theta(\varepsilon_\pm - \mu)$ in Eq. (13) forbid electron production inside a filled Fermi sphere (for $\varepsilon_\pm < \mu$) .

For the real part of M on the mass shell we obtain the representation

$$\mathrm{Re}\, M = -\frac{m_e^2}{\pi}\tau \ \mathrm{P}\int_0^\lambda dx \left[\frac{1}{\tau - \cosh^2(x-\psi)} + \frac{1}{\tau - \cosh^2(x+\psi)}\right] \ . \tag{14}$$

Here where P signifies a principal value, the parameters λ and ψ are defined as $\cosh\lambda = \mu/m_e$, $\tanh\psi = k_z/\omega$. The integral (14) can be expressed in terms of elementary functions.

3 Discussion

We shall confine our attention below to the limiting cases that are of interest for astrophysical applications.

For an axion on the mass shell

$$l^2 = 4m_e^2\tau = \omega^2 - k_z^2 = m_a^2 + k_\perp^2 > 0 \ , \tag{15}$$

and the condition (7) gives $k_\perp^2 \ll h$, so that $\exp(-k_\perp^2/2h) \simeq 1$. We note that the imaginary part of the polarization operator is formed by the contribution of real electrons and positrons, and the expression for it holds under the weaker condition $k_\perp^2 < 2h$. Therefore the exponential factor can be retained in Eq. (11).

For $\tau \ll 1$ (substantially below the threshold of the decay process $a \to e^-e^+$), we find from Eqs. (10), (14) and (8)

$$\Pi_R = \Pi_R^{(F)} + \Pi^{(M)} = -\frac{\alpha_a}{\pi} m_e^2 \frac{H}{H_0}\tau\,(2 - \nu_+ - \nu_-) \ . \tag{16}$$

Here

$$\nu_\pm = \tanh(\lambda \pm \psi) = \frac{\nu\omega \pm k_z}{\omega \pm \nu k_z} \ , \quad \nu = \tanh\lambda = \left[1 - (m_e/\mu)^2\right]^{1/2} \ .$$

We note that $\Pi_R < 0$ and if the axion moves in the direction of the field $\mathbf{H}$ ($k_\perp = 0$) , then according to Eqs. (15) and (16) $\Pi_R \to 0$ in the limit of a massless axion ($m_a \to 0$) .

At high energies ($\tau \gg (\mu/m_e)^2 \gg 1$) we obtain for the polarization operator the asymptotic representation

$$\Pi_R = \frac{\alpha_a}{\pi} m_e^2 \frac{H}{H_0}\left[\ln\left[\tau\left(\frac{m_e}{\mu}\right)^2\right] - i\pi\right] \simeq \frac{2\alpha_a}{\pi} eH\left[\ln\frac{k_\perp}{2\mu} - i\frac{\pi}{2}\right] \ , \tag{17}$$

and it does not depend on the electron mass m_e as should be the case in this limit.

Let us write the dispersion relation (4) in the form

$$\omega^2 = k_\perp^2 + k_z^2 + m_a^2 + \Pi_R(k) \ . \tag{18}$$

It follows from Eqs. (16) - (18) that in a magnetized medium a radiative shift of the axion mass is generated — a dynamic mass, whose square, according to the definition in [15], is

$$\delta m_a^2 = \mathrm{Re}\,\Pi_R \ .$$

For $\tau \gtrsim 1$ and $\mu/m_e \gg 1$ we obtain the estimate

$$\delta m_a \sim g_{ae} m_e \left(\frac{H}{H_0}\right)^{1/2} \sim 10^6 g_{ae} \left(\frac{H}{10^{13}\ \mathrm{G}}\right)^{1/2} \mathrm{eV} \ . \tag{19}$$

For $g_{ae} \sim 10^{-13}$ (see [4,10]) and $H \gtrsim 10^{17}$ G (such fields [18,19] and even $H \sim 10^{18} - 10^{20}$ G [20] can exist in the interior regions of neutron stars), Eq. (19) gives $\delta m_a \gtrsim 10^{-5}$ eV.

4 Conclusion

In summary, under the conditions of strongly magnetized neutron stars a dynamic axion mass, which can fall within the existing limits on the axion mass [3,4,12] — 10^{-5} eV $\lesssim m_a \lesssim 10^{-2}$ eV — is generated. Therefore $\delta m_a \sim m_a$ and the dispersion relation (18) differs appreciably from the vacuum relation ($k^2 = m_a^2$).

References

[1] R. Peccei, H Quinn, *Phys. Rev. Lett.* **38**, 1440 (1977).

[2] S. Weinberg, *Phys. Rev. Lett.* **40**, 223 (1978); F. Wilczek, *Phys. Rev. Lett.* **40**, 279 (1978).

[3] Particle Data Group: C. Caso *et al.*, *Eur. Phys. J.* **C 3**, 1 (1998).

[4] G. Raffelt, *Phys. Rep.* **198**, 1 (1990); G. Raffelt, *"Stars as Laboratories for Fundamental Physics"*, (Univ. of Chicago Press, Chicago), 1996.

[5] V. Lipunov, *"Astrophysics of Neutron Stars"*, (Nauka, Moscow), 1987.

[6] A. Averin, A. Borisov, V. Zhukovskiĭ, A. Él'sabbakh, Preprint No. 3/1993 (Physics Faculty, Moscow State University), 1993.

[7] A. Borisov, K. Zhukovskiĭ, *Phys. At. Nuclei* **58**, 1218 (1995).

[8] A. Borisov, V. Grishina, *Vest. MGU, Fiz., Astron.*, No. 4, 24 (1996).

[9] A. Borisov, V. Grishina, *J. Exp. Theor. Phys.* **83**, 868 (1996).

[10] A. Borisov, V. Grishina, *J. Exp. Theor. Phys.* **79**, 837 (1994).

[11] M. Kachelriess, C. Wilke, G. Wunner, *Phys. Rev.* **D 56**, 1313 (1997).

[12] N. Mikheev, G. Raffelt, L. Vassilevskaya, *Phys. Rev.* **D 58**, 055008 (1998); E- print archive hep-ph/9803486.

[13] N. Mikheev, L. Vassilevskaya, *Phys. Lett.* **B 410**, 203 (1997).

[14] N. Mikheev, L. Vassilevskaya, *Phys. Lett.* **B 410**, 207 (1997); L. Vassilevskaya, N. Mikheev, A. Parkhomenko, *Phys. At. Nuclei* **60**, 2041 (1997).

[15] A. Borisov, A. Vshivtsev, V. Zhukovskiĭ, P. Éminov, *Physics - Uspekhi* **40**, 229 (1997).

[16] V. Skobelev, *Izv. Vyssh. Ucheb. Zaved., Fiz.*, No. 10, 142 (1975); Yu. Loskutov, V. Skobelev, *Phys. Lett.*, **A 56**, 151 (1976); V. Skobelev, Doctoral Dissertation in Physicomathematical Sciences (Moscow State University, Moscow), 1982.

[17] V. Berestetskiĭ, E. Lifshitz, L. Pitaevskiĭ, *"Quantum Electrodynamics"* (Pergamon Press, New York) 1982.

[18] I. Ternov, O. Dorofeev, *Phys. Part. Nuclei* **25**, 1 (1994).

[19] M. Bocquet, S. Bonazzola, E. Gourgoulhon, J. Novak, *Astron. Astrophys.* **301**, 757 (1995).

[20] D. Bandyopadhyay, S. Chakrabarty, S. Pal, *Phys. Rev. Lett.* **79**, 2176 (1997).

Mixing and CP violation with Quasidegenerate Majorana Neutrinos

G. C. Branco [a] M. N. Rebelo [b] J. I. Silva-Marcos [c]
Centro de Física das Interacções Fundamentais (CFIF),
Instituto Superior Técnico, P-1049-001, Lisboa, Portugal

Abstract. We study the exactly degenerate case for three lefthanded Majorana neutrinos building a general parametrization for the leptonic mixing matrix characterized by two angles and one CP violating phase and identify a weak-basis invariant relevant, in this case, for CP violation. After lifting the degeneracy, this parametrization accommodates the present data on atmospheric and solar neutrinos, as well as neutrinoless double beta decay. Some of the leptonic mixing ansätze suggested in the literature correspond to special cases of this parametrization.

1 Introduction

In the Standard Model (SM) neutrinos are massless and there is no mixing in the leptonic sector. Currently there are indications for neutrino oscillations in solar 1, atmospheric 2 and accelerator 3 experiments with the strongest evidence coming from the Super-Kamiokande atmospheric neutrino data 2. The LSND experiment is the only one that has not been confirmed independently. Neutrino oscillations are a clear sign of physics beyond the SM requiring the existence of massive neutrinos. The interpretation of the solar and atmospheric anomalies can be done in the framework of three lefthanded neutrinos, without additional sterile neutrinos. In our work 4, we have considered the case of three highly degenerate Majorana neutrinos and we analised in detail leptonic mixing and CP violation in the limit of exactly degenerate masses identifying, in this limit, a weak-basis invariant which controls the strength of CP violation. We showed that a two angle parametrization suggested by the exact degeneracy limit can fit all the present atmospheric and solar neutrino data in agreement with the experimental bound imposed by neutrinoless double beta decay. Our two angle parametrization has the interesting property of reproducing, for specific choices of the angles, several of the mixing schemes proposed in the literature such as bimaximal mixing 5, democratic mixing 6 as well as the scheme suggested by Georgi and Glashow 7.

2 The limit of exact degeneracy

The experimental constraints on squared neutrino mass differences coming from solar and atmospheric experiments together with the assumption that neutrino masses might be of the order of $1eV$ lead to highly degenerate masses 8.

The terms of the Lagrangean relevant for our discussion are

$$\mathcal{L}_{\text{mass}} = -(\nu_{L_\alpha})^T C^{-1} m_{\alpha\beta} \nu_{L_\beta} + \text{h.c.} \tag{1}$$

[a] e-mail: d2003@beta.ist.utl.pt

[b] On sabbatical leave, visiting SLAC - Stanford Linear Accelerator Center, partially supported by Department of Energy, contract DE-AC03-76SF00515, FLAD - Fundação Luso Americana para o Desenvolvimento and GTAE - Grupo Teórico de Altas Energias. e-mail: rebelo@slac.stanford.edu, rebelo@beta.ist.utl.pt

[c] e-mail: juca@gtae2.ist.utl.pt

and

$$\mathcal{L}_{\rm W} = \frac{g}{2} \left(\bar{e}, \quad \bar{\mu}, \quad \bar{\tau} \right)_L \gamma_\mu U \begin{pmatrix} \nu_1 \\ \nu_2 \\ \nu_3 \end{pmatrix}_L W^\mu + \text{ h.c.} \tag{2}$$

$\mathcal{L}_{\rm mass}$ is a generic Majorana mass term for the three lefthanded neutrinos where $m = (m_{\alpha\beta})$ is a 3×3 complex symmetric mass matrix, and ν_{L_α} denote weak eigenstates. In principle the matrix m could be an effective Majorana mass matrix within a framework with three left-handed and three right-handed neutrinos. We shall work in the weak-basis (WB) where the charged lepton mass matrix is diagonal, real and positive. The neutrino mass matrix can be diagonalized by the transformation

$$U^T \cdot m \cdot U = \text{diag}(m_{\nu_1}, \; m_{\nu_2}, \; m_{\nu_3}) \tag{3}$$

so that the weak eigenstates ν_{L_α}, are related to the mass eigenstates, ν_{L_i}, by $\nu_{L_\alpha} = U_{\alpha i} \; \nu_{L_i}$ and the fields in the charged current given by Eq.(2) are already physical fields.

In general the neutrino diagonalization matrix U considered above can be parametrized by three angles and three phases that are CP violating. It is well known that in the case of Dirac neutrinos only three angles and one phase are required to parametrize U and that in the limit of exact degeneracy U can be rotated away into the unit matrix through a redefinition of the neutrino fields. In this respect Majorana neutrinos are fundamentally different and only if the theory is CP invariant and the three degenerate neutrinos have the same CP parity, can the matrix U be rotated away.

In the limit of exact degeneracy with μ the common neutrino mass we shall denote the mixing matrix by U_o and define a dimensionless mass matrix by Z_o given by $Z_o = m/\mu$. From Eq(3) we obtain

$$Z_o = U_o^\star U_o^\dagger \tag{4}$$

so that Z_o is a unitary symmetric matrix and can be written without loss of generality as

$$Z_o = K^* \begin{pmatrix} c_\theta & s_\theta c_\phi & s_\theta s_\phi \\ s_\theta c_\phi & w_1 & w_2 \\ s_\theta s_\phi & w_2 & w_3 \end{pmatrix} K^* \tag{5}$$

where c and s stand for cosine and sine respectively, the w_i may be complex entries and K is a diagonal unitary matrix . After a WB transformation under which $Z_o \to K \cdot Z_o \cdot K$, Z_o transforms into

$$\begin{aligned} Z_o = & \begin{pmatrix} 1 & 0 & 0 \\ 0 & c_\phi & s_\phi \\ 0 & s_\phi & -c_\phi \end{pmatrix} \begin{pmatrix} c_\theta & s_\theta & 0 \\ s_\theta & z_{22} & z_{23} \\ 0 & z_{23} & z_{33} \end{pmatrix} \times \\ & \times \begin{pmatrix} 1 & 0 & 0 \\ 0 & c_\phi & s_\phi \\ 0 & s_\phi & -c_\phi \end{pmatrix}. \end{aligned} \tag{6}$$

Unitarity of Z_o, requires that either s_θ or z_{23} vanish. The case $s_\theta = 0$ leads to CP

invariance. Assuming $s_\theta \neq 0$ the most general form for Z_o is given by:

$$Z_o = \begin{pmatrix} 1 & 0 & 0 \\ 0 & c_\phi & s_\phi \\ 0 & s_\phi & -c_\phi \end{pmatrix} \begin{pmatrix} c_\theta & s_\theta & 0 \\ s_\theta & -c_\theta & 0 \\ 0 & 0 & e^{i\alpha} \end{pmatrix} \times \\ \times \begin{pmatrix} 1 & 0 & 0 \\ 0 & c_\phi & s_\phi \\ 0 & s_\phi & -c_\phi \end{pmatrix} . \tag{7}$$

In the cases $\alpha = 0, \pi$ there is, once again, CP conservation. It can be readily verified that this parametrization does not include the trivial case where CP is a good symmetry and all neutrinos have the same CP parity 9, corresponding to the eigenvalues $(1, 1, 1)$. In fact in the case of CP consevation Z_o is diagonalized by an orthogonal transformation leaving invariant both $\mathrm{Tr}(Z_o)$ and $\det(Z_o)$ and there is no choice of parameters in Eq.(7) leading to a trace and determinant corresponding to this particular case. On the other hand the set of eigenvalues $(1, -1, 1)$ and $(1, -1, -1)$ corresponding to one neutrino with opposite CP parity to the other two can be obtained for $\alpha = 0$ and $\alpha = \pi$, respectively. The diagonalization of the matrix Z_o through the transformation of Eq.(3), together with the requirement of positive diagonal elements requires a U_o matrix given by

$$U_o = \begin{pmatrix} 1 & 0 & 0 \\ 0 & c_\phi & s_\phi \\ 0 & s_\phi & -c_\phi \end{pmatrix} \begin{pmatrix} \cos(\frac{\theta}{2}) & \sin(\frac{\theta}{2}) & 0 \\ \sin(\frac{\theta}{2}) & -\cos(\frac{\theta}{2}) & 0 \\ 0 & 0 & e^{-i\alpha/2} \end{pmatrix} \times \\ \times \begin{pmatrix} 1 & 0 & 0 \\ 0 & i & 0 \\ 0 & 0 & 1 \end{pmatrix} . \tag{8}$$

U_o is not an orthogonal matrix even in the CP conserving limit, i.e., for $\alpha = 0, \pi$, as a result it cannot be rotated away through a redefinition of the neutrino fields.

From this discussion we see that in the case of three degenerate Majorana neutrinos the parametrization of U requires two angles and one phase and there may be CP violation 10.It can be shown that a necessary and sufficient condition for CP invariance, in the degenerate limit, is:

$$G \equiv \mathrm{Tr}[\,(m \cdot h \cdot m^\star)\,,\ h^\star]^3 \ = \ 0 \tag{9}$$

where $h = m_\ell \cdot m_\ell^\dagger$, and m_ℓ denotes the charged lepton mass matrix. G is a WB invariant and can be written as

$$\begin{aligned} G &= 6i\ \Delta_m\ \mathrm{Im}[(Z_o)_{11}(Z_o)_{22}(Z_o)^\star_{12}(Z_o)^\star_{21}] \\ &= \tfrac{3i}{2}\ \Delta_m\ \cos(\theta)\sin^2(\theta)\ \sin^2(2\phi)\ \sin(\alpha) \end{aligned} \tag{10}$$

where $\Delta_m = \mu^6\ (m_\tau^2 - m_\mu^2\ )^2(m_\tau^2 - m_e^2\ )^2(m_\mu^2 - m_e^2\ )^2$ is a multiplicative factor which contains the different masses of the charged leptons and the common neutrino mass μ. In Refs.10 11 various examples of CP-odd WB-invariants were constructed, but all of those invariants automatically vanish in the limit of exact degeneracy whilst the invariant of Eq.(9) only vanishes if CP is conserved. It was shown in Ref. 4 that the imposition of maximal CP violation leads to a structure of the Majorana neutrino mass of the type that one obtains in the framework of universal strength for Yukawa couplings 12.

3 Lifting the degeneracy. Phenomenological implications

In the limit of exact degeneracy, the leptonic mixing matrix U_o is param- etrized by two angles θ, ϕ and one phase α and is defined only up to an arbitrary orthogonal transformation $U_o \to U_o \cdot O$. The physically interesting case corresponds to quasidegenerate neutrinos. Let us assume that the degeneracy is lifted through a small perturbation:

$$Z = Z_o + \varepsilon\, Q \tag{11}$$

where ε is a small parameter and Q is a symmetric complex matrix of order one. It was shown in Ref. 4 that in the presence of a small perturbation around the degeneracy limit, the mixing matrix becomes, to leading order, $U_o \cdot O$, where O is no longer arbitrary, being the orthogonal matrix which diagonalizes the symmetric real matrix A, defined by $A = \mathrm{Re}(U_o^T \cdot Q \cdot U_o)$. As a result, for quasidegenerate neutrinos, to leading order, only one CP violating phase appears in the leptonic mixing, namely the phase α present in U_o and the question of whether the two angle parametrization given by Eq.(8) can accommodate the present experimental data on atmospheric and solar neutrinos, as well as the constraints on double beta decay immediately arises. Of course this corresponds to the case where the matrix $U_o^T \cdot Q \cdot U_o$ is already a real and diagonal matrix lifting the degeneracy as required experimentally.

The constraints arising from neutrinoless double beta decay put an upper bound on $< m >$, an average neutrino mass, given in standard notation by

$$< m > = \sum_i U_{ei}^2\, m_{\nu_i} \;=\; m_{ee}^{\star} \tag{12}$$

where the U_{ei} denote the elements of the first row of the mixing matrix U, and m_{ee} is the $(1,1)$ element of the mass matrix m. At present, the strongest bound is $| < m > | = |m_{ee}| < 0.2\ eV$ 13. In the limit of exact degeneracy, we have $m_{ee} = \mu\ \cos(\theta)$, where we have used the parametrization of Eq.(8). If we fix $\mu = 1\ eV$, then neutrino masses are equal to a precision sufficient to neglect their differences, and the experimental bound on m_{ee} immediately translates into a single bound on the parameter θ, namely $|\cos(\theta)| < 0.2$.

In our framework, without sterile neutrinos, the atmospheric neutrino data supports the existence of oscillations of atmospheric neutrinos to tau neutrinos with a large mixing angle satisfying the bound $\sin^2(2\theta_{\mathrm{atm}}) > 0.82$, and the neutrino mass square difference in the range $5 \times 10^{-4}\ eV^2 < \Delta m^2_{\mathrm{atm}} <$
$< 6 \times 10^{-3}\ eV^2$. This interpretation is further supported by recent data from the CHOOZ reactor netrino experiment 14 leading to the upper bound $| U_{e3} | \leq (0.22 - 0.14)$.

In the context of three left-handed neutrinos, the probability for a neutrino ν_α to oscillate to other neutrinos is

$$1 - P(\nu_\alpha \to \nu_\alpha) = 4 \sum_{i<j} U_{\alpha i} U_{\alpha i}^{\star} U_{\alpha j}^{\star} U_{\alpha j} \sin^2 \left[\frac{\Delta m_{ji}^2 L}{4E} \right] \tag{13}$$

where $\Delta m_{ji}^2 = |m_j^2 - m_i^2|$, E is the neutrino energy and L denotes the distance travelled by the neutrino between the source and the detector. Since in the range L/E that is relevant for atmospheric neutrinos the term in $\sin^2[(\Delta m_{21}^2/4)(L/E)]$ can be

disregarded, we may identify $\sin^2(2\theta_{\rm atm})$ with $4(U_{21}U_{21}^\star \cdot U_{23}^\star U_{23} + U_{22}U_{22}^\star U_{23}^\star U_{23})$. In the framework of our two-angle parametrization of Eq.(8), the above combination of matrix elements has a simple form and one obtains $\sin^2(2\theta_{\rm atm}) = \sin^2(2\phi)$, i.e., $\theta_{\rm atm}$ can be identified with the angle ϕ and thus the atmospheric neutrino data leads to the constraint $\sin^2(2\phi) > 0.82$.

The discrepancy between the observed and the calculated 15 solar neutrino fluxes also requires neutrino oscillations, although at this stage various schemes are still possible, namely within the framework of the MSW mechanism 16 there is a small angle solution $\sin^2(2\theta_{\rm sol}) \approx 7 \times 10^{-3}$ with $\Delta m^2_{\rm sol} \approx 6 \times 10^{-6}\ eV^2$, and a large angle solution $\sin^2(2\theta_{\rm sol}) \sim 0.65 - 0.97$ with $\Delta m^2_{\rm sol} \sim (2-20) \times 10^{-5}\ eV^2$. Another solution could be vacuum oscillations with $\sin^2(2\theta_{\rm sol}) \approx 0.9$ and $\Delta m^2_{\rm sol} \approx 10^{-10}\ eV^2$. Since in our two-angle parametrization one has $U_{13} = 0$ we obtain $\sin^2(2\theta_{\rm sol}) = 4U_{11}U_{11}^\star U_{12}^\star U_{12}$ leading to $\sin^2(2\theta_{\rm sol}) = \sin^2(\theta)$, i.e., in our parametrization $2\theta_{\rm sol} = \theta$.

We see that each of the experiments considered above independently constrains a single parameter. Also, it is clear from Eq.(12), that with small solar neutrino mixing the bound from double beta decay would not be satisfied for quasidegenerate neutrinos with masses of the order of 1 eV.

Finally we show that some of the neutrino mixing schemes proposed in the literature correspond to specific cases of the two-angle parametrization suggested by Eq.(8).

(a) *Bimaximal Mixing* 5: In this scheme the lines of the neutrino mixing matrix have the following structure:

$$L_1 = \left(\tfrac{1}{\sqrt{2}}, \tfrac{-1}{\sqrt{2}}, 0\right); L_2 = \left(\tfrac{1}{2}, \tfrac{1}{2}, \tfrac{1}{\sqrt{2}}\right); L_3 = \left(\tfrac{-1}{2}, \tfrac{-1}{2}, \tfrac{1}{\sqrt{2}}\right). \tag{14}$$

This pattern of neutrino mixing is obtained within the two-angle parametrization for the following values of θ, ϕ and α:

$$\alpha = 0; \cos\frac{\theta}{2} = -\sin\frac{\theta}{2} = -\cos\phi = \sin\phi = \frac{1}{\sqrt{2}} \tag{15}$$

(b) *Democratic Mixing* 6: In this case the neutrino mixing matrix has, to a very good approximation, the following form:

$$L_1 = \left(\tfrac{1}{\sqrt{2}}, \tfrac{-1}{\sqrt{2}}, 0\right); L_2 = \left(\tfrac{1}{\sqrt{6}}, \tfrac{1}{\sqrt{6}}, \tfrac{-2}{\sqrt{6}}\right); L_3 = \left(\tfrac{1}{\sqrt{3}}, \tfrac{1}{\sqrt{3}}, \tfrac{1}{\sqrt{3}}\right). \tag{16}$$

Within the two-angle parametrization, one obtains the democratic mixing for the following values of the parameters:

$$\begin{gathered} \alpha = 0; \cos(\theta/2) = -\sin(\theta/2) = \tfrac{1}{\sqrt{2}}; \\ \cos(\phi) = \tfrac{1}{\sqrt{2}}\ \sin(\phi) = \tfrac{-1}{\sqrt{3}} \end{gathered} \tag{17}$$

In the above analysis, we have not paid attention to the factors "i" appearing in our two-angle parametrization of Eq.(8). As we have previously emphasized, these factors of "i" have to do with the fact that in the construction of the two-angle parametrization, we have implicitly assumed that in the limit of CP invariance (i.e. $\sin(\alpha) \to 0$), one of the Majorana neutrinos has relative CP parity opposite to the other two. The factors of "i" do not play any rôle in the analysis of atmospheric and solar neutrino data, but are crucial in the analysis of double beta decay.

(c) *Georgi-Glashow mass matrix* 7: Using an analysis of the present neutrino data Georgi and Glashow have suggested the following approximate form for the Majorana neutrino mass matrix

$$(m)_{1i} = \mu\left(0, \frac{1}{\sqrt{2}}, \frac{1}{\sqrt{2}}\right); (m)_{2i} = \mu\left(\frac{1}{\sqrt{2}}, \frac{1}{2}, \frac{-1}{2}\right); \\ (m)_{3i} = \mu\left(\frac{1}{\sqrt{2}}, \frac{-1}{2}, \frac{1}{2}\right). \tag{18}$$

From Eq.(7) it follows that this neutrino mass matrix is obtained, within the two-angle parametrization for the following values of its parameters,

$$\alpha = 0; \quad \sin(\theta) = 1; \quad \cos(\phi) = \sin(\phi) = \frac{1}{\sqrt{2}} \tag{19}$$

Acknowledgments

M. N. R is grateful to the Organizers of the the 9th Lomonosov Conference on Elementary Particle Physics for the warm hospitality. M. N. R. received financial support from FCT - Fundação de Ciência e Tecnologia through GTAE - Grupo Teórico de Altas Energias and CFIF - Centro de Física das Interacções Fundamentais, to participate at the Conference.

References

[1] Y. Suzuki, Talk given at the XIX Intern. Symp. on Lepton and Photon Interactions at High Energies, Stanford University, USA, August 9-14, 1999.

[2] A. Mann, Talk given at the XIX Intern. Symp. on Lepton and Photon Interactions at High Energies, Stanford University, USA, August 9-14, 1999.

[3] LSND Collaboration, C. Athanassopoulos et. al., *Phys. Rev. Lett.* **8**, 1774 (1998); *Phys. Rev.* **C58**, 2489 (1998).

[4] G. C. Branco, M. N. Rebelo and J. I. Silva-Marcos, *Phys. Rev. Lett.* **82**, 683 (1999).

[5] F. Vissani, hep-ph/9708483; B. Barger, S. Pakvasa, T. Weiler and K. Whisnant, *Phys. Lett.* **B437**, 107 (1998); A. Baltz, A. S. Goldhaber and M. Goldhaber, *Phys. Rev. Lett.* **81**, 5730 (1998); M. Jezabek and A. Sumino, *Phys. Lett.* **B440**, 327 (1998)

[6] H. Fritzsch and Z. Z. Xing, *Phys. Lett.* **B372**, 265 (1996); M. Fukugita, M. Tanimoto and T. Yanagida, *Phys. Rev.* **D 57**, 4429 (1998); Y. Koide, *Phys. Rev.* **D 39**, 1391 (1989).

[7] H. Georgi and S. L. Glashow, hep-ph/9808293.

[8] D.O. Caldwell and R.N. Mohapatra, *Phys. Rev.* **D 48**, 3259 (1993); A.S. Joshipura, *Z. Phys.* **C 64**, 31 (1994); S.T. Petcov and A.Yu. Smirnov, *Phys. Lett.* **B322**, 109 (1994); P. Bamert and C. P. Burgess *Phys. Lett.* **B329**, 289 (1994).

[9] L. Wolfenstein, *Phys. Lett.* **B107**, 77 (1981).

[10] G.C. Branco, L. Lavoura and M.N. Rebelo, *Phys. Lett.* **B180**, 264 (1986).

[11] F. del Aguila, J. A. Aguilar-Saavedra, and M. Zralek, *Comput. Phys. Commun.* **100**, 231 (1997).

[12] G.C. Branco, M.N. Rebelo and J.I. Silva-Marcos, *Phys. Lett.* **B428**, 136 (1998).
[13] L. Baudis et al., *Phys. Rev. Lett.* **83**, 41 (1999).
[14] CHOOZ Collaboration, M. Apollonio et al., *Phys. Lett.* **B446**, 415 (1999).
[15] J. N. Bahcall and M.H. Pinsonneault, *Rev. Mod. Phys.* **64**, 885 (1992); J. N. Bahcall, S. Basu and M.H. Pinsonneault, *Phys. Lett.* **B433**, 1 (1998).
[16] L. Wolfenstein, *Phys. Rev.* **D 17**,2369 (1978); *ibid* **D 20**,2634(1979);S.P.Mikheyev,A.Yu.Smirnov, *Sov. J.Nucl.Phys.***42**,913(1985);*ibid NuovoCim.***C9**,17(1986).

Solar neutrino oscillations in Extensions of the Standard Model

O.M.Boyarkin
Department of Physics, Minsk State Pedagogical University,
Soviet Street 18 , Minsk, 220050, Belarus

Abstract. The solar neutrino problem is considered within the left right model and the two Higgs doublet model. It is shown that the physical Higgs bosons could significantly influence on the value of the solar matter potential.

In this work we are going to investigate the problem of the solar neutrinos within two extensions of the SM having the massive neutrino. First we consider the asymmetric LRM ($g_L \neq g_R$) [1,2] with the bi-doublet and two triplets. The spectrum of the physical Higgs bosons consists of: 4 doubly charged scalars $\Delta_{1,2}^{(\pm\pm)}$, 4 singly charged scalars $h^{(\pm)}$ and $\tilde{\delta}^{(\pm)}$, 4 neutral scalars $S_{1,2,3,4}$ and 2 neutral pseudoscalars $P_{1,2}$. We shall use the Higgs potential proposed by the authours of Ref. [3] and take the Yukawa Lagrangian in the form

$$\mathcal{L}_Y = -\sum_{a,b}\{h_{ab}\overline{\Psi}_{aL}\Phi\Psi_{bR} + h'_{ab}\overline{\Psi}_{aL}\tilde{\Phi}\Psi_{bR} + if_{ab}[\Psi_{aL}^T C\tau_2(\vec{\tau}\cdot\vec{\Delta}_L)\Psi_{bL}+$$

$$+(L\to R)] + conj.\}, \tag{1}$$

where Ψ_{aL} (Ψ_{aR}) describes the left-handed (right-handed) lepton doublet, $\tau_{1,2,3}$ are the Pauli matrices, C is the charge conjugation matrix, $\tilde{\Phi} = \tau_2\Phi^*\tau_2$, a and b label different generations, h_{ab}, h'_{ab} and $f_{ab} = f_{ba}$ are the bidoublet and the triplet Yukawa coupling constants (YCC's) determining the interactions between leptons and the Higgs bosons. With the help of Eq.(1) we obtain the Lagrangian describing the interaction between leptons and the singly charged Higgs bosons

$$\mathcal{L}_l = \sum_{a,b}\{[\frac{h'_{ab}k_2 - h_{ab}k_1}{2k_+}\overline{\nu}_a(1-\gamma_5)l_b - \frac{h_{ab}k_2 - h'_{ab}k_1}{2k_+}\overline{N}_a(1+$$

$$+\gamma_5)l_b]h^{(+)} + \frac{f_{ab}}{\sqrt{2}}[\overline{l^c}_a(1+\gamma_5)\nu_b\left(\frac{\beta k_0^2}{(\alpha+\rho_1-\rho_3/2)v_R^2}h^{(+)} - \tilde{\delta}^{(+)}\right) +$$

$$+\overline{l^c_a}(1-\gamma_5)N_b\left(\frac{k_0}{v_R}h^{(+)} + \frac{\beta k_0}{(\alpha+\rho_1-\rho_3/2)v_R}\tilde{\delta}^{(+)}\right)] + conj.\}, \tag{2}$$

where k_1, k_2, v_L and v_R are the vacuum expectation values of the neutral components of the bidoublet, the left handed and the right handed triplets, respectively,

$$k_\pm = \sqrt{k_1^2 \pm k_2^2}, \qquad k_0 = \frac{k_-^2}{\sqrt{2}k_+}, \qquad \alpha = \frac{\alpha_3 k_+^2}{2k_-^2},$$

α_i, ρ_i and β_i are the constants entering the Higgs potential.

Further on we shall consider the case when the neutrino transition magnetic dipole moments are very small. Since the interaction with the solar magnetic field is absent, the evolution equation for the neutrino flux consisting of the left-handed and the right-handed light neutrinos is decoupled on the two independent systems which of them

describes the neutrinos with the same helicity. The subject of our investigation will be the neutrino flux including the ν_{eL}, $\nu_{\mu L}$ and $\nu_{\tau L}$. In vacuum the weak eigenstates the evolution in time is given in ultrarelativistic limit $E \gg max(m_1, m_2, m_3)$ through the Schrodinger-like equation

$$i\frac{d}{dz}\begin{pmatrix}\nu_e\\ \nu_\mu\\ \nu_\tau\end{pmatrix} = \mathcal{H}^v \begin{pmatrix}\nu_e\\ \nu_\mu\\ \nu_\tau\end{pmatrix}. \tag{3}$$

where

$$\mathcal{H}^v_{11} = \frac{1}{6E}(3s^2_{13} - 1)\Delta m^2_{32} + (1 - 3c^2_{12}c^2_{13})\Delta m^2_{21},$$

$$\mathcal{H}^v_{22} = \frac{1}{6E}[(3c_{13}s^2_{23} - 1)\Delta m^2_{32} + (1 - 3b^2_1)\Delta m^2_{21}],$$

$$\mathcal{H}^v_{12} = \frac{c_{13}}{2E}(s_{13}s_{23}\Delta m^2_{32} + c_{12}b_1\Delta m^2_{21}),$$

$$\mathcal{H}^v_{23} = \frac{1}{2E}(c^2_{13}c_{23}s_{23}\Delta m^2_{32} + b_1 b'_1\Delta m^2_{21}),$$

$$b_1 = c_{23}s_{12} + c_{12}s_{23}s_{13}, \qquad b'_1 = b_1(\varphi_{12} \to \varphi_{12} - \frac{\pi}{2}),$$

$$\Delta m^2_{ik} = m^2_i - m^2_k,$$

$$\mathcal{H}^v_{33} = \mathcal{H}^v_{22}(\varphi_{12} \to \varphi_{12} - \frac{\pi}{2}), \qquad \mathcal{H}^v_{13} = \mathcal{H}^v_{12}(\varphi_{12} \to \varphi_{12} + \frac{\pi}{2}),$$

$c_{ik} = \cos\varphi_{ik}$ and $s_{ik} = \sin\varphi_{ik}$.

Owing to the charged current contributions to the $\nu_{l_aL}e^-$ forward scattering, a matter modifies both the diagonal and the nondiagonal elements of the Hamiltonian $\mathcal{H}^v$. In the LRM apart from the diagrams with the W- and the Z-exchanges there are the additional diagrams with the virtual singly charged Higgs bosons (see, Fig.1). They give the following contributions to the solar matter potential (SMP)

$$V^H_{ee} = \left(\frac{\alpha^2_{ee}}{4m^2_h} - \frac{f^2_{ee}}{2m^2_{\tilde{\delta}}}\right)n_e, \qquad V^H_{ab} = \left(\frac{\alpha_{ea}\alpha_{eb}}{4m^2_h} - \frac{f_{ea}f_{eb}}{2m^2_{\tilde{\delta}}}\right)n_e,$$

where

$$\alpha_{ab} = \frac{h'_{ab}k_2 - h_{ab}k_1}{k_+},$$

$a, b = e, \mu, \tau$ and n_e (n_n) is the electron (neutron) density. Adding these contributions to those coming from the diagrams with the W- and Z-exchanges we obtain for the SMP the expression

$$V_{ee} = \frac{g^2_L}{4m^2_W}(\frac{1}{2}n_n - n_e) + V^H_{ee}, \qquad V_{aa} = \frac{g^2_L}{8m^2_W}n_n + V^H_{aa}, \qquad V_{ab} = V^H_{ab}.$$

Then the evolution equation for the flavor neutrino functions is given by

$$i\frac{d}{dz}\Psi = \mathcal{H}^m\Psi, \tag{4}$$

where

$$\mathcal{H}^m_{12} = \mathcal{H}^v_{12} + V_{e\mu}, \qquad \mathcal{H}^m_{13} = \mathcal{H}^v_{13} + V_{e\tau}, \qquad \mathcal{H}^m_{23} = \mathcal{H}^v_{23} + V_{\mu\tau},$$

$$\mathcal{H}^m_{11} = \mathcal{H}^v_{11} - \left(\frac{g_L^2}{4m_W^2} - \frac{\alpha_{ee}^2}{4m_h^2} + \frac{f_{ee}^2}{2m_{\tilde{\delta}}^2}\right) n_e, \qquad \mathcal{H}^m_{22} = \mathcal{H}^v_{22} + \left(\frac{\alpha_{\mu e}^2}{4m_h^2} - \right.$$
$$\left. - \frac{f_{\mu e}^2}{2m_{\tilde{\delta}}^2}\right) n_e, \qquad \mathcal{H}^m_{33} = \mathcal{H}^v_{33} + \left(\frac{\alpha_{\tau e}^2}{4m_h^2} - \frac{f_{\tau e}^2}{2m_{\tilde{\delta}}^2}\right) n_e.$$

There are altogether three resonance transitions which occur between neutrinos having the same helicity but different flavor, and thus correspond the MSW resonances. The resonance densities can be approximately found by equating pairs of diagonal elements of $\mathcal{H}^m$.

$$\frac{1}{2E}[(s_{13}^2 - c_{13}^2 s_{23}^2)\Delta_{32} + (\beta^2 - c_{12}^2 c_{13}^2)\Delta_{21}] = \left(\frac{g_L^2}{4m_W^2} - \frac{\alpha_{ee}^2 - \alpha_{\mu e}^2}{4m_h^2} + \right.$$
$$\left. + \frac{f_{ee}^2 - f_{\mu e}^2}{2m_{\tilde{\delta}}^2}\right) n_e, \tag{5}$$

$$\frac{1}{2E}[(s_{13}^2 - c_{13}^2 c_{23}^2)\Delta_{32} + (b_1'^2 - c_{12}^2 c_{13}^2)\Delta_{21}] = \left(\frac{g_L^2}{4m_W^2} - \frac{\alpha_{ee}^2 - \alpha_{\tau e}^2}{4m_h^2} + \right.$$
$$\left. \frac{f_{ee}^2 - f_{\tau e}^2}{2m_{\tilde{\delta}}^2}\right) n_e, \tag{6}$$

$$\frac{1}{2E}[c_{13}^2(s_{23}^2 - c_{23}^2)\Delta_{32} + (b_1'^2 - b_1^2)\Delta_{21}] = \left(\frac{\alpha_{\tau e}^2 - \alpha_{\mu e}^2}{4m_h^2} - \right.$$
$$\left. - \frac{f_{\tau e}^2 - f_{\mu e}^2}{2m_{\tilde{\delta}}^2}\right) n_e. \tag{7}$$

Equations (5)-(7) represent the resonant conditions for the channels $\nu_{eL} \leftrightarrow \nu_{\mu L}$, $\nu_{eL} \leftrightarrow \nu_{\tau L}$ and $\nu_{\mu L} \leftrightarrow \nu_{\tau L}$, respectively.

Now we discuss the solar neutrino problem within the model based on the $SU(2)_L \times U(1)_Y$ gauge group involving the two Higgs doublets (THDM)[4]

$$\Phi_j(\frac{1}{2}, 1) = \begin{pmatrix} \Phi_j^+ \\ \Phi_j^0 \end{pmatrix}, \qquad (j = 1, 2)$$

In general, such model will generate the fermion flavor violation at the tree level. To protect the model from such terms, the ad hoc discrete symmetry on the THDM scalar potential and the Yukawa interaction is proposed and there appears two different versions of the THDM depending on whether up-type and down-type fermions couple to the same or different scalar doublets. The model wherein the mentioned discrete symmetry is absent and, as a result, the flavor changing neutral current appears at the tree level is called as the general two Higgs doublet model (GTHDM). In this model we shall use for the Yukawa Lagrangian and the Higgs potential the expressions proposed in Ref. [5]. In the sector of the physical Higgs bosons we have: 2 neutral CP-even scalar particles H^0 and h^0, a neutral CP-odd scalar particle A^0, and 2 singly-charged scalars $H^\pm$. The Lagrangians describing the interaction between the Higgs bosons and leptons have the form

$$\mathcal{L}_c = -\sqrt{2}v^{-1}\tan\beta \sum_a m_a \overline{\nu}_{aL} l_{aR} H^+ + \sum_{a,b} \kappa_{ab} \overline{\nu}_{aL} l_{bR} H^+$$

$$+conj., \tag{8}$$

$$\mathcal{L}_n = \frac{1}{\sqrt{2}} \sum_{a,b} \{\bar{l}_{aL} l_{bR} [(h^d_{ab} c_\alpha + h'^d_{ab} s_\alpha) H^0 + (h'^d_{ab} c_\alpha - h^d_{ab} s_\alpha) h^0 + i(h'^d_{ab} c_\beta -$$

$$-h^d_{ab} s_\beta) A^0] + (l \to \nu, d \to u) + conj.\}, \tag{9}$$

where

$$\tan 2\alpha = \frac{v_1 v_2 (\lambda_3 + \lambda_5)}{\lambda_2 v_2^2 - \lambda_1 v_1^2}, \qquad \tan\beta = \frac{v_2}{v_1},$$

$$\kappa_{ab} = h'^d_{ab} c_\beta^{-1} + h^u_{ab} s_\beta - h'^u_{ab} c_\beta,$$

and λ_k are the parameters of the potential V. In the GTHDM the SMP is defined by the expressions

$$V'_{ee} = [-\frac{g_L^2}{4m_W^2} + \frac{(-\sqrt{2} v^{-1} \tan\beta m_e + \kappa_{ee})^2}{4m_H^2} + \mathcal{V}_{ee}] n_e,$$

$$V'_{ab} = \left(\mathcal{V}_{ab} + \frac{\kappa_{ab}^2}{4m_H^2}\right) n_e, \qquad a, b \neq e^-,$$

where

$$\mathcal{V}_{ab} = \sum_{S_i} \frac{(h^d_{ee} c_\alpha + h'^d_{ee} s_\alpha)(h^u_{ab} c_\alpha + h'^u_{ab} s_\alpha)}{8m^2_{S_i}}, \qquad S_i = H^0, h^0, A^0.$$

For describing the neutrino flux consisting of ν_{eL}, $\nu_{\mu L}$ and $\nu_{\tau L}$ we can use the expressions obtained for the LRM having made in them the substitution $V_{ab} \to V'_{ab}$.

Now the basic question is: how large could be the corrections to the SMP connected with the Higgs bosons? To answer on it we must call attention to the low energy experiments of the elastic scattering off neutrinos on electrons. For the ultimate determination of $V - A$ form in these processes it is necessary to detect the final charged lepton and the neutrino. Since at present it is impossible experimentally, one could not say here about the eventual establishing the $V - A$ structure. Situation is the same as in the case of direct (or inverse) leptonic decays

$$\mu^- \to e^- \bar{\nu}_e \nu_\mu, \qquad \tau^- \to e^- \bar{\nu}_e \nu_\tau.$$

All results of such decays at low energies may be parametrized in terms of amplitudes $g^\gamma_{\lambda\lambda'}$ and the Fermi coupling constant G_F, using the matrix elements [6]

$$\frac{4G_F}{\sqrt{2}} \sum g^\gamma_{\lambda\lambda'} < \bar{e}_\lambda \mid \Gamma_\gamma \mid \nu_{en} >< \bar{\nu}_{Xm} \mid \Gamma_\gamma \mid X_{\lambda'} >, \tag{10}$$

where the type of interaction - $\Gamma^S = 1$ for scalar, $\Gamma^V = \gamma_\mu$ for vector, $\gamma^T = \frac{1}{\sqrt{2}}\sigma_{\mu\nu}$ for tensor is labelled by γ and the chiral projections of the leptons - left, right - by λ, λ'. The helicities n and m of the ν_e and ν_μ are then determined by the values of γ, λ and λ'. The ten complex amplitudes $g^\gamma_{\lambda\lambda'}$ and G_F constitute 19 independent (real) parameters to be determined by experiment. The SM interactions corresponds to one single amplitude g^V_{LL} being unity and all the others being zero. In the LRM we have

three nonvanishing amplitudes, namely g^V_{LL}, g^S_{LL}, and g^S_{RR}. For the muon decay at the 90% CL the current experimental limits on these are [6]

$$| g^V_{LL} |> 0.96, \qquad | g^S_{LL} |< 0.55, \qquad | g^S_{RR} |< 0.066.$$

The experimental bounds for non-standard couplings in tau decay are less restrictive. At 90% CL the constraints on the couplings relevant to the case are [7]

$$| g^V_{LL} |> 1., \qquad | g^S_{LL} |< 1., \qquad | g^S_{RR} |< 0.27.$$

In the GTHDM the process of the inverse muon (tau) decay is described the five nonvanishing amplitudes g^V_{LL}, g^S_{RR}, g^S_{LL}, g^S_{LR}, and g^S_{RL}. As we see it is appeared the two new amplitudes compared with the LRM. The current bounds for them are

$$| g^S_{LR} |< 0.125, \qquad | g^S_{RL} |< 0.424,$$

for the muon case, and

$$| g^S_{LR} |< 0.36, \qquad | g^S_{RL} |< 1.,$$

for the tau case.

In conclusion, it has been shown that in the extensions of the SM the interaction between neutrinos and physical Higgs bosons could significantly change the value of the SMP compared with the SM prediction. For example, in the LRM when $f_{ee} \simeq f_{\mu\mu} \gg f_{e\mu}$, this change may reach 55%. Therefore, in these extensions of the SM the existing bounds on the neutrino oscillation parameters should be revised.

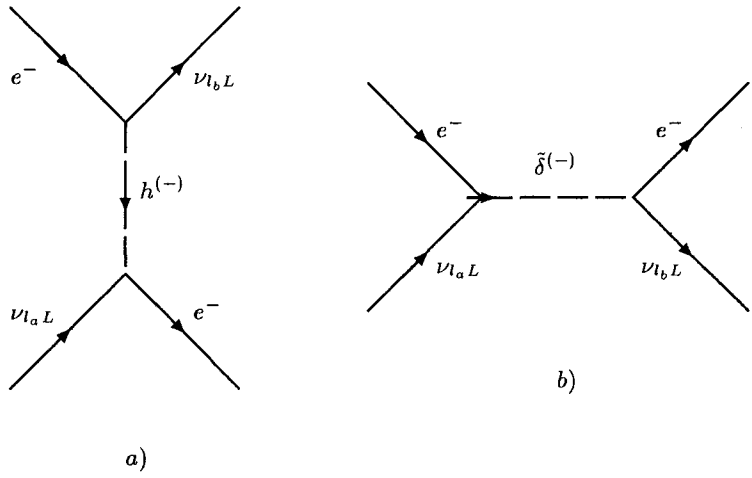

Fig. 1

References

[1] J.C.Pati and A.Salam, *Phys. Rev.* **D**10, 275 (1974); R.N.Mohapatra and J.C.Pati, *Phys. Rev.*,**D**11, 566, 2558 (1975); G.Senjanovich and R.N.Mohapatra, *Phys. Rev.*,**D**12, 1502 (1975).

[2] O.M.Boyarkin, *Acta Phys. Polonica* **B**23, 1031 (1992); O.M.Boyarkin, *Phys. Rev.* **D**50, 2247 (1994).

[3] N.G.Deshpande et al., *Phys. Rev.* **D**44, 837 (1991).

[4] M.Sher, *Physics Reports*, 179, 273 (1989).

[5] G.C. Branco et al., *Nucl. Phys.* **B**259, 306 (1985).

[6] W.Fetscher, H.-J.Gerber and K.F.Johnson, *Phys. Lett.* **B**173, 102 (1986).

[7] W.Lohmann and J.Raab, DESY 95 - 188, Oktober 1995.

Covariant Treatment of Neutrino Spin (Flavour) Conversion in Matter under the Influence of Electromagnetic Fields

M.S.Dvornikov, A.M. Egorov, A.E. Lobanov, A.I. Studenikin[a]
Department of Theoretical Physics, Moscow State University, 119899 Moscow, Russia

Abstract. Within the recently proposed [1, 2] Lorentz invariant formalism for description of neutrino spin evolution in presence of an arbitrary electromagnetic fields effects of matter motion and polarization are considered.

In [1, 2] the Lorentz invariant formalism for neutrino motion in nonmoving and isotropic matter under the influence of an arbitrary configuration of electromagnetic fields have been developed. We have derived the neutrino spin evolution Hamiltonian that accounts not only for the transversal to the neutrino momentum components of electromagnetic field but also for the longitudinal components. With the using of the proposed Hamiltonian it is possible to consider neutrino spin precession in an arbitrary configuration of electromagnetic fields including those that contain strong longitudinal components. We have also considered the new types of resonances in the neutrino spin precession $\nu_L \leftrightarrow \nu_R$ that could appear when neutrinos propagate in matter under the influence of different electromagnetic field configurations.

In the studies [1, 2] of the neutrino spin evolution we have focused mainly on description of influence of different electromagnetic fields, while modeling the matter we confined ourselves to the most simple case of nonmoving and unpolarized matter. Now we should like go to further and to generalize our approach for the case of moving and polarized homogeneous matter.

To derive the equation for the neutrino spin evolution in electromagnetic field $F_{\mu\nu}$ in such a matter we again start from the Bargmann-Michel-Telegdi (BMT) equation [3] for the spin vector S^μ of a neutral particle that has the following form

$$\frac{dS^\mu}{d\tau} = 2\mu\big\{F^{\mu\nu}S_\nu - u^\mu(u_\nu F^{\nu\lambda}S_\lambda)\big\} + 2\epsilon\big\{\tilde{F}^{\mu\nu}S_\nu - u^\mu(u_\nu \tilde{F}^{\nu\lambda}S_\lambda)\big\}, \qquad (1)$$

This form of the BMT equation corresponds to the case of the particle moving with constant speed, $\vec{\beta} = const$, $(u_\mu = (\gamma, \gamma\vec{\beta}), \gamma = (1-\beta^2)^{-1/2})$, in presence of an electromagnetic field $F_{\mu\nu}$. Here μ is the fermion magnetic moment and $\tilde{F}_{\mu\nu}$ is the dual electromagnetic field tensor. The neutrino spin vector also satisfies the usual conditions, $S^2 = -1$ and $S^\mu u_\mu = 0$. Equation (1) covers also the case of a neutral fermion having static non-vanishing electric dipole moment, ϵ. Note that the term proportional to ϵ violates T invariance.

The BMT spin evolution equation (1) is derived in the frame of electrodynamics, the model which is P invariant. Our aim is to generalize this equation for the case when effects of various neutrino interactions (for example, weak interaction for which P invariance is broken) with moving and polarized matter are also taken into account. Effects of possible P nonconservation and non-trivial properties of matter (i.e., its motion and polarization) have to be reflected in the equation that describes the neutrino spin evolution in an electromagnetic field.

[a]E-mail: studenik@srdlan.npi.msu.su

The Lorentz invariant generalization of eq.(1) for our case can be obtained by the substitution of the electromagnetic field tensor $F_{\mu\nu} = (\vec{E}, \vec{B})$ in the following way:

$$F_{\mu\nu} \to F_{\mu\nu} + G_{\mu\nu}. \tag{2}$$

In evaluation of the tensor $G_{\mu\nu}$ we demand that the neutrino evolution equation has to be linear over the neutrino spin vector S_μ, electromagnetic field $F_{\mu\nu}$, and such characteristics of matter (which is composed of different fermions, $f = e,\ n,\ p...$) as fermions currents

$$j_f^\mu = (n_f, n_f \vec{v}_f), \tag{3}$$

and fermions polarizations

$$\lambda_f^\mu = \Big(n_f(\vec{\zeta}_f \vec{v}_f), n_f \vec{\zeta}_f \sqrt{1 - v_f^2} + \frac{n_f \vec{v}_f (\vec{\zeta}_f \vec{v}_f)}{1 + \sqrt{1 - v_f^2}}\Big). \tag{4}$$

Here n_f, $\vec{v}_f$, and $\vec{\zeta}_f$ $(0 \leq |\vec{\zeta}_f|^2 \leq 1)$ denote, respectively, the number density of the background fermions f, the speed of the reference frame in which the mean momentum of fermions f is zero, and the mean value of the polarization vectors of the background fermions f in the above mentioned reference frame. For each type of fermions f there are only three vectors, u_μ^f, j_μ^f, and λ_μ^f, using which the tensor $G_{\mu\nu}$ have to be constructed. If j_μ^f and λ_μ^f are slowly varying functions in space and time (this condition is similar to one imposed on the electromagnetic field tensor $F_{\mu\nu}$ in the derivation of the BMT equation) then one can construct only four tensors (for each of the fermions f) linear in respect to the characteristics of matter:

$$G_1^{\mu\nu} = \epsilon^{\mu\nu\rho\lambda} u_\lambda j_\rho, \quad G_2^{\mu\nu} = \epsilon^{\mu\nu\rho\lambda} u_\lambda \lambda_\rho, \tag{5}$$

$$G_3^{\mu\nu} = u^\mu j^\nu - j^\mu u^\nu, \quad G_4^{\mu\nu} = u^\mu \lambda^\nu - \lambda^\mu u^\nu. \tag{6}$$

Thus, in general case of neutrino interaction with different background fermions f we introduce for description of matter effects antisymmetric tensor

$$G^{\mu\nu} = \epsilon^{\mu\nu\rho\lambda} g_\rho^{(1)} u_\lambda - (g^{(2)\mu} u^\nu - u^\mu g^{(2)\nu}), \tag{7}$$

where

$$g^{(1)\mu} = \sum_f \rho_f^{(1)} j_f^\mu + \rho_f^{(2)} \lambda_f^\mu, \quad g^{(2)\mu} = \sum_f \xi_f^{(1)} j_f^\mu + \xi_f^{(2)} \lambda_f^\mu. \tag{8}$$

Summation is performed over fermions f of the background. The explicit expressions for the coefficients $\rho_f^{(1),(2)}$ and $\xi_f^{(1),(2)}$ could be found if the particular model of neutrino interaction is chosen. In the usual notations the antisymmetric tensor $G_{\mu\nu}$ can be written in the form,

$$G_{\mu\nu} = \big(-\vec{P},\ \vec{M}\big), \tag{9}$$

where

$$\vec{M} = \gamma\big\{(g_0^{(1)} \vec{\beta} - \vec{g}^{(1)}) - [\vec{\beta} \times \vec{g}^{(2)}]\big\}, \ \vec{P} = -\gamma\big\{(g_0^{(2)} \vec{\beta} - \vec{g}^{(2)}) + [\vec{\beta} \times \vec{g}^{(1)}]\big\}. \tag{10}$$

It worth to note that the substitution (2) implies that the magnetic $\vec{B}$ and electric $\vec{E}$ fields are shifted by the vectors $\vec{M}$ and $\vec{P}$, respectively:

$$\vec{B} \to \vec{B} + \vec{M}, \quad \vec{E} \to \vec{E} - \vec{P}. \tag{11}$$

In the case of nonmoving, $\vec{v}_f = 0$, and unpolarized, $\vec{\zeta}_f = 0$, matter we get, confirming our previous result [1,2],

$$G_{\mu\nu} = \Big(\gamma\vec{\beta}\sum_f \xi_f^{(1)} n_f, \gamma\vec{\beta}\sum_f \rho_f^{(1)} n_f\Big). \tag{12}$$

We finally arrive to the following equation for the evolution of the three-dimensional neutrino spin vector $\vec{S}$ accounting for the direct neutrino interaction with electromagnetic field $F_{\mu\nu}$ and matter (which is discribed by the tensor $G_{\mu\nu}$):

$$\frac{d\vec{S}}{dt} = \frac{2\mu}{\gamma}\Big[\vec{S}\times(\vec{B}_0 + \vec{M}_0)\Big] + \frac{2\epsilon}{\gamma}\Big[\vec{S}\times(\vec{E}_0 - \vec{P}_0)\Big]. \tag{13}$$

The derivative in the left-hand side of eq.(13) is taken with respect to time t in the laboratory frame, whereas the values $\vec{B}_0$ and $\vec{E}_0$ are the magnetic and electric fields in the neutrino rest frame given in terms of the transversal, $\vec{F}_\perp$, and longitudinal, $\vec{F}_\parallel$, in respect to the direction of the neutrino motion field $\vec{F} = \vec{B}, \vec{E}$ components in the laboratory frame,

$$\vec{B}_0 = \gamma\big(\vec{B}_\perp + \frac{1}{\gamma}\vec{B}_\parallel + \sqrt{1-\frac{1}{\gamma^2}}\big[\vec{E}_\perp\times\vec{n}\big]\big),$$

$$\vec{E}_0 = \gamma\big(\vec{E}_\perp + \frac{1}{\gamma}\vec{E}_\parallel - \sqrt{1-\frac{1}{\gamma^2}}\big[\vec{B}_\perp\times\vec{n}\big]\big), \vec{n} = \vec{\beta}/\beta. \tag{14}$$

The influence of matter on the neutrino spin evolution in eq.(13) is given by the vectors $\vec{M}_0$ and $\vec{P}_0$ which in the rest frame of neutrino can be expressed in terms of quantities determined in the laboratory frame

$$\vec{M}_0 = \gamma\vec{\beta}\Big(g_0^{(1)} - \frac{\vec{\beta}\vec{g}^{(1)}}{1+\gamma^{-1}}\Big) - \vec{g}^{(1)}, \tag{15}$$

$$\vec{P}_0 = -\gamma\vec{\beta}\Big(g_0^{(2)} - \frac{\vec{\beta}\vec{g}^{(2)}}{1+\gamma^{-1}}\Big) + \vec{g}^{(2)}. \tag{16}$$

Let us determine the coefficients $\rho_f^{(i)}$ and $\xi_f^{(i)}$ in eq.(8) for the particular case of the electron neutrino propagation in moving and polarized electron gas. We consider the standard model of interaction supplied with $SU(2)$-singlet right-handed neutrino ν_R. The neutrino effective interaction Lagrangian reads

$$L_{eff} = -f^\mu\Big(\bar{\nu}\gamma_\mu\frac{1+\gamma^5}{2}\nu\Big), \tag{17}$$

where

$$f^\mu = \frac{G_F}{\sqrt{2}}\Big((1+4\sin^2\theta_W)j_e^\mu - \lambda_e^\mu\Big). \tag{18}$$

In this case neutrino electric dipole moment vanishes, $\epsilon = 0$, so that the coefficients $\xi_e^{(i)} = 0$, and from the obvious relation, $f_\mu = 2\mu g_\mu^{(1)}$, it follows

$$\rho_e^{(1)} = \frac{G_F}{2\mu\sqrt{2}}(1+4\sin^2\theta_W),\ \rho_e^{(2)} = -\frac{G_F}{2\mu\sqrt{2}}. \tag{19}$$

If for the neutrino magnetic moment we take the vacuum one-loop contribution [4,5]

$$\mu_\nu = \frac{3}{8\sqrt{2}\pi^2} e G_F m_\nu,$$

then

$$\rho^{(1)} = \frac{4\pi^2}{3em_\nu}(1 + 4\sin^2\theta_W), \quad \rho^{(2)} = -\frac{4\pi^2}{3em_\nu}.$$

On the base of eqs.(8) and (15) it is possible to show that in the case of the relativistic flux of electrons, $v_e \sim 1$, and the parallel motion of neutrinos and electrons matter effect contribution to the neutrino spin evolution equation (13) is suppressed. The same phenomenon can exist for neutrino flavour oscillations in the relativistic flux of electrons.

Finally, we should like to note that solutions of the derived eq.(13) for the neutrino spin evolution in moving and polarized matter and, correspondingly, the neutrino oscillation probabilities and effective mixing angles θ_{eff} can be obtained for different configurations of electromagnetic fields in a way similar to that discribed in [1,2,7].

To conclude, we note that the equation analogues to (13) can be derived [6] in quantum theory by using the Heizenberg equation for the neutrino spin operator.

Acknowledgements

We should like to thank Anatoly Borisov and Pavel Eminov for discussions on the relativistic quantum statistics.

References

[1] A.Egorov, A.Lobanov, A.Studenikin, in: New Worlds in Astroparticle Physics, ed. by A.Mourao, M.Pimento, P.Sa, World Scientific, Singapore, p.153, 1999; hep-ph/9902447.

[2] A.Egorov, A.Lobanov, A.Studenikin, Phys.Lett.B491 (2000) 137, hep-ph/9910476.

[3] V.Bargmann, L.Michel, V.Telegdi, *Phys.Rev.Lett.* **2**, 435 (1959).

[4] B.Lee, R.Shrock, PR **16**, 1444 (1977).

[5] K.Fujikawa, R.Shrock, *Phys.Rev.Lett.* **45**, 963 (1980).

[6] M.Dvornikov, A.Lobanov, A.Studenikin, to be published.

[7] A.Egorov, A.Lobanov, A.Studenikin, in: Results and Perspectives in Particle Physics, ed. by M.Greco, Frascati Physics Series, 2000.

PULSAR VELOCITY PUZZLE AND NONSTANDARD NEUTRINO OSCILLATIONS

R. HORVAT [a]

"Rudjer Bošković" Institute, P.O.Box 1016, 10001 Zagreb, Croatia

Abstract. We consider a string-inspired scheme in which an extremely light (or a strictly massless) scalar particle, coupled ultra-weakly to both neutrinos and to a constituent of the matter, gives rise to sizeable neutrino masses within a medium. We then show how the conventional mechanism of neutrino oscillations based on such a scheme can solve the pulsar velocity problem without being in conflict with cosmological bounds on stable neutrino masses.

1 Introduction

It has been known for a while [1] that pulsars have very large peculiar velocities; the average value from a sample of about a hundred of pulsars being around 500 kms^{-1} [2]. The origin of such high velocities is still unclear. Let us recall that pulsars are fast-rotating neutron stars which are assumed to have very large surface magnetic fields. They are born in the explosion of a supernova.

Some explanations of the origin of high velocities of pulsars which are not directly related to neutrino emission from a star [3, 4] can hardly explain pulsar velocities in excess of 100 kms^{-1}. As the data suggest that a newly born neutron star receives a strong kick at birth, and that more than 99% of the binding energy is emitted in form of neutrinos, it is easy to estimate that only a 1% asymmetry in the distribution of the escaping neutrinos could generate the observed kick of the pulsars. Recently a possibility of a cumulative build-up of the asymmetry due to some parity-violating interactions has been put forward as an explanation of the pulsar velocity problem (PVP) [5]. However shortly after it was noticed that any such asymmetry is necessarily washed out in thermodynamic equilibrium, even if the scattering amplitudes are asymmetric [6]. So it has become clear that any viable solution of the PVP should rely on some out-of-equilibrium effect; the most obvious candidate being free streaming of neutrinos from their neutrinospheres.

2 Pulsar velocities from standard and nonstandard neutrino oscillations

It was stressed first by Kusenko and Segrè [7] that any explanation of the PVP in terms of neutrino oscillations should satisfy the following two conditions: (a) strong magnetic field inside a neutron star, $B \sim 2 \times 10^{15} - 10^{16}$ G [7, 8] (a different value according to different authors); and (b) adiabatic neutrino oscillations $\nu_e - \nu_{\nu_\mu,\nu_\tau,s}$ occurring at some point inside the ν_e-neutrinosphere but outside the $\nu_{\nu_\mu,\nu_\tau,s}$-neutrinosphere, where s denotes a sterile neutrino. In addition to these conditions, the key ingredient in generation of the required asymmetry is a modification of the MSW resonant condition in the presence of an external magnetic field [9]. Thus, the origin of the observed velocities of pulsars lies in the angular dependence of the neutrino resonance surface, caused by the strong background magnetic field present during a SN explosion [7]. For

[a] e-mail: horvat@lei3.irb.hr

active-active transitions, the resonant condition is met for the value of the neutrino mass squared difference, $\Delta m^2 \sim 10^4$ eV^2, no matter whether the resonant conversion is between ν_e and ν_μ or ν_e and ν_τ. Later on, Kusenko and Segrè found that ordinary-sterile resonant neutrino oscillations may also play a role in the understanding of the pulsar kicks [10]. Now, a value of the neutrino mass squared difference which is required is somewhat larger, $\Delta m^2 \sim 1$ keV^2. But in any of the above mechanism, the value of Δm^2 is in conflict with cosmological bounds on neutrino masses, unless $\nu_\mu(\nu_\tau)$ is unstable. Also, these values of Δm^2 are not preferred by neutrino oscillation solution neither of the solar neutrino problem nor the atmospheric neutrino anomaly.

Mainly in order to avoid the conflict with cosmological constraints, two nonstandard oscillation schemes have been put forward recently in that respect. The first proposal [11] for generation of pulsar space velocities contains resonant oscillations of massless neutrinos in a particle physics model based on a small violation of universality in the weak interaction sector. Another mechanism [12] relates the high birth velocities of pulsars with a kind of neutrino oscillations based on the assumption that neutrinos violate the equivalence principle (VEP). The important check for those models comes from an analysis [13] of the Super-Kamiokande (SK) data on atmospheric neutrino deficit which also includes the observed angular distribution of the high energy upward going muons. By studying the energy dependence of the neutrino oscillation length associated to transitions, it was shown there that the best explanation of the data is achieved when the oscillation length depends linearly on neutrino energy (as in the standard-oscillation scenario). On the other hand, the models of Refs. [11, 12] appear to be disfavored by the present data as the neutrino oscillation length is proportional to the inverse of the neutrino energy and is independent of the energy, respectively.

Thus, the main problem in explaining the PVP in terms of neutrino oscillations is to find a model which is in agreement with cosmological constraints and which, at the same time, gives a good fit to the recent atmospheric data from the SK experiment.

3 Model based on the scenario of Damour and Polyakov from string theory

We suggest here that the intervening matter may induce appreciable masses for neutrinos, if they couple to an extremely light (or a strictly massless) scalar particle. Such a large effect may occur even if the scalar is assumed to interact with neutrinos only gravitationally (or even weaker) [14], i.e. via coupling constants suppressed by the inverse of the Planck mass. By inducing a nonzero mass squared difference for neutrinos within a medium, such exotic interactions may produce neutrino oscillations even for degenerate-in-mass neutrinos [14, 15]. It is necessary for this to occur that the coupling constants representing interactions at the Planck scale are not universal but rather species-dependent, thereby violating the equivalence principle . It is important to stress that the masslessness of the scalar and VEP (the ingredients necessary for the efficient generation of neutrino masses and oscillations), are at the same time a basic outcome of a scenario of Damour and Polyakov [16] in string theory, in which the string dilaton field may remain massless in the low-energy world and violates the equivalence principle. One should not confuse the above scheme with another one,

where the neutrino mixing is generated by a VEP induced by a breakdown of universality in the gravitational coupling strength between the conventional spin-2 particles and the neutrinos, which had been proposed first in [17] and discussed afterwards in several papers over the past ten years (see e.g. [18] and the references therein).

The relevant Lagrangian density reads [16],

$$\mathcal{L} = \sqrt{4\pi G_N}\, \beta_A m_A \bar{\psi}_A \psi_A \phi \quad , \tag{1}$$

where ψ_A and ϕ is a matter field of type A and the dilaton field, respectively. Here G_N is the Newton's gravitational constant and β_A is the strength of the coupling of the dilaton to A-type particles.

From a viewpoint of Thermal Field Theoery (TFT) [19], neutrino masses within a medium are generated in the above scheme via a tadpole graph. It consists of a medium-induced loop (in which real particles are circulating) and also of a one-loop resummed propagator for the scalar. The contribution to the induced neutrino mass as given by the medium-induced tadpole graph reveals several salient features which we are now going to discuss. First of all, it depends only on the ratio of couplings but not on their absolute values. From a viewpoint of perturbation expansion, this means that apparently of order $O(g^2)$, it is actually of order $O(1)$. Since the only information on β's are the weak upper limits (see below), it is quite obvious that the ratio is practically unconstrained - this gives us an opportunity to accommodate practically any value for the neutrino mass in the problem very easily. In the presence of nonuniversal β's the mechanism will produce neutrino oscillation; as a special feature we stress that even for degenerate-in-mass neutrinos the mechanism will still produce oscillations. In the following we assume, for the sake of demonstration, a complete degeneracy for the oscillatory neutrinos $i = 1, 2$, i.e.

$$m^*_{\nu_i} = m_0 + m^{ind}_{\nu_i} \quad , \tag{2}$$

where m_0 is the common mass from the vacuum.

If, for the sake of simplicity, one deals with the case where the mass and the gravitational eigenstates are identical, then it is easy to show that the evolution equation as well as the expression for flavor survival probability as a function of distance L (for say two flavors with mixing angle θ) have precisely the same form as in the standard-oscillation mechanism,

$$P(\nu_e \to \nu_e) = 1 - \sin^2(2\theta)\sin^2\left(\frac{L\Delta m^{*2}}{4E}\right) \quad . \tag{3}$$

We assume that the largest contribution to the induced neutrino mass inside a supernova core comes from interactions with the nucleons. Using the real-time formulation [20] of TFT, together with the relevant distribution functions for nucleons, we find by explicit calculation a contribution to the induced masses for neutrinos in a supernova core as

$$\Delta m^{*2} \simeq 2\left(\frac{\Delta\beta}{\beta_N}\right)\left(\frac{T(r_0)}{m_N}\right) m_0^2 \quad , \tag{4}$$

where $T(r_0)$ is the temperature at the resonant point and $\Delta\beta \equiv \beta_{\nu_2} - \beta_{\nu_1}$ characterizes a VEP. Setting Δm^{*2} at the level $\sim 10^4$ eV^2, $m_0 \sim 1$ eV (as to be in

agreement with cosmological constraints on stable neutrino masses as well as the SK data), $T(r_0) \sim$ (a few) MeV, we obtain $\Delta\beta/\beta_N \sim 10^6$. Similarly for active-sterile transitions, $\Delta\beta/\beta_N \sim 10^8$.

4 Discussion

Let us notice that the solution of the PVP requires that the neutrino-dilaton coupling be much greater than the coupling of the dilaton to ordinary matter. We mention a limit for ordinary matter coming from conventional solar-system gravity experiments. The present experimental data give upper limits of order 10^{-3} for a possible admixture of a scalar component to the relativistic gravitational interaction, $\beta^2_{ext} < 10^{-3}$ [21]. There is also a limit on β_ν obtained recently from quintessential cosmology [22],

$$\beta_\nu^2 \ll 4 \times 10^{-6} \left(\frac{\mathrm{eV}}{m_\nu}\right)^3 . \tag{5}$$

Hence both coupling should be less than unity (and at the same time we need $\beta_\nu >> \beta_N$). This however represents a certain deegre of fine-tuning in the theory. Indeed, from a traditional viewpoint, the expected values for the β's are of order of unity since they represent interactions at the Planck scale. The solution to the fine-tuning problem was given in the work of Damour and Polyakov [16] in the form of a *least coupling principle.* It is based on a mechanism which provides that a (universal) coupling of the scalar (the string dilaton field in their example) with the rest of the world, being dependent on the VEV of ϕ and hence time dependent, has a minimum close to the present value of the ϕ's VEV. Therefore, the present-day value for β's can naturally be much less than unity. We have to assume however that the mechanism is also operative for quintessence since in their paper Damour and Polyakov dealt with the string dilaton, which, as a recent analysis [23] shows, cannot provide us with the negative equation of state, and therefore is useless for the dynamical component of quintessence.

On the other hand, due to differences in cosmological evolution it is conceivable that the present-day values of β_N's are much closer to the minimum, and therefore can be much less than β_ν's.

We can therefore conclude that the above string-inspired scheme can lead to a viable solution of the PVP in terms of neutrino oscillations.

Acknowledgments

The author acknowledges the support of the Croatian Ministry of Science and Technology under the contract 1 – 03 – 068.

References

[1] J. E. Gunn and J. P. Ostriker, *Astrophys. J.* 160, 979 (1970); A. G. Lyne and M. J. Salter, *MNRAS* 261, 113 (1993).
[2] A. G. Lyne and D. R. Lorimer, *Nature (London)* 369, 127 (1994).
[3] J. R. Gott, J. E. Gunn and K. P. Ostriker, *Astrophys. J. Lett.* 60, L91 (1971).

[4] E. R. Harrison and E. P. Tademaru, *Astrophys. J.* 201, 447 (1975).
[5] C. J. Horowitz and G. Li, *Phys. Rev. Lett.* 80, 3694 (1998); D. Lai and Y.-Z. Qian, *Astrophys. J.* 495, L103 (1998); 501, L155 (1998); H.-Th. Janka, *astro-ph/9801320.*
[6] A. Kusenko, G. Segrè and A. Vilenkin, *Phys. Lett.* B 437, 359 (1998).
[7] A. Kusenko and G. Segrè, *Phys. Rev. Lett.* 77, 4872 (1996).
[8] Y. Z. Qian, *Phys. Rev. Lett.* 79, 2750 (1997).
[9] J. C. D'Olivo, J. F. Nieves and P. B. Pal, *Phys. Rev.* D 40, 3679 (1989).
[10] A. Kusenko and G. Segrè, *Phys. Lett.* B 396, 197 (1997).
[11] D. Grasso, H. Nunokawa and J. W. F. Valle, *Phys. Rev. Lett.* 81, 2412 (1998).
[12] R. Horvat, *Mod. Phys. Lett.* A 13, 2379 (1998).
[13] G. L. Folgi, E. Lisi, A. Marrone and G. Scioscia, *hep-ph/9904248.*
[14] R. Horvat, *Phys. Rev.* D 58, 125020 (1998).
[15] A. Halprin and C. N. Leung, *Phys. Lett.* B 416, 361 (1998).
[16] T. Damour and A. M. Polyakov, *Gen. Rel. Grav.* 26, 1171 (1994); *Nucl. Phys.* B 423, 532 (1994).
[17] M. Gasperini, *Phys. Rev.* D 38, 2635 (1988); D 39 3606 (1989).
[18] A. Halprin, C. N. Leung and J. Pantaleone, *Phys. Rev.* D 53, 5365 (1996).
[19] See e.g. M. Le Bellac, *"Thermal Field Theory"* (Cambridge University Press, Cambridge, 1996).
[20] A. J. Niemi and G. W. Semenoff, *Nucl. Phys.* B 230, 181 (1984); R. L. Kobes and G. W. Semenoff, *Nucl. Phys.* B 260, 714 (1985); B 272, 329 (1986).
[21] R. D. Reasenberg et al., *Astrophys. J.* 234, L219 (1979).
[22] R. Horvat, *Mod. Phys. Lett.* A 14, 2245 (1999).
[23] P. Binetruy, *hep-ph/9810553.*

Kinematic Projecting of Pulsar Profiles

V.A. Bordovitsyn[a], V.Ya. Epp[b], V.G. Bulenok
Tomsk State University, pr. Lenina 36, Tomsk, 634050 Russia

Abstract. We suggest a technique for construction of profiles of incoherent pulsar emission using instantaneous angular distribution of radiation from relativistic source moving in the neutron star magnetosphere. In the general case the indicatrix of radiation depends on the kinematic parameters of radiation source such as velocity and acceleration. The method is illustrated by calculation of the profiles of pulsar radiation based on synchrotron radiation indicatrix. This technique can be easily generalized for the case of other types of relativistic particles radiation. The considered profiles are compared with observed ones. A good agreement was found with profiles of γ-pulsars — Geminga, Crab and Vela.

1 Introduction

There is no clear conception of the nature of pulsar electromagnetic radiation. We accept the well known point of view suggested by I.S. Shklovsky [1] that at least the high frequency part of radiation represents the incoherent synchrotron radiation.

There are different models of pulsar radiation based on various physical processes which are sometimes contradictory and insufficiently conditioned. We suggest a technique of kinematic projecting of synchrotron radiation [2] which gives the pulsar radiation profiles including the phase dependence of polarization characteristics [3, 4, 5]. Then one can analyze the coherence effects and possible mechanisms of pulsar radiation.

The suggested technique of determination of the pulsar radiation profiles is as a matter of fact a kinematic projecting of relativistic radiation regardless to the specific source of the radiation. The role of such sources of radiation can play relativistic charged particles such as electrons, magnetic particles (neutrons) or even bunches of those particles. The main source of information in this technique is the highly directed indicatrix of the instantaneous angular distribution of relativistic radiation, which is specified by the kinematic and dynamic characteristics of the emitting object in every specific case. It is known [1, 6] that there are two models of radiation geometry. The first one is due to two beams of curvature radiation associated with the magnetic poles. The second one is associated with synchrotron radiation in a plane orthogonal to the magnetic axis of pulsar. We restrict our consideration with the second model of radiation, though it is possible to apply this technique in the first case too.

2 Transformation of angular distribution into the pulse profile

We start from the indicatrix of synchrotron radiation averaged over the period. Because of high energy of particles the main part of radiation is concentrated near the plane of symmetry which we call the light plane. Directions, assigned to radiation maximum, are situated in the light plane. Axis orthogonal to the light plane coincides

[a]e-mail: bord@mail.tomsknet.ru
[b]e-mail: epp@tspu.edu.ru

with the direction of pulsar magnetic moment $\boldsymbol{\mu}$. Vector $\boldsymbol{\mu}$ is precessing around the pulsar axis of rotation $\boldsymbol{M}$ with the angular velocity Ω.

We assume that the angular velocity ω of the emitting particles is much more than Ω: $\omega = eH/(m_0 c\gamma) \gg \Omega$, here e is the charge, m_0 is the rest mass, c is the speed of light, $\gamma = \sqrt{1-\beta^2}$ is the relativistic Lorentz factor, $\beta = u/c$, u is the particle velocity. It follows from the last inequality that $\gamma \ll eH/(m_0 c\Omega)$.

Let us estimate the order of γ-factor satisfying the last condition. It can be taken for pulsars that $\Omega \approx 10\ s^{-1}$, $H \approx 10^{12}$ Oe not far from the surface and $H \approx 10^6$ Oe in the periphery of magnetosphere (near the light cylinder). Then the last inequaliey is always satisfied in available relativistic and even ultrarelativistic case.

We introduce the coordinate system shown in Fig. 1. Direction of the angular velocity of pulsar is parallel to the Z-axis. The pulsar magnetic axis defined by unit vector $\boldsymbol{k}$ is specified by the angles κ and Ωt. The unit vector of the observer's direction is given by the angles δ and λ. We assume that vector $\boldsymbol{k}$ is situated in the plane YZ at the moment $t = 0$.

We present the angular distribution of radiation averaged over the period of particle motion in a form

$$\overline{dW} = W\ \rho(\theta)\ \sin\theta d\theta,$$

where W is the total power of radiation, and $\rho(\theta)$ is the function of the angular distribution of radiation normalized to unity.

In the case of synchrotron radiation [3]

$$W = \frac{2}{3}\frac{e^2}{c}\,\omega^2\beta^2\gamma^4 = W_{\mathrm{SR}}$$

and

$$\rho(\theta) = \frac{3}{8}\gamma^{-4}\left\{\frac{2+\beta^2\sin^2\theta}{(1-\beta\cos\theta)^{5/2}} - \frac{\sin^2\theta(4+\beta^2\sin^2\theta)}{4\gamma^2(1-\beta\cos\theta)^{7/2}}\right\}. \tag{1}$$

It is obvious that the angle θ varies in the course of time, as the unit vector $\boldsymbol{k}$ setting the position of light plane, is precessing around the Z axis. It is easy to show that

$$\cos\theta(t) = \cos\delta\cos\kappa + \sin\delta\sin\kappa\sin(\Omega t - \lambda). \tag{2}$$

If we know $\theta(t)$, we determine the radiation profile $\rho(t)$ and the power $\overline{dW}$ emitted in the directions of the angle interval $\sin\theta d\theta$. The maximum of radiation will be observed at the moment of intersection of the observation direction by the light plane when $\cos\theta = 0$, i.e. when

$$\sin(\Omega t - \lambda) = -\cot\delta\cot\kappa. \tag{3}$$

The latter equation has a solution when $|\cot\delta\cot\kappa| \leq 1$. Equation (3) has two roots within the precession period which are equal at $\delta = \pi/2 \pm \kappa$. In other words, the light plane intersects the observation direction twice within the period, if the angle between the vector $\boldsymbol{n}$ and plane XY is less than κ.

If the light plane intersects the observation direction (or touches it), then the angle λ can be chosen such that the observation direction has been situated in the light

plane at $t = 0$. the radiation pulse under this initial condition takes on the maximum value $\rho(\theta = \pi/2)$ at $t = 0$. Thereat it follows from the equation (3) that

$$\sin\lambda = \cot\delta\cot\kappa, \tag{4}$$

$$\sin\kappa = \frac{\cos\delta}{\sqrt{\cos^2\delta + \sin^2\delta\sin^2\lambda}}, \quad 0 < \kappa, \quad \delta \leq \pi/2.$$

It follows from equation (4)that for the same acute angles κ and $\delta \leq \pi/2 - \kappa$, the term $\sin\lambda$ takes equal values within the range $0 < \lambda < \pi$, i.e. λ_1 and $\lambda_2 = \pi - \lambda_1$, which corresponds to two possible intersections of the observation direction and the light plane. At $\lambda_1 = \lambda_2 = \pi/2$ we have $\kappa = \pi/2 - \delta$. In this case the observation direction only touches the light plane. Note that equation (4) is symmetric relative to the angles κ and δ. It means that the positions of the two peaks of profiles will not change if we swap κ and δ. The case of $\kappa = 0$ is special. It follows from equation (2) that in this case $\cos\theta = \cos\delta$ =const and pulsar is observed as a source of synchrotron radiation with constant luminosity and angular distribution of radiation defined by relation (1).

In the ultrarelativistic case of $\gamma \gg 1$ the main part of radiation is concentrated near the light plane $\theta \approx \pi/2$. Thereat duration of the radiation pulse is much less than Ω^{-1}. It allows to expand the function $\rho(\theta)$ in a series in small angles $\psi = \pi/2 - \theta$, or small Ωt. To a first approximation in Ωt we get

$$\psi = \cos\delta\cos\kappa + \sin\delta\sin\kappa(\Omega t\cos\lambda - \sin\lambda). \tag{5}$$

We specify the initial conditions in accordance with equation (4)

$$\psi = \Omega t\sin\delta\sin\kappa\cos\lambda = \pm\Omega t\sqrt{\sin^2\delta\sin^2\kappa - \cos^2\delta\cos^2\kappa}. \tag{6}$$

We introduce another angular variable

$$\chi = \gamma\psi = \gamma\overline{\omega}t, \quad \overline{\omega} = \Omega\sin\delta\sin\kappa\sin\lambda. \tag{7}$$

The variable $\overline{\omega}$ has a sense of angular velocity at which the observer's direction intersects the light plane. The highest velocity corresponds to passage through the radiation maximum. In this case δ and λ are associated with the direction in the light plane.

3 Comparison with the observed profiles

We have considered a simple model of pulsar emission. Some of the obtained profiles are close in shape to really observed profiles. In this section we compare the profiles of γ-ray pulsars, the Crab [7], Vela [8] and Geminga [9, 10] with the profiles obtained from synchrotron radiation indicatrix. As one can see from Figs. 3 and 4, the variation of angles κ and δ gives a wide variety of profiles. But it does not mean that you can produce any profile this way. In particular, profiles obtained by this method have a certain relationship between the width of peaks, phase position and the level of plato between them. Thus, not every observed profile can be built with help of the used

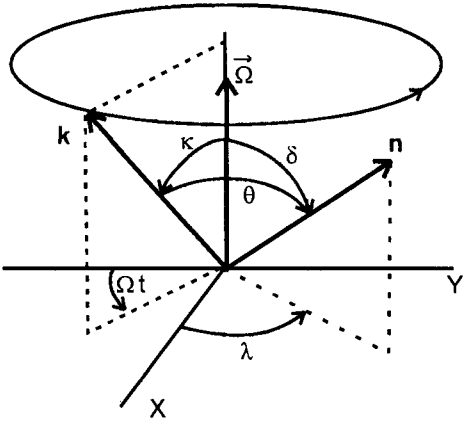

Figure 1: The coordinate system.

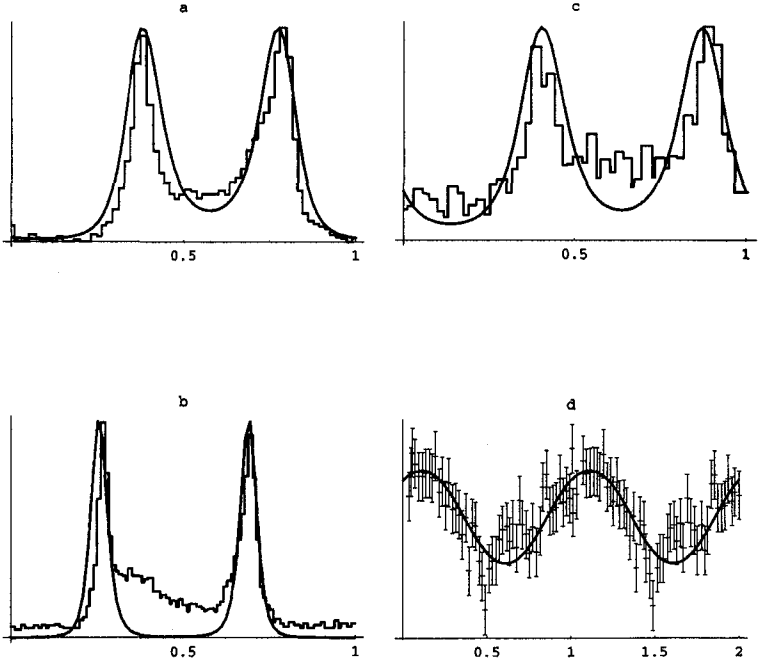

Figure 2: Profiles of γ-ray pulsars. Smooth lines show the model results, histograms display observed profiles. a — Crab; b — Vela ; c — Geminga, γ-ray profile ; d — Geminga, X-ray profile

model. But if a calculated profile fits an observed one, it can mean that the suggested model is adequate and we obtain some information about the angles δ and κ.

Fig. 2 shows the calculated and observed profiles for three well known γ-ray pulsars. The energy interval for electrons (or positron) was chosen for following reason. Most pulsars exhibit two sharp peaks within a period, if the energy of photons lies in the region $E_\gamma \geq 1$ MeV. Knowing the critical frequency of synchrotron radiation $\omega_\gamma \sim eH\gamma^2/mc$ we can estimate the Lorentz-factor of particles $\gamma^2 \geq mcE_\gamma/eH\hbar$. For the magnetic field of order $H \sim 10^{12}$ Oe we obtain $\gamma \geq 10$ or for the particle velocity $\beta \geq 0.99$. Specific values of β for Figs 5 were selected in a way to obtain the best fit of peaks width. It is obvious that the greater is the particle energy the narrower are the peaks.

It is believed that the pulsar in the Crab Nebula has an inclination angle close to $\pi/2$. That is why we have chosen $\kappa = 85°$. Then the best fit to the observed pulse profile measured by BATSE [7] gives the value $\delta = 15°$ (see Fig. 2a). Fig. 2b shows the Vela pulse profile for energy of photons above 100 MeV detected by EGRET [8] along with calculated profile for angles $\delta = 10°$, $\kappa = 88°$ and $\beta = 0.999$. The difference occurs in a bridge between the two pulses. It can be caused by the dispersion of particle orbits in the pulsar magnitosphere. Next two figures show Geminga profiles. Fig. 2c displays observed γ-profile for $E_\gamma > 100$ MeV [9] along with calculated one for $\delta = 89°$, $\kappa = 10°$ and $\beta = 0.992$. Soft X-ray profile is plotted in Fig. 2d in the 0.53–1.5 keV band measured by ROSAT [10] and a profile calculated for angles $\delta = 80°$, $\kappa = 4°$ and $\beta = 0.94$. We see good agreement between the model and observed profile though it is thought that the soft X-ray radiation is due to thermal blackbody emission [10].

4 Discussion

The profiles shown on Figs 2 are calculated for moderately relativistic electrons. In doing this we tried to fit the shape of profiles. But all the calculations were made for a single particle. It is evident that in a real situation radiation is emitted by an ensemble of particles with a spread in energies and orbit orientation. On averaging over this parameters the pulse width can grow significantly. But without regard on averaging we can obtain some information about the pulsar magnetic axis orientation from the relative position of pulses in the radiation profile. According to equation (3) the maximum of radiation occurs at $t_{1,2}$ given by

$$\Omega t_{1,2} = \pm \arccos(\cot\delta \cot\kappa) \tag{8}$$

If we know the phase distance between the pulses, we will find the relationship between angles δ and κ by use of equation (8).

We suppose here that γ-radiation of pulsars is a synchrotron radiation of particles with their orbits orthogonal to the magnetic axis of pulsar. The probability of detection of such pulsar in a γ-ray band according to this model is equal to $p = \sin\kappa$. Thus, with the most probability we can detect pulsars with its magnetic axis orthogonal to the axis of rotation. Thereby the gap between pules in γ-ray region should be close to 0.5 of period. That is what we see in most cases of detected γ-ray pulsars.

The discussed model does not pretend to give entire interpretation of the pulsar radiation. The main purpose of this paper is to show how to find the light profile of a rotating source when the indicatrix of radiation is known in a rest frame. We have chosen the synchrotron radiation mechanism as an widely spread example. Considered method can be used for curvature radiation or a more complicated source.

Acknowledgments

This work was supported by Ministry of General and Professional Education of Russia, Competitive Center of Fundamental Research.

References

[1] I.S. Shklovsky *Stars*, (Nauka, Moscow) p.384, 1977.
[2] V.G. Bagrov *Optika i Spektroskopija* 18, 541 (1965).
[3] V.G. Bagrov, V.A. Bordovitsyn , G.F. Kopytov *Izv. Vuzov. Fiz.* N 6, 86 (1972).
[4] V.G. Bagrov, V.A. Bordovitsyn, G.F. Kopytov, V.Ya. Epp *Izv. Vuzov. Fiz.* N 1, 46 (1974).
[5] *Synchrotron Radiation and Its Development.* Ed. V.A. Bordovitsyn, (World Scientific, Singapore) 1999.
[6] R.N. Manchester, J.H. Taylor *Pulsars*, (W.H. Freeman and Company) 1977.
[7] G. Fishman *GRO Newsletter* 1, 6 (1992).
[8] J.M. Fierro, P.F. Michelson, and P.L. Nolan *ApJ* 494, 734 (1998).
[9] J.K. Daugherty and A.K. Harding *ApJ* 458, 278 (1996).
[10] J.P. Halpern and M. Ruderman *ApJ* 415, 286 (1993).

Neutral particle radiation in electromagnetic field

A.E. Lobanov, O.S. Pavlova

Abstract. The total radiation power of a classical neutral particle with anomalous magnetic and electrical moments moving in an arbitrary electromagnetic field has been found. The result was obtained under the assumption that spin evolution of the particle was determined by the generalized Bargmann-Michel-Telegdi equation.

As is well known, external electromagnetic fields can have considerable influence on processes involving neutral particles, and this influence may be caused not only by the vacuum polarization, but also by the inner electromagnetic structure of heavy particles, for example, neutron. Therefore the investigation of the effect of external fields on the processes involving neutrons is one of the important problems of high energy physics.

The inner electromagnetic structure of neutron manifests itself more obviously in the fact that it has anomalous magnetic moment (AMM). The studies show that the account of only this factor leads to nontrivial results. It was found that the interaction of the neutron AMM with electromagnetic field greatly changes the probability of β-decay in the strong field [1], which is very important, for example, in the physics of pulsar [2]. The neutron radiation is another interesting process.

The radiation of a neutral particle moving in an arbitrary electromagnetic field attracts steady attention for a long time. The study of this phenomenon was carried out by using both quantum theory and classical electrodynamics. The QED methods were used to investigate neutral particle radiation in the electromagnetic fields of special types: homogeneous fields [3,4], the plane-wave fields [5-8] and other fields [9]. The classical description of this phenomenon was employed in a number of articles [10, 11].

In using quantum approach the choice of field models was determined by existing the exact solutions of the Dirac equation. Notice that in this case the exact solution of the Dirac equation is necessary for calculating the radiation power both for polarized particles and unpolarized particles. When we use the classical description, we have the same situation for polarized particles, i.e., the exact solutions of the equation of motion (Lorentz's equation) and the equation of spin evolution (the Bargmann–Michel–Telegi equation (BMT)) allows us to calculate the radiation power both for the neutral particle and for the charged particle moving in the electromagnetic field.

The problem is essentially simplified if the radiation of a neutral unpolarized particle is considered. The principle difference between classical and quantum descriptions consists in the fact that the recoil during the emission of the radiation is not taken into account in the classical approach. In the QED the act of emission leads to the change of the particle moment and its polarization, which means that this process are described by the initial and terminal values of particle moment and polarization. However, in the classical theory the act of emission does not change these values since the recoil is absent.

Since for a neutral particle the solution of the Lorentz's equation for 4–velocity is of the form $u^\mu = \text{const}$, the Lorentz transformation to the particle rest frame will be determined by the constant operator. In the rest frame, the polarization vector is the only vector describing the particle. If we perform the averaging over spin

directions (which, in quantum theory, corresponds to the description of radiation of an unpolarized particle), then the only vectors that can enter the expression for radiation energy will be the intensities of electric and magnetic fields in the particle rest frame. This fact means that there exists an universal formula for the radiation energy of neutral unpolarized particle in the arbitrary inhomogeneous electromagnetic fields, which is actually true.

Consider the radiation of a neutral unpolarized particle, which is caused by its anomalous magnetic moment (AMM) μ. The classical formula for the total radiation energy is of the form [12]

$$\mathcal{E} = \int I dt, \tag{1}$$

the covariant form of the radiation power being written as

$$I = -\frac{2}{3}\langle \ddot{\mu}^\nu \ddot{\mu}_\nu \rangle, \tag{2}$$

Here dots designate the differentiation with respect to proper time τ, the angle brackets mean the averaging over spin states, and $\hbar = c = 1$.

We restrict ourselves to the standard assumption that the magnetic momemt is proportional to the spin vector

$$\mu^\nu = \mu_0 S^\nu. \tag{3}$$

Then the evolution of spin vector is described by the BMT equation [13]

$$\dot{S}^\nu = 2\mu_0 \{F^{\nu\alpha} S_\alpha - u^\nu (u_\alpha F^{\alpha\beta} S_\beta)\}, \tag{4}$$

whose solution satisfies the additional conditions $(SS) = -1$ and (Su)=0.

To make the comparison with quantum mechanical description easier, instead of 4-vector a^ν we will use the two dimension spin-tensor $\underset{\sim}{a} = a^0\sigma_0 + \boldsymbol{a\sigma}$ and $\tilde{a} = a^0\sigma_0 - \boldsymbol{a\sigma}$, where σ_ν are the Pauli matrices (designations are used according to [14]). Then the spin evolution is determined by

$$\underset{\sim}{S}(\tau) = \underset{\sim}{L}\underset{\sim}{R}\underset{\sim}{L}^{-1}\underset{\sim}{S}_0(\underset{\sim}{L}^{-1})^+\underset{\sim}{R}^+\underset{\sim}{L}^+. \tag{5}$$

Here $S_0 \equiv S(\tau_0)$ is the polarization at the initial moment of time τ_0, L^{-1} is the operator of transition into the particle rest frame

$$\underset{\sim}{L}^{-1} = \frac{1+\tilde{u}}{\sqrt{2(1+u^0)}}, \qquad \underset{\sim}{L} = \frac{1+\underset{\sim}{u}}{\sqrt{2(1+u^0)}};$$

nd R is the rotation operator satisfying the equation

$$\dot{\underset{\sim}{R}} = i\mu_0 \underset{\sim}{H}_0 \underset{\sim}{R}, \tag{6}$$

where

$$\mathbf{H}_0(x) \equiv \mathbf{H}_0 = u^0\mathbf{H} - \mathbf{u}\times\mathbf{E} - \frac{\mathbf{u}(\mathbf{uH})}{1+u^0} \quad - \tag{7}$$

is the magnetic field at the point where the particle is located in its rest frame $x^\nu = u^\nu \tau$.

Using the spin–tensor, we can rewrite the formula (2) in the form

$$I = -\frac{\mu_0^2}{3} Sp\langle \ddot{\underset{\sim}{S}} \ddot{\tilde{S}} \rangle. \tag{8}$$

After simple algebra with regard for formula (5) for the radiation power of unpolarized particle, hence we obtain

$$I = \frac{\mu_0^2}{3} Sp \sum_i (\underset{\sim}{R}\sigma_i \underset{\sim}{R}^+)^{\cdot\cdot} (\underset{\sim}{R}\sigma_i \underset{\sim}{R}^+)^{\cdot\cdot}. \tag{9}$$

In (9) summation with respect to i corresponds to the averaging over initial spin states and to the summation over final spin states.

From (6) and (9) we arrive at the final result

$$I = \frac{16}{3}\mu_0^2\{4(\mu_0 \mathbf{H}_0)^4 + (\mu_0 \dot{\mathbf{H}}_0)^2\}. \tag{10}$$

Thus, as noted above, the radiation power of an unpolarized neutral particle in the arbitrary electromagnetic field is expressed only through its intensity in the particle rest frame and their derivatives with respect to the proper time.

Now we make a few remarks with reference to formula (1). It is the convention of quantum mechanics that, if the integral in (1) converges on the interval $(-\infty, +\infty)$, then this formula describes the total energy emitted while the particle flies through the field region. If the finite limit

$$\lim_{T\to\infty} \frac{1}{2T} \int_{-T}^{T} I dt, \tag{11}$$

exists, then the expression (11) determines the radiation energy per unit time in the periodic and quasi–periodic fields. If the limit in (11) does not exist, then formula (1) does not have the quantum analog, or in more exact terms, this divergence means that in solving the quantum problem the bound states (discrete energy spectrum) can be observed (see, for example, [15]).

We easily verify that, substituting into formula (10) the fields which were ealier used for calculations both by quantum and classical methods, we obtain the complete agreement with the results found when we neglect the terms describing the recoil, i.e., the terms having the next order of smallness with respect to the Planck constant.

Discuss the possibility of using the classical approximation at greater length. As we have already mentioned, the quantum corrections can be neglected if the energy of emitted photons is small comparing to the energy of emitting particle. This requirement leads to the restrictions of two kinds. First, the binding energy in the rest frame has to be essentially smaller than the rest energy of the particle $\mu_0 H_0/m \ll 1$. Second, the field should have few changes at the distances of the order of the Kompton wave length $\dot{H}_0/mH_0 \ll 1$. It is expedient to rewrite these conditions using the Gaussian units. Then, if we take into account that $\mu_0 \sim e\hbar/mc$ and introduce the so-called critical magnetic field $H_{cr} = m^2c^3/e\hbar$, the above conditions assume the

form $H_0/H_{cr} \ll 1$ and $(H_0/H_{cr})(\omega/\omega_c) \ll 1$. Here ω is the characteristic frequency of external field, nd $\omega_c = eH/mc$ is the cyclotron frequency. Hence we see that for neutron these conditions are necessarily met for reasonable values of field intensities and their gradients. It is essential that the above estimates are not weaker than those which permit us to neglect the change of effective mass in the external field and also the Stern–Gerlach effect in deriving the BMT equation [16, 17]. All that has been said above confirms the validity of classical approach to solving the problem on the radiation of neutral unpolarized particle in the external field.

It is interesting to compare in the order of magnitude the radiation power I of the neutral particle (neutron) which is determined by (10) and the classical radiation power I_0 of charged particle (see, for example, [12]) having the similar mass and energy (proton). We easily find

$$\frac{I}{I_0} \sim max\left\{\left(\frac{H_0}{H_{cr}}\right)^2, \left(\frac{u_0\hbar\omega}{mc^2}\right)^2\right\}.$$

Thus, the radiation power of charge and that of magnetic moment becomes comparable in the extrastrong fields, or in the fields having very high frequency, which can exist near the astrophysical objects, for example, pulsar.

In conclusion it should be noted that just obtained formula can be generalized to the case when the particle has, in addition to AMM, the electric moment (it is natural that static limit of electric moment ϵ_0 exists only in the theories with the violation of T–invariance). In this case the evolution of spin vector is described by the generalized BMT equation [12,17]

$$\dot{S}^\nu = 2\mu_0\{F^{\nu\alpha}S_\alpha - u^\nu(u_\alpha F^{\alpha\beta}S_\beta)\} + 2\epsilon_0\{H^{\nu\alpha}S_\alpha - u^\nu(u_\alpha H^{\alpha\beta}S_\beta)\}, \qquad (12)$$

where $H^{\nu\alpha} = -\frac{1}{2}e^{\nu\alpha\beta\gamma}F_{\beta\gamma}$ is the dual tensor.

The generalization of formula (10) assumes the form

$$I = \frac{16}{3}(\mu_0^2 + \epsilon_0^2)\{4(\epsilon_0\mathbf{E}_0 + \mu_0\mathbf{H}_0)^4 + (\epsilon_0\dot{\mathbf{E}}_0 + \mu_0\dot{\mathbf{H}}_0)^2\}. \qquad (13)$$

where

$$\mathbf{E}_0(x) \equiv \mathbf{E}_0 = u^0\mathbf{E} + \mathbf{u}\times\mathbf{H} - \frac{\mathbf{u}(\mathbf{uE})}{1+u^0}$$

is the electrical field at the point of particle location in its rest frame. The results obtained by using (13) are consistent with that found ealier in [19].

Authors are very greatful to V. . Bordovitzyn, . V. Borisov and V. Ch. Zhukovsky for fruitful discussion.

References

[1] I.M.Ternov, V.N.Rodionov, V.Zhulego, O.S.Pavlova , A.E.Lobanov, O.F.Dorofeev, *Yad. Fiz.* 45, 1357 (1987).

[2] O.F.Dorofeev, V.N.Rodionov, I.M.Ternov, *Pis'ma v Zh. Eksp. Teor. Fiz.* 40, 159 (1985).

[3] I.M.Ternov, V.G.Bagrov, A.M.Khapaev, *Zh.Eksp.Teor.Fiz.* 48, 921 (1965).

[4] I.M.Ternov, V.G.Bagrov, V..Kruzhkov, A.M.Khapaev, *Izv.Vyssh.Uchebn.Zaved.Fiz.* 4, 30 (1967).
[5] V.V.Skobelev, *Zh.Eksp.Teor.Fiz.* 94, 48 (1988); 95, 391 (1989).
[6] V.A. Bordovitsyn, *Izv.Vyssh.Uchebn.Zaved.Fiz.* 1, 131 (1971).
[7] I.M.Ternov, V.G.Bagrov, V.A.Bordovitsyn, Ju.A.Markin, *Zh.Eksp.Teor.Fiz.* 52, 1584 (1967).
[8] A.S.Vshivtsev, R.A.Potapov, I.M.Ternov, *Zh.Eksp.Teor.Fiz.* 105, 1108 (1994).
[9] I.M.Ternov, V.G.Bagrov, V.R.Khalilov, *Vest. Mosk. Univ. (3)* 2, 113 (1969).
[10] V.A.Bordovitsyn, V.S.Gushchina, *Izv.Vyssh.Uchebn.Zaved.Fiz.* 2, 60 (1993); 3, 73 (1993); 1, 53 (1994); 2, 63 (1995); 3, 83 (1995).
[11] V.A.Bordovitsyn, *Izv.Vyssh.Uchebn.Zaved.Fiz.* 11, 39 (1993).
[12] L.D.Landau, E.M.Lifshitz, *Teorya polya (The theory of fields)*, (Moscow) 1960.
[13] V.Bargmann, L.Michel, V.Telegdi, *Phys. Rev. Lett.* 2, 435 (1959).
[14] N.N.Bogolubov, A.A.Logunov, A.I.Oksak , I.T.Todorov, *Obshchie printsipi kvantivoy teorii polya (The General basis of the Quantum Theory of Fields)*, (Moscow) 1987.
[15] I.M.Ternov, V.G.Bagrov, *Yad. Fiz.* 4, 797 (1965).
[16] I.M.Ternov, V.R.Khalilov, O.S.Pavlova, *Izv. Vyssh. Uchebn. Zaved. Fiz.* 12, 89 (1978); 2, 68 (1979).
[17] I.M.Ternov, *Vvedenye v fiziku spina relyativistskih chastits (The introduction to physics of relativistic particle spin)*, (Moscow) 1997.
[18] V.S.Popov, *Zh.Eksp.Teor.Fiz.* 38, 1584 (1960).
[19] V.G.Bagrov, V.V.Bozrikov, D.M.Gitman, Yu.I.Klimenko, A.I.Khudomyasov, *Izv.Vyssh.Uchebn.Zaved.Fiz.* 6, 150; 7, 138 (1974).

Radiation of Relativistic Particles in a Quasi-Homogeneous Magnetic Field

V. Epp [a], T.G. Mitrofanova

Tomsk State Pedagogical University, 634041 Tomsk Russia

Abstract. Spectrum of radiation of a relativistic particle moving in a nonhomogeneous magnetic field is considered. The spectrum depends on the pitch-angle α between the velocity direction and a line tangent to the field line. In case of very small α the particle generates so-called curvature radiation, in an intermediate case undulator-kind radiation is produced. In this paper we present the calculations of radiation properties in a case when both curvature and undulator radiation is observed.

It is well known that the spectrum of radiation of a relativistic particle depends on the pitch-angle α between the velocity direction and a line tangent to the field line. One can distinguish three specific cases

1. $\alpha \gg \gamma^{-1}$ synchrotron radiation,
2. $\alpha \leq \gamma^{-1}$ undulator radiation,
3. $\alpha \ll \gamma^{-1}$ curvature radiation,

where $\gamma = (1 - V^2/C^2)^{-1/2}$, V is the particle velocity, c is the speed of light.

Radiation of the particle in the first case is assumed to be synchrotrone one with the radius of the orbit equal to the radius of a helix. The maximum in the radiation spectrum falls on high number of harmonics.

The radiation in the second case is formed along all path of the particle and is assumed to be of undulator type, when the main part of radiation power is emitted in some few first harmonics. The third case is usually realized in a strong magnetic field when the orthogonal component of velocity vanishes quickly due to synchrotron radiation and the particle moves almost along the field line. This approximation is usually accepted for the particles in the pulsar magnitosphere. Corresponding radiation is called curvature radiation. General formula for the cases 1 and 3 were obtained in refs [1, 2]. The principle point of these papers is that the equations of motion were expanded in power series with respect to time t in the vicinity of fixed moment $t = 0$. But if $\alpha \leq \gamma^{-1}$, the radiation spectrum is formed along rather great part of the particle path. This part can include several loops of the helix. In this case one can expand in a series only slowly varying functions in equation of motion. The rapidly oscillating part of motion produces radiation of undulator type.

In this paper we present the calculations of radiation properties in a case when both curvature and undulator radiation is observed.

In a general case the curved magnetic field line can be approximated with an arc of a circle. If the magnetic field does not depend on the coordinate orthogonal to the plane of magnetic line, the field $\vec{H}(\vec{r})$ can be represented in a form $H_r = 0$, $H_\varphi = H(r)$, $H_z = 0$, where r,φ,z are the cylindrical coordinates.

It follows immediately from the condition $rot\vec{H} = 0$, that $H(r) = I/r$, where $I = const$. This is the field of a straight current or the field of toroidal solenoid in its inner part.

[a] e-mail: epp@tspu.edu.ru

Let us consider equations of motion of a charged particle in such field. It is easy to find three first integrals of motion: energy, axial momentum and z-component of momentum. Thus, we can rewrite the equations of motion in terms of first-order equations

$$\begin{aligned} \dot{r}^2 &= V^2 - U(r), \\ \dot{\varphi} &= V_{0\varphi}\frac{r_0}{r^2}, \\ \dot{z} &= V_{0z} + \mathcal{E}c\ln\frac{r}{r_0}, \end{aligned} \tag{1}$$

where $V = const$ is the particle velocity, $V_{0\varphi}$ and V_{0z} are axial and z-components of velocity respectively, r_0 is the initial coordinate, $\mathcal{E} = eI/mc^2\gamma$, e and m are the charge and mass of the particle.

The function

$$U(r) = (V_{0z} - \mathcal{E}c\ln\frac{r}{r_0})^2 + \frac{V_{0\varphi}^2 r_0^2}{r^2}$$

plays the role of effective potential energy. It has the only minimum at $r = r_m$, which is given by equation

$$r_m^2(V_{0z} + \mathcal{E}c\ln\frac{r_m}{r_0}) = \frac{V_{0\varphi}^2 r_0^2}{\mathcal{E}c}. \tag{2}$$

Solution of eqs (1) gives a great variety of trajectories, which are rather complicated. We are interested only in motion in a quasi-uniform magnetic field. It means that the particle path lies in a small interval $\triangle r \ll r_0$. Thus, we consider the particle motion in the vicinity of minimum of effective potential energy. If the initial state is $r_0 = r_m$, $\dot{r}_0 = 0$, then the solution of eqs (1) is

$$r(t) = r_0, \quad \varphi(t) = \frac{V_{0\varphi}}{r_0}t, \quad z(t) = V_{0z}. \tag{3}$$

Note that this solution is valid for arbitrary r_0. It follows from eq.(2) that the only condition realizing the motion of eq.(3) is that

$$V_{0z} = \frac{V_{0\varphi}^2}{\mathcal{E}c}, \quad V_{0r} = 0.$$

In this case the particle moves along a helix with radius r_0 and constant angle η between the magnetic field line and velocity direction.

$$\tan\eta = \frac{V_{0\varphi}}{\mathcal{E}c}. \tag{4}$$

It is usually assumed in astrophysical applications that after the particle radiates out all the transversal energy, it moves along the magnetic field line. Eq. (4) shows that it is true only if $V_{0\varphi} \ll \mathcal{E}c$. Generally speaking, the angle η can significantly differ from zero.

We assume further that the magnetic field is quasi-uniform, i.e. $\mathcal{E} \gg 1$ and $\eta \ll 1$. Expanding the function $U(r)$ in a power series with respect to small $(r - r_m)/r_m$ we obtain the following solution of eqs (1)

$$\begin{aligned} r &= r_m + a\sin(\omega_0 t + \delta), \\ \varphi &= \frac{V_{0\varphi}}{r_m} t, \\ z &= a\cos(\omega_0 t + \delta), \end{aligned} \tag{5}$$

with $a = r_m\sqrt{V^2 - V_{0\varphi}^2}/\mathcal{E}c$, $\omega_0 = \mathcal{E}c/r_m$ and δ is an arbitrary initial phase. According to eqs (5), the particle moves along a curved helix.

Let us calculate the spectral and angular distribution of radiation. We start with a well known formulae [3]

$$\frac{d\mathcal{E}_j}{d\Omega d\omega} = \frac{cR^2}{4\pi^2}|E_j(\omega)|^2, \tag{6}$$

$$E_j(\omega) = \frac{ei\omega}{cR} e^{ikR} \int\limits_{-\infty}^{\infty} \beta_j(t) e^{i(\omega t - \vec{k}\vec{r})} dt, \tag{7}$$

where $\beta_j(t) = (\vec{V}\vec{e}_j)/c$, $\vec{e}_j$ are the unite vectors of polarization. Let the wave vector $\vec{k}$ lay in the coordinate pane yz and denote by χ the angle between $\vec{k}$ and axis y. Then $\vec{e}_\sigma = (-1, 0, 0)$, $\vec{e}_\pi = (0, \sin\chi, \cos\chi)$.

We assume that the particle is ultrarelativistic one and the pitch- angle satisfies the inequality $\alpha \ll \gamma^{-1}$. This allows us to expand expression (7) in a power series with respect to small $\frac{V_{0\varphi}}{r_0} t$, but keeping unexpanded functions of $\omega_0 t$. As a result we obtain

$$\omega t - \vec{k}\vec{r} = \frac{\omega t}{2}(\gamma^{-2} + \chi^2) + \frac{\omega V_{0\varphi}}{6r_0} t^3, \tag{8}$$

$$\beta_\sigma(t) = \frac{V_{0\varphi}}{r_0} t - \frac{a\omega_0}{c}\cos(\omega_0 t - \delta), \tag{9}$$

$$\beta_\pi(t) = \chi - \frac{a\omega_0}{c}\sin(\omega_0 t - \delta). \tag{10}$$

After integration in equation (7) and substitution in eq. (6) we find

$$\begin{aligned} \frac{d\mathcal{E}_\sigma}{d\Omega d\omega} &= A[(1+\psi^2)^2 K_{\frac{2}{3}}^2(q) - k\sin\delta K_{\frac{2}{3}}(q) f(v) + \frac{1}{4}k^2 f^2(p)], \\ \frac{d\mathcal{E}_\pi}{d\Omega d\omega} &= A[\psi^2(1+\psi^2) K_{\frac{1}{3}}^2(q) + k\sin\delta K_{\frac{1}{3}}(q) f(v) + \frac{1}{4}k^2 f^2(p)], \end{aligned} \tag{11}$$

where

$$\begin{aligned} A &= \frac{4e^2\omega_0^2\nu^2 r_0^2}{3c\pi^2 V_{0\varphi}^2}, \quad \psi = \gamma\chi, \quad k = \frac{a\omega_0\gamma}{V_{0\varphi}}, \quad \nu = \frac{\omega}{2\gamma^2\omega_0}, \\ q &= \frac{r_0\omega(1+\psi^2)^{3/2}}{3\gamma^3 V_{0\varphi}}, \quad N = \frac{\omega_0 r_0}{V_{0\varphi}\gamma}. \end{aligned}$$

The function $f(p)$ is defined by following expression

$$f(p) = \begin{cases} \frac{\pi}{\sqrt{3}}\sqrt{-\eta}[J_{-1/3}(p) + J_{1/3}(p)], & p = \frac{2}{3}\nu N(-\eta)^{3/2}, \quad \eta \leq 0, \\ \sqrt{\eta}K_{1/3}(p), & p = \frac{2}{3}\nu N\eta^{3/2}, \quad \eta \geq 0, \end{cases}$$

$$\eta = 1 + \psi^2 - \nu^{-1}.$$

We see that equations (11) consist of three terms. The first gives the typical synchrotron radiation emitted from an arc of a circle of radius r_0. Thus, it is a curvature radiation. The third term is proportional to transversal part of the particle velocity $V_\perp = a\omega_0$. Parameter $k = V_\perp\gamma/V_{0\varphi}$ is the well known undulator parameter [4, 5]. Hence, the third term in eqs (11) represents the undulator radiation. It is evident that the second term describes some kind of interference of curvature and undulator radiation.

Let us estimate the characteristic frequencies of each part of radiation. The main part of curvature radiation is emitted at frequencies defined by $q \sim 1$, i.e. $\omega \sim \omega_{cr} \sim \frac{V_{0\varphi}}{r_0}\gamma^3$. The undulator part of radiation is generated at frequencies, at which $p \sim 1$, i.e.

$$\nu \left|1 + \psi^2 - 1/\nu\right|^{3/2} \sim 1.$$

This gives

$$\nu \sim \frac{1}{1+\psi^2} \pm \frac{1}{N},$$

thus, $\nu \sim 1$, or $\omega \sim \omega_{ur} \sim \omega_0\gamma^2$. This means that in adopted assumptions ($k \ll 1$) the undulator radiation contains only first harmonic of basic frequency ω_0 shifted by Doppler effect. The ratio $\omega_{ur}/\omega_{cr} \sim N \gg 1$ shows that the curvature and undulator radiation are far separated in spectrum. It means that even when the intensity of one part of radiation is much less then another one, we can distinguish the curvature and undulator radiation. The intermediate part of radiation, which is given by

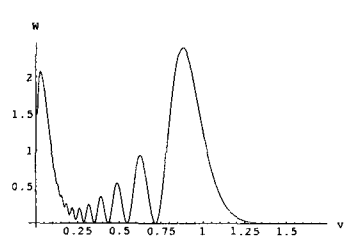

Figure 1: Spectrum of radiation for σ-component at an angle $\chi = 0$. The initial phase is $\delta = 0$.

the second term in eqs (11) strongly depends on the initial phase δ. If we observe

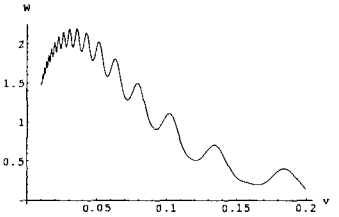

Figure 2: Spectrum of radiation for σ-component at an angle $\chi = 0$. The initial phase is $\delta = \pi/6$.

radiation of an incoherent bunch of particles then this term should be averaged over δ. As a result this term vanishes.

Figures 1 and 2 show the dependence of spectrum of radiation on parameters k, δ and N. The low-frequency part exhibits the curvature radiation while the high-frequency part represents the undulator radiation. We see that the undulator radiation is emitted at basic harmonic $\nu \approx 1$, and the curvature radiation is situated around frequency $\omega_{cr} \approx \omega_{ur}/N$, i.e. $\nu \approx 0.05$. Figure 2 demonstrates the influence of initial phase upon the shape of the spectrum. The small oscillations of the spectrum curve is highly dependent on the value of the initial phase δ.

The dependence on the pitch-angle α is included in the undulator parameter k. Formula (11) show that the undulator part of radiation increases with increasing α.

References

[1] J.L.Zhang and K.S.Cheng, *Phys. Lett.* **A** 208, 47 (1995).

[2] K.S.Cheng and J.L.Zhang, *ApJ* 463, 271 (1996).

[3] L.Landau and E.Lifshitz, *The Classical Theory of Fields* (Pergamon, London), 1962.

[4] M.M.Nikitin and V.Ya.Epp, *Undulator Radiation* (Energoatomizdat, Moscow), 1988.

[5] *Synchrotron Radiation Theory and Its Development.* Ed. by V.A. Bordovitsyn. (World Scientific, Singapore), 1999.

SPIN-ORBITAL MOTION AND THOMAS PRECESSION IN THE CLASSICAL AND QUANTUM THEORIES

V.A. Bordovitsyn [a] and A.N. Myagkii

Physics Faculty of Tomsk State University, 634050 Tomsk, Russia

Abstract. The motion of a magnetic spin particle in electromagnetic fields is considered on the basis of general principles of the classical relativistic theory. The problem of noncollinearity of the momentum and velocity of a particle with spin, the origin and the meaning of Thomas precession in dynamics of the spin particle are also considered.

1 Introduction

In the initial form the classical spin theory was constructed by Ya.I. Frenkel [1] almost at the same time when the spin was discovered. The main theses of quantum spin theory were formulated by W. Pauli. Later with appearance of the Dirac relativistic equation the quantum spin theory was consecutively developed.

For a long time the classical and quantum spin theories developed independently from each other. It seemed that there was no connection between them. A large number of authors, including the authors of well-known books [2, 3, 4], assumed that there was no the classical spin theory in general (see also [5]).

The situation had changed when the Bargmann-Michel-Telegdi (BMT) classical spin equation [6] and respectively the Frenkel spin equation [7] were obtained on the basis of the relativistic quasiclassical spin theory [8–11] and on the basis of the Heisenberg equations of motion in the relativistic quantum mechanics [12]. Moreover, it was found that even purely quantum effect such as spin-flip radiation has classical description [13].

Nevertheless there is no united point of view about the fundamental principles of construction of the classical spin theory in the modern scientific and educational literature. There is a great variety of the classical methods of spin description, which are not confirmed with each other in many respects (see, for example, [14]). In this work the attempt in constructing of a correct classical spin theory was made on the basis of the general principles of classical electrodynamics.

These points will be discussed more fully in our next paper.

2 Spin and problem of the noncollinearity of momentum and velocity

We introduce the density tensor of total angular momentum of a particle in the electromagnetic field

$$M^{\alpha\lambda\beta} = R^{[\alpha}\mathcal{P}^{\lambda\beta]} = R^{\alpha}\mathcal{P}^{\lambda\beta} - R^{\beta}\mathcal{P}^{\lambda\alpha},$$

where

$$\mathcal{P}^{\alpha\beta} = \mathcal{P}_e^{\alpha\beta} + \tilde{\mathcal{P}}^{\alpha\beta},$$

$$\mathcal{P}_e^{\alpha\beta} = c\int_{-\infty}^{\infty} d\tau' P^{\alpha}(\tau')v^{\beta}(\tau')\delta\left(R^{\rho} - r^{\rho}(\tau')\right),$$

[a] e-mail: bord@mail.tomsknet.ru

$$\tilde{\mathcal{P}}^{\alpha\beta} = -\frac{1}{4\pi}\left(H^{\alpha\rho}H_{\rho}{}^{\beta} + \frac{1}{4}g^{\alpha\beta}H_{\rho\gamma}H^{\rho\gamma}\right).$$

The conservation law of angular momentum in differential form is

$$D_{\lambda}M^{\alpha\lambda\beta} = 0.$$

If we then act as in Ref. [15] one obtains the following equation of motion of the angular momentum $M^{\alpha\beta}$

$$\frac{dM^{\alpha\beta}}{d\tau} = \mu H^{[\alpha\rho}\Pi_{\rho}{}^{\beta]} + r^{[\alpha}\left(\frac{e}{c}H^{\beta]\rho}v_{\rho} + \frac{\mu}{2}H_{\rho\lambda}\partial^{\beta]}\Pi^{\rho\lambda}\right),$$

or, taking into account the momentum form of the equation of motion[7]

$$\frac{dP^{\alpha}}{d\tau} = \frac{e}{c}H^{\alpha\beta}v_{\beta} + \frac{\mu}{2}\Pi_{\rho\lambda}\partial^{\alpha}H^{\rho\lambda}, \tag{1}$$

we obtain

$$\frac{dM^{\alpha\beta}}{d\tau} = \frac{d}{d\tau}\left(r^{[\alpha}P^{\beta]}\right) - v^{[\alpha}P^{\beta]} + \mu H^{[\alpha\rho}\Pi_{\rho}{}^{\beta]}. \tag{2}$$

Using the definition of orbital momentum

$$L^{\alpha\beta} = r^{\alpha}P^{\beta} - r^{\beta}P^{\alpha}$$

we can represent the equation (2) as

$$\frac{dM^{\alpha\beta}}{d\tau} = \frac{d}{d\tau}\left(L^{\alpha\beta} + S^{\alpha\beta}\right).$$

It follows that $S^{\alpha\beta}$ is the spin moment of the particle. By separating from $S^{\alpha\beta}$ the factor $\hbar/2$ we come to the dimensionless spin equation

$$\frac{\hbar}{2}\frac{d\,\Pi^{\alpha\beta}}{d\tau} = -v^{[\alpha}P^{\beta]} + \mu H^{[\alpha\rho}\Pi_{\rho}{}^{\beta]}. \tag{3}$$

It is also evident that $\Pi_{\alpha\beta}\left(d\Pi^{\alpha\beta}/d\tau\right) = 0$, i.e. $\Pi_{\alpha\beta}\Pi^{\alpha\beta} = \text{const}$ is well known spin invariant. We emphasize that equation (3) was derived under assumption that the Frenkel condition

$$v_{\alpha}\Pi^{\alpha\beta} = 0 \tag{4}$$

is valid.

If, as usual, the momentum of a particle is defined by relation $P^{\alpha} = mv^{\alpha}$, i.e. momentum and velocity are collinear, the spin equation (3) can be simplified to

$$\frac{\hbar}{2}\frac{d\,\Pi^{\alpha\beta}}{d\tau} = \mu H^{[\alpha\rho}\Pi_{\rho}{}^{\beta]}.$$

This equation differs essentially from experimentally verified BMT equation since formally it does not contain in the pure state the terms with anomalous magnetic moment $\mu_a = \mu - \mu_0 = \mu_0(g-2)/2$. Matters can be improved by replacement

$$P^{\alpha} = mv^{\alpha} + \vec{Z}^{\alpha}. \tag{5}$$

The first term contains a factor

$$m = m_0 \left(1 - \frac{\mu}{2m_0c^2}\, H_{\alpha\beta}\Pi^{\alpha\beta}\right), \tag{6}$$

which can be presented as the mass of a particle with spin. The spin mass (6) was introduced in the works of many authors (see Refs. [7, 14, 17] et al.) by various means. Additional term $\vec{Z}^{\,\alpha}$ must be concerned with anomalous magnetic moment in a way. In general, it leads to noncollinearity of the momentum and the velocity of the spin particle. Taken along, this fact is not unexpected. It is reasonable that the spin particle moving along curved trajectory executes a peculiar trembling motion (Zitterbewegung).

Notice that the relation of the type (5) was first adduced in the original Frenkel theory [1]. Thus we can say that the first definition of spin mass m was made by Ya.I.Frenkel (m is the Langrange uncertain multiplier λ in the Frenkel original theory).

Next we shall assume that the additional term $\vec{Z}^{\,\alpha}$ is space-like vector which satisfies condition

$$v_\alpha \vec{Z}^{\,\alpha} = 0. \tag{7}$$

It follows that in the system of rest the particle energy is equal to mc^2 and contains the potential energy of the intrinsic magnetic moment of the particle (see definition m in (6)). According to (5) and (7) we obtain

$$v_\alpha P^\alpha = -mc^2. \tag{8}$$

By substituting (5) into the spin equation (3) we have

$$\frac{\hbar}{2}\frac{d\Pi^{\alpha\beta}}{d\tau} = -v^{[\alpha}\,\vec{Z}^{\,\beta]} + \mu H^{[\alpha\rho}\Pi_\rho{}^{\beta]}. \tag{9}$$

It is interesting that the spin mass drops out of the equation. To determine $\vec{Z}^{\,\alpha}$ equation (9) should be multiplied by v_β. With regard for the equation of motion (see [7])

$$m\,\frac{dv^\rho}{d\tau} = \frac{e}{c}\, H^{\rho\lambda}v_\lambda + \frac{\mu}{2}\,\Pi_{\alpha\beta}\,\vec{\partial}^{\rho}H^{\alpha\beta}, \tag{10}$$

where

$$\vec{\partial}^{\rho} = \partial^\rho + \frac{1}{c^2}\, v^\rho v_\lambda \partial^\lambda$$

is the space-like derivative and the Frenkel condition (4) we obtain

$$\vec{Z}^{\,\alpha} = \Pi^{\alpha\beta}\left(\frac{\mu\hbar}{4mc^2}\Pi_{\rho\lambda}\,\vec{\partial}_\beta\, H^{\rho\lambda} - \frac{\mu_a}{c^2}H_{\beta\rho}v^\rho\right). \tag{11}$$

Thus, here we can see not only the expected anomalous magnetic moment μ_a but also a gradient in field term which is proportional to $\hbar$. Since $\vec{Z}^{\,\alpha} \sim \hbar^2$, $\hbar(g-2)$ the spin mass in (11) is replaced by the rest mass m_0.

It is significant from definition of $\vec{Z}^{\,\alpha}$ (11) it follows that a free particle does not undergo the spin perturbation of trajectory. If we assume that $g = 2$ (anomalous

magnetic moment is absent) $\vec{Z}^{\alpha}$ will coincide with the expression found by Frenkel[b] in a different way

$$\vec{Z}^{\alpha}|_{g=2} = \frac{1}{4}\frac{\mu_0\hbar}{m_0c^2}\Pi^{\alpha\beta}\Pi_{\rho\lambda}\,\vec{\partial}_{\beta}\,H^{\rho\lambda}.$$

For arbitrary values of g the expression $\vec{Z}^{\alpha}$ in (11) is associated with definition of the momentum in the Corben theory [16].

By substituting $\vec{Z}^{\alpha}$ (11) into equation (9) we obtain the spin equation

$$\frac{d\Pi^{\alpha\beta}}{d\tau} = \frac{\mu}{\hbar s}H^{[\alpha\rho}\Pi_{\rho}{}^{\beta]} + v^{[\alpha}\Pi^{\beta]\rho}\left[\frac{(g-2)e}{2m_0c^3}H_{\rho\lambda}v^{\lambda} - \frac{\mu}{2m_0c^2}\Pi_{\eta\lambda}\vec{\partial}_{\rho}H^{\eta\lambda}\right]. \tag{12}$$

This equation is written with an accuracy to terms of orders $\hbar$, $g-2$. The spin equation (12) was first obtained by H.Corben [16] (see also [19]). In particular case of uniform fields this equation transforms to the tensor form of the BMT spin equation (see [7]).

Instead of the Frenkel condition (4) many authors (see, for example, Ref. [14]) use the auxiliary condition [c]

$$P_{\alpha}\Pi^{\alpha\beta} = 0. \tag{13}$$

But it is very interesting that in the Shirokov formalism the spin equation (3) has the same form as in the Frenkel formalism. (see also in Ref. [20] p.51).

3 Thomas precession as a kinematical spin-orbit effect

The equation (12) is considerably simplified via introduction of a certain effective field with physically distinguished kinematical part which meets the Thomas precession

$$H^{\alpha\beta}_{\text{eff}} = \vec{H}^{\alpha\beta} + \frac{2m_0}{egc}\,v^{[\alpha}w^{\beta]}, \tag{14}$$

where

$$w^{\beta} = \frac{e}{m_0c}\,H^{\beta\rho}v_{\rho},$$

$\vec{H}^{\alpha\beta}$ is the space-like part of an electromagnetic field

$$\vec{H}^{\alpha\beta} = H^{\alpha\beta} + \frac{1}{c^2}\,v^{[\alpha}v_{\rho}H^{\rho\beta]}, \quad v_{\alpha}\,\vec{H}^{\alpha\beta} = 0.$$

---

[b] In notation of Frenkel we have (see formula (22a) in Ref. [1])

$$\vec{Z}^{\alpha} = -\mu^{\alpha\beta}a_{\beta}, \quad a^{\beta} = -\frac{1}{2e_0c}\mu_{\rho\lambda}\partial^{\beta}H^{\rho\lambda}.$$

[c] It will be noted that the condition (13) was first formulated by Yu.M. Shirokov [21] for spin four-vector. As it is known (see, for example, [18]) the spin four-vector S^{μ} is connected with tensor $\Pi^{\alpha\beta}$ by relation

$$S^{\mu} = \frac{1}{2m_0c}\varepsilon^{\mu\nu\alpha\beta}\Pi_{\alpha\beta}P_{\nu}, \quad \Pi^{\alpha\beta} = \frac{1}{m_0c}\varepsilon^{\alpha\beta\rho\sigma}S_{\rho}P_{\sigma}.$$

It follows that in the Shirokov formalism condition (13) have the form $P_{\mu}S^{\mu} = 0$. Sometimes the condition (13) is called as Nakano condition [22].

Then the spin equation (12) takes the simple form

$$\frac{d\,\Pi^{\mu\nu}}{d\tau} = \frac{eg}{2m_0 c} H_{\rm eff}^{[\mu\rho}\Pi_\rho{}^{\nu]}.$$

The equation for spin vector $\boldsymbol{\zeta}$ in the rest frame is also considerably simplified [23, 24]

$$\frac{d\boldsymbol{\zeta}}{dt} = [\boldsymbol{\Omega}\boldsymbol{\zeta}],$$

where

$$\boldsymbol{\Omega} = \boldsymbol{\Omega}_{\rm L} + \boldsymbol{\Omega}_{\rm Th},$$

consists of two fundamentally different parts: the Larmor frequency

$$\boldsymbol{\Omega}_{\rm L} = -\frac{eg}{2m_0 c}\left(\frac{1}{\gamma}\,\boldsymbol{H} - [\boldsymbol{\beta}\boldsymbol{E}] - \frac{\gamma}{\gamma+1}[\boldsymbol{\beta}[\boldsymbol{\beta}\boldsymbol{H}]]\right)$$

and the Thomas precession frequency which, as known, has the kinematical origin ($\boldsymbol{a}$ is the particle acceleration)

$$\boldsymbol{\Omega}_{\rm Th} = -\frac{e}{m_0 c}\,\frac{\gamma}{\gamma+1}\,([\boldsymbol{\beta}\boldsymbol{E}] + [\boldsymbol{\beta}[\boldsymbol{\beta}\boldsymbol{H}]]) = -\frac{1}{c}\,\frac{\gamma^2}{\gamma+1}\,[\boldsymbol{\beta}\boldsymbol{a}].$$

Thus one can compare the kinematical field

$$H_{\rm Th}^{\alpha\beta} = \frac{2m_0}{egc}\,v^{[\alpha}w^{\beta]}$$

with Thomas precession, so that

$$H_{\rm eff}^{\alpha\beta} = \vec{H}^{\,\alpha\beta} + H_{\rm Th}^{\alpha\beta}.$$

The Thomas precession [25] is considered in a large number papers (see [24–26] et al.). Here we show how the separation of spin equations into dynamical and kinematical parts can be carried out via covariant form of spin equation (12).

References

[1] J.Frenkel, *Zs. Phys.* **37**, 243 (1926).

[2] Mc.Graw-Hill, *"Encyclopedia of Physics"*, (McGraw-Hill, N.Y.) "Electron spin", 1983.

[3] L.D.Landau and E.M.Lifshitz, *"Quantum mechanics. Non-Relativistic Theory"*, (Pergamon, Oxford) sec. 54, 1958.

[4] A.A.Sokolov, Yu.M.Loskutov, I.M.Ternov, *"Quantum Mechanics"*, (Holt, Reinhart and Winston, N.Y.) sec. 16, 1966.

[5] H.C.Corben, *Am. J. Phys.* **61**, 551 (1993).

[6] V.Bargmann, L.Michel, and V.L.Telegdi, *Phys. Rev. Lett.* **2**, 435 (1959).

[7] I.M.Ternov, V.A.Bordovitsyn, *Ann. d. Phys.* **39**, 295 (1982).

[8] S.I.Rubinov, J.B.Keller, *Phys. Rev.* **131**, 2789 (1961).

[9] K.Rafanelli, R.Schiller, *Phys. Rev.* **B**135, 279 (1964).

[10] M.Rosen, *Nuovo Cim.* **33**, 1667 (1964).
[11] M.Kolsrud, *Nuovo Cim.* **39**, 504 (1965).
[12] I.M.Ternov, V.A.Bordovitsyn, *Vestn. Mosk. Univ., Ser.III* **21**, N 3, 8 (1980).
[13] V.A.Bordovitsyn, V.S.Gushchina, A.N.Myagkii, *NIM* **A**405, 256 (1998).
[14] S.R.de Groot and L.G.Suttorp, *"Foundation of Electrodynamics"*, (North-Holland, Amsterdam) sec. IV.3., 1972.
[15] H.van Dam and Th.W.Ruijgrok, *Physica* **A**104, 281 (1980).
[16] H.C.Corben, *Phys. Rev.* **121**, 1833 (1961).
[17] V.A.Bordovitsyn, *Izv. Vyssh. Uchebn. Zaved., Fiz.* N 3, 109 (1982).
[18] V.A.Bordovitsyn, I.M.Ternov, *Theor. Math. Phys.* **51**, 327 (1982).
[19] P.Nyborg, *Nuovo Cim.* **31**, 1209 (1964); **32**, 1131 (1964).
[20] C.Teitelboim, D.Villarroel, Ch.G.van Weert, *Riv. Nuovo Cim.* **3**, 1 (1980).
[21] Yu.M.Shirokov, *Zh. Exper. Theor. Fiz.* **21**, 748 (1951).
[22] T.Nakano, *Progr. Theor. Phys.* **15**, 333 (1956).
[23] H.Bacry, *"Theses Dr. Sc. Phys."*, (Masson, Paris) 13, 1963.
[24] V.A.Bordovitsyn, S.V.Sorokin, *Izv. Vyssh. Uchebn. Zaved., Fiz.* N 8, 125 (1983).
[25] L.H.Thomas, *Nature* **117**, 264 (1926).
[26] H.C.Corben, *"Classical and quantum theories of spining particles"*, (Holden-Day, San Francisco) 1964.

LATE GRAVITATIONAL COLLAPSE, QUANTUM MINIHOLES AND THE BIRTH OF A NEW UNIVERSE

M.L. FIL'CHENKOV[a]

Institute of Gravitation and Cosmology, Peoples' Friendship University of Russia, 6 Miklukho-Maklaya Street, Moscow 117198, Russia

Abstract. Quantization of Friedmann's world is considered. The birth of the Universe and creation of a new universe in the laboratory are examples of tunnelling processes. The last stages of the gravitational collapse of compact astrophysical objects (such as stars, quasars and galactic active nuclei) in our space-time are followed by tunnelling into another space-time. A reasonable probability of this tunnelling is obtainable only for miniholes whose properties are briefly discussed.

1 Introduction

The latest stages of gravitational collapse and the earliest stages of evolution of the Universe will be considered. Since these phenomena are taking place at tiny scales, they should be analyzed in the framework of quantum gravity. Without going into details, it is sufficient to say here that we shall use the so-called Wheeler-DeWitt equation $\hat{H}\psi = 0$ ($\hat{H}$ is the Hamiltonian, ψ is the wave function) having the form of Schrödinger's equation for a dependence on only the scale factor and of Klein-Gordon's equation for its dependence on the scale factor and the scalar field [1, 2, 3].

2 Quantization of Friedmann's World

Einstein's equations read:

$$\frac{\dot{a}^2}{2} - \frac{4\pi G\varepsilon a^2}{3c^2} = -\frac{kc^2}{2}, \tag{1}$$

$$\ddot{a} = -\frac{4\pi G}{3c^2}(\varepsilon + 3p)a. \tag{2}$$

The equation of state is

$$p = \alpha\varepsilon. \tag{3}$$

From formulae (1)-(3) we obtain

$$\dot{\varepsilon}a + 3(1+\alpha)\dot{a}\varepsilon = 0. \tag{4}$$

Whence

$$\varepsilon = \varepsilon_0 \left(\frac{a}{r_0}\right)^{-3(1+\alpha)}, \tag{5}$$

where ε_0 and r_0 satisfy the relation

$$\frac{8\pi G\varepsilon_0}{3c^4} = \frac{1}{r_0^2}. \tag{6}$$

In the conformal time η, defined as

$$cdt = ad\eta, \tag{7}$$

[a]e-mail: fil@agmar.ru

the Hamiltonian has the form

$$H = \frac{1}{2}\left(\frac{da}{d\eta}\right)^2 - \frac{4\pi G\varepsilon a^4}{3c^4} + \frac{ka^2}{2} = 0, \tag{8}$$

the Lagrangian is

$$L = \frac{1}{2}\left(\frac{da}{d\eta}\right)^2 + \frac{4\pi G\varepsilon a^4}{3c^4} - \frac{ka^2}{2}. \tag{9}$$

The generalized momentum is defined as

$$P = \frac{\partial L}{\partial(\frac{da}{d\eta})} = \frac{da}{d\eta}. \tag{10}$$

The corresponding momentum operator is

$$\hat{P} = \frac{1}{i} l_{pl}^2 \frac{d}{da}. \tag{11}$$

Replacing the momentum by its operator in (8) and acting by $\hat{H}$ on the wave function ψ, we obtain Wheeler-DeWitt's equation for Friedmann's Universe

$$\frac{d^2\psi}{da^2} - V(a)\psi = 0, \tag{12}$$

where

$$V(a) = \frac{1}{l_{pl}^4}\left(ka^2 - \frac{8\pi G\varepsilon a^4}{3c^4}\right). \tag{13}$$

Generalize the energy density

$$\varepsilon = \varepsilon_0 \sum_{n=0}^{6} B_n (\frac{r_0}{a})^n \tag{14}$$

with

$$\sum_{n=0}^{6} B_n = 1, \tag{15}$$

where

$$n = 3(1+\alpha) \tag{16}$$

also taking account different states of matter other than the de Sitter vacuum (n=0 vacuum, n=1 domain walls, n=2 strings, n=3 dust, n=4 radiation, n=5 perfect gas, n=6 ultrastiff matter).

Separating a term independent of the scale factor in the potential (13), we reduce Wheeler-DeWitt's equation to Schrödinger's

$$-\frac{\hbar^2}{2m_{pl}}\frac{d^2\psi}{da^2} + [U(a) - E]\psi = 0 \tag{17}$$

with

$$V(a) = \frac{2m_{pl}}{\hbar^2}[U(a) - E]. \tag{18}$$

Restricting ourselves to radiation strings and vacuum, we obtain

$$U(a) = \frac{m_{pl}c^2a^2}{2l_{pl}^2}\left(k - B_2 - \frac{B_0a^2}{r_0^2}\right), \tag{19}$$

$$E = \frac{m_{pl}c^2}{2}\left(\frac{r_0}{l_{pl}}\right)^2 B_4. \tag{20}$$

3 Birth of the Universe. Creation of a New Universe in the Laboratory

The Universe is born of the de Sitter vacuum as a result of tunnelling through the potential barrier (19). The penetration factor is [4]

$$D = \exp\{-\frac{2}{\hbar}|\int_{a_1}^{a_2}\sqrt{2m(E-U)}\,da|\}, \tag{21}$$

where $a_1 = 0$, $a_2 = \sqrt{\frac{k-B_2}{B_0}}$, $k - B_2 > 0$, $B_0 > 0$.
For $E = 0$ we have

$$D = \exp\left\{-\frac{2}{3}\left(\frac{r_0}{l_{pl}}\right)^2\frac{(k-B_2)^{3/2}}{B_0}\right\}. \tag{22}$$

Guth and Farhi proposed twelve years ago that the de Sitter vacuum may be created in the laboratory by man-made processes of contraction up to higher densities unachievable by now [5]. Three year later they published the paper where some quantum arguments were presented in favour of this possibility 6. According to these papers at the scale $r_0 \approx 10^{-24}$ cm, typical for Grand Unification, there arises a domain whose mass required to be of the order of 10 kg (which follows from $r_0 \leq r_g$) and the energy density to be about 10^{76} g·cm^{-3}. The process takes place beyond the event horizon, hence a new universe is born in another space, otherwise all would be destroyed by the expanding universe.

If we substitute into (22) $r_0 \approx 10^{-24}$ cm, then for $|k| \leq 1$, $B_0 \leq 1$ and $|B_2| \leq 1$ we obtain

$$D \approx e^{-10^{18}}. \tag{23}$$

As seen from the latter, the birth or creation of a new universe is the most probable for

$$k - B_2 \ll 1. \tag{24}$$

This means that for a closed model we have

$$k = 1, \quad B_0 \ll 1, \quad B_2 \approx 1, \tag{25}$$

i.e. we obtain a string-dominant universe;
for a flat model we have

$$k = 0, \quad B_0 \approx 1, \quad B_2 \ll 1, \tag{26}$$

i.e. we obtain an inflation-dominant universe; for an open model we have

$$k = -1, \quad B_0 \approx 2, \quad B_2 \approx -1, \tag{27}$$

i.e. we obtain an inflation universe with an admixture of strings.

4 The Last Stages of the Gravitational Collapse

The geometry of collapse in a comoving frame of reference is the same as that of Friedmann's closed model [7]. Some difference arises due to a sudden change in the equation of state of the collapsing body from $p = \frac{\varepsilon}{3}$, $p = \frac{2}{3}\varepsilon$, $p = \varepsilon$ to $p = -\varepsilon$. The latter corresponds to the final stage of the gravitational collapse according to Gliner [8].

The potential takes the form

$$U(\gamma) = \frac{m_{pl}c^2}{2}[k\gamma^2 - B_0\gamma^4 - B_1\gamma^3 - B_2\gamma^2 - B_3\gamma - B_5\gamma^{-1} - B_6\gamma^{-2}$$
$$-B_5'(\gamma - \gamma_0)^{-1} - B_6'(\gamma - \gamma_0)^{-2}]. \tag{28}$$

For $\gamma \gg \sqrt[4]{2|E|/mc^2} \gg 1$ and $B_0 = 1$ Schrödinger's equation reduces to

$$\frac{d^2\psi}{d\gamma^2} + \gamma^4\psi = 0 \tag{29}$$

which has a solution

$$\psi = \gamma^{1/2} Z_{1/6}\left(\frac{\gamma^3}{3}\right) \tag{30}$$

with asymptotic behaviour

$$\psi = C_1 e^{i\frac{\gamma^3}{3}} + C_2 e^{-i\frac{\gamma^3}{3}}. \tag{31}$$

This formula corresponds to the classical inflation $\gamma = e^{t/t_{pl}}$ or deflation $\gamma = e^{-t/t_{pl}}$.

For $\gamma - \gamma_0 \ll 1$ and $B_0 = 1$ Schrödinger's equation takes the form

$$\frac{d^2\psi}{d\gamma^2} + \left[{\gamma_0}^4 - \frac{B_5}{\gamma - \gamma_0} + \frac{B_6}{(\gamma - \gamma_0)^2} + \frac{2E}{m_{pl}c^2}\right]\psi = 0. \tag{32}$$

The energy spectrum has a hydrogen-like form

$$E_p = -\frac{B_5'^2 m_{pl}c^2}{8\left(p + \frac{1}{2} + \sqrt{\frac{1}{4} - B_6'}\right)^2} - \frac{{\gamma_0}^4}{2}m_{pl}c^2. \tag{33}$$

A discrete spectrum exists provided

$${\gamma_0}^4 \leq \frac{2|E|}{m_{pl}c^2}, \tag{34}$$

$$B_6' \leq \frac{1}{4}. \tag{35}$$

If one assumes

$$E + Mc^2 = m_{pl}c^2, \tag{36}$$

then we obtain the relation

$${\gamma_0}^4 \leq \frac{2M}{m_{pl}} \tag{37}$$

allowing γ_0 to be estimated for collapsing bodies of different masses.
$\gamma_0 \leq 10^{10}$ for stars $M \sim 10M_\odot$, $\gamma_0 \leq 10^{12}$ for quasars and galactic active nuclei $M \sim 10^9 M_\odot$.

Matching (29) and (32) at $\gamma = \gamma_0 + 1$ simplifies the spectrum at $B_6' = 0 \quad n = p+1$ as follows

$$B_4 = -2n^2 + 2n\sqrt{n^2 - {\gamma_0}^4} \tag{38}$$

where $B_4 = -2{\gamma_0}^4$ at $n = {\gamma_0}^2$ and $B_4 = -{\gamma_0}^4$ for $n \gg {\gamma_0}^2$.

The WKB coefficient for penetration through the potential barrier is given by formula (21). For $|B_4| \gg 1$ we obtain

$$D \approx e^{-2\sqrt[4]{(-B_4)^3}}. \tag{39}$$

$D \leq e^{-10^{29}}$ for stars, $D \leq e^{-10^{35}}$ for stars and galactic active nuclei.

5 Conclusion

We have considered the total cycle from the quantum garavitational collapse of a body to the birth (creation) of new universe. Two approaches presented allowed one to find model parameters in terms of the string contribution to the total energy density(for $E < 0$) and of the mass of a collapsing body (for $E = 0$). This provides a possibility of considering these complicated phenomena from different reasonable viewponts.

Acknowledgement

I am grateful to A.I. Studenikin for providing me the possibility of participating in the 9th Lomonosov Conference on Elementary Particle Physics.

References

[1] B.S. DeWitt, *Phys. Rev.* **160**, 1113 (1967).
[2] A. Vilenkin, *Phys. Rev.* **D 30**, 509 (1984); *Nucl. Phys.* **B 252**, 141 (1985).
[3] M.L. Fil'chenkov, *Phys. Lett.* **B 354**, 208 (1995); **B 441**, 34 (1998).
[4] L.D. Landau, E.M. Lifshitz, *Quantum Mechanics. Nonrelativistic Theory* (Fizmatgiz, Moscow) 1963.
[5] E. Farhi, A.H. Guth, *Phys. Lett.* **B 183**, 149 (1987).
[6] E. Farhi, A.H. Guth, J. Guven, *Nucl. Phys.* **B 339**, 147 (1990).
[7] B.K. Harrison, K.S. Thorne, M. Wakano, J.A. Wheeler, *Gravitational Theory and Gravitational Collapse*, (Univ. Chicago Press, Chicago and London) 1965.
[8] E.B. Gliner, *Zh. Eksp. Teor. Fiz.* **49**, 542 (1965); *DAN SSSR* **192**, 771 (1970); E.B. Gliner, I.G. Dymnikova, *Pis'ma Astron. Zh.* **1**, N 95, 7 (1975); L.E. Gurevich, *Ap. Space Sci* **38**, 67 (1975).

ON ADELIC STRINGS

Branko DRAGOVICH[a]
Institute of Physics, P.O.Box 57, 11001 Belgrade, Yugoslavia, Steklov Mathematical Institute, Moscow, Russia

Abstract. New approach to p-adic and adelic strings, which takes into account that not only world sheet but also Minkowski space-time and string momenta can be p-adic and adelic, is formulated. p-Adic and adelic string amplitudes are considered within Feynman's path integral formalism. The adelic Veneziano amplitude is calculated. Some discreteness of string momenta is obtained. Also, adelic coupling constant is equal to unity.

1. Since ancient times, scientists have been interested in unification of human knowledge on Nature. Superstring theory, recently resulted in the M-theory, is the best modern candidate for "theory of everything". It unifies all fundamental interactions. Gravity, nonabelian gauge symmetry, supersymmetry and space-time dimension are the most significant predictions of string theory. Superstring theory is a synthesis of deep physical principles and modern mathematical methods. In spite of many significant achievements, there are a number of open questions. One of the main actual problems is the space-time structure at the Planck scale. To find an appropriate answer to this problem it seems unavoidable to extend the Riemannian geometry, which is the Archimedean one and related to real numbers, with the non-Archimedean geometry described by p-adic numbers. The corresponding mathematical instrument suitable for unification of Archimedean and non-Archimedean geometries, as well as of real and p-adic numbers, is the space of adeles.

Recall that the field of rational numbers Q plays an important role not only in mathematics but also in physics. All numerical results of measurements belong to Q. On Q there is the usual ($|\cdot|_\infty$) and p-adic ($|\cdot|_p$) absolute value, where p denotes a prime number. Completion of Q with respect to $|\cdot|_\infty$ and $|\cdot|_p$ yields the field of real ($R \equiv Q_\infty$) and p-adic (Q_p) numbers, respectively. Many properties of p-adic numbers and their functions 1 are very different in comparison with real numbers and classical analysis. Any $x \in Q_p$ can be presented in the form

$$x = p^\nu (x_0 + x_1 p + x_2 p^2 + \cdots), \quad x_0 \neq 0, \quad \nu \in Z, \tag{1}$$

where $x_i \in \{0, 1, ..., p-1\}$.

An adele a 2 is an infinite sequence

$$a = (a_\infty, a_2, a_3, ..., a_p, ...), \tag{2}$$

where $a_\infty \in R$ and $a_p \in Q_p$ with restriction that $a_p \in Z_p = \{x \in Q_p : x = x_0 + x_1 p + x_2 p^2 + \cdots\}$ for all but a finite set S of primes p. The set of all adeles A may be given in the form

$$A = \bigcup_S \mathcal{A}(S), \quad \mathcal{A}(S) = R \times \prod_{p \in S} Q_p \times \prod_{p \notin S} Z_p. \tag{3}$$

A has the structure of a topological ring.

[a]e-mail: dragovic@phy.bg.ac.yu

2. Since 1987, p-adic numbers and adeles have been successfully used in many branches of theoretical and mathematical physics (for a review, see, e.g. 3, 4, and 5). First applications were just in string theory. It was suggested 6 a hypothesis on the possible emergence of a non-Archimedean geometry at the Planck scale and initiated the corresponding string theory over Q_p and the Galois fields. It was also proposed generalization of the usual Veneziano and the Virasoro-Shapiro amplitude using multiplicative characters over various number fields. In 7, the Veneziano and the Virasoro-Shapiro p-adic string amplitudes are postulated as the Gel'fand-Graev beta functions, which are convolutions of the real-valued characters on the p-adic fields. After that it was put forward an interesting formula 8: the product of the Veneziano amplitude and its p-adic counterparts is equal to unity. In other words, the Veneziano amplitude can be presented as the infinite product of inverses of p-adic amplitudes. The similar property holds for the Virasoro-Shapiro amplitude. The product of an ordinary string amplitude and the corresponding p-adic counterparts is usually called adelic string amplitude. However, such adelic string amplitudes must be regularized 9 and they are not equal to a constant in a more complex case. This situation has been an obstacle to further progress in application of p-adic numbers in string theory. It seems to be a consequence of restricted employment of p-adic numbers in string amplitudes. In fact, a general feature of all these investigations was that only world sheet may be treated p-adically, while target space-time and momenta should be described by real numbers.

3. According to successful formulation of p-adic 10 and adelic 11 quantum mechanics, approach to p-adic and adelic string amplitudes should be modified. Here we give a new proposal to p-adic and adelic string amplitudes based on the following general assumptions:

(i) space-time and matter are adelic at the Planck (string) scale,

(ii) the Feynman path integral is an essential constituent of quantum theory,

(iii) ordinary classical and quantum theories are effective limits of the adelic ones.

Thus, a string is adelic, and has real and all p-adic faces simultaneously. We use term real (p-adic) string when we consider as dominant its real (p-adic) characteristics. In addition to the adelic Minkowski space-time, string world sheet and momenta are also adelic. However, string amplitude remains complex-valued in all these cases.

Recall that quantum amplitudes defined by means of path integral may be symbolically presented as

$$A(K) = \int A(X)\chi\left(-\frac{1}{h}S[X]\right)\mathcal{D}X, \tag{4}$$

where K and X denote classical momenta and configuration space, respectively. $\chi(a)$ is an additive character, $S[X]$ is a classical action and h is the Planck constant.

4. In the sequal, we briefly consider simple p-adic and adelic bosonic string amplitudes based on the functional integral (4). As is known 12, the scattering of two real bosonic strings in 26-dimensional space-time at the tree level can be described in terms of the path integral in 2-dimensional quantum field theory formalism as follows:

$$A_\infty(k_1, ..., k_4) = g_\infty^2 \int \mathcal{D}X \exp\left(\frac{2\pi i}{h}S_0[X]\right)$$

$$\times \prod_{j=1}^{4} \int d^2\sigma_j \exp\left(\frac{2\pi i}{h} k_\mu^{(j)} X^\mu(\sigma_j, \tau_j)\right), \tag{5}$$

where $\mathcal{D}X = \mathcal{D}X^0(\sigma,\tau)\mathcal{D}X^1(\sigma,\tau)...\mathcal{D}X^{25}(\sigma,\tau)$, $d^2\sigma_j = d\sigma_j d\tau_j$ and

$$S_0[X] = -\frac{T}{2}\int d^2\sigma \partial_\alpha X^\mu \partial^\alpha X_\mu \tag{6}$$

with $\alpha = 0, 1$ and $\mu = 0, 1, ..., 25$. Using the usual procedure 12 one can obtain the crossing symmetric Veneziano amplitude

$$A_\infty(k_1, ..., k_4) = g_\infty^2 \int_R |\, x \,|_\infty^{k_1 k_2} |\, 1 - x \,|_\infty^{k_2 k_3}\, dx \tag{7}$$

and similarly the Virasoro-Shapiro one for closed bosonic strings. As p-adic Veneziano amplitude, it was postulated 7 p-adic analogue of (7), i.e.

$$A_p(k_1, ..., k_4) = g_p^2 \int_{Q_p} |\, x \,|_p^{k_1 k_2} |\, 1 - x \,|_p^{k_2 k_3}\, dx, \tag{8}$$

where only the string world sheet (parametrized by x) is p-adic.

Expressions (7) and (8) are Gel'fand-Graev beta functions on R and Q_p, respectively. However, (8) cannot be derived from p-adic analogue of (5) and one may doubt validity of (8) as a p-adic string amplitude. Therefore, we take p-adic analogue of (5), i.e.

$$A_p(k_1, ..., k_4) = g_p^2 \int \mathcal{D}X \chi_p\left(-\frac{1}{h} S_0[X]\right)$$

$$\times \prod_{j=1}^{4} \int d^2\sigma_j \chi_p\left(-\frac{1}{h} k_\mu^{(j)} X^\mu(\sigma_j, \tau_j)\right), \tag{9}$$

to be p-adic string amplitude, where $\chi_p(u) = \exp(2\pi i \{u\}_p)$ is p-adic additive character and $\{u\}_p$ is the fractional part of $u \in Q_p$. In (9), all space-time coordinates X_μ, momenta k_i and world sheet (σ, τ) are p-adic.

Evaluation of (9), in an analogous way to the real case, leads to

$$A_p(k_1, ..., k_4) = g_p^2 \prod_{j=1}^{4} \int d^2\sigma_j$$

$$\times \chi_p\left(\frac{\sqrt{-1}}{2hT} \sum_{i<j} k_i k_j \log((\sigma_i - \sigma_j)^2 + (\tau_i - \tau_j)^2)\right). \tag{10}$$

Since p-adic character χ_p is complex-valued and logarithmic function is p-adic valued, amplitude (10) cannot be reduced to (8). p-Adic logarithmic function is

$$\log x = \sum_{n=1}^{\infty} (-1)^{n+1} \frac{(x-1)^n}{n}, \quad |\, x - 1 \,|_p < 1. \tag{11}$$

Due to (10) and (11) one obtains the system of equations

$$(\sigma_i - \sigma_j)^2 + (\tau_i - \tau_j)^2 \in 1 + pZ_p, \quad (i < j), \quad i, j = 1, ..., 4, \tag{12}$$

which determines possible p-adic values of the world sheet parameters σ_i and τ_i. Since (10) can be rewritten as

$$A_p(k_1, ..., k_4) = g_p^2 \prod_{j=1}^{4} \int d^2\sigma_j \chi_p(\sqrt{-1}$$

$$\times \log \prod_{i<j} ((\sigma_i - \sigma_j)^2 + (\tau_i - \tau_j)^2)^{\frac{k_i k_j}{2hT}}) \tag{13}$$

it has to be also satisfied

$$\prod_{i<j} ((\sigma_i - \sigma_j)^2 + (\tau_i - \tau_j)^2)^{\frac{k_i k_j}{2hT}} \in 1 + pZ_p. \tag{14}$$

Combining (12) and (14) one gets

$$\prod_{i<j} (1 + pZ_p)^{\frac{k_i k_j}{2hT}} \in 1 + pZ_p, \tag{15}$$

what is satisfied if

$$\mid \frac{k_i k_j}{2hT} \mid_p \leq 1. \tag{16}$$

Since in experiments $k_i, k_j \in Q$ and (17) has place for every p, it follows that string momenta have discrete values in units $h = T = 1$.

Amplitude (14) becomes

$$A_p(k_1, ..., k_4) = g_p^2 \prod_{j=1}^{4} \int d^2\sigma_j, \tag{17}$$

because $\chi_p(\sqrt{-1} \log u) = 1$.

5. Adelic string amplitude is product of real and all p-adic amplitudes, i.e.

$$A_A(k_1, ..., k_4) = A_\infty(k_1, ..., k_4) \prod_p A_p(k_1, ..., k_4). \tag{18}$$

In the case of the Veneziano amplitude and $(\sigma_i, \tau_j) \in \mathcal{A}(S) \times \mathcal{A}(S)$, where $\mathcal{A}(S)$ is defined in (3), we have

$$A_A(k_1, ..., k_4) = g_\infty^2 \int_R \mid x \mid_\infty^{k_1 k_2} \mid 1 - x \mid_\infty^{k_2 k_3} dx$$

$$\times \prod_{p \in S} g_p^2 \prod_{j=1}^{4} \int d^2\sigma_j \times \prod_{p \notin S} g_p^2. \tag{19}$$

There is a sense to take adelic coupling constant as

$$g_A^2 = | g |_\infty^2 \prod_p | g |_p^2 = 1, \quad 0 \neq g \in Q. \tag{20}$$

At the end, it follows that p-adic effects in the adelic Veneziano amplitude induce discreteness of string momenta and contribute to an effective coupling constant in the form

$$g_{ef}^2 = g_A^2 \prod_{p \in S} \prod_{j=1}^{4} \int d^2\sigma_j \geq 1.$$

Acknowledgements

The author wishes to thank A.I. Studenikin and the Organizing Committee of the 9th Lomonosov Conference on Elementary Particle Physics for invitation to participate and give a talk.

References

[1] W.H.Schikhof, *Ultrametric Calculus: an introduction to p-adic analysis*, (Cambridge University Press, Cambridge) 1984.
[2] I.M.Gel'fand, M.I.Graev and I.I.Piatetskii-Shapiro, *Representation Theory and Automorphic Functions*, (Nauka, Moscow) 1966.
[3] L.Brekke and P.G.O.Freund, *Phys. Rep.* **233**, 1 (1993).
[4] V.S.Vladimirov, I.V.Volovich and E.I.Zelenov, *p-Adic Analysis and Mathematical Physics*, (World Scientific, Singapore) 1994.
[5] A.Khrennikov, *p-Adic Distributions in Mathematical Physics*, (Kluwer Acad. Publishers, Dordrecht) 1994.
[6] I.V.Volovich, *Class. Quantum Grav.* **4**, L83 (1987).
[7] P.G.O.Freund and M.Olson, *Phys. Lett. B* **199**, 186 (1987).
[8] P.G.O.Freund and E.Witten, *Phys. Lett. B* **199**, 191 (1987).
[9] I.Ya.Aref'eva, B.Dragovich and I.V.Volovich, *Phys. Lett. B* **209**, 445 (1988).
[10] V.S.Vladimirov and I.V.Volovich, *Commun. Math. Phys.* **123**, 659 (1989).
[11] B.Dragovich, *Teor. Mat. Fizika* **101**, 1404 (1994).
[12] M.B.Green, J.H.Schwarz and E.Witten, *Superstring Theory*, (Cambridge University Press, Cambridge) 1984.

Collider searches for TeV scale Quantum Gravity with compact extra dimensions

P.Azzurri [a]
Laboratoire de l'Accélérateur Linéaire, IN2P3-CNRS
Univerisité Paris-Sud, B.P.34 F-98189 Orsay-CEDEX, France

Abstract. We review capabilities of collider experiments to detect signals of quantum gravity effects near the electro-weak scale, that could be observable in the framework of recently proposed scenarios of a low scale gravity propagating into large compact extra-dimensions. Most of the experimental data results presented are preliminary and subject to modifications.

1 Introduction

The enormity of the ratio between the scales of the gravitational interaction (set by the the Plank mass $M_P \sim G_N^{-1/2} \sim 10^{19}\,\mathrm{GeV}$) and the electro-weak interactions (set by $M_{EW} \sim 10^2\,\mathrm{GeV}$ is a major unresolved question of contemporary physics, known as the hierarchy problem. It has been suggested recently by Arkani-Hamed, Dimopoulos and Dvali (ADD) [1] that gravity may become strong at energies close to the electro-weak scale, offering a radical solution to the hierarchy problem. Under the hypothesis of the existence of n additional compact dimensions, a simple argument based on the Gauss law in arbitrary dimensions shows that the Plank scale is related to the radius of compactification (R) of the n extra dimensions by

$$M_P^2 \sim R^n M_S^{n+2}, \tag{1}$$

where M_S is the $(4+n)$-dimensional, fundamental gravitational scale. Thus the largeness of the 4-dimensional Plank scale (or smallness of the Newton's constant) can be attributed to the existence of large extra dimensions of volume R^n. Setting the gravitational scale near the electro-weak scale $M_S \sim 1\mathrm{TeV}$ in this scenario, offers a solution to the original gauge hierarchy problem, and leads to a rich low-energy phenomenology [2].

In order to evade the very strong constraints from electro-weak precision measurements on such theories with large extra dimensions, all Standard Model (SM) fields are assumed to propagate only on the ordinary four-dimensional hypersurface, while gravity can propagate in the extra dimensions.

1.1 Constraints from macroscopic gravitational experiments

Experimental searches for deviations from Newton's law of universal gravitation [3] commonly parametrise such possible new long-range gravitational forces as additional Yukawa interactions modifying the interaction potential as $V = -(G_N m_1 m_2/r_{12})\,[1+\alpha\exp(-r_{12}/\lambda]$, where α is the strength of the Yukawa force relative to gravity and λ is the range. The current experimental limits on α and λ are illustrated in Fig.1. In the ADD scenario of gravity propagating in compact extra dimensions if we impose $M_S \sim 1\mathrm{TeV}$ in equation 1, we obtain

$$R \sim 10^{31/n-17}\,\mathrm{cm}, \tag{2}$$

[a] e-mail: Paolo.Azzurri@cern.ch

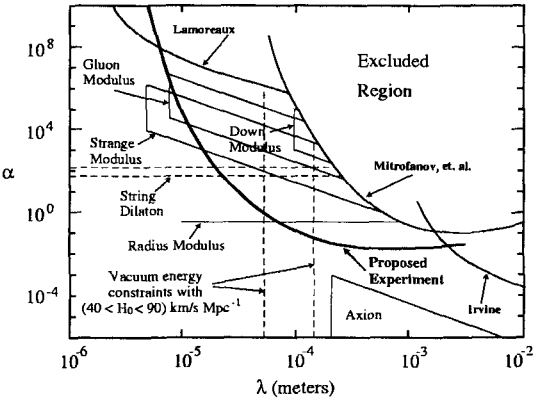

Figure 1: Parameter space for new gravitational Yukawa-type forces where α is the strength relative to gravity and the range λ. Limits from experiments are shown (bold lines), as well as some specific predictions for new long range forces (fine and dashed lines).

and we would observe Yukawa violations of Newton's law of magnitude $\alpha = 2n$ and range $\lambda = R$. As the experimental excluded region is $\lambda < 1$mm (for $\alpha > 2$), $n = 1$ is clearly impossible as it would imply $R \sim 10^8$Km (deviations of classical gravity on planetary scales), while $n \geq 2$ is allowed, as it implies $R \leq 1$mm, where Newton's law has not yet been tested.

1.2 Constraints from astrophysics and cosmology

Astrophysics bounds on the ADD framework come from the fact that strongly coupled gravitons can be produced copiously and escape in the extra dimensions, carrying away energy, for example from a hot supernova core. The phenomenology of supernova SN 1987A places strong constraints on this energy loss and allows to derive a bound on the fundamental Planck scale $M_S \geq 50$TeV for $n = 2$ [4]. Cosmological constraints derive from the possible presence of Cosmic Diffuse Gamma radiation (CDG) from graviton decays (e.g. in the process $\nu\bar{\nu} \to G \to \gamma\gamma$). The comparison of the predicted graviton contribution to the CDG spectrum with the measurements of the COMPTEL instrument lead to $M_S \geq 110$TeV for $n = 2$ [5]. These bounds disfavour a solution of the hierarchy problem in the ADD scenario for $n = 2$, so we shall pay attention to $n \geq 3$.

2 Phenomenology at collider experiments

The higher dimensional gravitons of the ADD scenario would appear in our four dimensional world, as towers of "Kaluza-Klein" (KK) modes, massive particles whose mass is determined by their momentum in the extra-dimensions, and is quantised in units of $1/R$. Starting from the linearised gravity (Fiertz-Pauli) Lagrangian, and performing the reduction to the four non-compactified dimensions, the $(4+n)$-dimensional graviton field is decomposed different four dimensional fields: one spin-

two field, $(n-1)$ spin-one fields and $n(n-1)/2$ spin-zero fields, and each of them is a expansion of KK modes as

$$h_{\mu\nu}(x,y) = \sum_n h^n_{\mu\nu}(x) \exp\left(i\frac{2\pi n \cdot y}{R}\right) \qquad (\text{spin}-2), \tag{3}$$

$$A_{\mu i}(x,y) = \sum_n A^n_{\mu i}(x) \exp\left(i\frac{2\pi n \cdot y}{R}\right) \qquad (\text{spin}-1), \tag{4}$$

$$\phi_{ij}(x,y) = \sum_n \phi^n_{ij}(x) \exp\left(i\frac{2\pi n \cdot y}{R}\right) \qquad (\text{spin}-0) \tag{5}$$

where $n = (n_1, \ldots, n_n)$ represent the KK states, $x = (x_0, x_1, x_2, x_3)$ are ordinary coordinates, $y = (y_1, \ldots, y_n)$ are coordinates in extra dimensions, $\mu, \nu = 0, 1, 2, 3$ and $i, j = 5, \ldots, 4+n$.

2.1 *Couplings of KK gravitons to matter*

Because of our ignorance about the underlying quantum gravity theory, only an Infrared effective theory of KK graviton interactions can be used to predict interaction rates. Such effective theory will be valid below the fundamental scale M_S and the contribution of the unknown ultraviolet physics is reabsorbed in unknown coefficients of the effective theory. In such low energy limit, the coupling of KK gravitons to SM particles is determined by general covariance, with a contribution to the interaction Lagrangian given by

$$\mathcal{L}_I = -\frac{1}{M_P} G^n_{\mu\nu} T^{\mu\nu}. \tag{6}$$

From equation 6 it follows that the $n(n-1)/2$ spin-zero gravitons all decouple from ordinary SM matter, except for the one that couples to the trace of the four dimensional energy-momentum tensor ($T^{\mu\nu}$), so that there is a scalar graviton field coupling at tree level proportionally to the mass of ordinary particles. The $(n-1)$ spin-one gravitons decouple completely from $T^{\mu\nu}$ and SM particles, playing no role. On the contrary the spin-two KK gravitons couple directly to $T^{\mu\nu}$, giving a large variety of couplings to the Electro-Weak and QCD theories[6]: some of such couplings are depicted in figure 2.

We will now discuss the possibilities of studying graviton productions or the effects of virtual graviton exchanges at high energy collider experiments.

2.2 *Rates for KK graviton emissions*

Experimentally KK gravitons can be produced at colliders in processes like $f\bar{f} \to \gamma G$, $f\bar{f} \to gG$, $f\bar{f} \to ZG$, $qg \to qG$ and $gg \to gG$. Even though the amplitude of the coupling of each single KK graviton to matter is suppressed by $1/M_P$, their mass splittings are very small compared to collider typical energies, so that a large number of different KK modes are accessible. Summing up the contributions of all KK modes compensates the $1/M_P$ factor and leads to a final squared amplitude suppressed by powers of M_S, $|A|^2 \sim 1/M_S^n$. Once produced, the $1/M_P$ suppression in the graviton decay rate into ordinary matter is not compensated by phase space and therefore its lifetime is $\tau_G \sim M_P^2/m_G^3 \sim (\text{TeV}/M_G)^3 10^3$ seconds. For experimental purposes, this means that the KK gravitons behave like massive, non-interacting, stable particles,

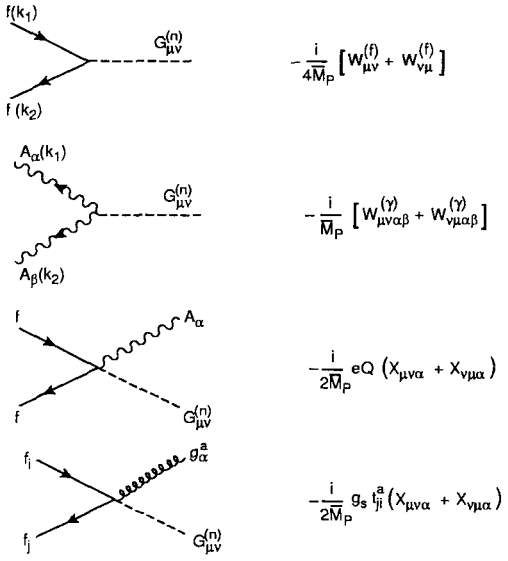

Figure 2: Some Feynman rules for Kaluza-Klein spin two graviton couplings to SM fields.

and its collider signatures are imbalance in final state momenta and missing mass. The emitted gravitons will have a distribution in mass described by the cross-section for producing single KK modes of a given mass, corresponding to the probability of emitting gravitons with different momenta in the extra dimensions.

2.3 Rates for KK graviton virtual exchanges

When evaluating the effects of virtual-graviton exchanges at tree level in scattering processes, the sum over the infinite tower of KK modes is dominated by the ultraviolet contributions so that a cutoff Λ, of order M_S has to be introduced. For phenomenological applications the amplitude of the physical process is then $A \sim q^2/\Lambda^4 \sim q^2/M_S^4$, where q^2 is the exchanged invariant mass. The rate for a pure graviton exchange process will then be suppressed by a factor $\sim 1/M_S^8$, while the SM-graviton interference terms will be suppressed by $\sim 1/M_S^4$, with a unknown phase sign with respect to the SM scattering amplitude. Moreover the graviton exchange operator gives a pure spin two (d-wave) contribution to the scattering process, a peculiar signature of the graviton presence.

3 Searches at e^+e^- colliders

The LEP e^+e^- collider at CERN has been operating since 1989. During its first phase (LEP-I, 1989-1995) it has been working at the Z resonance ($\sqrt{s} \simeq 91$GeV) delivering

about 5 million hadronic Z decays to the four experiments (ALEPH,DELPHI,OPAL,L3). During the second phase (LEP-II, 1995-2000) it has delivered up to 1999 a luminosity of about 500 pb^{-1} to each experiment at $\sqrt{s}$ ranging from 130GeV to 202GeV .

3.1 Direct search for $Z \to f\bar{f}\ G$ *at LEP-I*

The Z decay into $f\bar{f} + G$ is the best probe of the scalar (spin zero) KK modes of the graviton, as the scalar graviton (G_0) coupling to matter fields is proportional to their masses (in this case m_Z), and in other possible higher energy processes that may probe G_0 (as $f\bar{f} \to WG, ZG$, $f\bar{f} \to WW, WZ, ZZ$), the contribution of G_0 relative to G_2, is much more suppressed due to the higher energies. The expected Z branching ratio for this signal is proportional to $(M_Z/M_S)^{n+2}$, and the signature of the process is the presence of a virtual Z decay to $f\bar{f}$ accompanied by missing energy carried away by the graviton. The expected distribution of the emitted graviton mass (i.e. the missing mass) for different values of n is shown in figure 3.

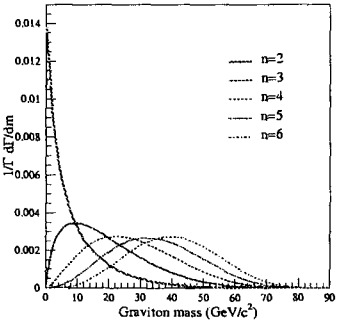

Figure 3: Normalised differential decay width of $Z \to f\bar{f}\ G$ as a function of the graviton mass and for different n, the number of compact extra dimensions.

Results from the ALEPH experiment [9], based on the search of acoplanar jet pairs in 4×10^6 hadronic Z decays, find no candidate events with an expected background of 1.4 events. From this results 95% Confidence Level (CL) limits M_S^{95} on M_S are calculated as a function of n, and vary from $M_S^{95} = 0.35$TeV for $n = 2$, to $M_S^{95} = 0.22$TeV for $n = 3$, down to $M_S^{95} = 0.12$TeV for $n = 6$.

3.2 Direct search for $e^+e^- \to \gamma G$ *at LEP-II*

Real gravitons can still be produced at the higher LEP-II energies directly via the process $e^+e^- \to \gamma G$, carrying away energy in the extra dimensions. Such process would manifests itself through an enhancement of the single photon cross section, and modifications of the expected single photon polar angle and energy distributions. The differential cross section for the graviton production is proportional to

$\alpha_{em}/s(\sqrt{s}/M_S)^{n+2}$, and is also a function of the fraction x_γ of the beam energy taken by the photon and of its polar emission angle θ, relative to the beam.

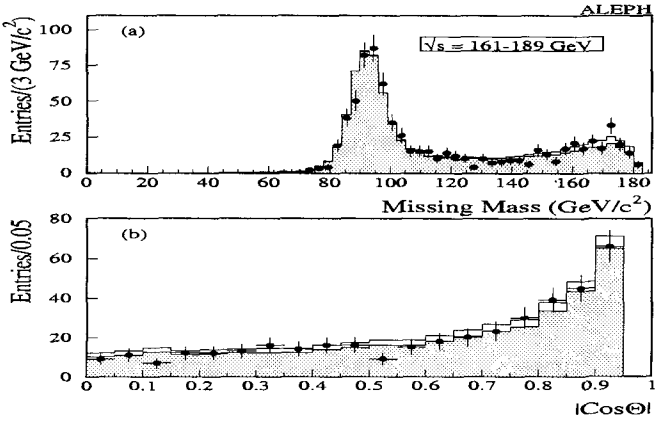

Figure 4: (a) Invariant missing mass distribution recoiling against the photon. (b) The polar angle (θ) distribution of the photon. The points with error bars are the combined data sample at $\sqrt{s} = 161 - 189$GeV , the shaded histogram is the normalised SM expectation, and the open histogram shows the expected γG additional contribution for two extra dimensions and M_S at the lower limit of 0.99 TeV.

The invariant mass distribution of the system recoiling against selected photon candidates and the distribution of the polar angle of the same photons for the ALEPH data sample [9] are shown in figure 4. These distributions are dominated by radiative returns to the Z , where the Z decays invisibly to $\nu\bar{\nu}$. The simulated detection efficiencies for the real graviton plus photon signals range from 0.45 (for $n = 2$) to 0.30 (for $n = 10$). As no significant statistical signal is observed, 95% CL lower limits are placed by the four LEP experiments on the fundamental mass scale M_S as a function of the number n of extra dimensions. The obtained limits for each individual experiment [9,10,14,19] range from $M_S^{95} \simeq 1.0$TeV for $n = 2$, to $M_S^{95} \simeq 0.8$TeV for $n = 3$, down to $M_S^{95} = 0.5$TeV for $n = 6$ and $M_S^{95} = 0.3$TeV for $n = 10$.

3.3 Direct search for $e^+e^- \to Z\ G$ *at LEP-II*

The direct graviton production associated with a Z boson has been studied by the L3 experiment [15], complementing the $G\gamma$ direct search. Only single hadronic Z decays are searched for, with a signal efficiency of 0.87, where in this case the selection analysis is made independent of n. Again the signal cross section is expected to be $\sigma_{ZG} \sim 1/M_S^{n+2}$ but no significant excess was found in the data up to $\sqrt{s} = 189$GeV .

A fit to the visible mass distribution of figure 5 yields 95% CL cross section limits and the corresponding lower limits on M_S as a function of n. The extracted results are $M_S^{95} = 0.6$TeV for $n = 2$, degraded to $M_S^{95} = 0.3$TeV for $n = 4$.

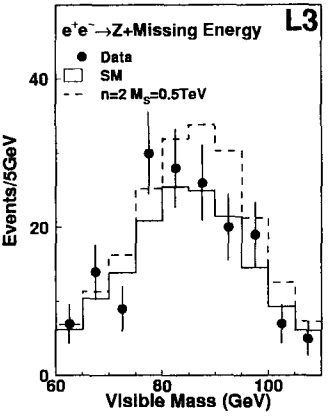

Figure 5: Visible mass for $e^+e^- \to Z\ G$ candidate events at $\sqrt{s}$ =188.7 GeV together with SM expectations, dominated by W pair and single W production. The effect of real graviton production with two extra space dimensions and $M_S = 1$TeV is also shown

3.4 Search for graviton exchanges in $e^+e^- \to \gamma\gamma$ *at LEP-II*

The s-channel KK graviton exchanges modify the SM differential cross section for photon pair production in e^+e^- collisions $d\sigma_{\gamma\gamma}/d\cos\theta$ by a term proportional to $\lambda s/M_S^4$, where λ can incorporate other possible model dependences but for simplicity it is chosen to be ± 1 just to allow for different signs in the interference.

All four LEP experiments have analysed their two-photon data samples searching for virtual graviton exchanges effects [9,12,13,17]. The two-photon polar angle distribution obtained by ALEPH is shown in figure 6, as no significant deviation from SM expectations is observed, 95% C.L. lower limits on M_S are derived for $\lambda = \pm 1$, leading to $M_S^{95} \simeq 0.7$TeV for each individual experiment with the data up to $\sqrt{s} = 189$GeV .

3.5 Search for graviton exchanges in $e^+e^- \to f\bar{f}$ *at LEP-II*

Also the $e^+e^- \to f\bar{f}$ SM differential cross sections would be modified due to the interference of additional s-channel spin two graviton exchange amplitudes. All LEP experiments results on difermion measurements at $\sqrt{s} = 130 - 189$GeV of differential cross sections $d\sigma_{f\bar{f}}/d\cos\theta$ for $f\bar{f} = e^+e^-, \mu^+\mu^-, \tau^+\tau^-, q\bar{q}$ have been searched for graviton exchange effects [9,11,16,18], the distributions from the L3 analysis of Bhabha events are shown in figure 7.

Again, as no signal-like deviation from the SM is observed, maximum likelihood fits are made to estimate 95% CL lower limits on the M_S parameter. The limits obtained by each experiment depend on the analysed $f\bar{f}$ channel and are: $M_S^{95} \simeq 0.8$TeV from e^+e^- events, $M_S^{95} \simeq 0.6$TeV from $\mu^+\mu^-$ events, $M_S^{95} \simeq 0.5$TeV from $\tau^+\tau^-$ events, and $M_S^{95} \simeq 0.5$TeV from $q\bar{q}$ events. These results show how the Bhabha channel is in fact the most sensitive to reveal possible virtual graviton exchanges.

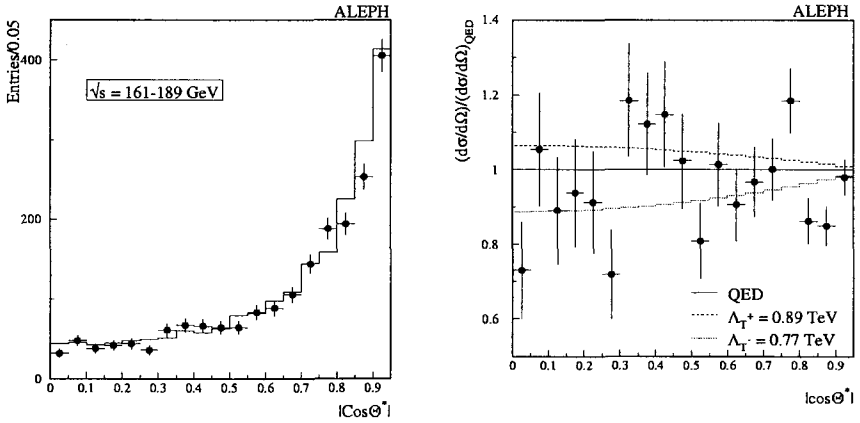

Figure 6: (left) The polar production angle (θ^*) for $e^+e^- \to \gamma\gamma$, with θ^* calculated in the two-photon rest frame. The points with error bars are the combined data sample for $\sqrt{s} = 161 - 189$GeV , the open histogram shows the absolutely normalised SM prediction (with some Bhabha contaminations). (right) The ratio of observed to SM predicted differential $e^+e^- \to \gamma\gamma$ cross section as a function of $\cos(\theta^*)$. The dashed and dotted lines correspond to the ratios which include the effects from virtual graviton exchanges, with $\Lambda_T^{\pm}$ (a cutoff with $\Lambda_T^4 = M_S^4\pi/2$) set to its 95% C.L. measured lower limits.

3.6 Search for graviton exchanges in $e^+e^- \to WW, ZZ$ *at LEP-II*

The contribution of virtual graviton exchange to the pair production of heavy bosons affects both the total cross-section and the angular distribution of the production angle. Such distributions have been studied by the L3 experiment [15], investigating for possible light scale gravity signals. Contrary to the fermion pair productions, where important distortions of the angular distributions occur, the signal effects in boson pair productions are mainly expected in the total cross section measures. The data distributions are analysed and a likelihood in terms of λ/M_S^4. No significant deviations from the SM are found and the likelihood functions are then integrated over the physical region for $\lambda = +1$ and $\lambda = -1$, to yield again 95% CL on M_S, with $M_S^{95} \simeq 0.8$TeV from Z Z processes, and $M_S^{95} \simeq 0.8$TeV from W^+W^-processes.

3.7 Combined results for virtual graviton effects at LEP-II

Assuming that the meaning of the cutoff parameter is the same for all investigated processes, it is possible to combine the likelihood curves obtained by all pair production processes into a single one, as done by the L3 collaboration and displayed in figure 8.

The combined 95% CL lower limits on M_S are $M_S^{95} = 0.9 - 1.0$TeV for $\lambda = +1$ or $\lambda = -1$, such limits are dominated by the sensitivity in the Bhabha, Z Z and W^+W^-channels.

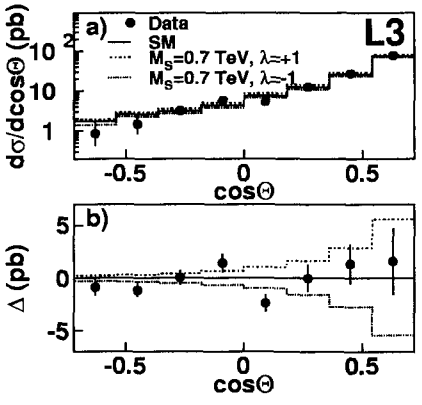

Figure 7: a) Differential cross section for Bhabha scattering in data and the SM expectations. Low Scale Gravity modifications for $M_S = 0.7$TeV are also displayed for $\lambda = \pm 1$ interference with the SM process. b) Differences Δ of the above with SM prediction.

4 Searches at e^+p colliders

The HERA collider enables the study of deep inelastic neutral current (NC) scattering $e^+p \rightarrow e^+ X$ at high momentum transfers $Q^2 \simeq 10^2 - 10^5 \mathrm{GeV}^2$, probing the structure of eq interactions at very short distances. The H1 experiment had analysed its data samples, corresponding to an integrated luminosity of 36 pb$^-$1 collected at $\sqrt{s} = 300$GeV , in search for low scale gravity effects [21].

The contributions of virtual graviton exchanges to deep inelastic scattering have been derived from ref.[6], applying the basic processes of elastic $e^+ q \rightarrow e^+ q$ and $e^+ g \rightarrow e^+ g$ scattering. Again the strength of graviton exchange to the cross section is characterised by the ratio λ/M_S^4. The differential cross section is fitted to the λ/M_S^4 parameter and as the result is compatible with the SM, lower limits at 95% CL are derived, yielding $M_S > 0.48$TeV for $\lambda = +1$ and $M_S > 0.72$TeV for $\lambda = -1$. Possible effects of graviton exchange in the data, as given by such exclusion limits, are illustrated in figure 9.

5 Searches at $p\bar{p}$ colliders

5.1 Searches for real graviton emissions at hadron colliders

Hadron colliders offer as well a rich phenomenology for low scale gravity scenarios. Direct real graviton productions can occur from subprocesses $q\bar{q} \rightarrow qG$, $qg \rightarrow qG$, $gg \rightarrow qG$ and $q\bar{q} \rightarrow \gamma G$. For the fist three processes the experimental signal would be $p\bar{p} \rightarrow$ jet + $\not{E}_T$, where $\not{E}_T$ is the event transverse missing energy. The last process would originate events with a photon and missing energy but would be expected to have a lower rate caused by the smallness of the electromagnetic coupling and

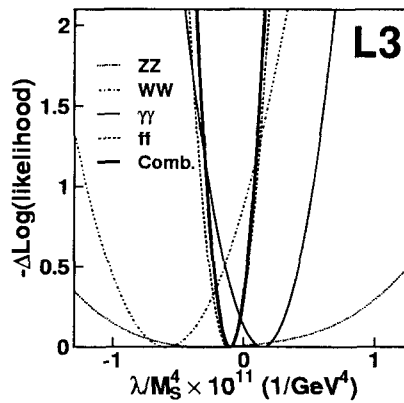

Figure 8: Difference with respect to the minimum of the negative logarithm of the individual and combined likelihood functions of the LEP2 vector boson pair, and fermion pair production data, in terms of λ/M_S^4.

the lower luminosity of $q\bar{q}$ over qg at large values of $\hat{s}/s$ in pp collisions. The SM background to these kind of signals at hadron colliders would the the transverse production of a Z boson decaying invisibly $Z \rightarrow \nu\bar{\nu}$, together with a parton or a photon. The sensitivity reach expected from these kind of signals at the Tevatron ($\sqrt{s} = 2$TeV) range from $M_S \simeq 0.8$TeV with $n = 4$ to $M_S \simeq 1.0$TeV with $n = 2$. At the LHC ($\sqrt{s} = 14$TeV) this will reach $M_S \simeq 5$TeV with $n = 4$ and $M_S \simeq 7$TeV with $n = 2$ [6].

The distribution of $\not{E}_T$ in jet + missing transverse energy events from CDF data is shown in figure 10, where no evidence of significant deviations from the SM expectations appear.

5.2 Searches for virtual graviton exchanges at hadron colliders

Similar to the case of e^+e^- colliders, boson and fermion pair productions at hadron colliders offer the possibility to detect virtual graviton exchanges interfering with ordinary SM productions.

The di-photon production channel appears to be a very interesting one as both the invariant mass $M_{\gamma\gamma}$ and the angular $d\sigma/d\cos\theta$ distributions would be sensibly affected by virtual KK graviton exchanges. Figure 11 shows possible signal effects and preliminary CDF data $M_{\gamma\gamma}$ distributions. The expected sensitivity reach from these signals is $M_S \simeq 1$TeV at the Tevatron with 100pb^{-1} (Run I), and should grow to $M_S \simeq 7$TeV at the LHC with 100fb^{-1} [22]

Di-lepton productions also appear to be quite sensitive to graviton interference effects. In this case at the Tevatron energies, the sensitivity is is fact quite small using only the invariant mass distribution M_{ll}, so that in fact the angular distribution

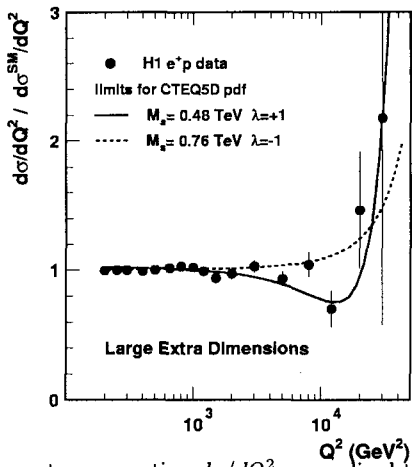

Figure 9: Neutral Current cross section $d\sigma/dQ^2$ normalised to the Standard Model using CTEQ5D parton distributions. H1 data are compared to the effect of graviton exchange given by the 95% CL lower limits on the scale M_S for positive ($\lambda = +1$) and negative($\lambda = -1$) coupling.

$d\sigma/d\cos\theta$, of the asymmetry is needed. At the LHC the $gg \to l^+l^-$ dominate and the effects are visible mostly on the M_{ll} distribution. As for the $gamma\gamma$ channel the expected reach in M_S are $M_S \simeq 1$TeV at the Tevatron (Run I) and $M_S \simeq 7$TeV at the LHC [7]. Distribution of expected graviton exchange effects on the lepton pair asymmetry and the expected M_S reach at the Tevatron are shown in figure 12.

Finally possible virtual graviton exchange effects on the production of weak bosons at hadron colliders have also been studied [23]. The effects on WW and ZZ production rates and distributions give a sensitivity reach of M_S around 0.6TeV , using the Tevatron data.

6 Conclusions

The experimental high energy physics community has reacted quickly to the Low Scale Gravity (LSG) proposals and is currently investigating such theories with the available collider data. For $n \geq 3$ it appears that even though they do not probe the M_S scale directly, virtual graviton exchanges have a better sensitivity to LSG compared to the possibilities to detect direct KK graviton production. The LEP, HERA and Tevatron experiments data appear to rule out such scenarios with gravity scales of $M_S \sim 1$TeV . In the future the NLC and LHC data will be able to provide a very stringent test of the ADD framework, probing low gravity scales up to $M_S \sim 10$TeV .

References

[1] N.Arkani-Hamed *et al.*, *Phys.Lett.* **B** 429, 263 (1998).

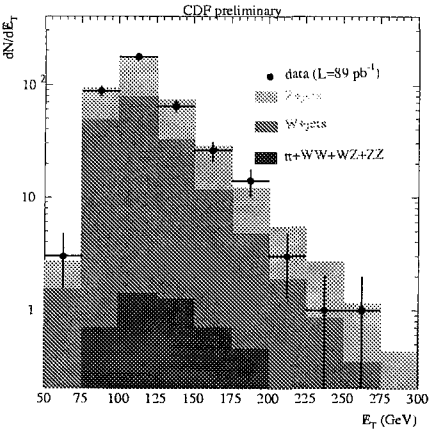

Figure 10: Distribution of transverse energy in jet + missing energy events from CDF Run I data.

[2] N.Arkani-Hamed *et al.*, *Phys.Rev.* **D** 59, 86004 (1999); I.Antoniadis *et al.*, *Phys.Lett.* **B** 436, 257 (1998); I.Antoniadis and C.Bachas, *Phys.Lett.* **B** 450, 83 (1999).

[3] J.C.Long, H.W.Chan, J.C.Price, *Nucl.Phys.* **B** 539 23 (1999).

[4] S.Cullen and M.Perelstein, *Phys.Rev.Lett.* 83, 268 (1999).

[5] L.J.Hall and D.Smith, *Phys.Rev.* **D** 60, 85008 (1999).

[6] G.F.Giudice *et al.*, *Nucl.Phys.* **B** 544, 3 (1999).

[7] J.Hewett, *Phys.Rev.Lett.* 82, 4765 (1999).

[8] K.Agashe and N.G.Deshpande, *Phys.Lett.* **B** 456, 60 (1999).

[9] ALEPH Collab., R.Barate *et al.*, *EPS-HEP#6-417* Contribution to EPS-HEP99 Tampere (July-1999).

[10] DELPHI Collab., P.Abreu *et al.*, *EPS-HEP#6-141* Contribution to EPS-HEP99 Tampere (July-1999).

[11] DELPHI Collab., P.Abreu *et al.*, *EPS-HEP#6-362* Contribution to EPS-HEP99 Tampere (July-1999); *CERN-EP* 2000-068 (2000).

[12] DELPHI Collab., P.Abreu *et al.*, *EPS-HEP#6-364* Contribution to EPS-HEP99 Tampere (July-1999).

[13] L3 Collab., M.Acciarri *et al.*, *Phys.Lett.* **B** 464, 135 (1999).

[14] L3 Collab., M.Acciarri *et al.*, *Phys.Lett.* **B** 470, 268 (1999).

[15] L3 Collab., M.Acciarri *et al.*, *Phys.Lett.* **B** 470, 281 (1999).

[16] L3 Collab., M.Acciarri *et al.*, *CERN-EP* 2000-061 (2000).

[17] OPAL Collab., G.Abbiendi *et al.*, *Phys.Lett.* **B** 465, 303 (1999).

[18] OPAL Collab., G.Abbiendi *et al.*, *CERN-EP*/99-097 (1999); to appear in *Eur.Phys.J.C.*

[19] OPAL Collab., G.Abbiendi *et al.*, *CERN-EP* 2000-050 (2000).

[20] S.Mele and E.Sanchez, *Phys.Rev.* **D** 61, 117901 (2000).

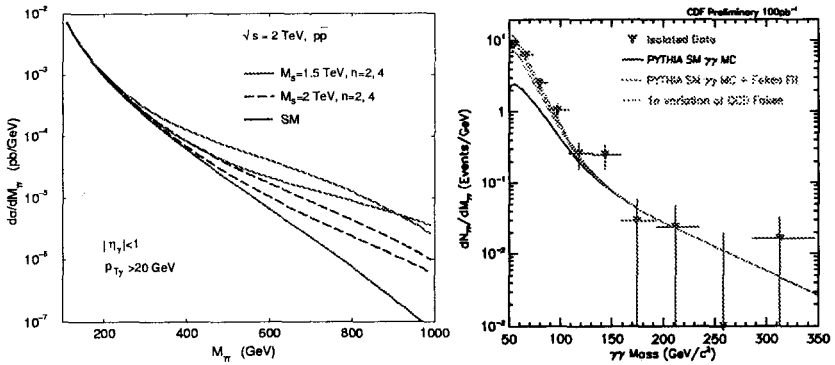

Figure 11: Differential distribution $d\sigma/dM_{\gamma\gamma}$ versus $M_{\gamma\gamma}$ for diphoton production at the 2 TeV Tevatron for Standard Model and low scale gravity with M_S=1.5, 2 TeV, and n=2,4. Cuts $|\eta_\gamma| < 1$ and $p_{T\gamma} > 20$ GeV are imposed.

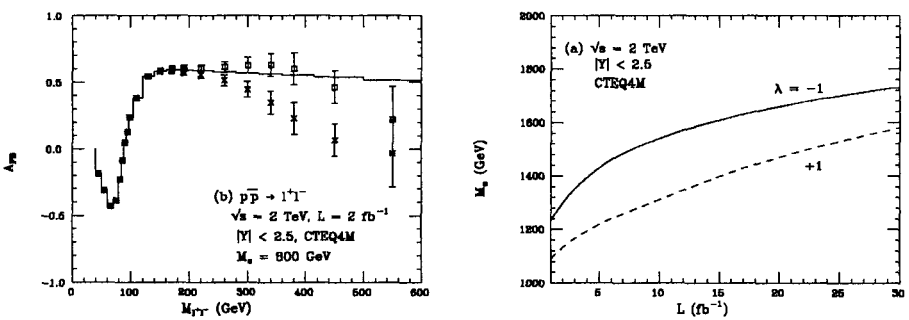

Figure 12: (left) Bin integrated lepton pair forward-backward asymmetry for Drell-Yan productions at the Tevatron Main Injector. The SM is represented by the solid histograms, the data points represent possible graviton exchanges with $M_S = 0.8$TeV and $\lambda = +1$ or$\lambda = -1$. (right) 95% CL search reach for the string scale M_S as a function of the integrated luminosity at the Tevatron with $\lambda = \pm 1$.

[21] H1 Collab., C.Adloff *et al.*, DESY 00-027. Submitted to *Phys.Lett.* **B**.
[22] K.Cheung, UCD-HEP-99-8, hep-ph/9904266.
[23] C.Balázs *et al.*, hep-ph/9904220.

Dynamics of Event Horizon Creation

A. A. SHATSKIY [a]

Physics Faculty of Lomonosov Moscow State University, 119899 Moscow, Russia

Abstract. The research was carried out on the radial motion of a substance in the spherically symmetric gravitational field in the comoving reference system for the realistic equation of substance state. The dynamics of event horizon formation was studied.

1 Introduction

In this work a particular but a physically real case of the spherically symmetric accretion to a central body, irrespective of rotation, was investigated. The following definitions were adopted: speed of light c and gravitational constant G are taken equal to 1. It is assumed that our system is a cooling off massive star without a horizon. Its substance rests in the initial moment (equation of state $P = \alpha\varepsilon$, where P - pressure in the substance, ε — energy density and α is constant). In the following moment the substance starts free falling. If the reaction of the moving substance to the gravitational field of the system is neglected, then, considering that the inequality system gravitation radius more then radius r is inevitably true in one of the points r, in this point, according to the Schwarzschield solution for the gravitational field in vacuum, the apparent horizon would form, i.e. the speed of the falling substance would reach the speed of light. In this case the achievement of the speed of light by the substance causes the interval sign to change and therefore is an invariant event not depending on the choice of a reference system.

2

The solution of such dynamic problem can be conveniently found by choosing a co-moving reference system. In this system the problem was solved in the literature for a particular case $\alpha = 0$. The substance rests in the chosen reference system and one can form an opinion about its movements only by the changes in the surrounding distances r which are connected with the center of the system and are defined as $2\pi r$. With this definition of radius r the metric can be conveniently presented in the form:

$$ds^2 = e^{\nu}dt^2 - e^{\lambda}dR^2 - r^2(d\theta^2 + sin^2\theta d\varphi^2) \tag{1}$$

Here R - coordinate of a particle of the substance in the comoving reference system or its index, e^{ν}, e^{λ}, r are in this case functions R and time t. It should be noted that with pressure equal to 0, i.e. when $\alpha = 0$, ν is also equal to 0, i.e. the reference system is at the same time a synchronous one.

3

Einstein equations for an unambiguous description of the system can be derived from literature. Let us assign indexes R to the particles so that in the initial moment

[a] e-mail: bruk@lpi.ru

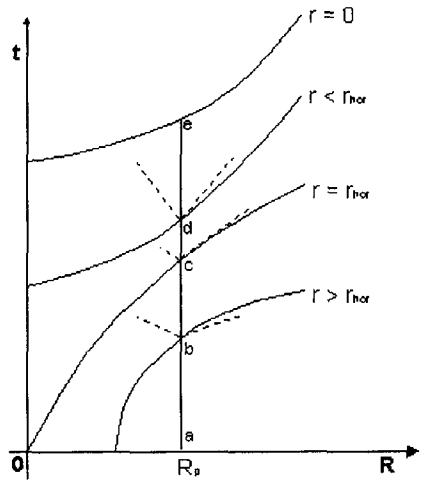

Figure 1:

$r = R$. An expression for the squared speed V^2 of the substance relative to the surfaces $r = const$ can be derived from the metric form (1): $V^2 = \dot{r}^2 e^{-\nu} e^{\lambda}/(r')^2$. Dot and accent marks mean time and coordinat derivatives respectively.

Einstein equations can be transformed to boil down to the equation:

$$r = \frac{2M + 2\alpha m}{1 - Q(1 - V^2)},$$

where it is noted: M — mass under the sphere with radius R in the initial moment, Q and m given in equations:

$$Q = (r')^2 e^{-\lambda} \quad and \quad m = \int_r^R 4\pi \tilde{r}^2 \varepsilon(R, \tilde{r}) d\tilde{r}|_{R=const}.$$

One can prove that the apparent horizon appears in that point and that moment where the speed of the falling substance reaches the speed of light in vacuum, i.e. where $V = 1$ (see Figure 1). Hence the radius of the horizon r_{hor} is defined by the formula:

$$r_{hor} = 2M + 2\alpha m(r_{hor}). \tag{2}$$

Thus, the horizon shifts to the greater value in comparison with its value in vacuum $r_{0_{hor}} = 2M$, by $2\alpha m(r_{hor})$ (see Figure 2). In this case it is reasonable to assume that in the vicinity of the horizon the ultrarelativistic equation of substance state is true under which $\alpha = 1/3$.

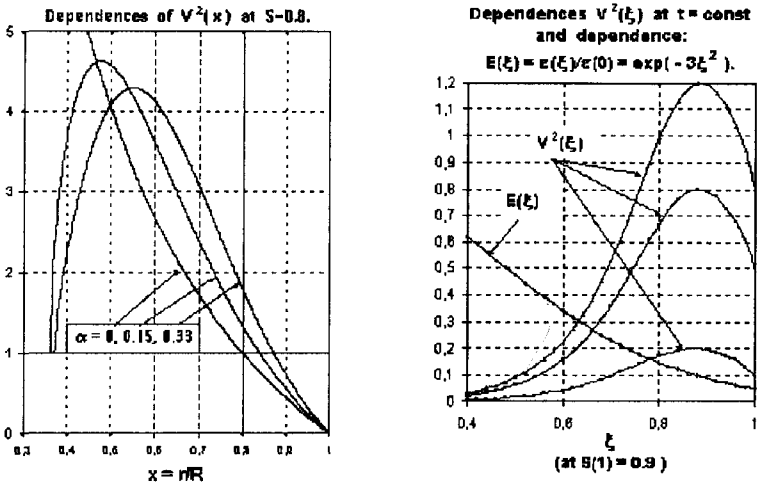

Figure 2: Dependences V^2 from $x = r/R$ at $R = const$ — left and from $\xi = R/R_*, (S(R_*) = 0.9, t = const)$ — right.

4 Summary.

1. Due to the "gravitation of pressure" effect we discovered the effect of the horizon shifting to the greater value in comparison with its Schwarzschield value.

2. According to the results of the detailed investigation it appears that the solution for a spherical layer of the substance with index R is fully defined by three non-dimensional parameters in the initial moment on this layer and in this sense is not dependent on the initial distribution of the substance of the system under and above this layer (a dependence is in the frames of these three parameters). Thus, by integrating we find a whole family of self-similar solutions.

3. The research shows that with a certain choice of initial parameters a local extremum of the curve $V(R)|_{t=const}$ appears which causes with $V = 1$ the second horizon to form in the system — a counterpart of Reisner-Nordstrem and Kerr-Newman solutions.

References

[1] L.D. Landau, E.M. Lifshits "The Theory of Field".
[2] I.D. Novikov, V.P Frolov "Physics of Black Holes". M., Science 1986.
[3] Choptuik, M. W., Phys. Rev. D **44**, 3124-3135 (1991).
[4] Shatskiy A.A., Andreev A.Yu. Zh.Éksp.Teor.Fiz., **116**, p.353-368, 8, (1999).

Programme of the 9th Lomonosov Conference on Elementary Particle Physics

20 September, MON

08.30 – 09.30 Registration

09.45 – 10.15 Welcome to the participants and Introduction to the Conference

10.15 - 13.00 **MORNING SESSION** (Auditorium 5-19)

Chairman: R.Faustov
10.15 E.Shabalin (ITEP, Moscow), *On the Fundamental Symmetries in Particle Physics* (40 min).
10.55 G.Tatishvili (JINR, Dubna), First Result on the Direct CP Violation Measurement with the NA48 Experiment at CERN (30 min)
11.25 B.Vallage (DAPNIA, Saclay), *NA48 Rare Decays Results* (30 min)

11.50 - 12.20 Tea break

12.20 Yu.Simonov (ITEP, Moscow), *Spontaneous Symmetry Breaking: Now and Forever* (40 min)

13.00 - 14.30 Lunch

14.30 - 18.10 **AFTERNOON SESSION** (Auditorium 5-19)

Chairman: A.Mourao
14.30 A.Slavnov (MSU), *Chiral Symmetry in Lattice Field Theory Models* (40 min)
15.10 I.Josa (CIEMAT, Madrid), *Higgs Searches at LEP* (25 min)

15.35 - 16.05 Tea break

16.05 S.Armstrong (University of Wisconsin-Madison), *Searches for Higgs* (40 min)
16.45 R.Santos (IST, Lisbon), L.Bruecher (IST, Lisbon), *Experimental Signatures of Fermiophobic Higgs* (25 min)
17.10 G.Boyarkina (Grodno, Belorussia), *S-Channel Higgs Physics Beyond the Standard Model* (20 min)
17.30 Special Session (Banquet)

21 September, TUE

9.30-13.40 **MORNING SESSION** (Conference Hall)

Chairman: A.Nikishov
9.30 P.Azzurri (University of Paris), *Quantum Gravity Effects* (40 min)
10.10 Yu.Loskutov (MSU), *Gravyweak Interactions and its Consequences* (25 min)
10.35 V.Braginsky (MSU), *How to Detect the Spacetime Foam* (30 min)

11.05 - 11.40 Tea break

Chairman: P.Nowosad
11.40 D. Galtsov (MSU), *Solitons in Gauge and Superstring Theory* (40 min)
12.20 A.Nikishov (FIAN, Russia), *On Energy-Momentum Tensor of Gravitational Field* (40 min)

13.00 - 15.00 Lunch

15.00-18.05 **AFTERNOON SESSION** (Conference Hall)

Chairman: A.Degr'e
15.00 V.Tioukov (INFN, Italy), *Results from the CHORUS Neutrino Oscillation Experiment at CERN* (40 min)
15.40 A.Mourao (IST/CENTRA, Lisbon), *Limits on the Neutrino Magnetic Moment from Solar Neutrino Experiments* (20 min)
16.00 M.Dvornikov, A.Egorov, A.Lobanov, A.Studenikin (MSU), *Neutrino Oscillatations in Electromagnetic Fields* (20 min)

16.20 - 16.40 Tea break.

16.40 O.Boyarkin (Grodno, Belorussia), *Neutrino Oscillations in the Extensions of the Standard Model* (20 min)
17.00 R.Horvat (Rudjer Boskovic Inst., Zagreb), *Pulsar Velocity Puzzle and Nonstandard Neutrino Oscillations* (20 min)
17.20 A.Husain (Tokyo Metropolitan University), *Neutrino Conversions in Active Galactic Nuclei* (20 min)
17.40 M.Rebelo (IST, Lisbon), *Degenerate and Quasidegenerate Majorana Neutrinos* (25 min)

22 September, WED

9.00-13.45 **MORNING SESSION** (Conference Hall)

Chairman: A.Studenikin
9.00 A.Kaidalov (ITEP, Moscow), *High-Energy Interactions of Hadrons and Nuclei and QCD*
(40 min)
9.40 I.Dremin (Lebedev Physical Institute, Moscow), *Perturbative and Non-Perturbative Effects in QCD Jet Evolution* (40 min)
10.20 A.Bassetto , L.Grigoulos, F.Vian (Univ. of Padova, Italy), *Two-Dimentional QCD and Instanton Contributions* (25 min)
10.45 T.Ziegler (J.Gutenberg University, Mainz), *Color Reconnection and Bose-Einstein* (25 min)
11.10 S.Kulagin (INR, Moscow), *Nuclear Shadowing Effects in Neutrino Deep Inelastic Scattering (15 min)*

11.25 - 11.45 Tea break

Chairman: A.Kaidalov
11.45 D.Shirkov, I.Solovtsov (JINR, Dubna), *Invariant analytic approach in perturbative QCD* (40 min)
12.25 M.Polikarpov (ITEP, Moscow), *Confinement in QCD, Lattice and Continue Point of View*
(40 min)
13.05 V.Belokurov, Yu.Solovyov, E.Shavgulidze (MSU), *Perturbative Theory with Convergent Series* (20 min)
13.25 A.Kataev (INR, Moscow), *Electron-Positron Annihilation: Experimental data vs QCD Theoretical Predictions in the Euclidian Region* (20 min)

13.45 - 15.00 Lunch

15.00 - 18.45 **AFTERNOON SESSION** (Conference Hall)

Chairman: A.Kataev
15.00 G.Bobbink (NIKHEF, Amsterdam), *QCD Studies at LEP* (25 min)
15.25 S.Alekhin (IHEP, Protvino), *Determination of α_s from Charged Leptons Deep Inelastic Scattering Data* (25 min)
15.50 A.Sidorov (JINR, Dubna), *A NLO QCD analysis of the spin structure function g_1 and higher twist corrections* (25 min)
16.15 A.Illarionov, A.Litvinenko, G.Lykasov (JINR, Dubna), *Polarization Phenomena in Fragmentation Processes of Type $dp \to \pi X$* (15 min)

16.30 - 16.50 Tea break

Chairman: O.Bojarkin
16.50 I.Cherednikov, S.Fedorov, M.Khalili, K.Sveshnikov (MSU),
3-phase hybrid quark bag models and renormalization of the Casimir energy (20 min)

17.10 A.Borisov, N.Zamorin (MSU), *Lepton Production by Neutrinos in an External Electromagnetic Field* (15 min)
17.25 A.Borisov, P.Sizin (MSU), *Propagation of Axions in a Strongly Magnetized Medium* (15 min)
17.40 A.Lobanov, O.Pavlova (MSU), *Neutral Particle Radiation in Electromagnetic Field* (20 min)
18.00 V.Epp, T.Mitrofanova (Tomsk University, Russia), *Radiation of Relativistic Particles in a Quasi-Homogeneous Magnetic Field* (20 min)
18.15 V.Bagrov, B.Samsonov (Russia), *Special Properties of Generalized Coherent States* (20 min)
18.35 V.Bordovitsyn, V.Gushchina, A.Myagkii (Russia), *Spin orbital motion and the Thomas Precession in the Classical and Quantum Theory* (15 min)

23 September, THU

09.00 – 18.00 Bus excursion to the Monastery St. Serge in the town of Sergiev-Posad

24 September, FRI

9.15-13.40 **MORNING SESSION** (Conference Hall)

Chairman: V.Savrin
9.15 A.Malinine (CERN), *B physics at LEP* (40 min)
9.55 A.Halley (CERN), *B_S Oscillations* (25 min)
10.20 A.Tricomi (ALEPH Coll., Univ. of Catania; INFN Bari), *Measurements of the b and c Asymmetries* (25 min)
10.45 J.Putz (University of Washington), *$D_S \rightarrow$ tau nu* (20 min)
11.05 D.Ebert (Humboldt Univ., Berlin), V.Galkin (NSK RAN), R.Faustov (FIAN, Moscow), *Weak Decay of Mesons With Heavy Quarks* (25 min)
11.30 D.Melikhov (Russia), N.Nikitin, F.Rizatdinova, S.Simula, L.Smirnova (Russia), *Probing the Standard Model in Rare Semileptonic B-Meson Decays with ATLAS Detector* (15 min)

11.50 - 12.10 Tea break
Chairman: G.Diambrini-Palazzi
12.10 J.-P. Vialle (LAPP, Annecy-le-Vieux), *First Results of the Alpha Magnetic Spectrometer (AMS) Experiment* (30 min)
12.40 A.Cherepashuk (Russia), *Modern Observational Status of Black Hole Problem* (40 min)
13.20 V.Lipunov (MSU), *The Cosmic GRB Phenomena* (40 min)

14.00 - 15.00 Lunch
15.00 - 18.45 **AFTERNOON SESSION** (Conference Hall)
Chairman: P.Nowosad
15.00 V.Bordovitsyn, V.Bulenok, V.Epp, V.Gushchina (Russia), *Kinematic Projection of the Pulsar Emission Profiles* (20 min)
15.20 A.Zakharov (ITEP, Moscow), *Possible Observational Evidences of Non-Compact (Non-Baryonic) Microlenses (Neutralino Stars)* (25 min)
15.45 M.Fil'chenkov (Institute of Gravitation and Cosmology, Moscow), *Late Gravitational Collapse, Quantum Miniholes and the Birth of a New Universe* (15 min)
16.00 B.Dragovich (Belgrade, Yugoslavia), *On Adelic Strings* (20 min)
16.20 A.Shatskiy (MSU), *The Dynamics of Event Horizon Creation* (15 min)

16.35 - 17.05 Tea break
Chairman: B.Dragovich
17.05 O.Khrustalev, E.Spirina, M.Tchitchikina (MSU), *Quantum Field of Nonstanionary Polaron* (20 min)
17.25 P.Nowosad (Brazil), *Bogomolny-Type Equations As Symmetry-Restoring of the Geometry of Elementary Particles* (20 min)
17.45 J.Smulsky (Tyumen, Russia), *New Fundamental Trajectories* (20 min)
18.05 A.Nesterenko (MSU), *The Quark-Antiquark Potential in the Analytic Approach to QCD* (15 min)
18.20 E.Bubelev (JINR, Dubna), I.Kuchin (PhTI, Min.-Ac.Sci., Almaty, Kazakh Republic), *What Stands Behind the Rising Elementary Act Cross Section* (15 min)
18.35 S.Kopylov (STE «Brainstorm», Moscow), *Dirac Equation, SU(2) Model and Octanions* (15 min)

25 September, SAT

9.00 - 13.35 **MORNING SESSION** (Auditorium 5-19)

Chairman: J.Dias de Deus
9.00 A.Degr'e (LAPP, Annecy-le-Vieux), *Precision EW tests at LEP* (40 min)
9.40 A.Balandras (LAPP, Annecy-le-Vieux), *SUSY Searches at LEP* (40 min)

10.20 - 11.00 Tea break

11.00 H.J.Lee (Humboldt University, Berlin), *W properties at LEP* (25 min)
11.25 M.Chalmers (University of Glasgow), *W mass* (25 min)
11.50 G.Passaleva (INFN, Florence), *Two Photon Physics at LEP* (25 min)

12.15 - 15.00 Lunch

15.00 - 18.15 **AFTERNOON SESSION** (Auditorium 5-19)

Chairman: V.Matveev
15.00 W.Lohmann (DESY, Zeuthen), *Tau Physics at LEP* (40 min)
15.40 A.Kounine (MIT, Cambridge), *LEP Physics Results* (40 min)

16.20 - 16.50 Tea break

16.50 G.Diambrini-Palazzi (Univ. of Rome), *Macroscopic Quantum Coherence: New Results and Possible Application to Quantum Computer* (40 min)
17.10 J.Dias de Deus (IST, Lisbon), *Physics of Quark Gluon Plasma* (40 min)
17-50 L.Soloviev (IHEP, Protvino), *String Quark Model of Mesons* (25 min)

18.15 **Closing**
19.00 **Banquet**

World Scientific
www.worldscientific.com
4722 hc

ISBN 981-02-4644-7
9 789810 246440